# NASA TECHNICAL
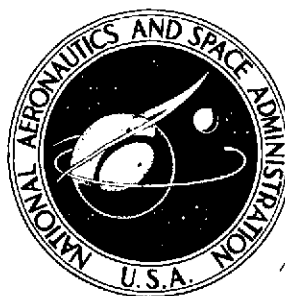# MEMORANDUM

NASA TM X-3079

(NASA-TM-X-3079)   A WIND TUNNEL                    N75-11896
INVESTIGATION OF THE WAKE NEAR THE
TRAILING EDGE OF A DEFLECTED EXTERNALLY
BLOWN FLAP (NASA)   190 p HC $7.00                  Unclas
                                    CSCL 01A H1/02   03883

# A WIND-TUNNEL INVESTIGATION OF
# THE WAKE NEAR THE TRAILING EDGE
# OF A DEFLECTED EXTERNALLY BLOWN FLAP

*by William G. Johnson, Jr., and Gerald E. Kardas*

*Langley Research Center*
*Hampton, Va. 23665*

| 1. Report No. NASA TM X-3079 | 2. Government Accession No. | 3. Recipient's Catalog No. |
|---|---|---|
| 4. Title and Subtitle A WIND-TUNNEL INVESTIGATION OF THE WAKE NEAR THE TRAILING EDGE OF A DEFLECTED EXTERNALLY BLOWN FLAP | | 5. Report Date October 1974 |
| | | 6. Performing Organization Code |
| 7. Author(s) William G. Johnson, Jr., and Gerald E. Kardas | | 8. Performing Organization Report No. L-9665 |
| 9. Performing Organization Name and Address NASA Langley Research Center Hampton, Va. 23665 | | 10. Work Unit No. 760-61-02-03 |
| | | 11. Contract or Grant No. |
| 12. Sponsoring Agency Name and Address National Aeronautics and Space Administration Washington, D.C. 20546 | | 13. Type of Report and Period Covered Technical Memorandum |
| | | 14. Sponsoring Agency Code |

16. Abstract

An investigation was made to determine the behavior of the flow near the trailing edge (that is, in the near wake) of a deflected externally blown flap. The model tested was a general research model of a swept-wing, jet-powered STOL transport with externally blown flaps. The model was tested with four engine simulators mounted on pylons under the wing. Tests were conducted in the Langley V/STOL tunnel over an angle-of-attack range of $0^{\circ}$ to $16^{\circ}$ and a thrust-coefficient range from 0 to approximately 4 at a Reynolds number of $0.461 \times 10^6$ based on the wing reference chord.

The results of this investigation are presented primarily as plots of the individual velocity vectors obtained from the wake survey. These data are used to extend an earlier analysis to isolate the effects of the engine thrust on the behavior of the flow at the flap trailing edge. Results of a comparison with a jet-flap theory are also shown.

| 17. Key Words (Suggested by Author(s)) Externally blown flap Wake surveys Propulsive lift Jet-flap theory | 18. Distribution Statement Unclassified — Unlimited STAR Category 01 |
|---|---|
| 19. Security Classif. (of this report) Unclassified | 20. Security Classif. (of this page) Unclassified | 21. No. of Pages 188 | 22. Price* $8.00 |

# A WIND-TUNNEL INVESTIGATION OF THE WAKE

## NEAR THE TRAILING EDGE OF A DEFLECTED

## EXTERNALLY BLOWN FLAP

By William G. Johnson, Jr., and Gerald E. Kardas*
Langley Research Center

## SUMMARY

An investigation was made to determine the behavior of the flow near the trailing edge (that is, in the near wake) of a deflected externally blown flap. The model tested was a general research model of a swept-wing, jet-powered STOL transport with externally blown flaps. The model was tested with four engine simulators mounted on pylons under the wing. Tests were conducted in the Langley V/STOL tunnel over an angle-of-attack range of $0^O$ to $16^O$ and a thrust-coefficient range from 0 to approximately 4 at a Reynolds number of $0.461 \times 10^6$ based on the wing reference chord.

The results of this investigation are presented primarily as plots of the individual velocity vectors obtained from the wake survey. These data are used to extend an earlier analysis to isolate the effects of the engine thrust on the behavior of the flow at the flap trailing edge. Results of a comparison with a jet-flap theory are also shown.

## INTRODUCTION

The process of developing propulsive-lift technology for application to short take-off and landing (STOL) aircraft has led to extensive research on high-lift concepts such as the externally blown flap, internally blown flap, augmenter wing, and upper-surface blown flap.

The present investigation was made to determine the behavior of the flow near the trailing edge (that is, in the near wake) of a deflected externally blown flap. The model tested was a general research model of a swept-wing, jet-powered STOL transport with externally blown flaps. The model was tested with four engine simulators mounted on pylons under the wing. Tests were conducted in the Langley V/STOL tunnel over an angle-of-attack range of $0^O$ to $16^O$ and a thrust-coefficient range from 0 to approximately 4. The free-stream dynamic pressure of 384 $N/m^2$ (8 $lbf/ft^2$) gave a Reynolds number of $0.461 \times 10^6$ based on the wing reference chord of 26.97 cm (10.62 in.). The total pressures and three velocity components were measured in the near wake. From the velocity components, the total velocity and downwash angles were determined.

---

An earlier analysis of these data using a jet-flap theory was reported in reference 1. The present paper extends this analysis to isolate the effects of the engine thrust on the behavior of the flow at the flap trailing edge. Related changes in the results of the comparison with a jet-flap theory are also shown.

## SYMBOLS

The measurements of this investigation are presented in the International System of Units (SI) with the U.S. Customary Units being indicated in parentheses. The measurements and calculations were made in the U.S. Customary Units. Factors relating the two systems are given in reference 2.

b      wing span, m  (ft)

c      local chord of wing with flaps undeflected, m  (ft)

$C_L$      lift coefficient, $\dfrac{\text{Lift}}{q_\infty S}$

$C_T$      total engine gross thrust coefficient, $\dfrac{T}{q_\infty S}$

$C_\mu$      momentum coefficient, $\displaystyle\int_{\eta_1}^{\eta_2} C_\mu{}^* \, d\eta$

$C_\mu{}^*$      section-momentum coefficient determined from wake-survey measurements

$d_{min}$      minimum distance between probe and flap trailing edge, cm  (in.)

$F_A$      axial force, N  (lbf)

$F_N$      normal force, N  (lbf)

g      gravitational acceleration constant, 9.8 m/sec$^2$ (32.2 ft/sec$^2$)

$p_t$      total pressure measured in near wake, N/m$^2$  (lbf/ft$^2$)

$p_\infty$      free-stream static pressure, N/m$^2$  (lbf/ft$^2$)

$q_\infty$      free-stream dynamic pressure, N/m$^2$  (lbf/ft$^2$)

R      universal gas constant, 29.27 kg-m/kg-K (53.35 ft-lb/lb-$^\circ$R)

| | |
|---|---|
| $S$ | wing area, $m^2$ $(ft^2)$ |
| $T$ | gross static thrust, N (lb) |
| $T_\infty$ | free-stream temperature, K $(^0R)$ |
| $V_B$ | power-off flow velocity in near wake, m/sec (ft/sec) |
| $V_B'$ | power-on flow velocity in near wake, m/sec (ft/sec) |
| $V_j$ | magnitude of individual streamwise velocity vector, m/sec (ft/sec) |
| $V_j^*$ | magnitude of the local average streamwise velocity vector at each spanwise survey station, m/sec (ft/sec) |
| $\Delta V_j^*$ | change in the magnitude of $V_j^*$ produced by addition of engine exhaust, m/sec (ft/sec) |
| $V_\infty$ | free-stream velocity, m/sec (ft/sec) |
| $y$ | distance measured spanwise on wing, m (ft) |
| $\alpha$ | angle of attack of wing chord line (also fuselage center line), deg |
| $\gamma$ | ratio of specific heats, 1.4 for air |
| $\delta_j$ | averaged jet- or thrust-deflection angle, deg |
| $\delta_j^*$ | section jet- or thrust-deflection angle, deg |
| $\Delta\delta_j^*$ | change in section jet- or thrust-deflection angle produced by addition of engine exhaust, deg |
| $\eta$ | spanwise location of survey station, $\dfrac{y}{b/2}$ |
| $\eta^*$ | static thrust recovery efficiency, $\dfrac{\sqrt{F_A^2 + F_N^2}}{T}$ |
| $\tau$ | jet thickness measured at flap trailing edge, m (ft) |

$\tau'$      distance from initial indication of jet wake, $0 \leqq \tau' \leqq \tau$; positive direction is up, m (ft)

Subscripts:

1      inboard limit

2      outboard limit

## MODEL AND APPARATUS

The near-wake investigation was conducted with a general research model of a four-engine, externally blown flap airplane. A three-view drawing of the model is shown in figure 1(a).

The wing had a nominal 30° quarter-chord sweep. The 35-percent-wing chord double-slotted flap system was deflected to 35° from the flap zero position by use of fixed-angle flap bracket. For this flap configuration, the 15-percent wing chord vane was deflected 11.2°. The leading-edge slat system consisted of a 15-percent wing chord slat from the fuselage to the outboard engine pylon and a 25-percent chord slat from the outboard pylon to the wing tip. The leading-edge slat deflection was 50°. A schematic of the complete high lift flap system is shown in figure 1(b). The vertical and horizontal tails were not installed for this investigation.

Four air ejector engine simulators, shown schematically in figure 2, were used to simulate the jet propulsion system. Each engine simulator was a two-part ejector with individual compressed air supply lines and control valves to provide the exhaust flow characteristics of the fan and gas generator which would represent a fan-jet engine bypass of 10.0, where bypass ratio is defined as the ratio of the total fan exit flow to total gas-generator exit flow. The size and position of the simulators are shown in figure 3.

A split-film total vector anemometer (described in ref. 3) was used to measure the three components of velocity in the near wake. The three split-film sensors were arranged in a mutually orthogonal pattern. The anemometer was mounted on a traverse assembly fixed to the model so that one sensor was alined horizontally perpendicular to free stream and the other two sensors formed a vertical plane which was coplanar with free stream. A shielded total head (Kiel) probe was mounted on the traverse assembly slightly above the anemometer and was used to measure total pressure in the near wake. Photographs of the survey instrumentation installed on the model are shown in figures 4(a) to 4(c).

4

## TEST AND PROCEDURES

Tests were conducted in the Langley V/STOL tunnel at a nominal free-stream dynamic pressure of 384 N/m$^2$ (8 lbf/ft$^2$) for a Reynolds number of $0.461 \times 10^6$ based on the wing reference chord of 26.97 cm (10.62 in.). Most of the tests were made over an angle-of-attack range of 0$^\text{o}$ to 16$^\text{o}$ and a total gross thrust coefficient range up to about 4.0.

For the near-wake investigation, the split-film total-vector anemometer and Kiel probe were moved laterally on the traverse assembly to each spanwise location indicated in figure 5. The probes were then pitched in a vertical arc with a radius of 41.96 cm (16.52 in.) through the wake near the flap trailing edge. The probe elevation angle was referenced to the wing element chord line; that is, an elevation angle of 0$^\text{o}$ was parallel to the wing chord line. A calibration of the response of the horizontal anemometer sensor to the flow angle provided a means of determining the local flow deflection angle relative to the probe axis. The voltage outputs from the anemometer were filtered to obtain steady values at each data point.

## PRESENTATION OF DATA

The data obtained from the investigation of the near wake of a deflected externally blown flap are presented in figures 6 to 148 for the conditions shown in the following table:

| $C_T$ | $\alpha$, deg | Figure |
|:---:|:---:|:---:|
| 0.0 | 0 | 6 to 16 |
|  | 4 | 17 to 27 |
|  | 8 | 28 to 38 |
|  | 12 | 39 to 49 |
|  | 16 | 50 to 60 |
| 1.0 | 12 | 61 to 71 |
|  | 16 | 72 to 82 |
| 2.0 | 0 | 83 to 93 |
|  | 8 | 94 to 104 |
|  | 12 | 105 to 115 |
|  | 16 | 116 to 126 |
| 4.0 | 0 | 127 to 137 |
|  | 8 | 138 to 148 |

Each figure represents a single survey location and consists of three parts. The measured streamwise velocity vectors shown in part (a) of each figure were determined from the velocity components measured by the two sensors located vertically coplanar to free stream. Dots on the vectors indicate the number of units of free-stream velocity in the magnitude of the local velocity vector. The vectors show the direction of the flow at the survey station relative to both the illustrated chord lines of the wing, vane, and flap elements and the free-stream velocity vector shown below the chord lines. The plots of total velocity as a function of probe elevation angle (part (b) of each figure) show the magnitude of the total velocity. The total velocity includes the streamwise and sidewash components. The plot of downwash angle as a function of probe elevation angle (part (c) of each figure) shows a downwash angle (referenced to the wing chord line) computed by combining the probe elevation angle and the local flow deflection angle.

The value of the free-stream velocity, as indicated in figures 6 to 148, was determined from the free-stream temperature $T_\infty$, the free-stream dynamic pressure $q_\infty$, and the free-stream static pressure $p_\infty$ by the following equation:

$$V_\infty = \sqrt{\gamma g R T_\infty} \sqrt{\frac{2q_\infty}{\gamma p_\infty}} \tag{1}$$

Total pressures $p_t$ measured in the near wake by the Kiel probe appear to be in error and are not presented.

## DISCUSSION OF RESULTS

All the power-off $\left(C_T = 0\right)$ streamwise velocity profiles presented in part (a) of figures 6 to 60 show a region of low-velocity flow behind the flap system. This low-velocity region is probably the separated flow region in the wake of the flap system. As power is added (figs. 61 to 148), the engine efflux eliminates the velocity defect and produces a high velocity region just below the flap trailing edge. The size, general symmetry, and inclination of this flow field indicate that most of the exhaust flow is passing well below the flap system with little impingement and turning. Although this engine flow is not turned as might be desired for a direct thrust contribution to lift, it has a significant influence on the free-stream flow throughout the survey region as shown in the higher than free-stream velocities above the wing and the lower than free-stream velocities below the engine exhaust flow.

### Determination of $C_\mu{}^*$

The velocity profiles for the power-on data reasonably illustrate the thickness of the engine-exhaust flow in the near wake. A jet thickness $\tau$ was defined as the wake

region in which the change in the local velocity vectors exceeded 0.3 m/sec (1 ft/sec). It should be noted that the physical location of this region within the total survey changes with the values of thrust coefficient. It should also be noted that the jet thickness region did not always include the velocity defect region associated with the power-off conditions. The velocity vectors within the jet thickness were integrated to obtain a section-momentum coefficient $C_\mu^*$ at each spanwise station. This integration was performed by using the following equation:

$$C_\mu^* = \frac{\int_0^T V_B'^2 d\tau' - \int_0^T V_B^2 d\tau'}{\frac{1}{2} V_\infty^2 c} \qquad (2)$$

The original form of this equation derived as equation (17) in reference 1 was based on a conclusion from the Kiel probe data that the total pressures were approximately equal for the power-on and the power-off conditions. Additional analysis of these data indicated possible error in the total pressures measured by the Kiel probe. The equation used for determining the section-momentum coefficient in the present analysis can be obtained by taking the difference in the basic momentum equations for power off and power on and by assuming that the static pressures in the jet wake are constant from power off to power on. The results of this integration are shown in figures 149 to 151 where the section-momentum coefficient is presented as a function of spanwise location. The results were extrapolated to the edge of the fuselage ($\eta = 0.126$) and to the most outboard extent of the wing felt to be impacted by the spread engine exhaust flow ($\eta = 0.6$). These section-momentum coefficient $\left(C_\mu^*\right)$ distributions were then integrated spanwise to obtain the total momentum coefficient $\left(C_\mu\right)$ due to engine thrust at the flap trailing edge.

The efficiency of turning the engine exhaust flow through some angle $\delta_j$ is defined as $\eta^*$. The value of $\eta^*$ can be determined from the data which were obtained at static conditions and presented in figure 152 for each engine thrust level of the wake survey data. The product of $\eta^*$ and the engine thrust coefficient $C_T$ obtained from the static-force tests gives a predicted value for the momentum coefficient at the flap trailing edge. This value is compared in figure 153 with the integrated value of engine momentum coefficient $C_\mu$ determined from the wake surveys. The good agreement indicates that for this model configuration, the use of $\eta^*$ obtained from static-force tests is a reasonably accurate means of determining the engine momentum coefficient at the flap trailing edge.

Determination of $\delta_j$

In part (c) of figures 6 to 148, the downwash angles for each wake survey station were presented as a function of probe elevation. Within the limits used to determine $C_\mu^*$, a variation of local downwash angles can be obtained. A mean turning angle $\delta_j^*$ was determined for each spanwise survey station by using the following equation:

$$\delta_j{}^* = \frac{\sum\limits_1^n V_j \delta_{j,l}}{\sum\limits_1^n V_j} \tag{3}$$

where $\delta_{j,l}$ is the local downwash angle minus the wing angle of attack, $V_j$ is the magnitude of the corresponding streamwise velocity vector, and n is the number of measured velocity vectors between the chosen limits. The results of this procedure for both power-off and power-on data are shown in figures 154 to 156 as spanwise distributions of $\delta_j{}^*$. The spanwise limits of these distributions are not extrapolated beyond the measured values since the turning angles for the free-stream flow beyond these spanwise survey stations could not be estimated. The differences in the power-off distributions shown for similar angles of attack (for example, figs. 154(a) and 155(c)) are a result of integrating the different segments of the power-off surveys required to match the specific power-on jet thickness. This procedure was similar to that discussed earlier for the determination of $C_\mu{}^*$. Subtracting the power-off distributions from the power-on distributions results in the distributions in figures 157 to 159 which show the change in $\delta_j{}^*$ due to power $\Delta\delta_j{}^*$ as a function of the spanwise location.

Several approaches were tried during the present investigation to relate a value of $\delta_j$ obtained from the wake survey data to the value of $\delta_j$ obtained from the static force data of figure 152. Figure 160 shows the results from two of these approaches where $\delta_j$ is plotted as a function of the angle of attack. The solid symbols represent the value of $\delta_j$ determined from the static-force data

$$\delta_j = \arctan \frac{F_N}{F_A} \tag{4}$$

The centered symbols are values of $\delta_j$ determined by a spanwise integration of $\delta_j{}^*$:

$$\delta_j = \frac{\int_{\eta_1}^{\eta_2} \left(\Delta V_j{}^*\right)\left(\delta_j{}^*\right)}{\int_{\eta_1}^{\eta_2} \left(\Delta V_j{}^*\right)} \tag{5}$$

The uncentered symbols are values of $\delta_j$ determined by a spanwise integration of $\Delta\delta_j{}^*$:

$$\delta_j = \frac{\int_{\eta_1}^{\eta_2} \left(\Delta V_j{}^*\right)\left(\Delta\delta_j{}^*\right)}{\int_{\eta_1}^{\eta_2} \left(\Delta V_j{}^*\right)} \tag{6}$$

8

These data show that the $\delta_j$ based on $\delta_j^*$ (eq. (5)) is nearly constant with angle of attack, and the $\delta_j$ based on $\Delta\delta_j^*$ (eq. (6)) increases significantly with increasing angle of attack which might suggest a sizable influence of the free-stream flow on the jet-stream deflection angle. These data, as shown in figure 160, however, do not indicate a definite relationship between wake-survey deflection angles and deflection angles obtained from static-force data.

## Relationship of $C_\mu$ to $\delta_j$

The data in figure 152 show an averaged variation of turning angle with the thrust level or velocity: the higher the thrust, the lower the turning angle. A comparison of the spanwise distributions of $C_\mu^*$ (figs. 149 to 151) and $\delta_j^*$ (figs. 157 to 159) relative to the engine center lines shows the same variation to generally exist at the individual spanwise stations. For the $C_\mu^*$ distributions, the peak values occur inboard of the corresponding engine center line; the lower values, on the center line. For the $\delta_j^*$ distributions, the peak values occur on the engine center line and the lower values generally off the center line. This result supports the conclusion drawn earlier from the velocity profiles that for this model configuration, the higher thrust flow passes under the flap system with little flap impingement and turning.

## Comparison With Theory

With the understanding of the near-wake flow characteristics obtained from this analysis, appropriate data from the wake surveys were used as input parameters to a jet-flap analytical method. (See ref. 4.) The results of the computation are compared with the experimental lift coefficients in figure 161 as a function of angle of attack. The surveys were made at $q_\infty = 383.04$ N/m$^2$ (8.0 lbf/ft$^2$). Since the experimental lift coefficients for $C_T = 1$ at this dynamic pressure are not available, data at a $q_\infty = 813.96$ N/m$^2$ (17.0 lbf/ft$^2$) are shown to provide the necessary comparison data. Adding the higher dynamic pressure data to the other comparisons shows that for power-off $\left(C_T = 0\right)$ and $C_T = 2$, the differences shown for the two levels of dynamic pressure are relatively small; therefore the differences for the $C_T = 1$ data are expected to be similar to those for the $C_T = 0$ and $C_T = 2$ data.

The $C_T = 4$ data, however, show that the higher level of dynamic pressure resulted in a lower level of lift coefficient. A study of this result shows that at the lower dynamic pressure, a lower level of thrust was required to produce the desired thrust coefficient. As concluded earlier, the lower velocity exhaust flow turns better and, in turn, produces higher values of lift per unit of thrust at forward velocity.

The two analytical comparisons for each thrust coefficient show the effects of the differences in the jet-deflection angles discussed in figure 160. The broken lines

represent the results from use of the distribution of total jet-deflection angles $\delta_j{}^*$ (summarized as the centered symbols in fig. 160) as input. The solid lines represent the results with the distributions of the power-induced changes in the jet-deflection angles $\Delta\delta_j{}^*$ (summarized as the uncentered symbols in fig. 160) used as input. Both of the methods used to describe the distributions of jet-deflection angles produced analytical results similar to the corresponding experimental data. Better results might have been obtained by using a survey region which had been extended to free-stream conditions both above and below the wing. Further improvement could also have resulted from additional surveys being made along the complete wing semispan.

## CONCLUSIONS

A wind-tunnel investigation has been conducted to develop an understanding of the behavior of the flow near the trailing edge (that is, in the near wake) of a deflected externally blown flap. An analysis of the data resulted in the following conclusions:

1. For this model configuration, the use of the static thrust recovery efficiency factor $\eta^*$ obtained from static force tests is a reasonably accurate means of determining the engine-momentum coefficient at the flap trailing edge.

2. For this model configuration, the higher thrust flow passes under the flap system with little flap impingement and turning.

3. Both of the methods used to describe the distributions of jet-deflection angles produced analytical results similar to the corresponding experimental data.

Langley Research Center,
   National Aeronautics and Space Administration,
      Hampton, Va., June 20, 1974.

## REFERENCES

1. Kardas, Gerald Eugene: Analysis of an Externally Blown Flap High-Lift System Using a Jet-Flap-Wing Theory. M.S. Thesis, George Washington Univ., 1973.

2. Mechtly, E. A.: The International System of Units — Physical Constants and Conversion Factors (Second Revision). NASA SP-7012, 1973.

3. Olin, J. G.; and Kiland, R. S.: Split-Film Anemometer Sensors for Three-Dimensional Velocity-Vector Measurement. Aircraft Wake Trubulence and Its Detection, Plenum Press, Inc., 1971, pp. 57-79.

4. Lissaman, Peter B. S.: Analysis of High-Aspect-Ratio Jet-Flap Wings of Arbitrary Geometry. NASA CR-2179, 1973.

Wing:
  Airfoil section: 9.3% thick supercritical
  Area, sqm (sq.ft)                    .483 (5.202)
  Wing reference chord, m(ft)          .270 (.885)
  Span, m(ft)                          1.902 (6.240)
  Aspect ratio                         7.48
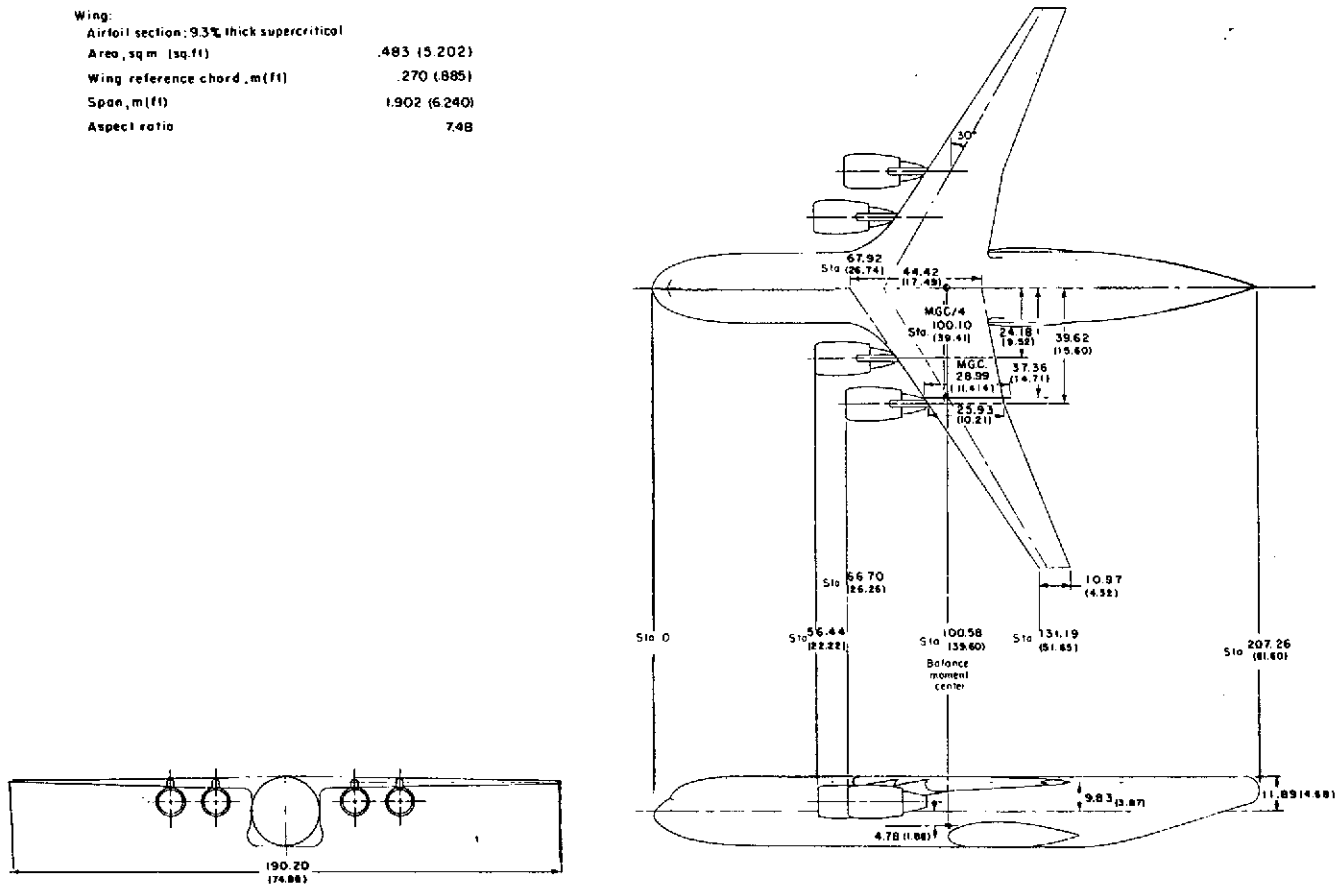


Figure 1.- Three-view drawing of model.   All dimensions are in
centimeters; parenthetical values are in inches.
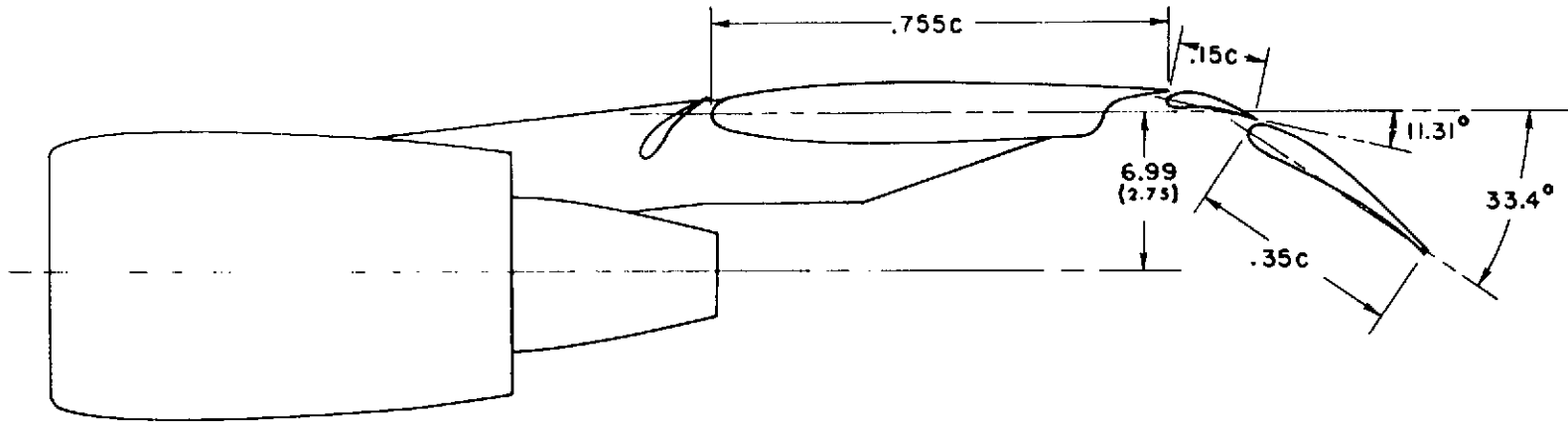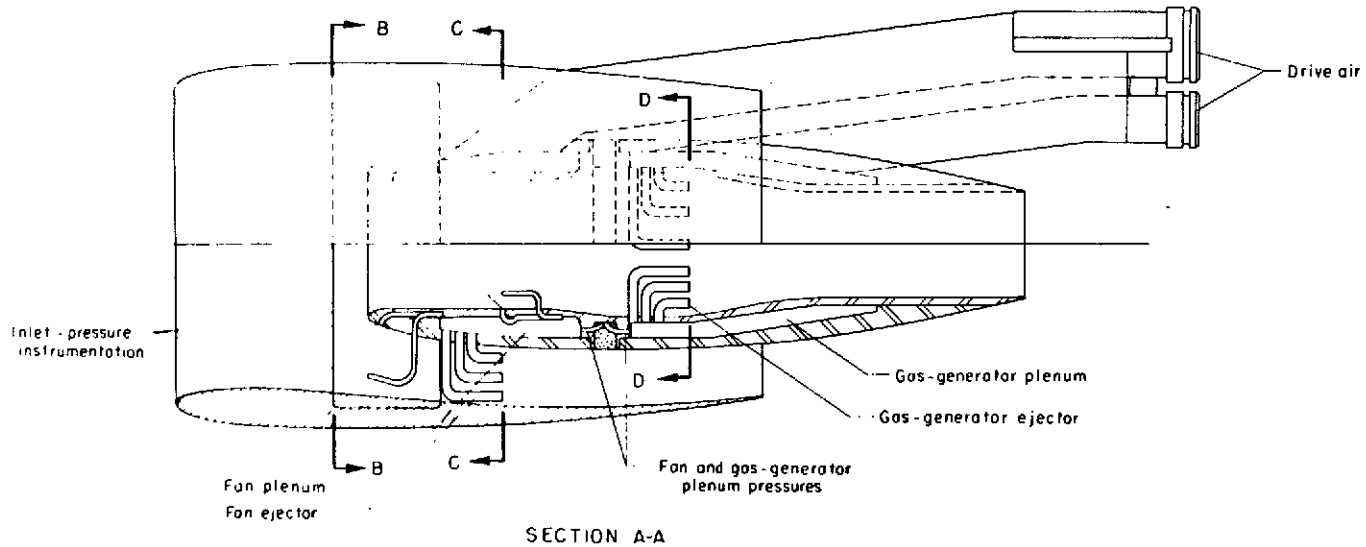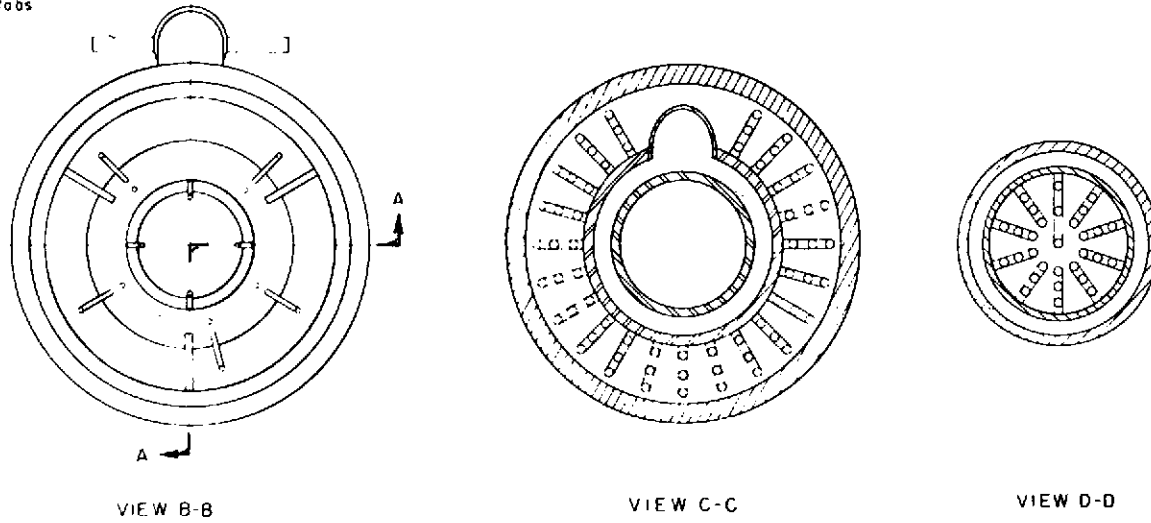
Figure 1.- Concluded.

Figure 2.- Schematic of dual air-ejector engine simulator.
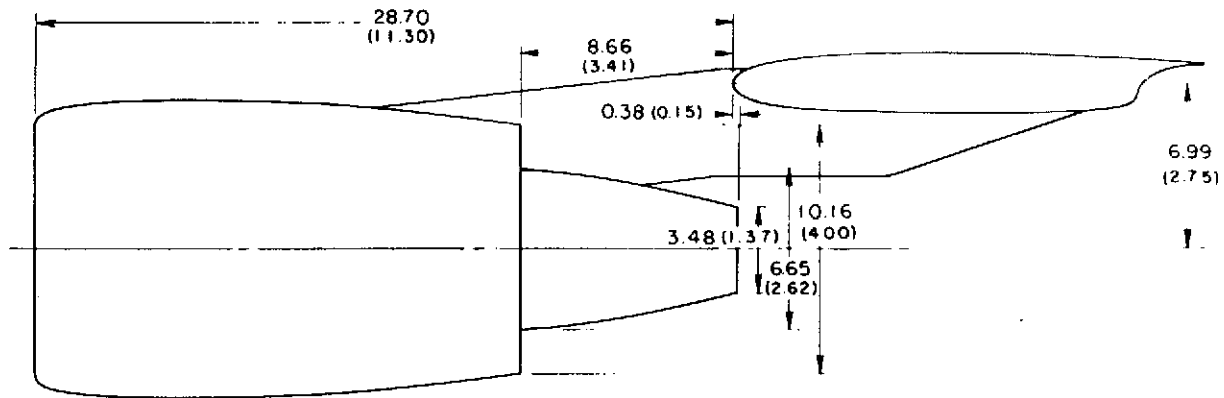
BPR 10.0 SIMULATOR

Figure 3.- Size and location details for engine simulator installation. All
dimensions are in centimeters; parenthetical values are in inches.
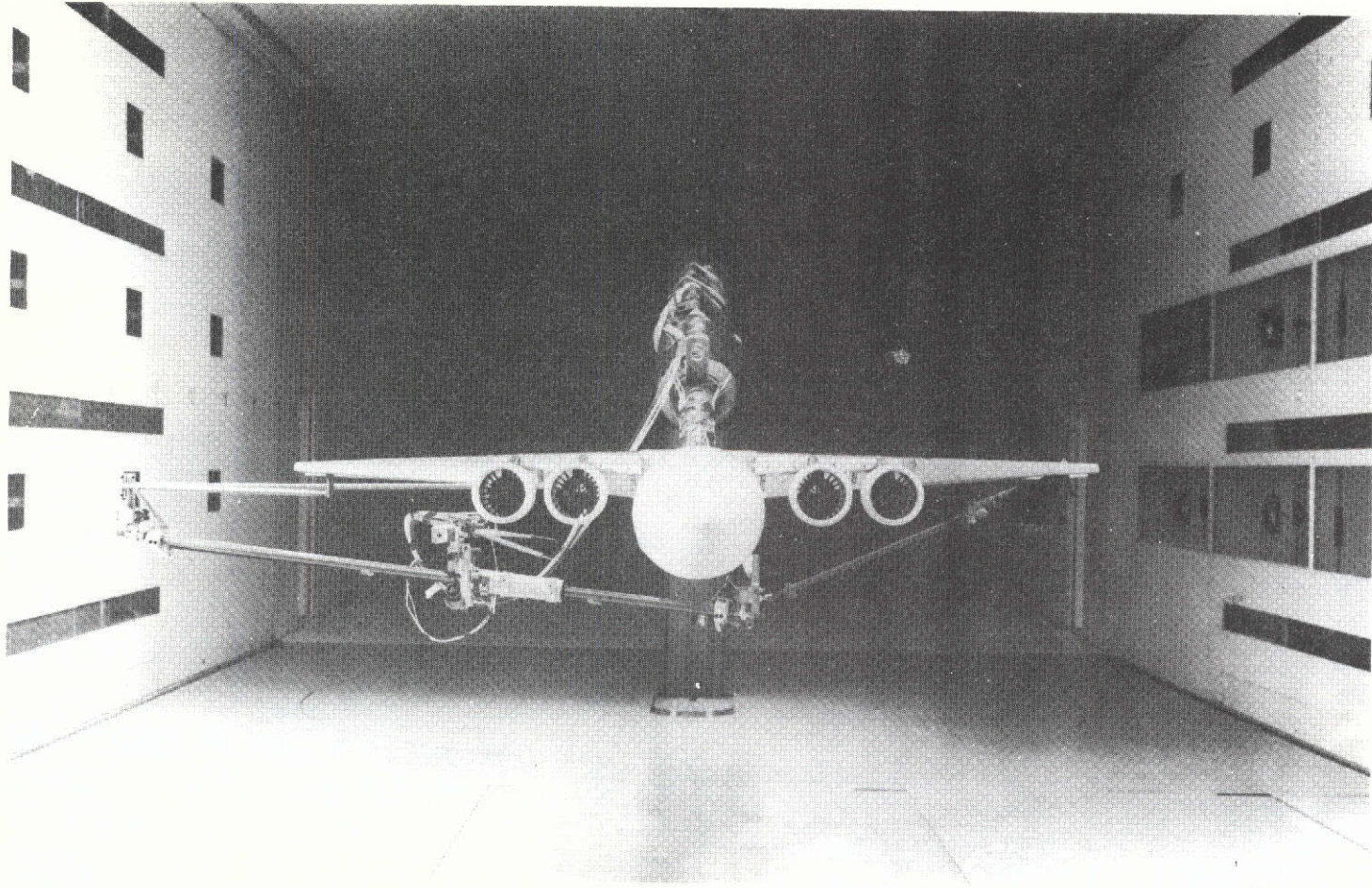
L-71-6522

(a) Front view.

Figure 4.- Photographs of models with probes mounted on traverse assembly.
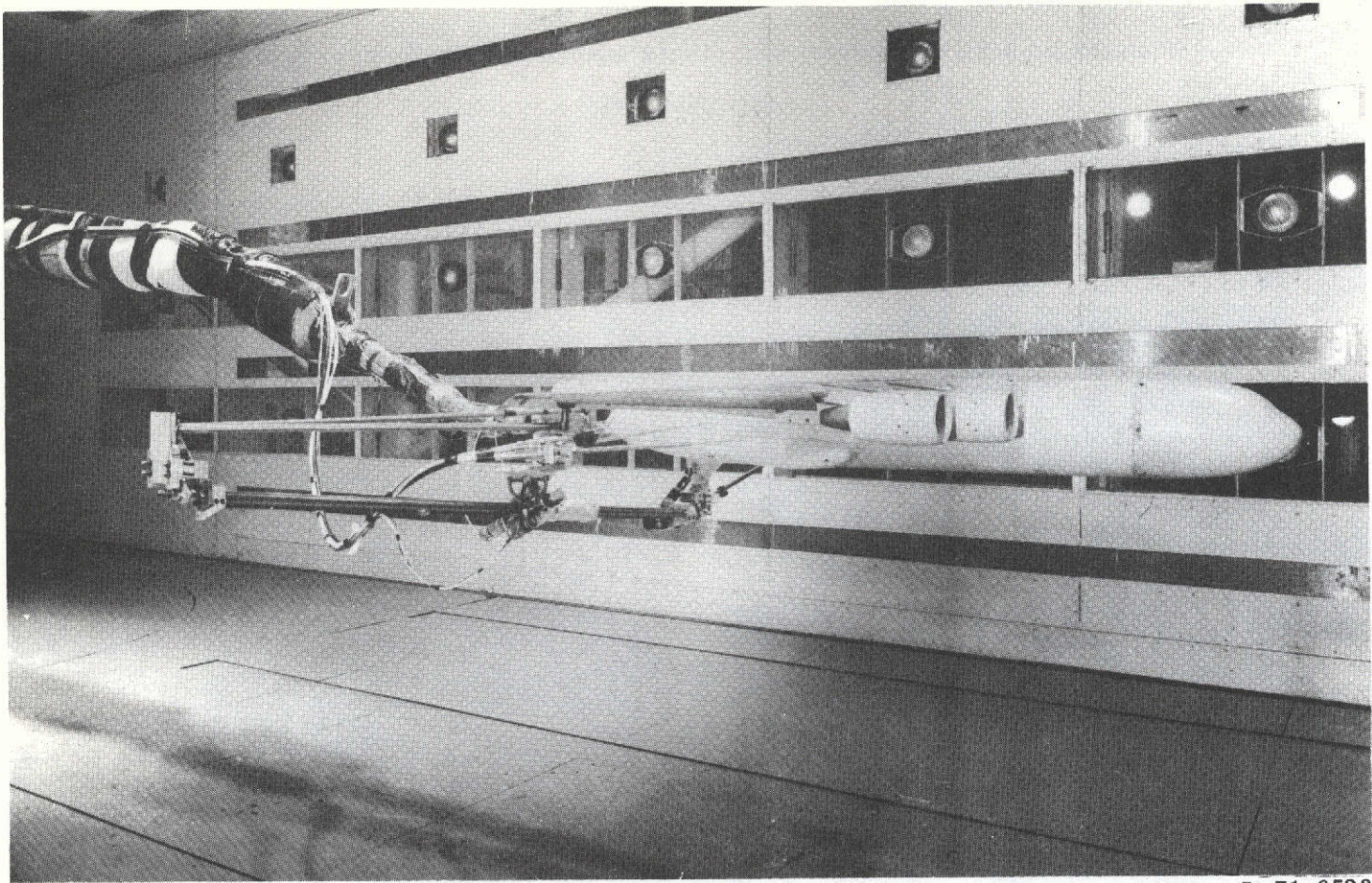
L-71-6523

(b) Side view.

Figure 4.- Continued.
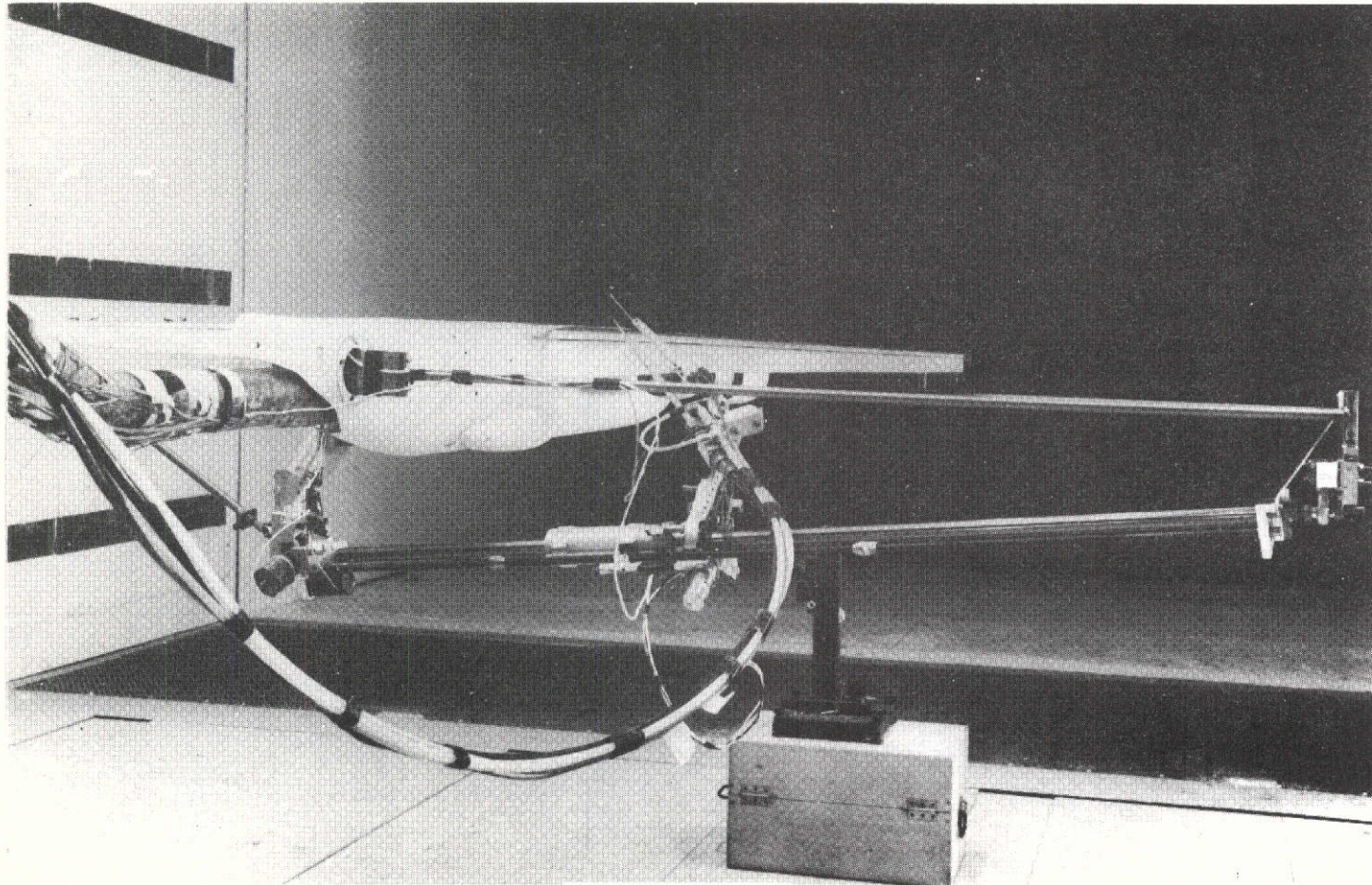
L-71-6524

(c) Rear view.

Figure 4.- Concluded.
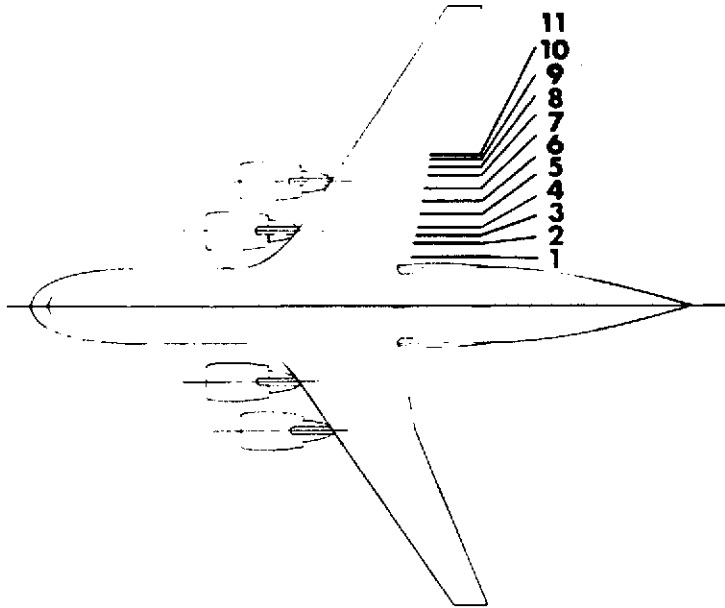
| Position | $\eta$ | $d_{min.}$, cm(in.) |
|----------|--------|---------------------|
| 1 | 0.163 | 4.125 (1.624) |
| 2 | .201 | |
| 3 | .228 | |
| 4 | .254 | |
| 5 | .295 | |
| 6 | .335 | |
| 7 | .376 | |
| 8 | .417 | 2.847 (1.121) |
| 9 | .443 | 2.035 (0.801) |
| 10 | .470 | 1.194 (0.470) |
| 11 | .483 | 0.787 (0.310) |

Figure 5.- Nominal near-wake survey locations.
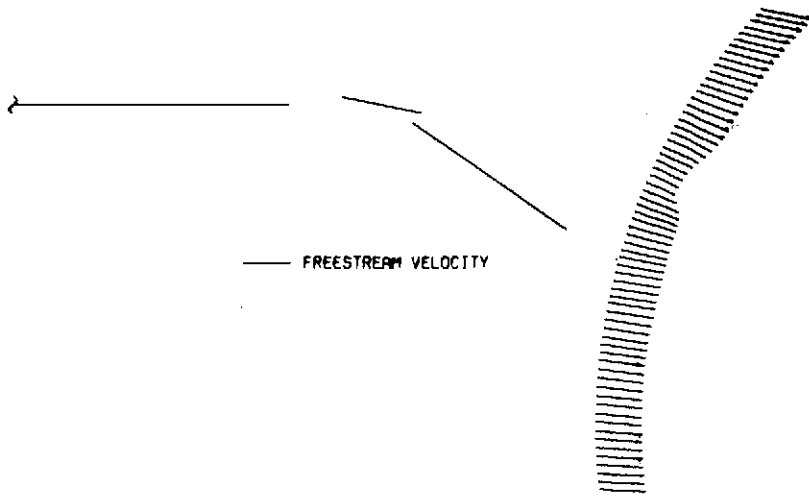
(a) Streamwise velocity profile.
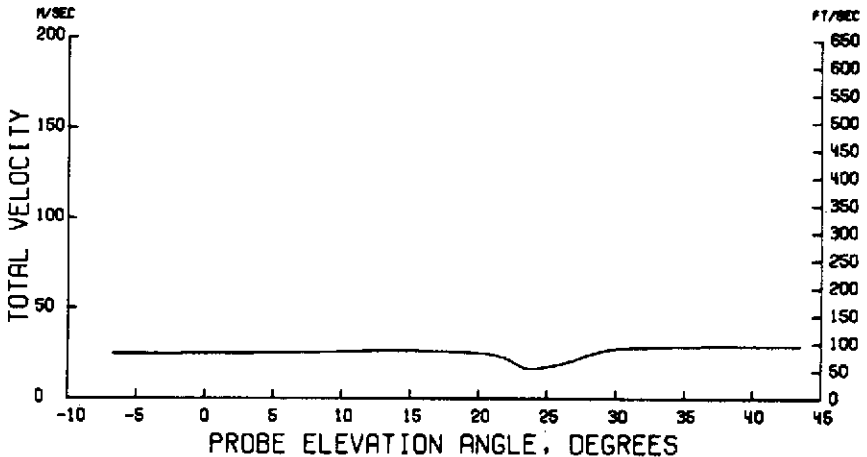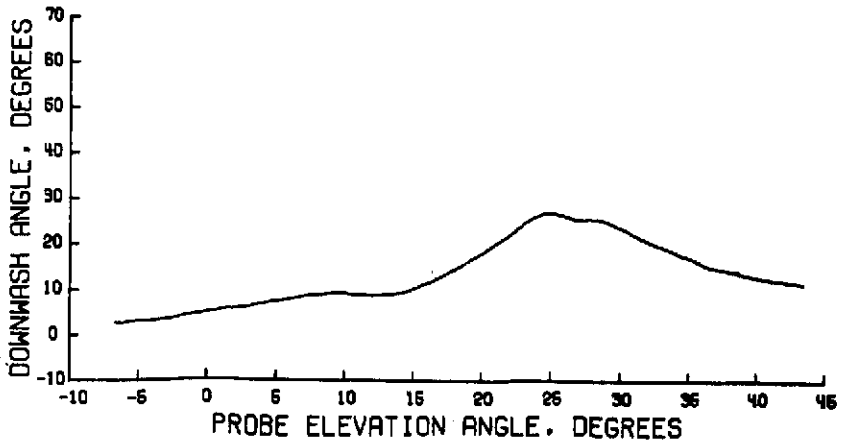


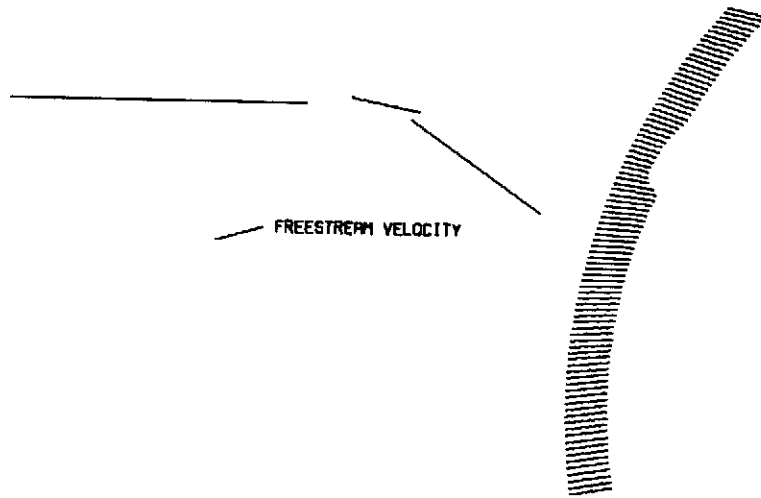(b) Total velocity.



(c) Downwash angle.

Figure 6.- Wake survey results for $\eta = 0.162$; $\alpha = 0^O$; $C_T = 0$;
$V_\infty = 25.47$ m/sec (83.57 ft/sec).
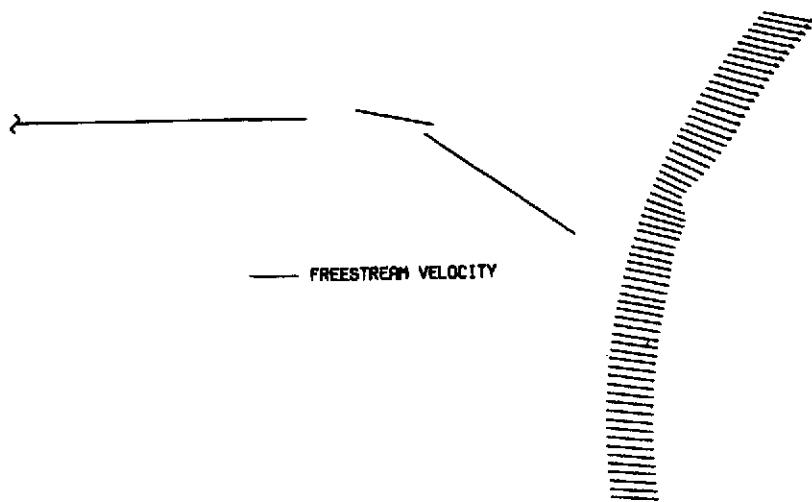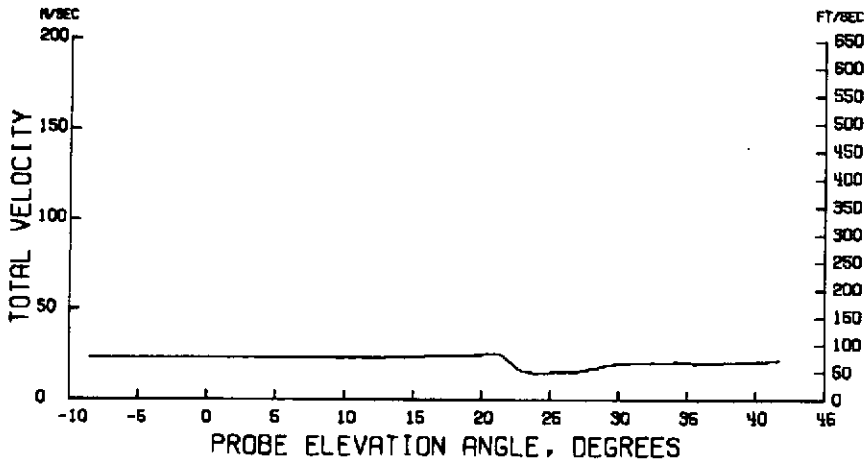
(a) Streamwise velocity profile.
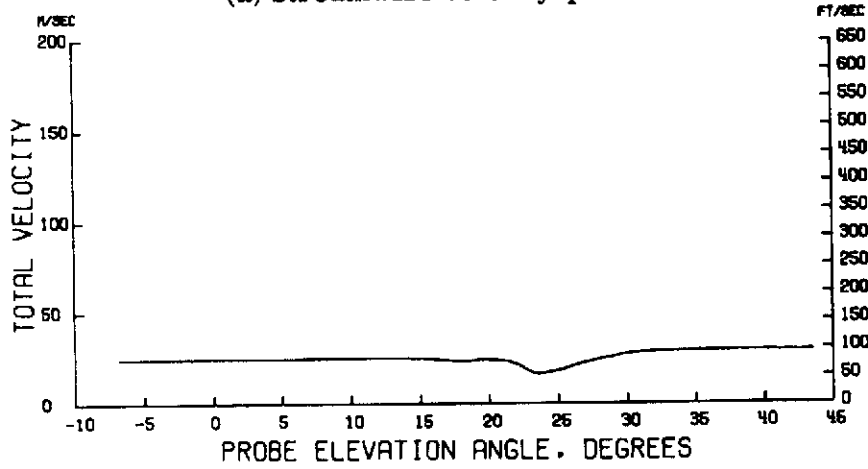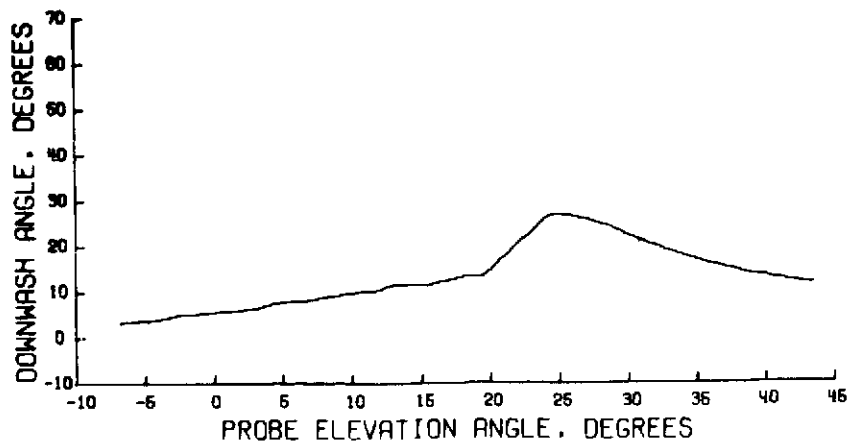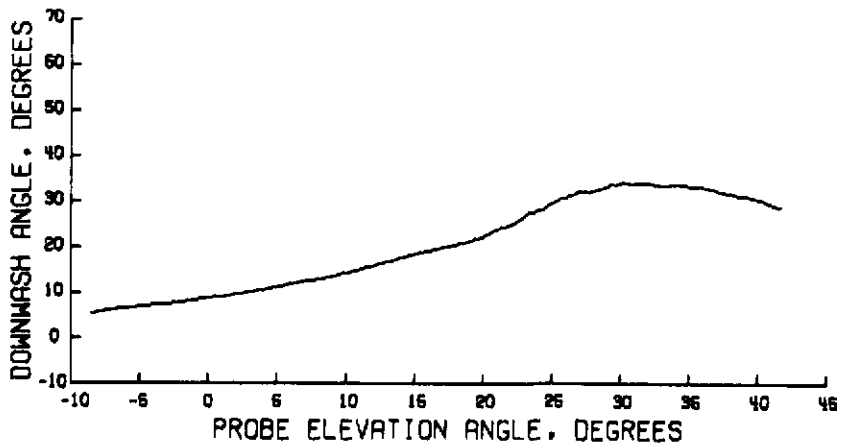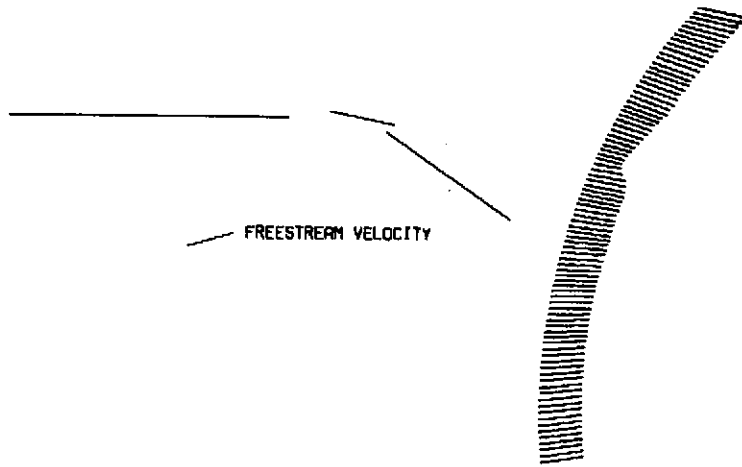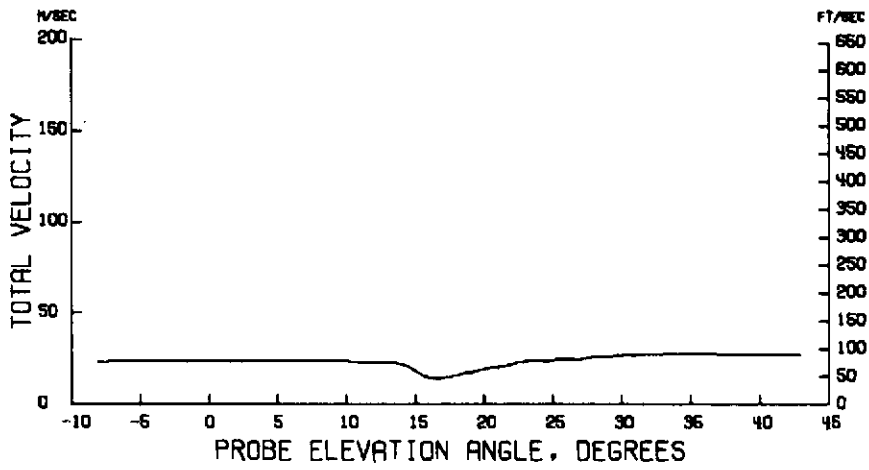


(b) Total velocity.



(c) Downwash angle.

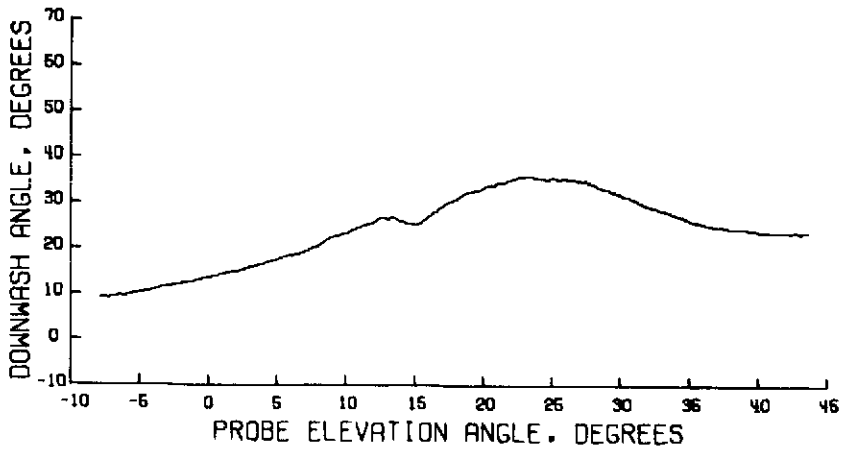Figure 7.- Wake survey results for $\eta = 0.201$; $\sigma = 0^O$; $C_T = 0$; $V_\infty = 25.48$ m/sec (83.60 ft/sec).
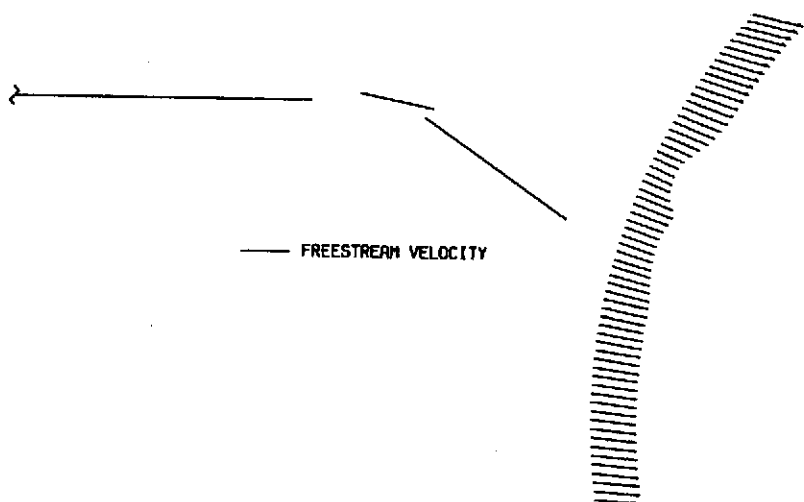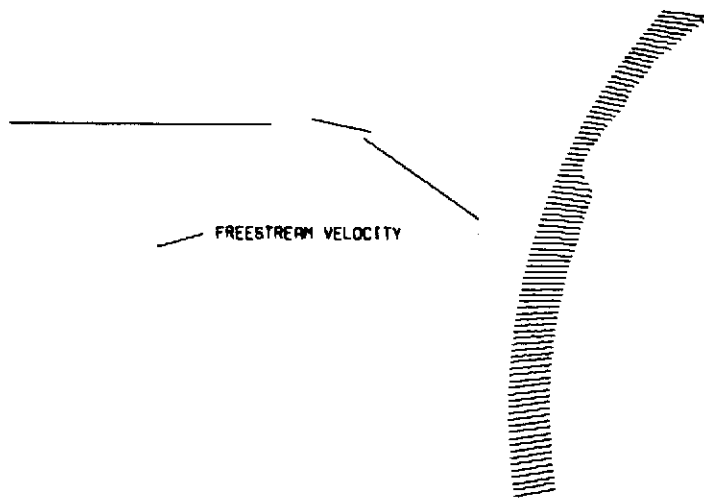
(a) Streamwise velocity profile.
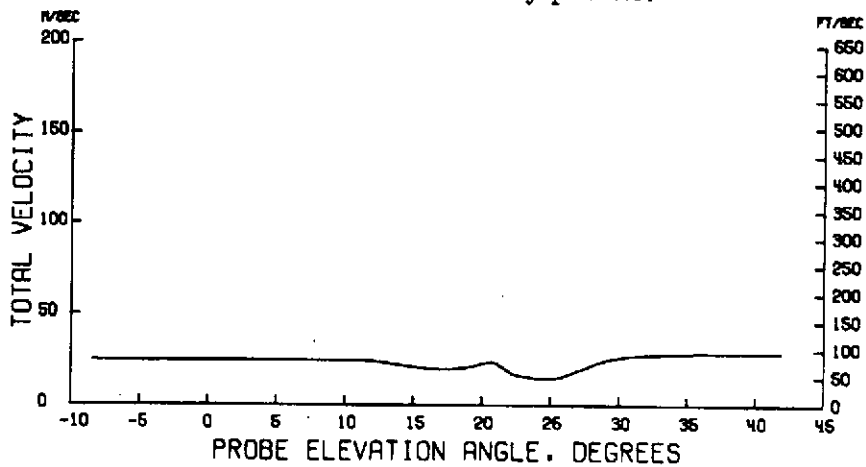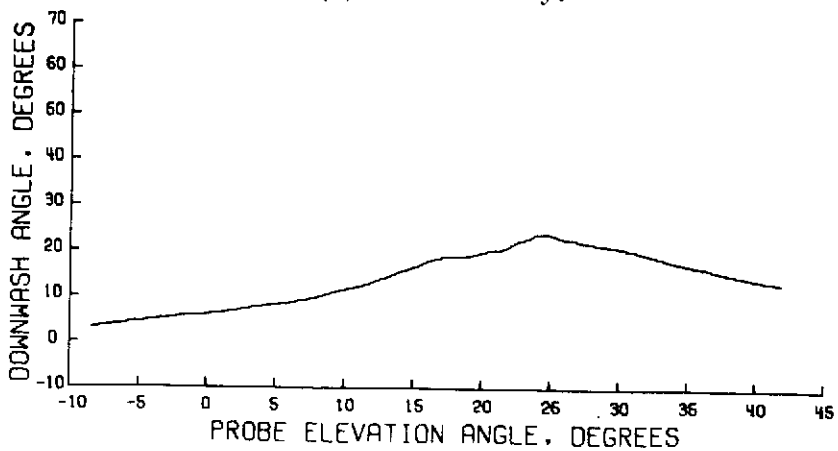


(b) Total velocity.
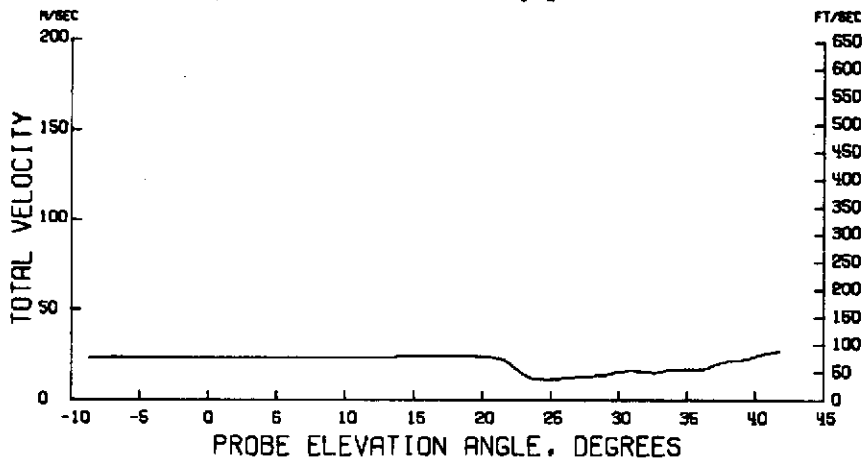


(c) Downwash angle.

Figure 8.- Wake survey results for $\eta = 0.227$; $\alpha = 0^{O}$; $C_T = 0$;
$V_{\infty} = 25.44$ m/sec (83.48 ft/sec).
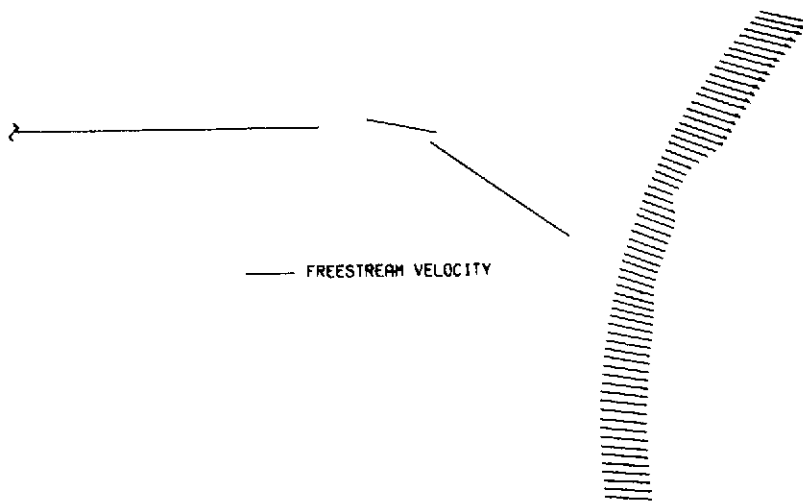
(a) Streamwise velocity profile.
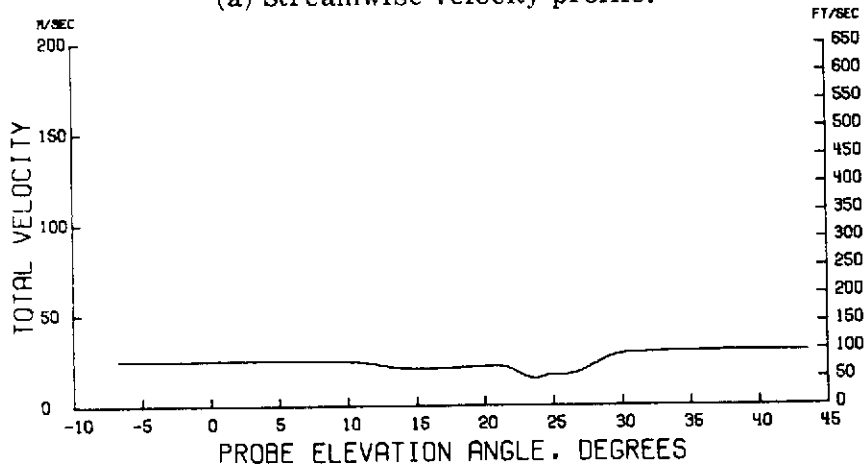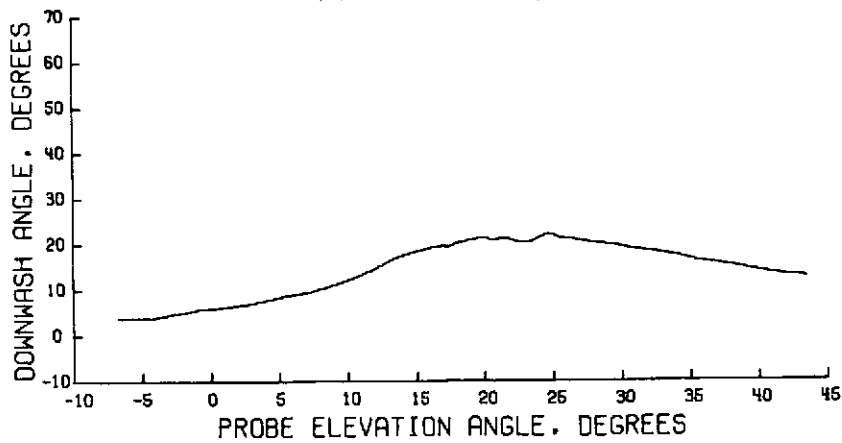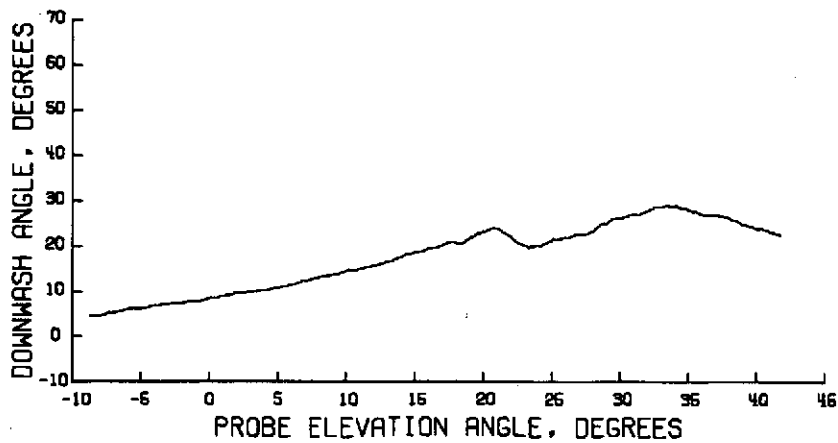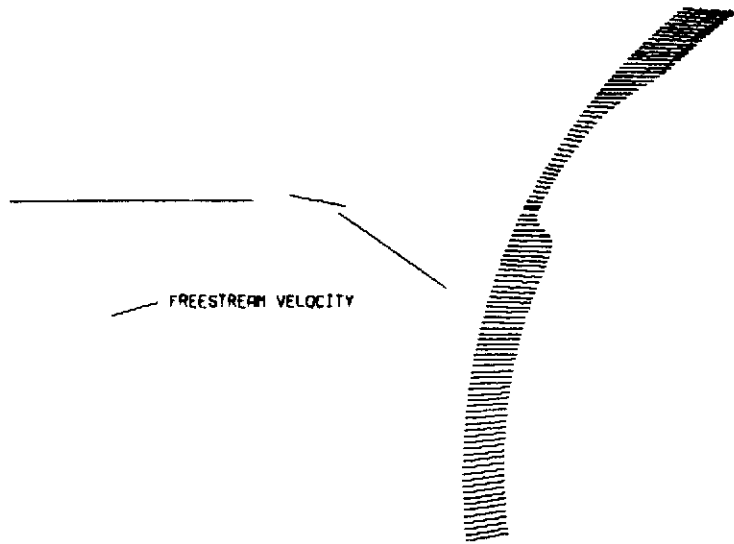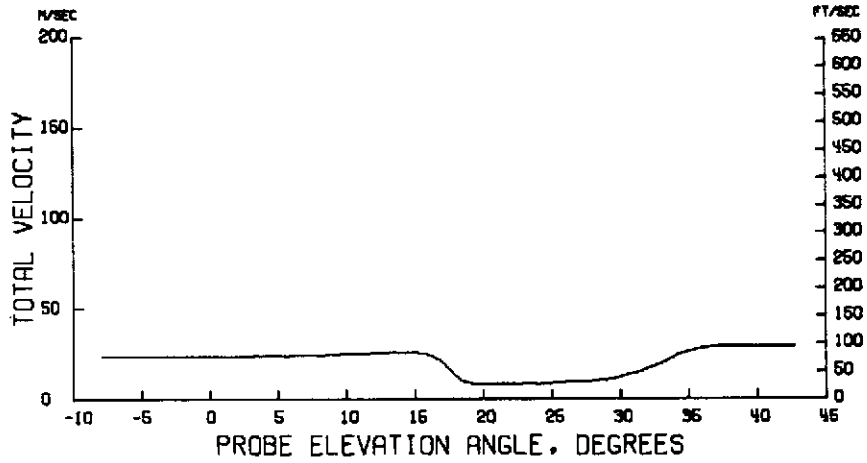


(b) Total velocity.



(c) Downwash angle.

Figure 9.- Wake survey results for  $\eta = 0.253$ ;   $\alpha = 0^O$ ;   $C_T = 0$ ;
$V_\infty = 25.53$  m/sec   (83.77 ft/sec).
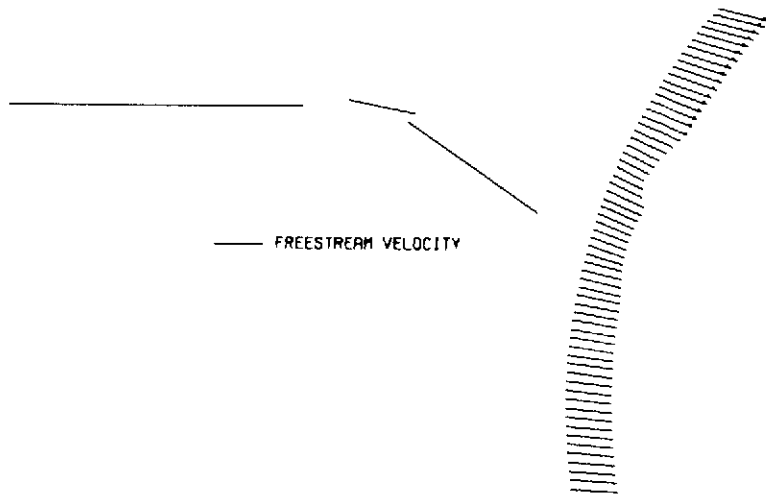
(a) Streamwise velocity profile.
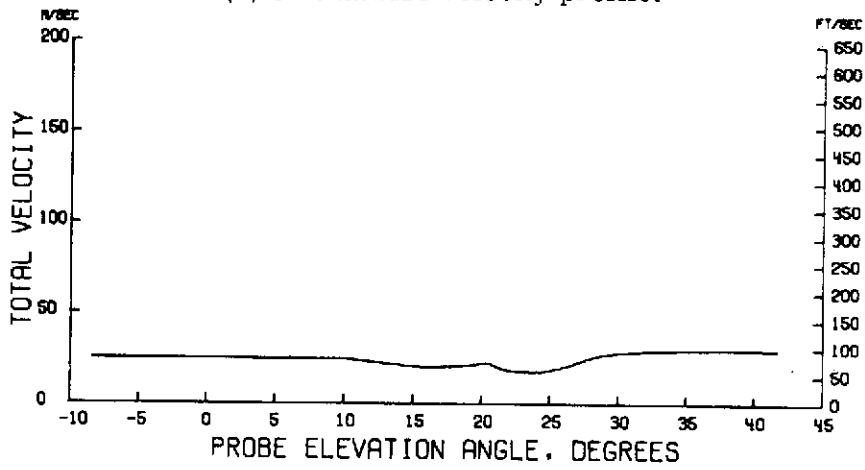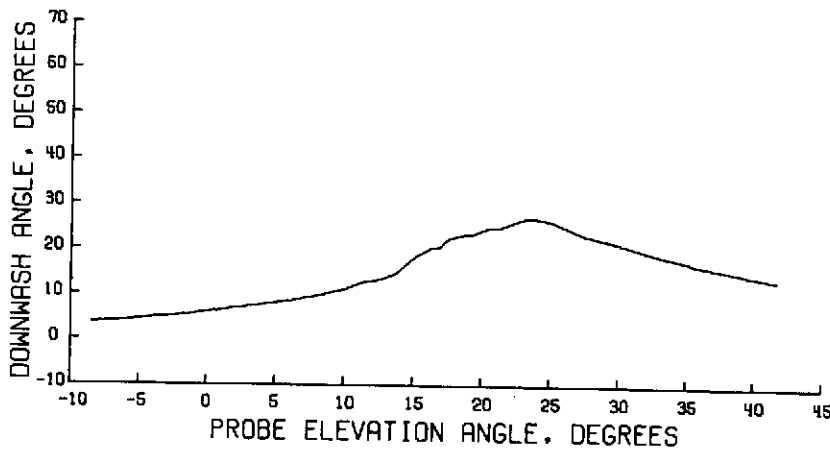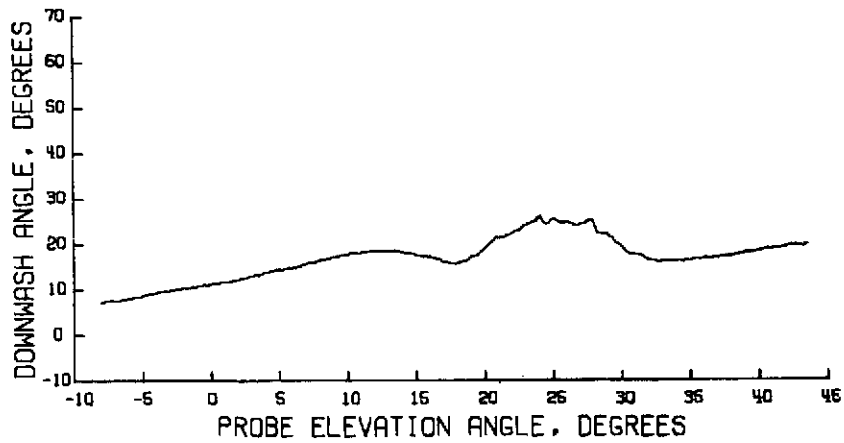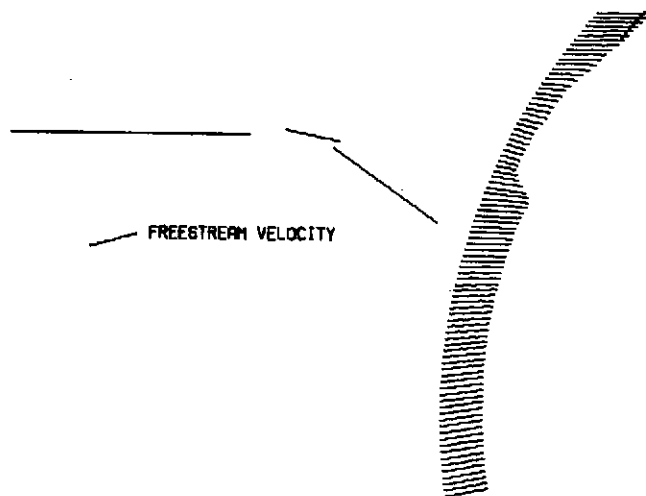


(b) Total velocity.



(c) Downwash angle.

Figure 10.- Wake survey results for $\eta = 0.294$; $\alpha = 0^{\circ}$; $C_T = 0$; $V_{\infty} = 25.53$ m/sec (83.79 ft/sec).
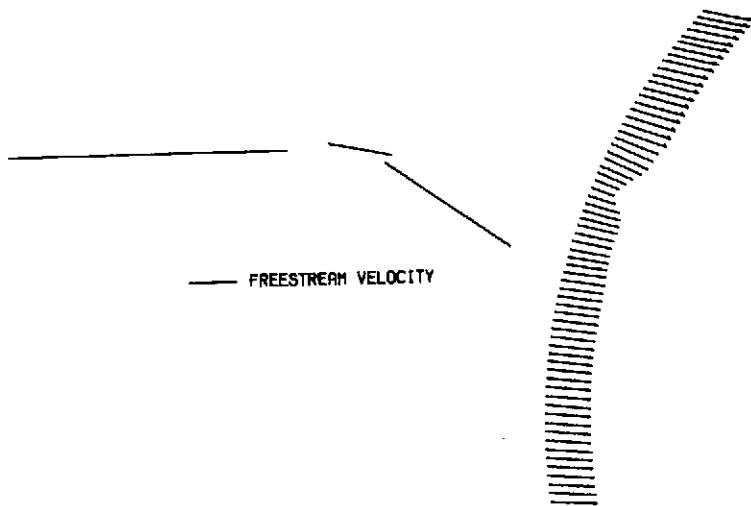
(a) Streamwise velocity profile.
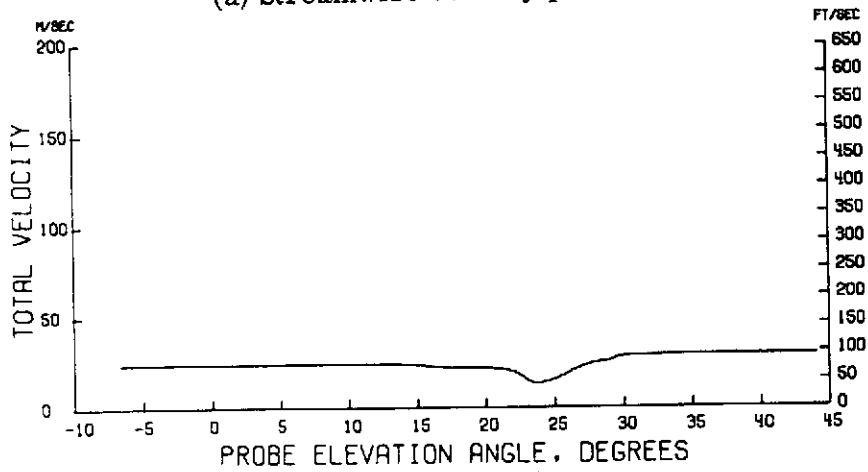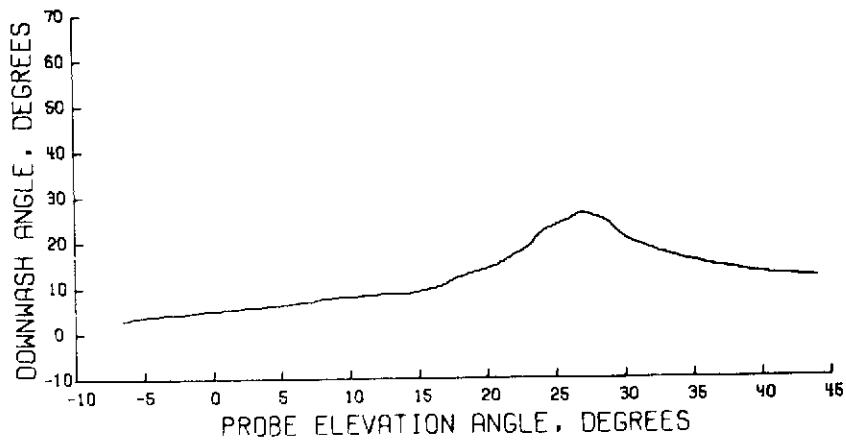


(b) Total velocity.



(c) Downwash angle.

Figure 11.- Wake survey results for $\eta = 0.336$; $\alpha = 0^O$; $C_T = 0$; $V_\infty = 25.39$ m/sec (83.31 ft/sec).
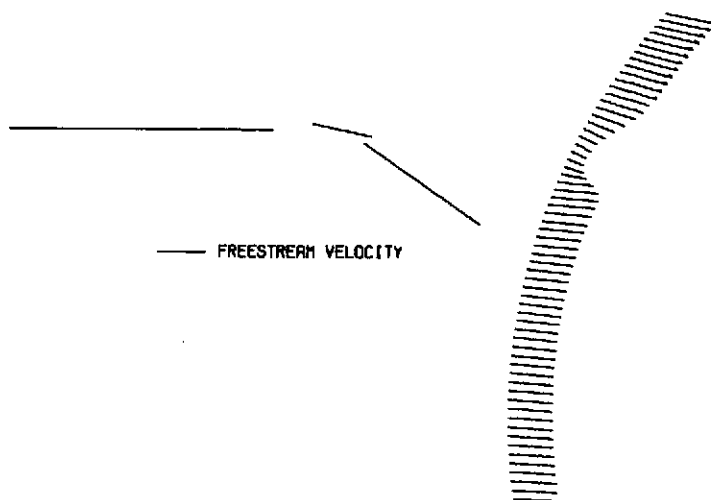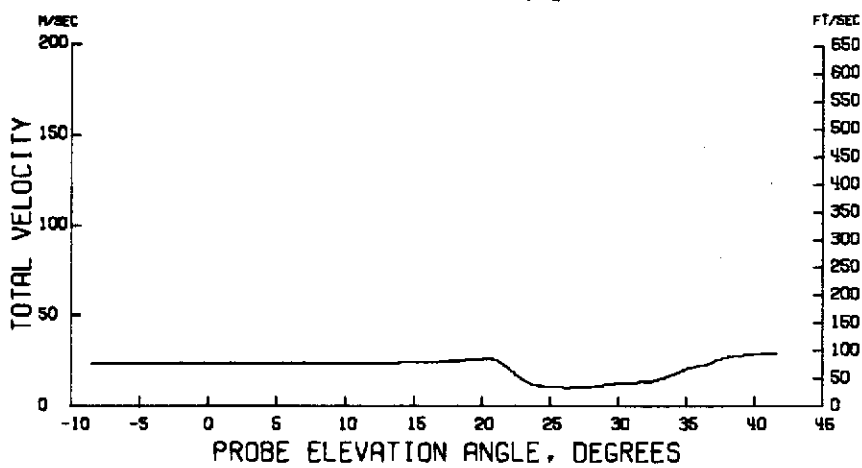
(a) Streamwise velocity profile.
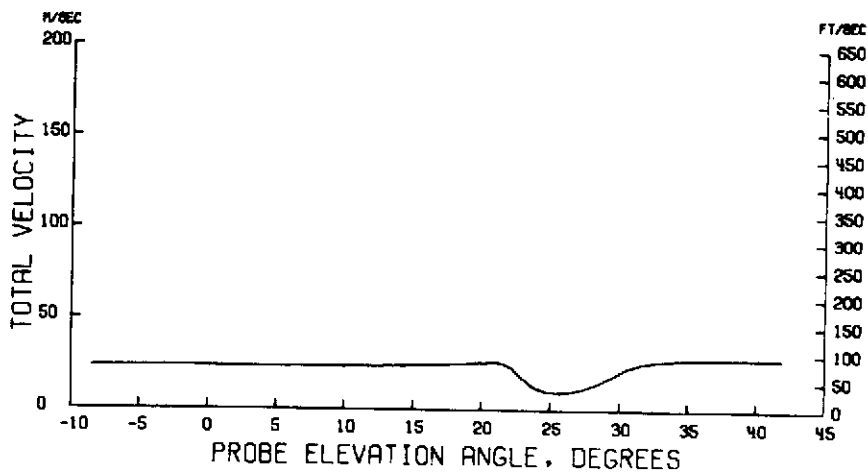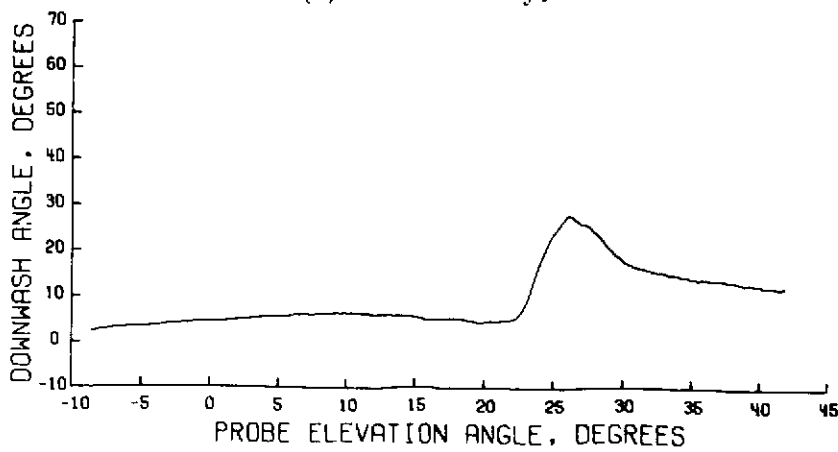


(b) Total velocity.



(c) Downwash angle.

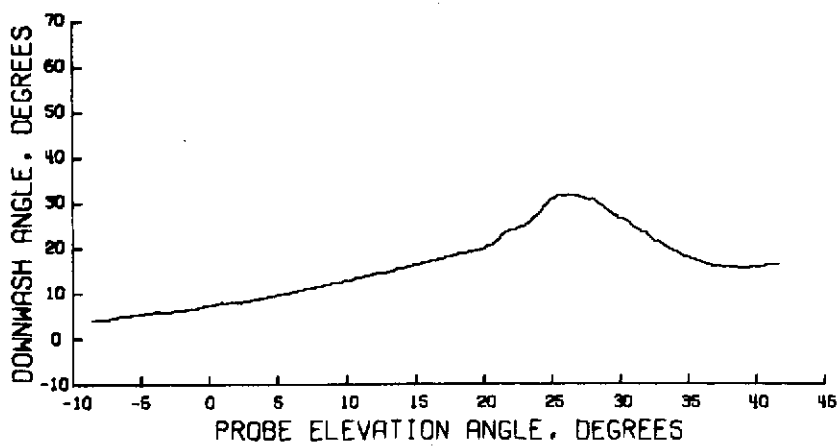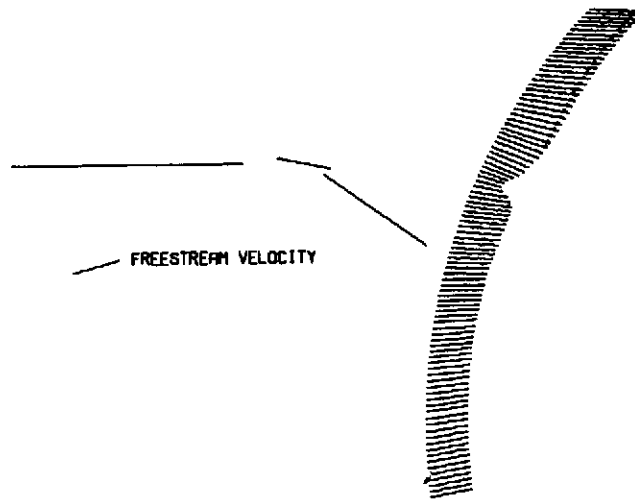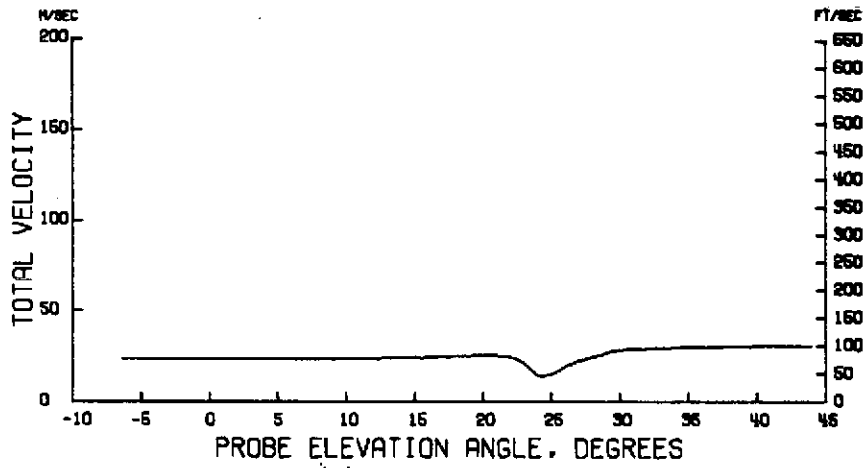Figure 12.- Wake survey results for $\eta = 0.376$; $\alpha = 0^O$; $C_T = 0$;
$V_\infty = 25.41$ m/sec  (83.39 ft/sec).
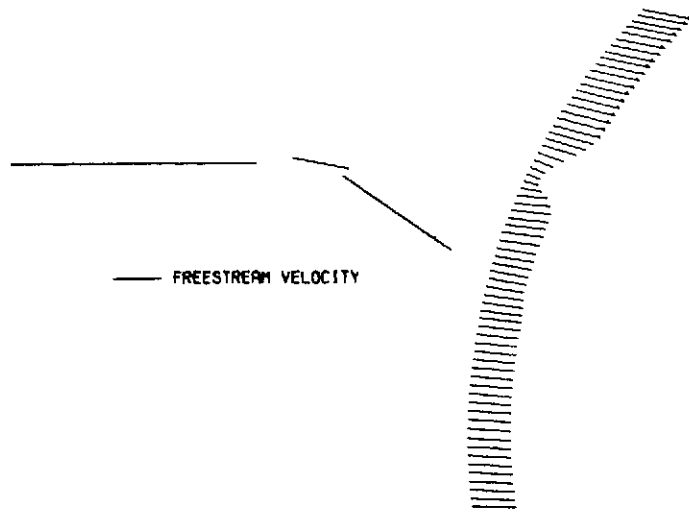
(a) Streamwise velocity profile.
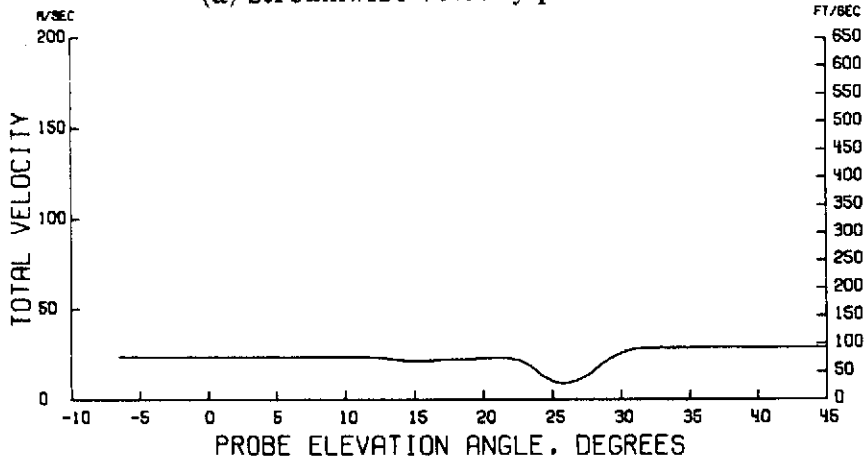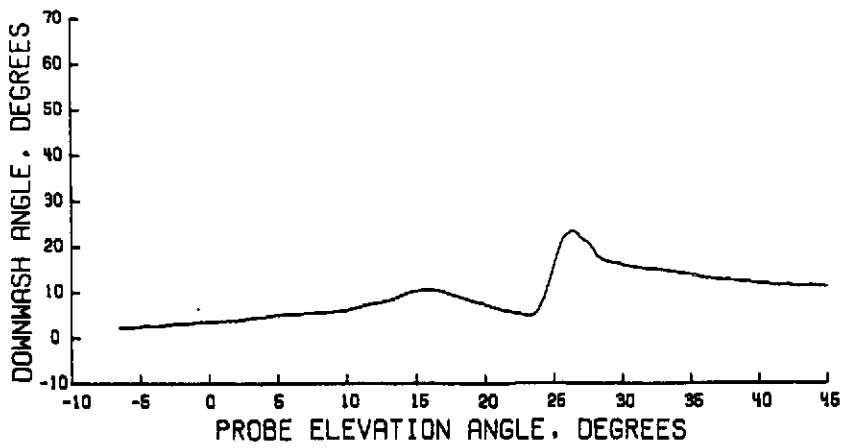


(b) Total velocity.



(c) Downwash angle.

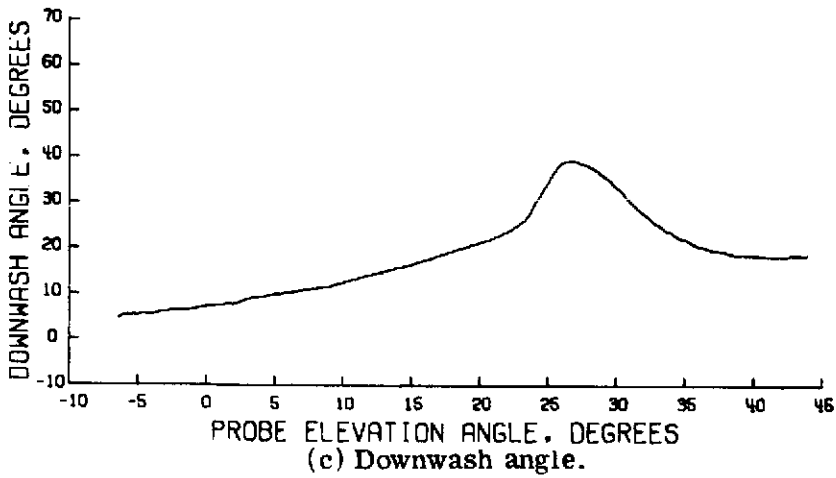Figure 13.- Wake survey results for $\eta = 0.417$; $\alpha = 0^{O}$; $C_T = 0$; $V_\infty = 25.33$ m/sec (83.12 ft/sec).
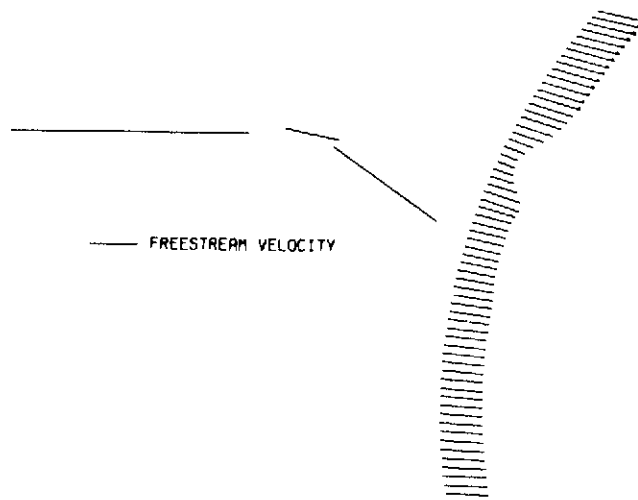
(a) Streamwise velocity profile.
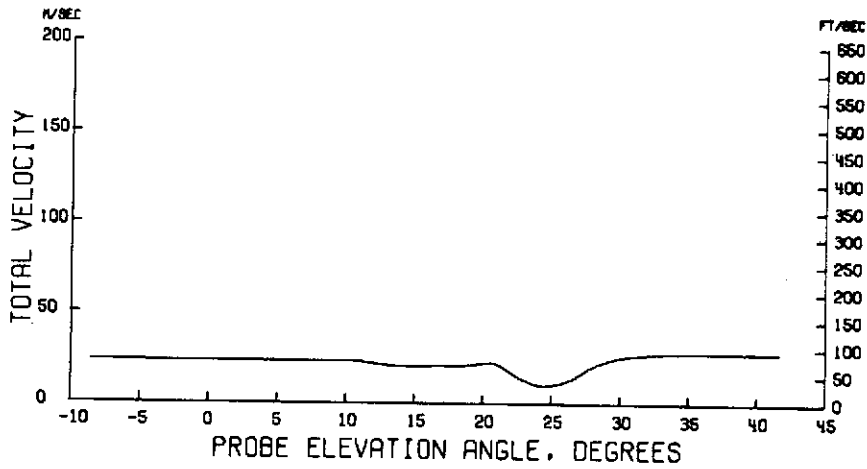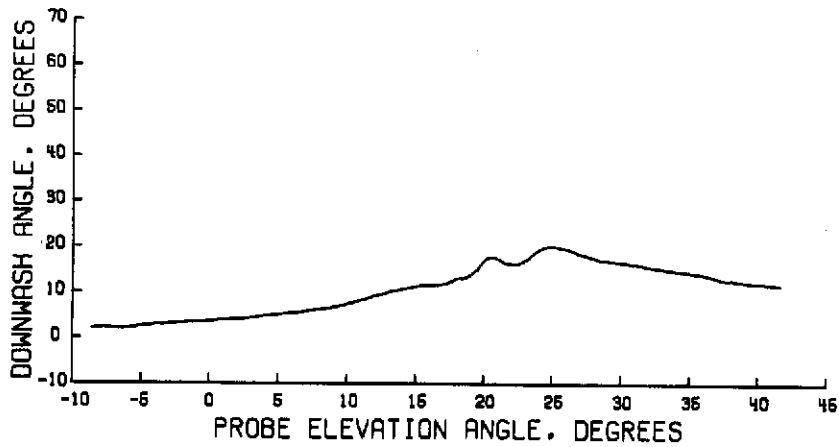


(b) Total velocity.



(c) Downwash angle.

Figure 14.- Wake survey results for $\eta = 0.442$; $\alpha = 0^O$; $C_T = 0$; $V_\infty = 25.41$ m/sec (83.36 ft/sec).
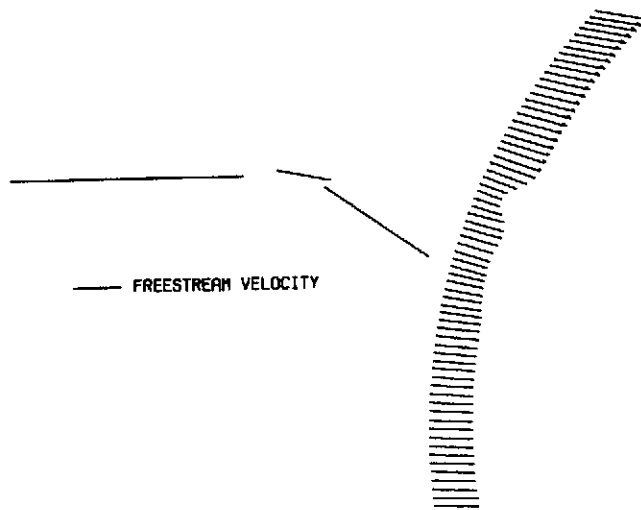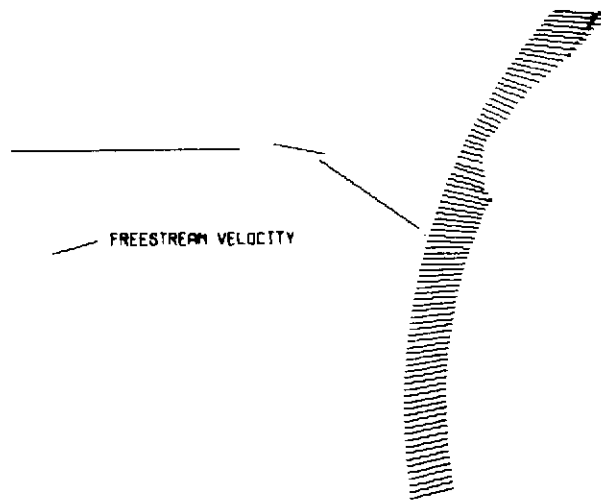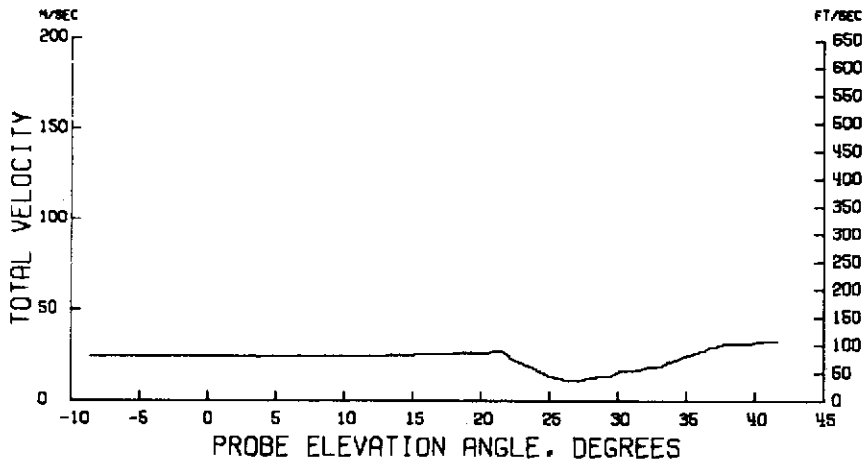
(a) Streamwise velocity profile.
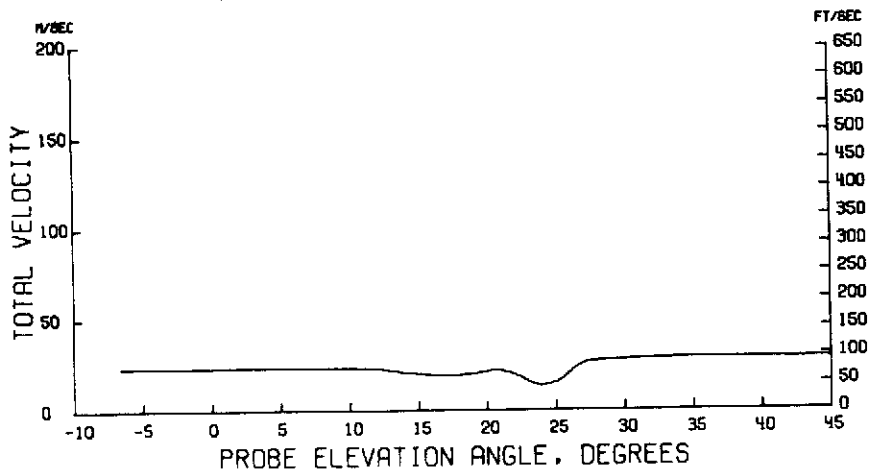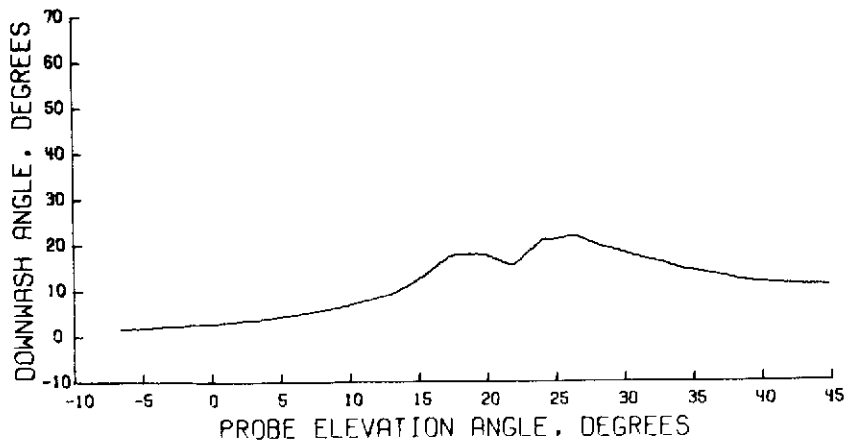


(b) Total velocity.



(c) Downwash angle.

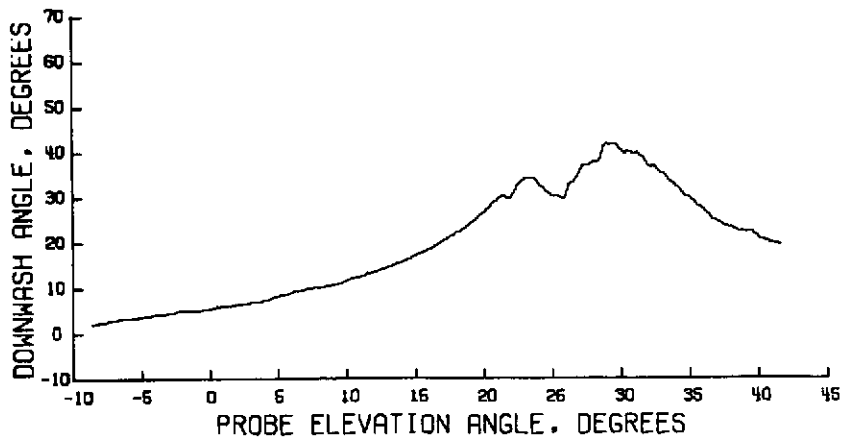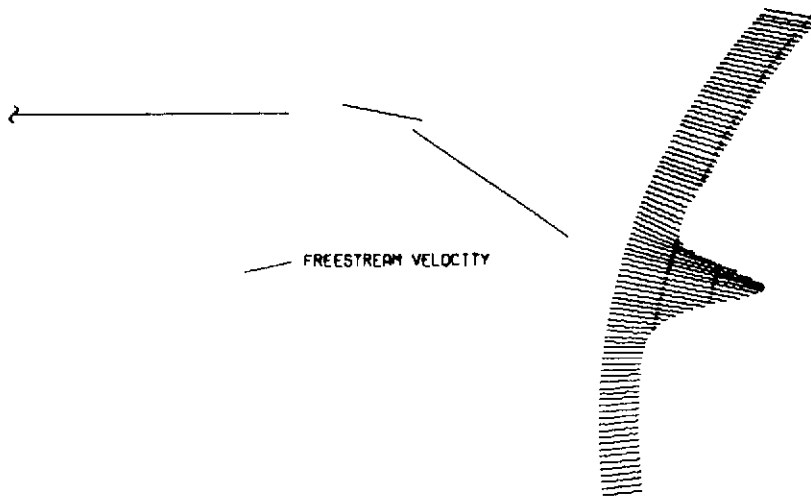Figure 15.- Wake survey results for $\eta = 0.469$; $\alpha = 0^O$; $C_T = 0$;
$V_\infty = 25.37$ m/sec (83.24 ft/sec).
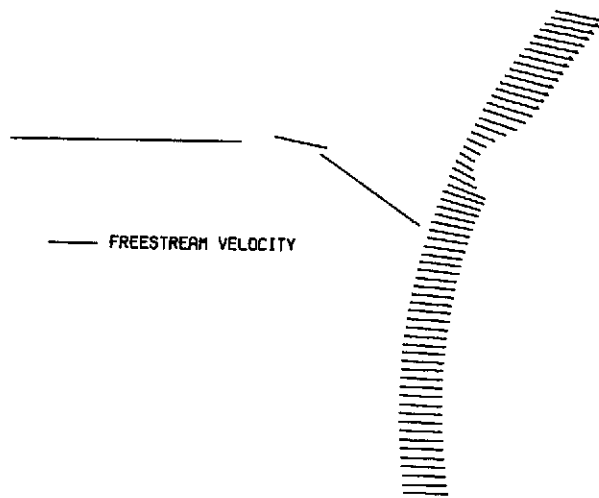
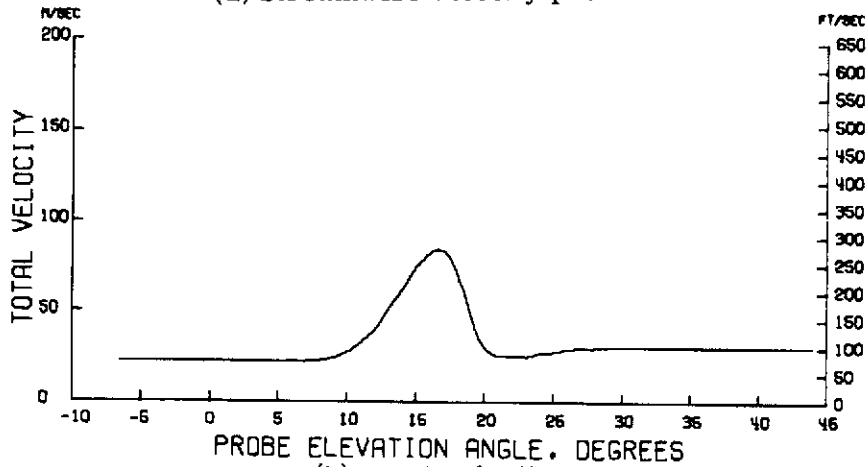(a) Streamwise velocity profile.
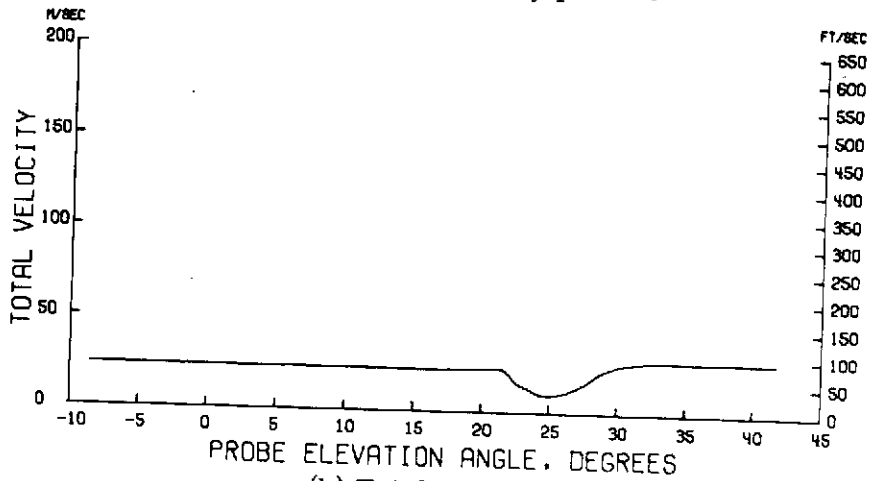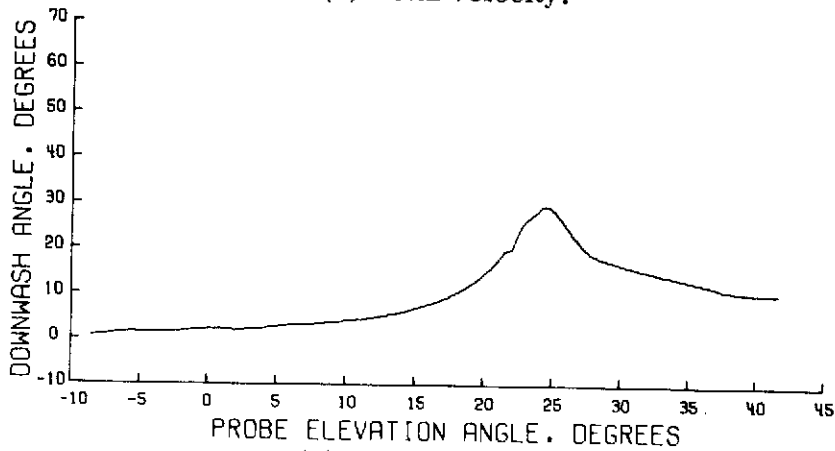


(b) Total velocity.



(c) Downwash angle.

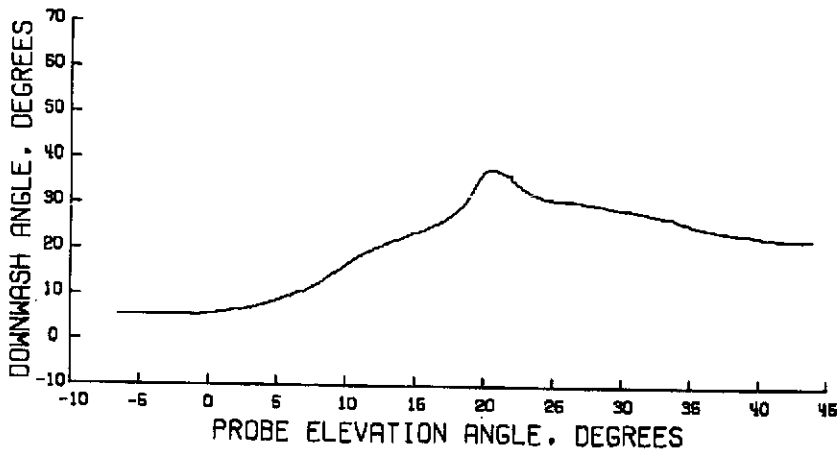Figure 16.- Wake survey results for $\eta = 0.563$; $\alpha = 0^O$; $C_T = 0$; $V_\infty = 25.36$ m/sec (83.21 ft/sec).
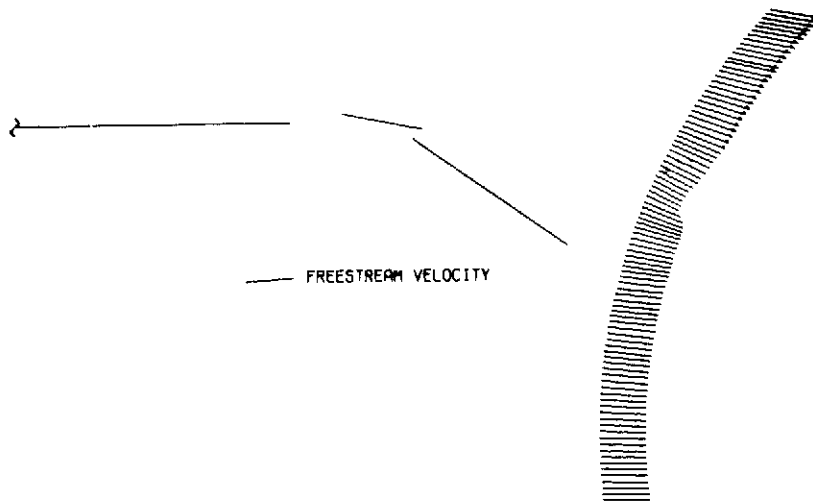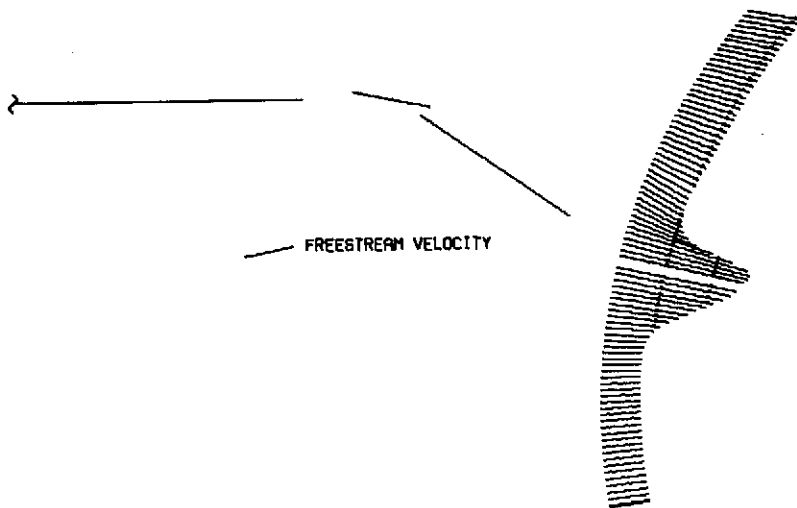
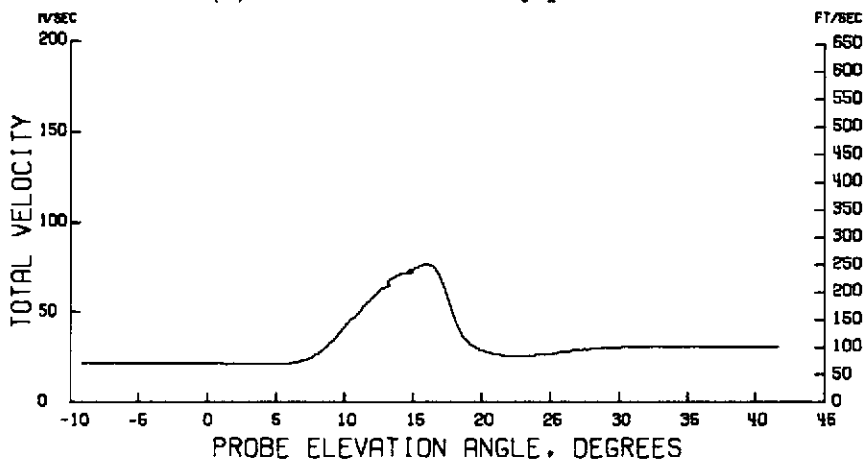(a) Streamwise velocity profile.
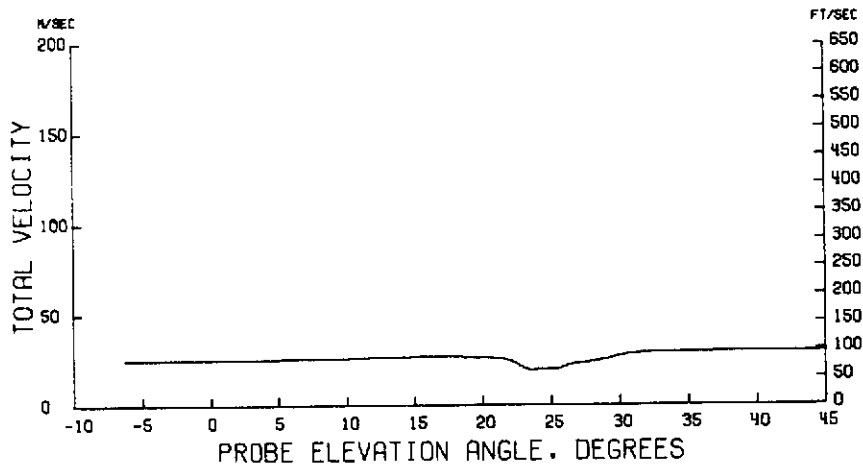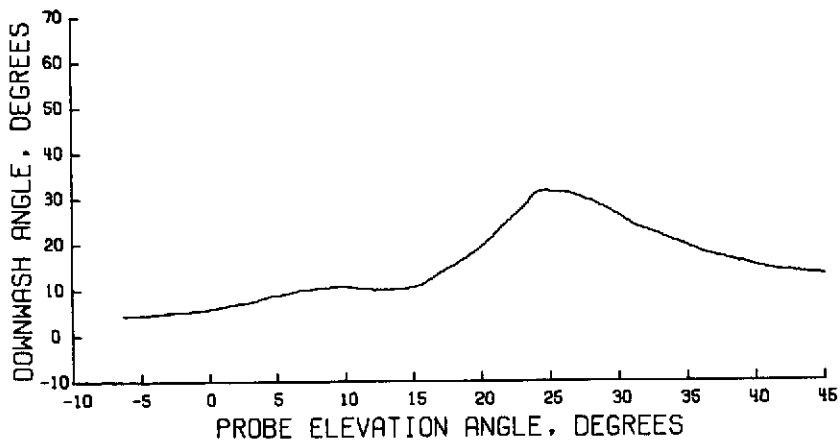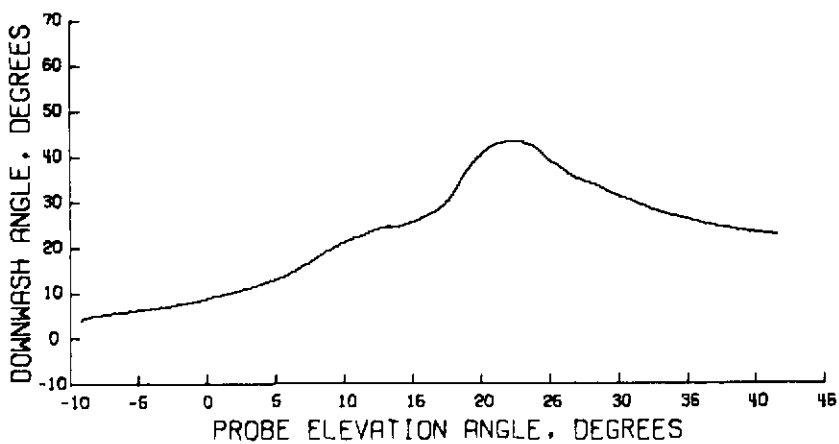


(b) Total velocity.



(c) Downwash angle.

Figure 17.- Wake survey results for $\eta = 0.162$; $\alpha = 4^O$; $C_T = 0$;
$V_\infty = 25.43$ m/sec (83.44 ft/sec).

— FREESTREAM VELOCITY
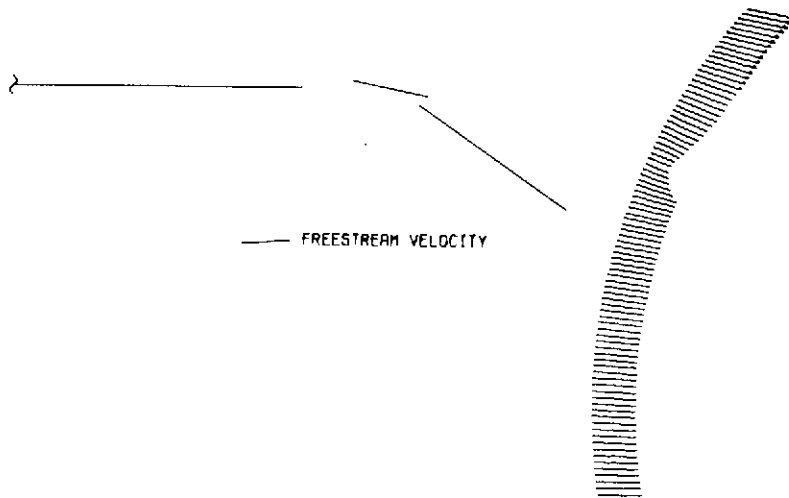
(a) Streamwise velocity profile.
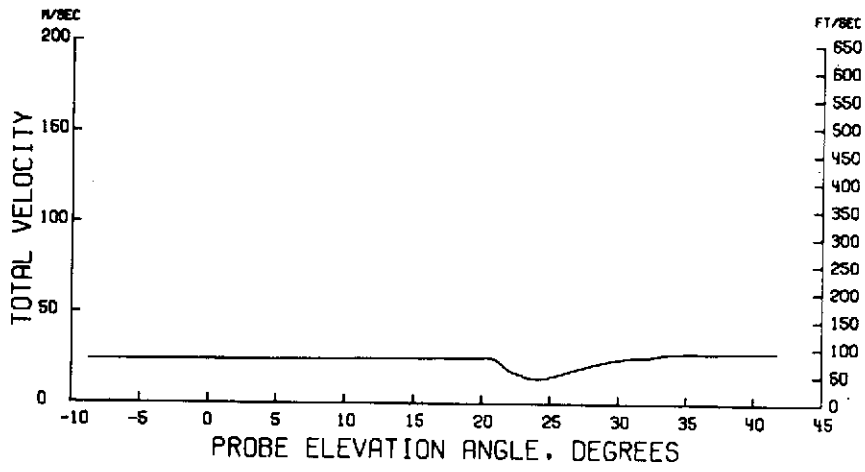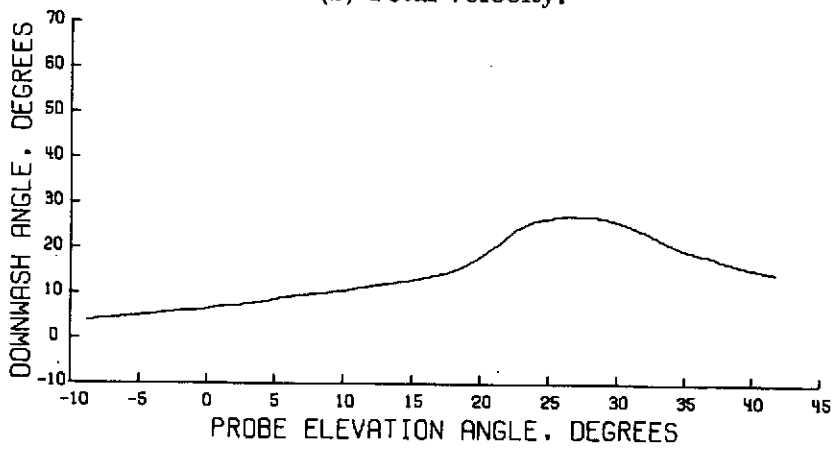


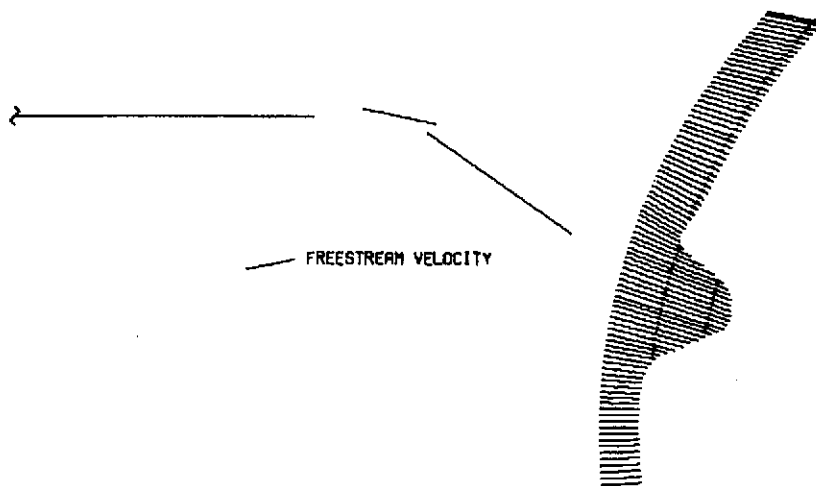(b) Total velocity.



(c) Downwash angle.

Figure 18.- Wake survey results for $\eta = 0.200$; $\alpha = 4^{\circ}$; $C_T = 0$; $V_{\infty} = 25.41$ m/sec (83.37 ft/sec).

FREESTREAM VELOCITY
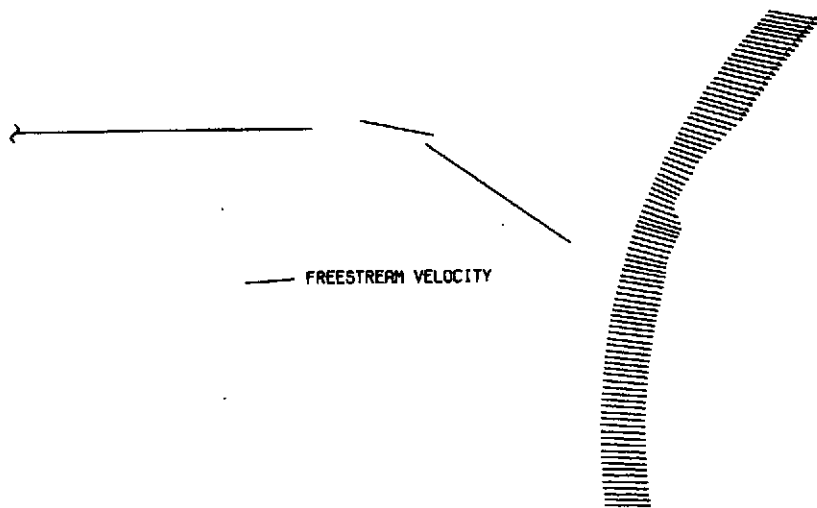
(a) Streamwise velocity profile.
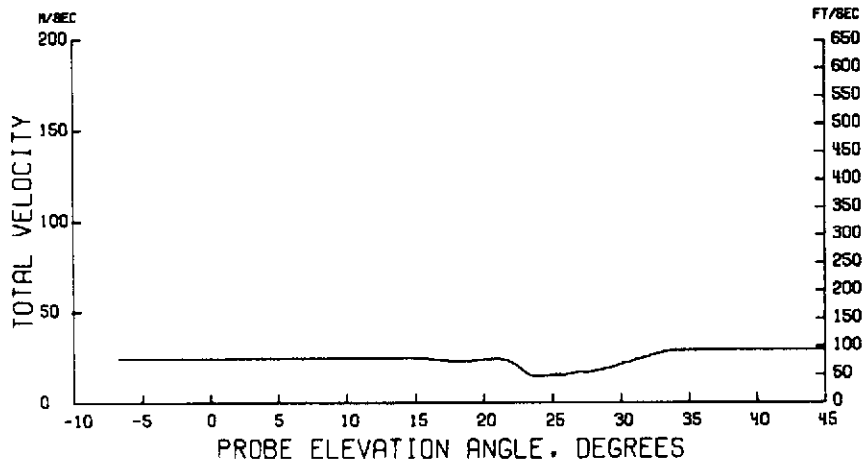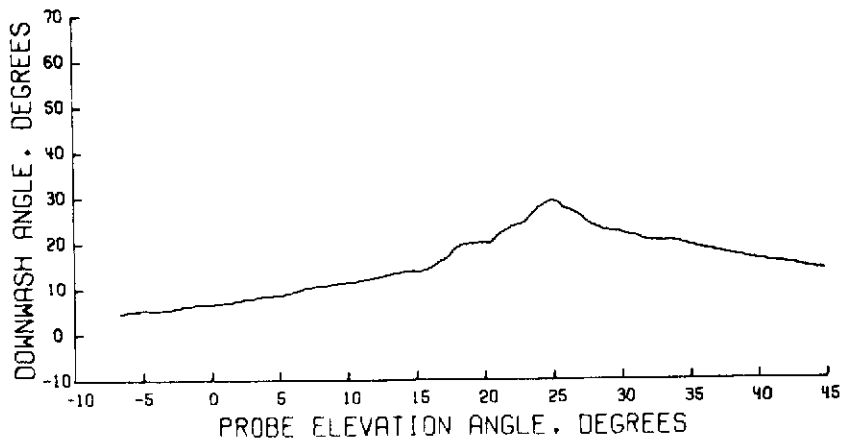


(b) Total velocity.



(c) Downwash angle.

Figure 19.- Wake survey results for $\eta = 0.227$; $\alpha = 4^O$; $C_T = 0$;
$V_\infty = 25.47$ m/sec (83.56 ft/sec).
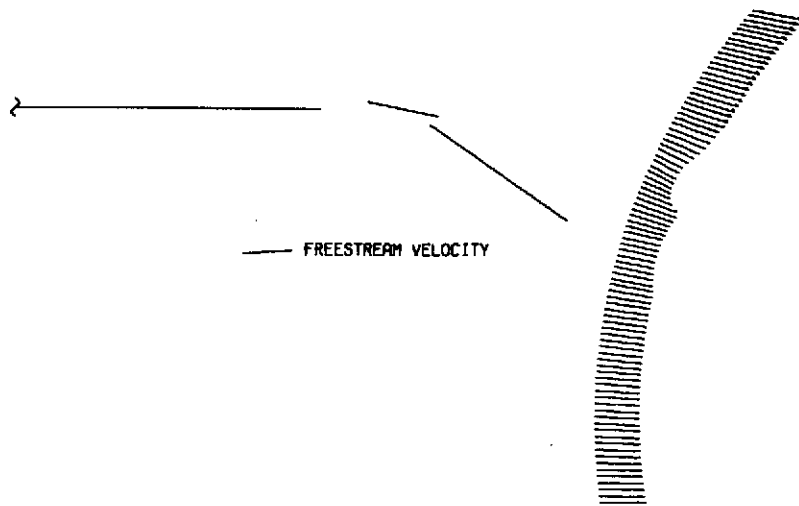
(a) Streamwise velocity profile.
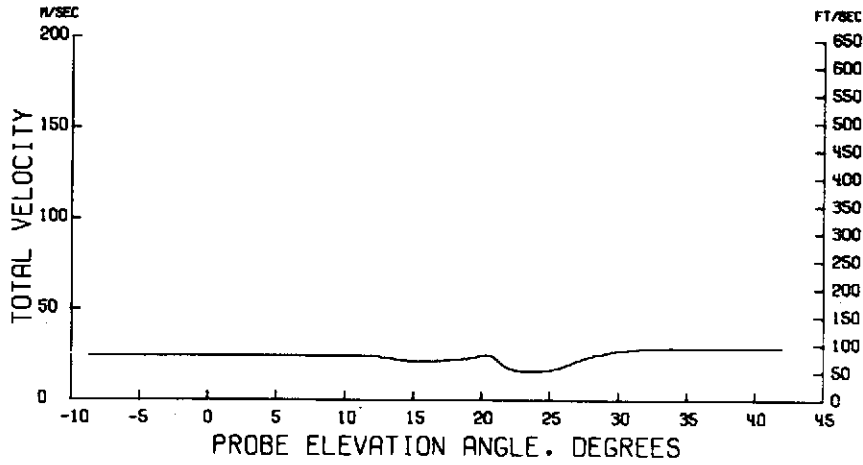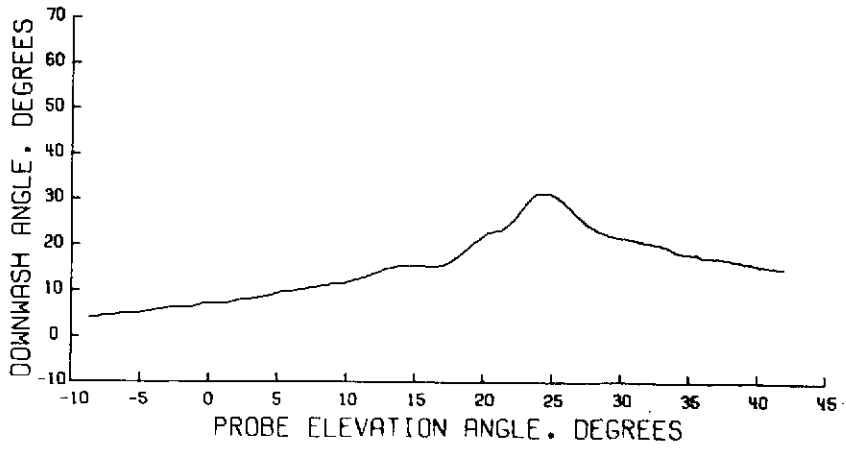


(b) Total velocity.



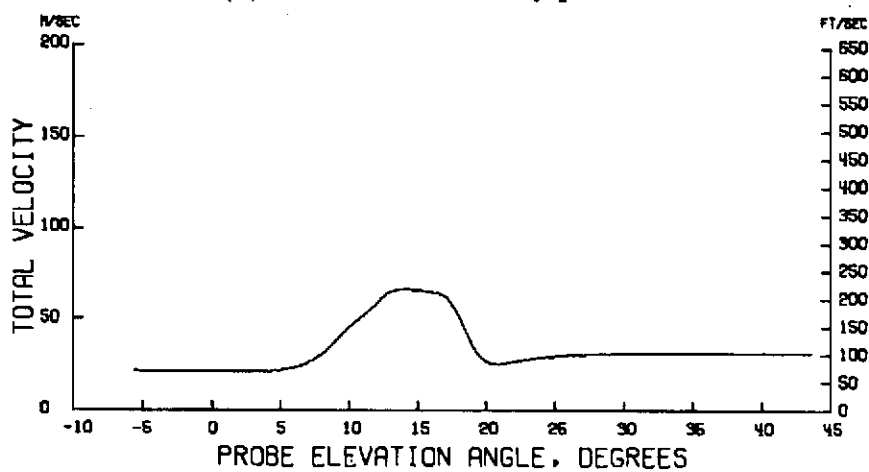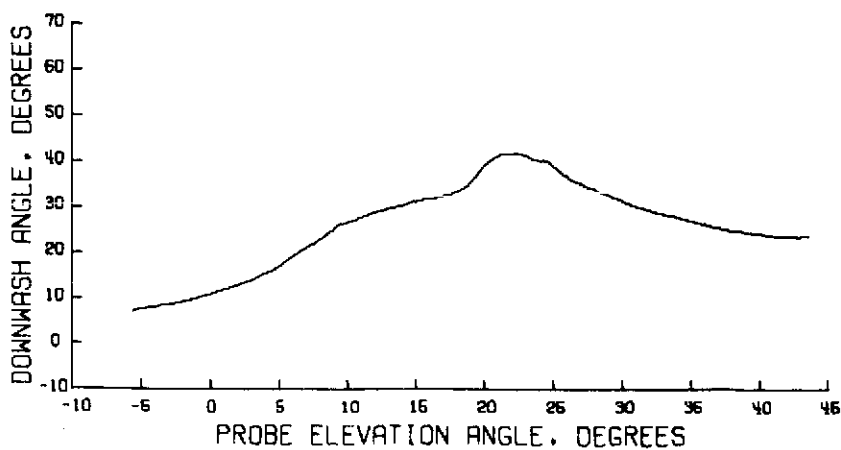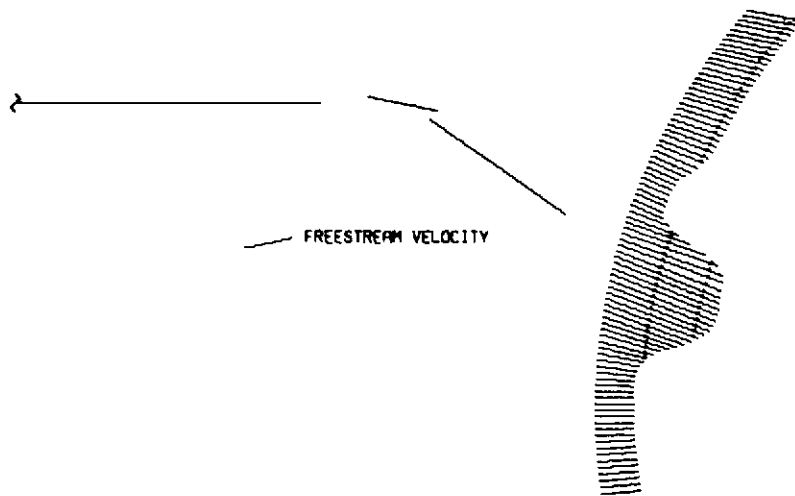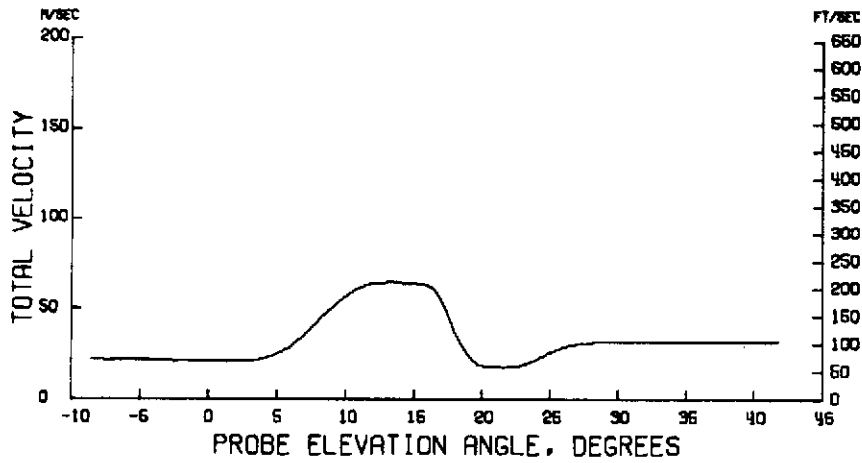(c) Downwash angle.

Figure 20.- Wake survey results for $\eta = 0.253$; $\alpha = 4^O$; $C_T = 0$; $V_\infty = 25.49$ m/sec (83.63 ft/sec).
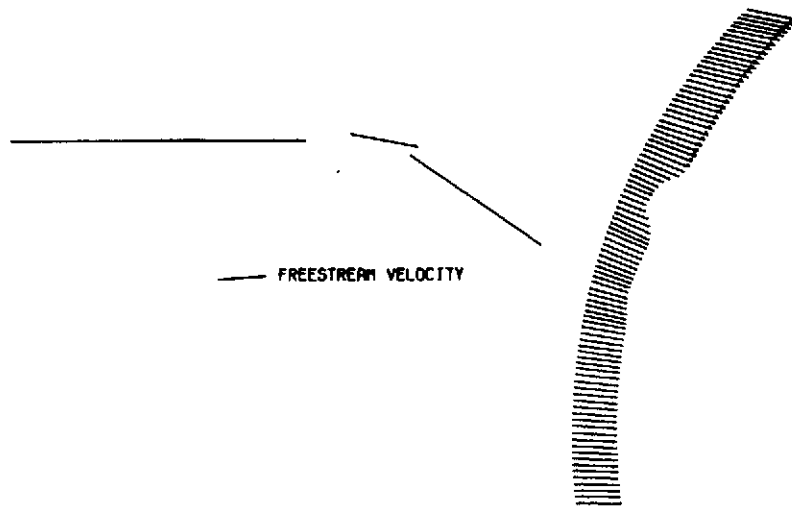
(a) Streamwise velocity profile.
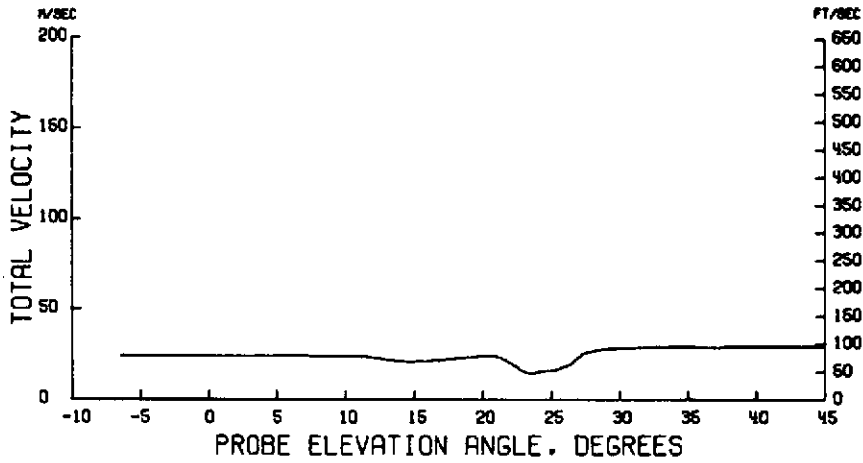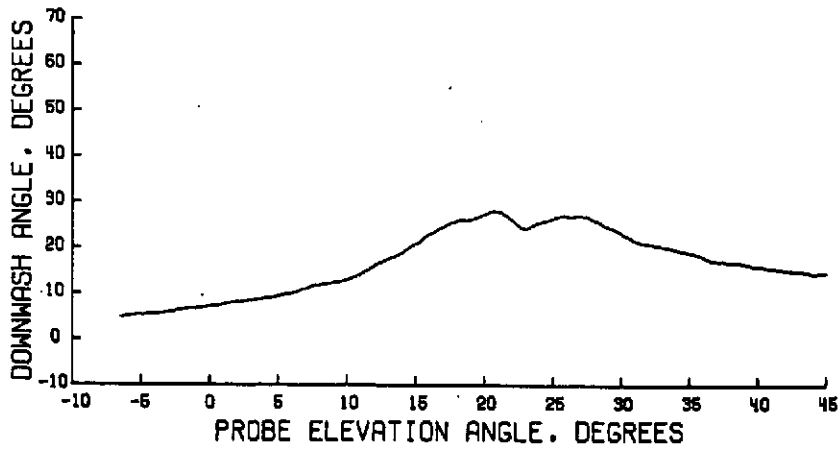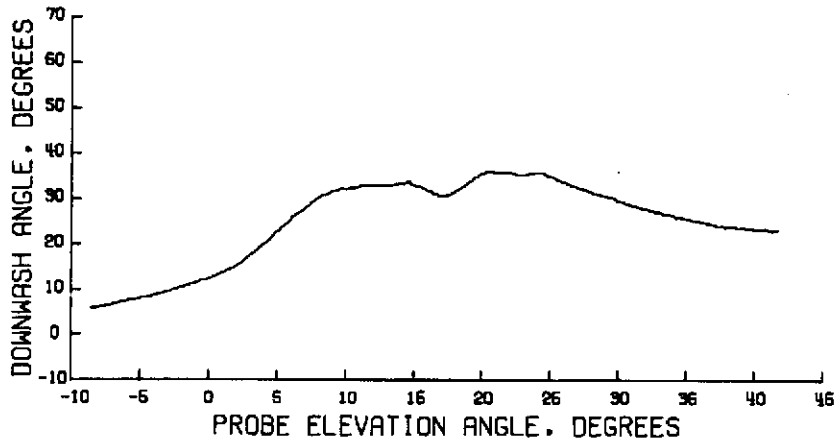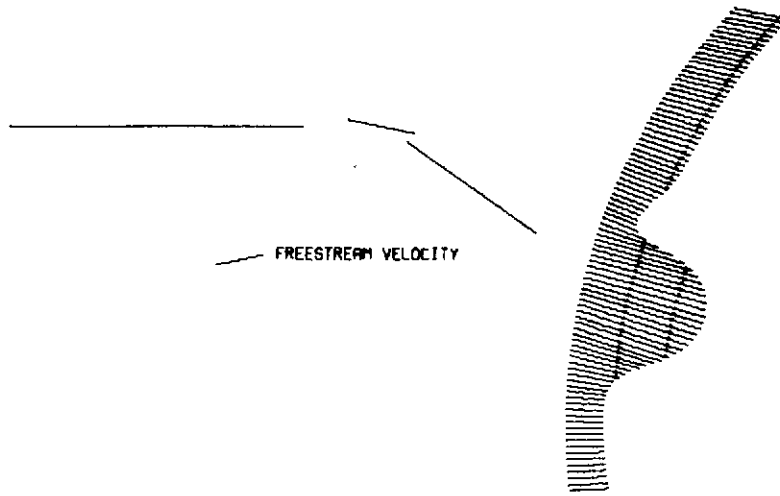


(b) Total velocity.



(c) Downwash angle.

Figure 21.- Wake survey results for $\eta = 0.294$; $\alpha = 4^{\circ}$; $C_T = 0$;
$V_{\infty} = 25.45$ m/sec (83.50 ft/sec).
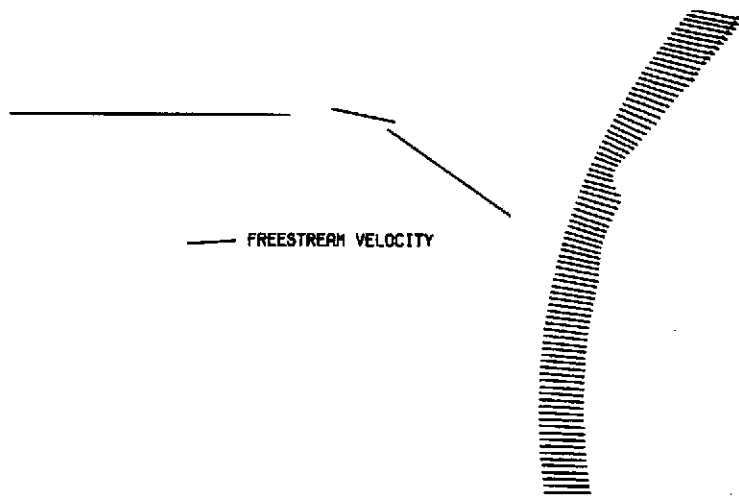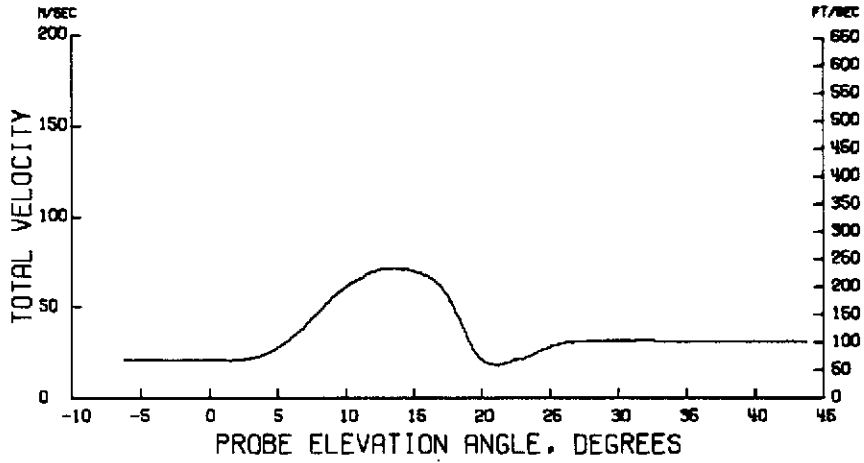
(a) Streamwise velocity profile.
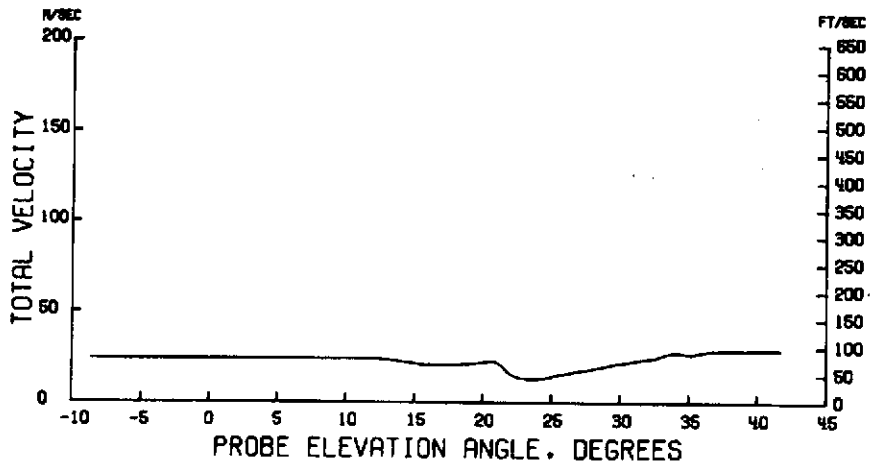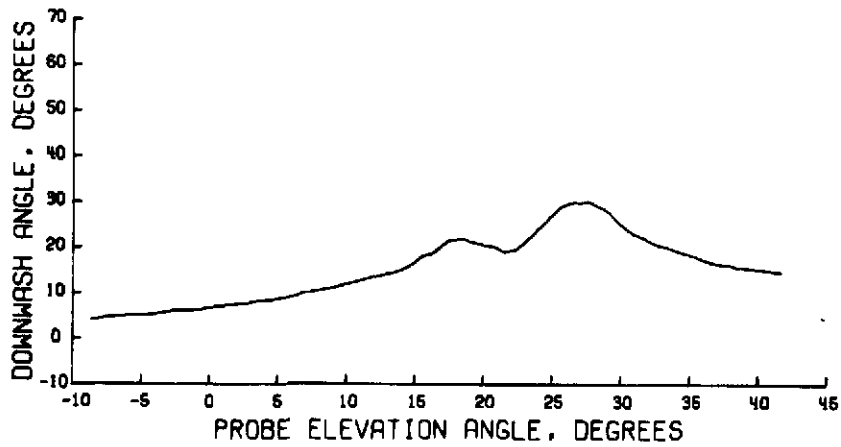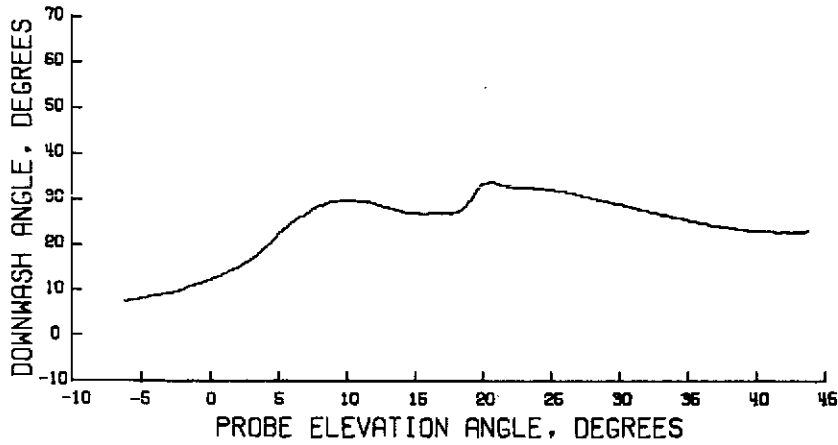


(b) Total velocity.



(c) Downwash angle.

Figure 22.- Wake survey results for $\eta = 0.335$; $\alpha = 4^O$; $C_T = 0$; $V_\infty = 25.42$ m/sec (83.43 ft/sec).
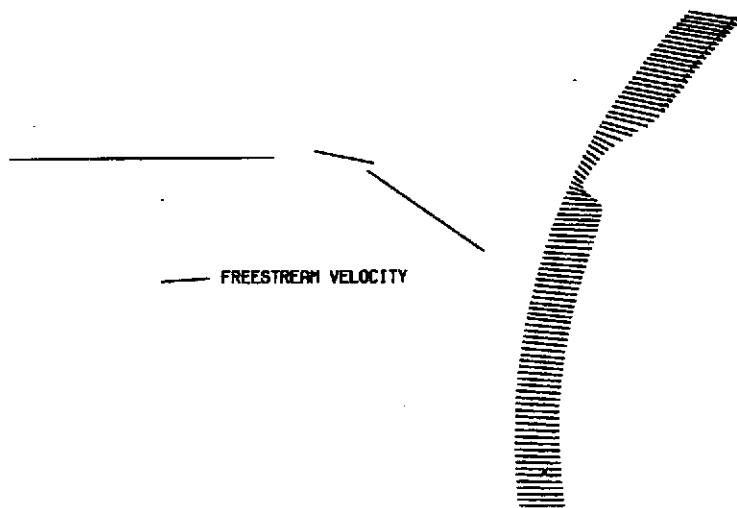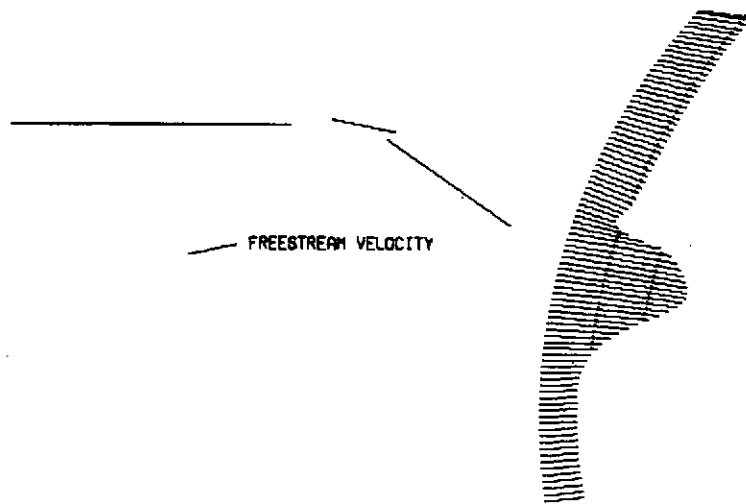
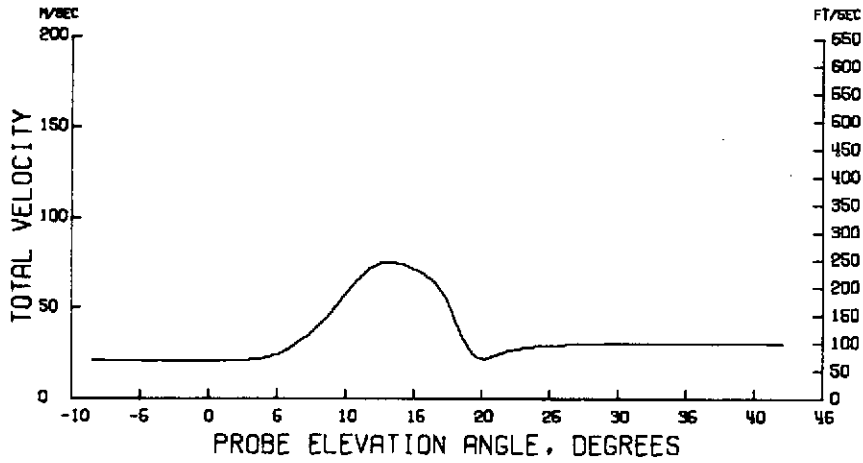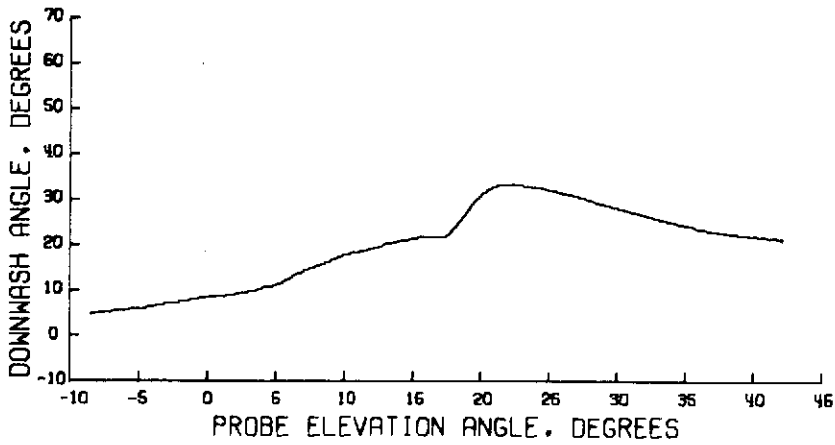(a) Streamwise velocity profile.
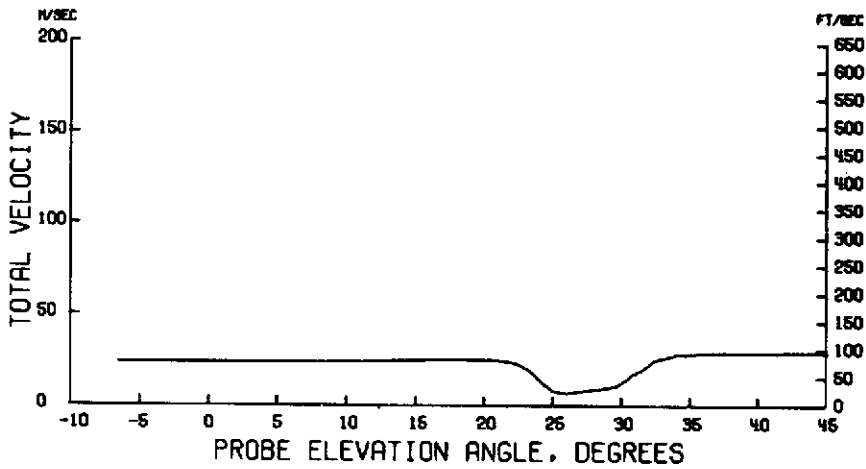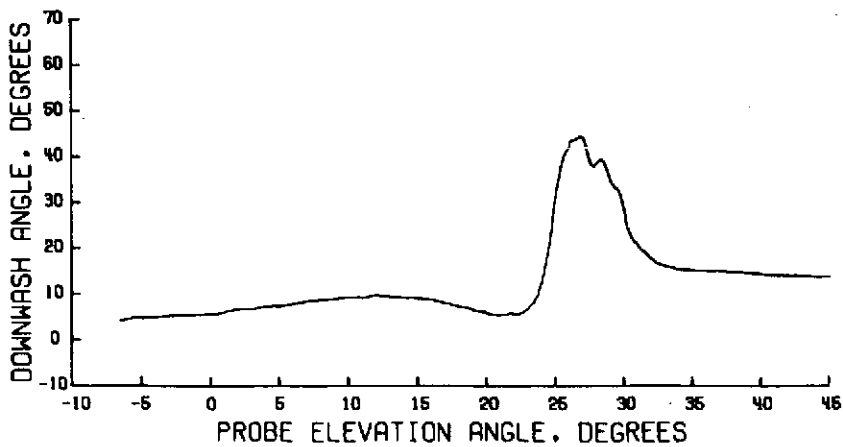


(b) Total velocity.



(c) Downwash angle.

Figure 23.- Wake survey results for $\eta = 0.375$; $\alpha = 4^O$; $C_T = 0$; $V_\infty = 25.49$ m/sec (83.65 ft/sec).
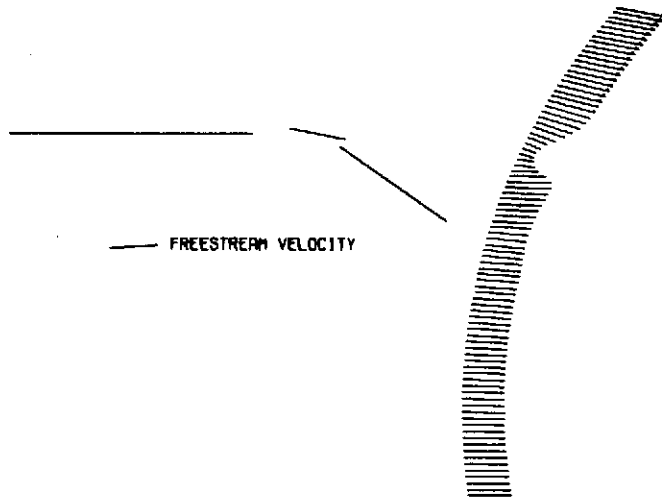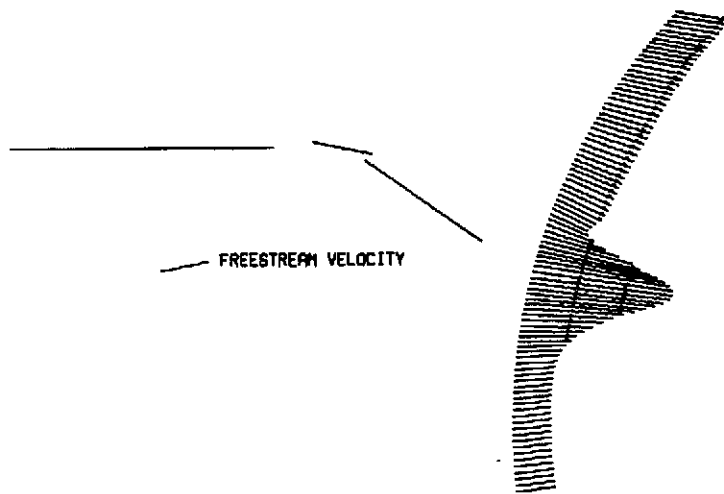
(a) Streamwise velocity profile.
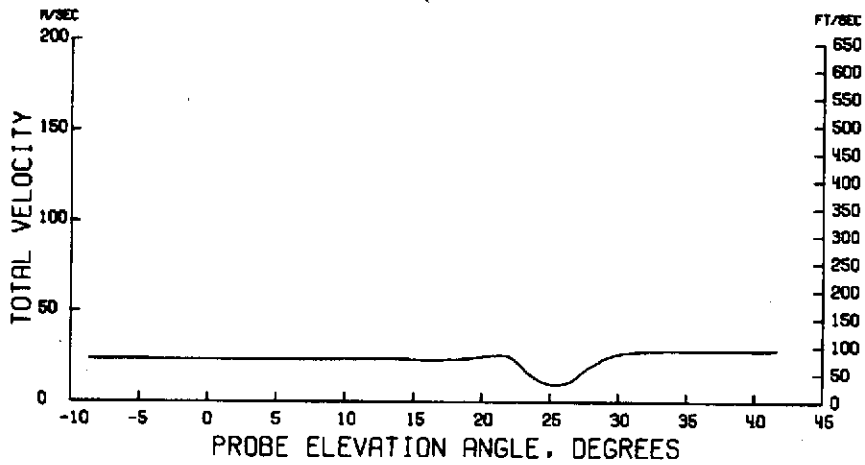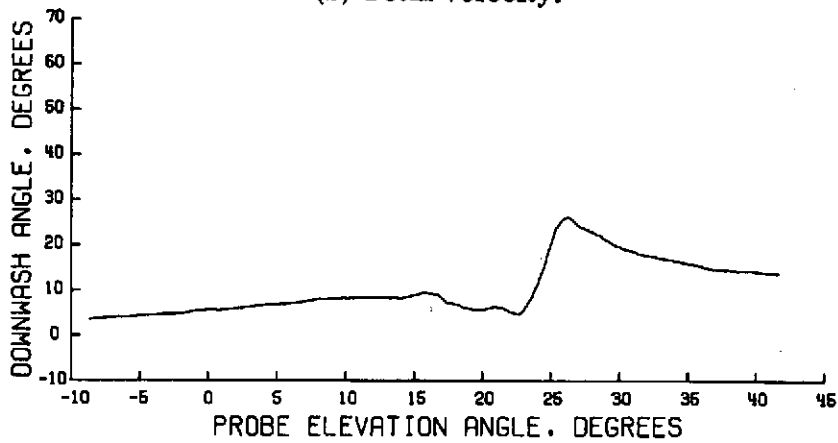


(b) Total velocity.



(c) Downwash angle.

Figure 24.- Wake survey results for $\eta = 0.416$; $\alpha = 4^{\circ}$; $C_T = 0$; $V_{\infty} = 25.40$ m/sec  (83.34 ft/sec).
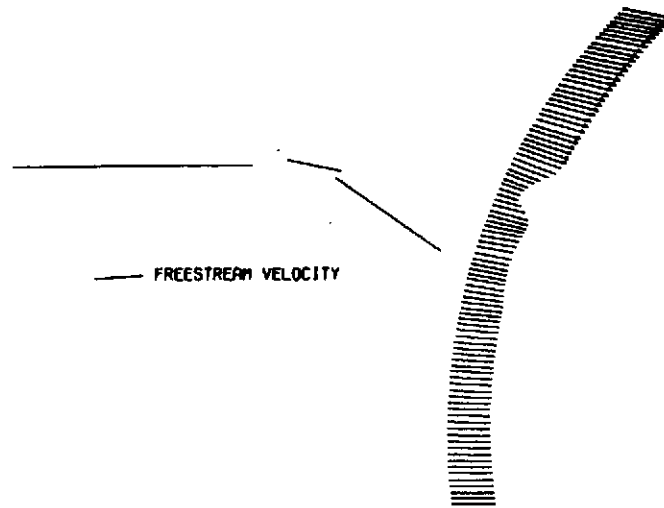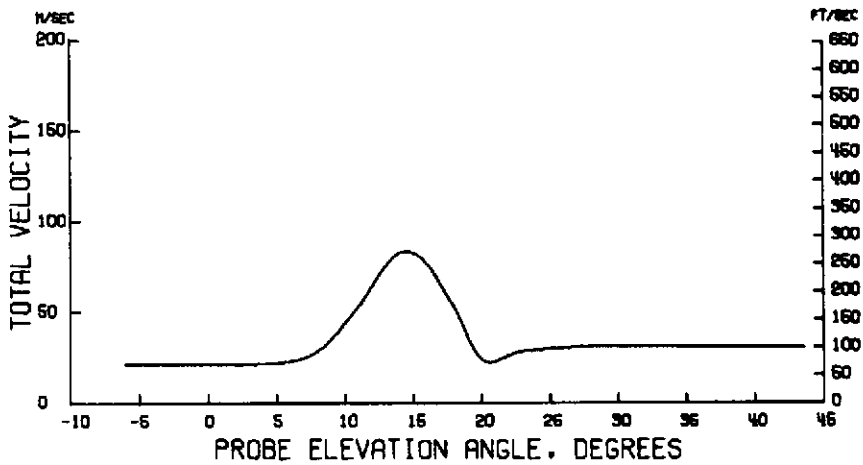
(a) Streamwise velocity profile.
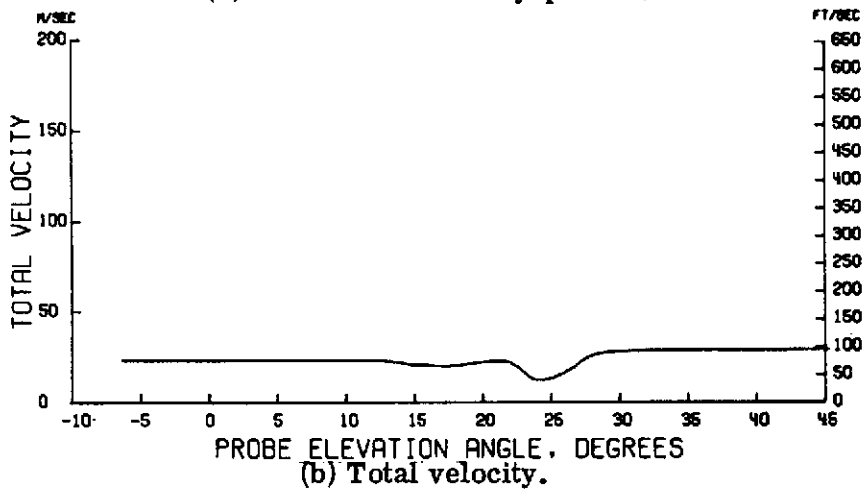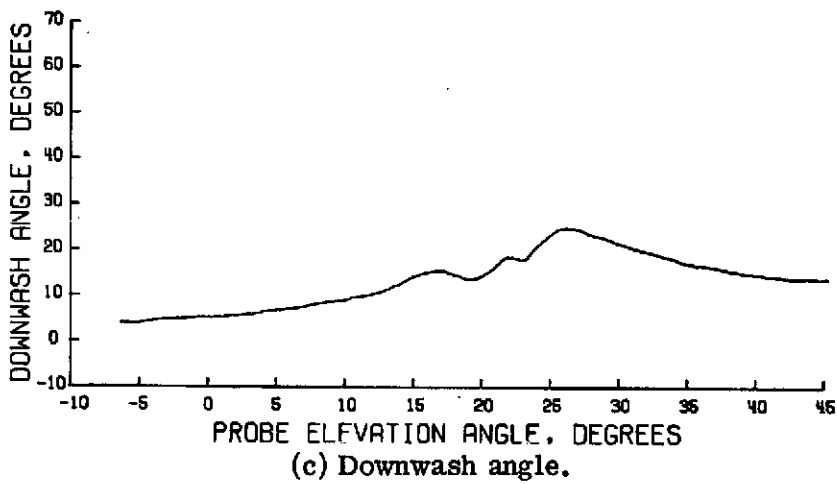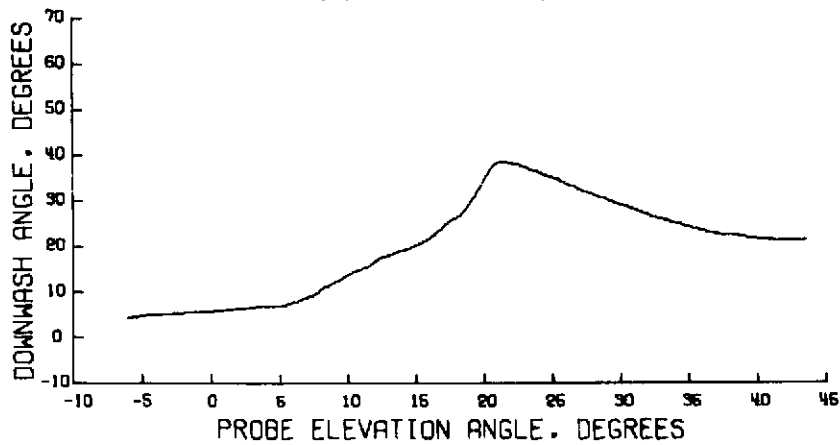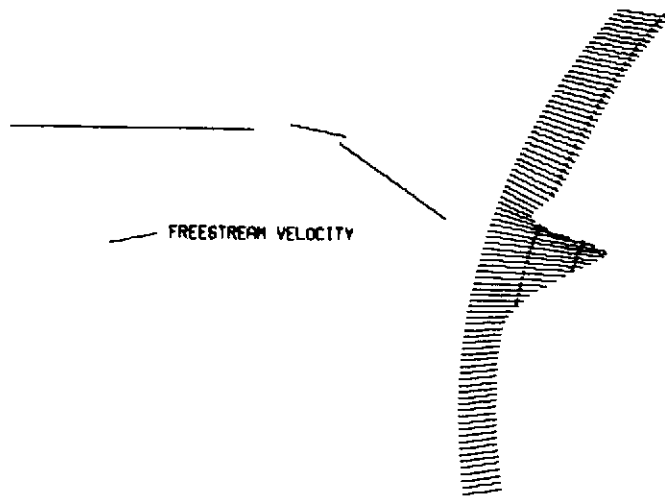


(b) Total velocity.



(c) Downwash angle.

Figure 25.- Wake survey results for $\eta = 0.442$; $\alpha = 4^O$; $C_T = 0$; $V_\infty = 25.38$ m/sec (83.29 ft/sec).
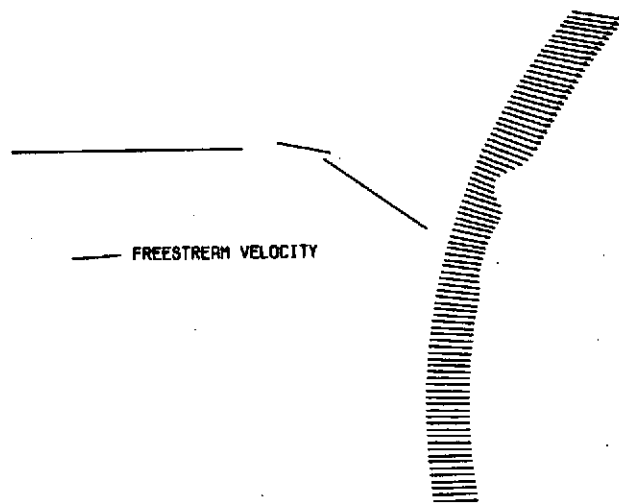
(a) Streamwise velocity profile.
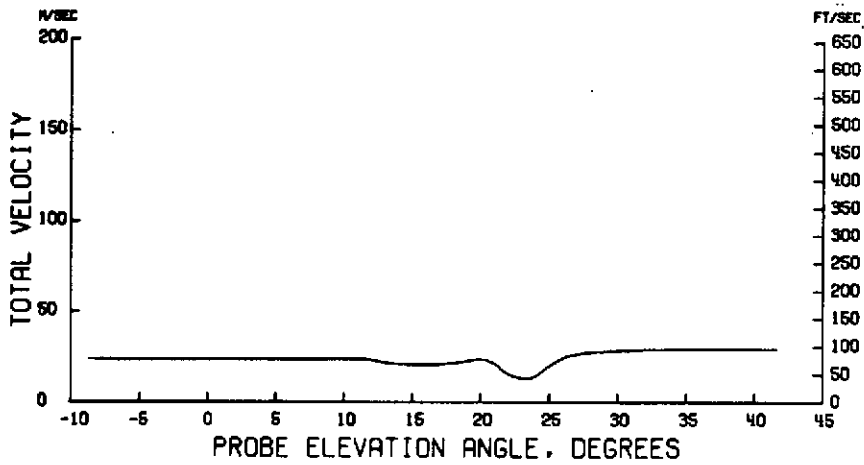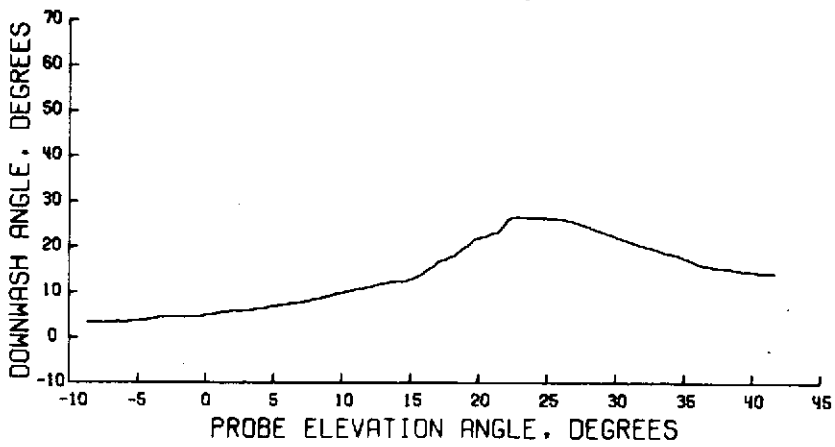


(b) Total velocity.



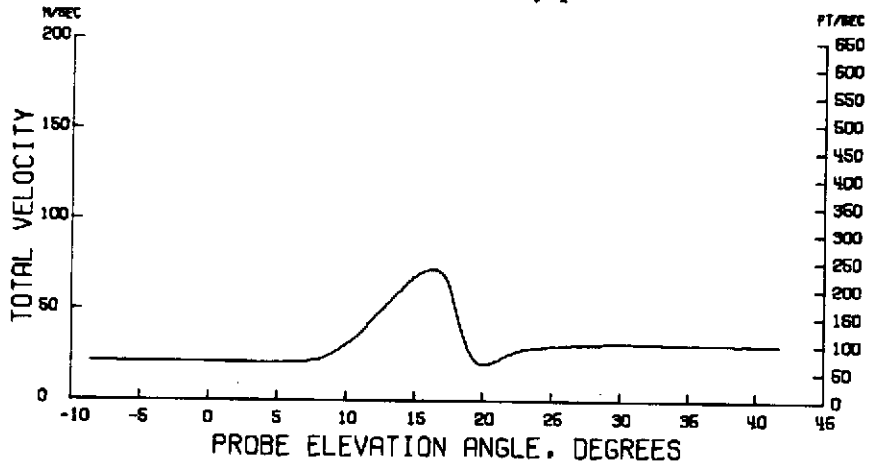(c) Downwash angle.

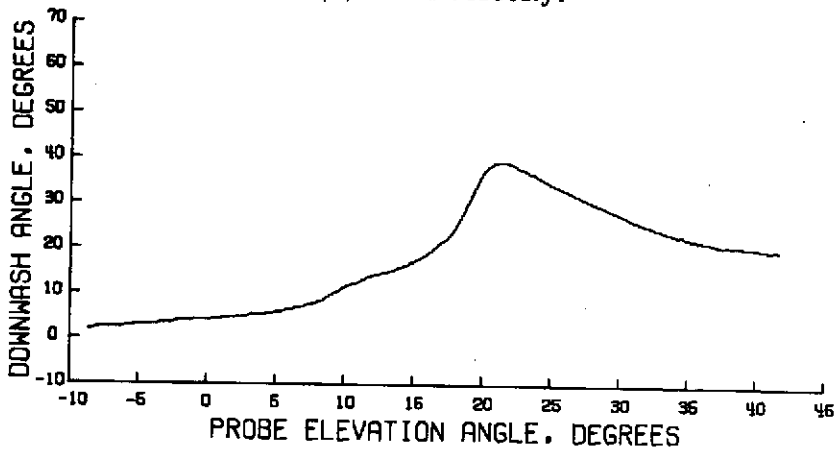Figure 26.- Wake survey results for $\eta = 0.469$; $\alpha = 4^O$; $C_T = 0$;
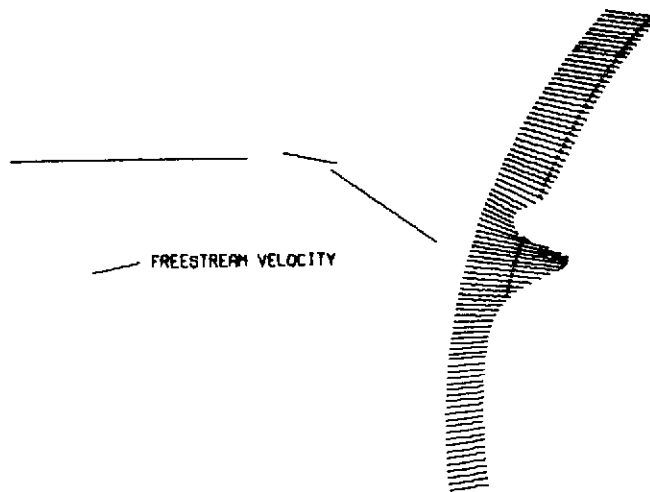$V_\infty = 25.44$ m/sec (83.47 ft/sec).
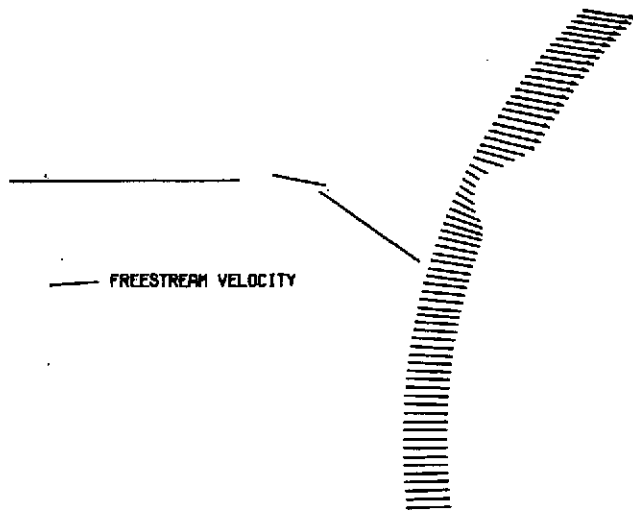
(a) Streamwise velocity profile.
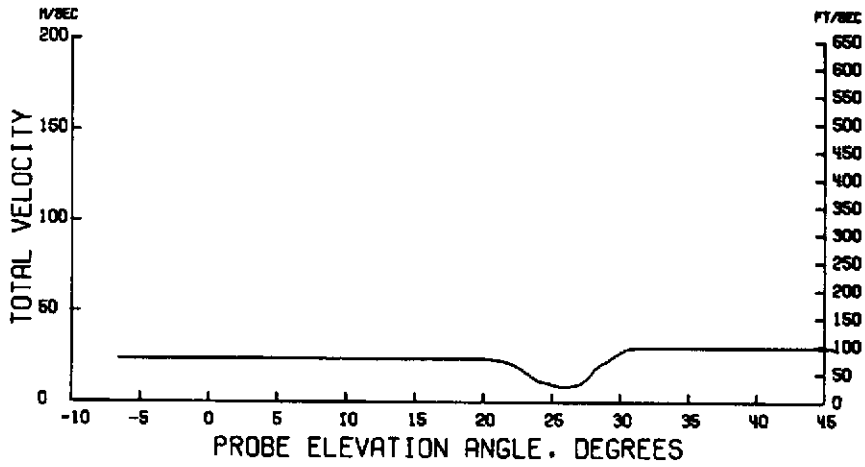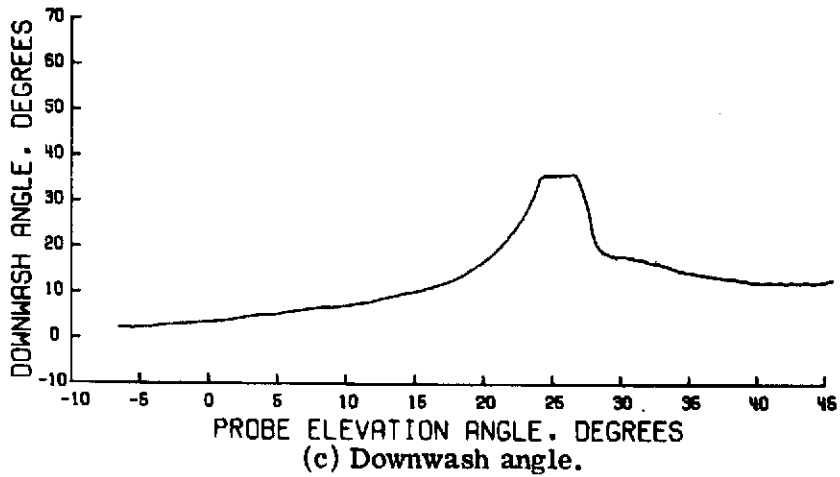


(b) Total velocity.



(c) Downwash angle.

Figure 27.- Wake survey results for $\eta = 0.564$; $\alpha = 4^O$; $C_T = 0$;
$V_\infty = 25.36$ m/sec (83.21 ft/sec).
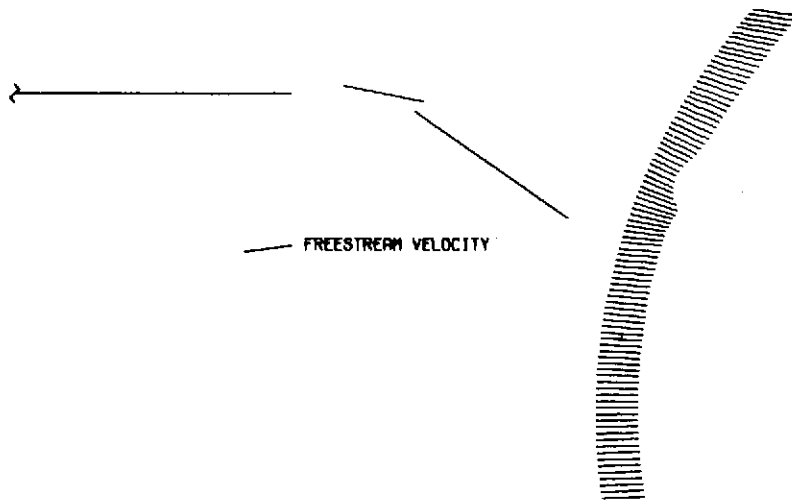
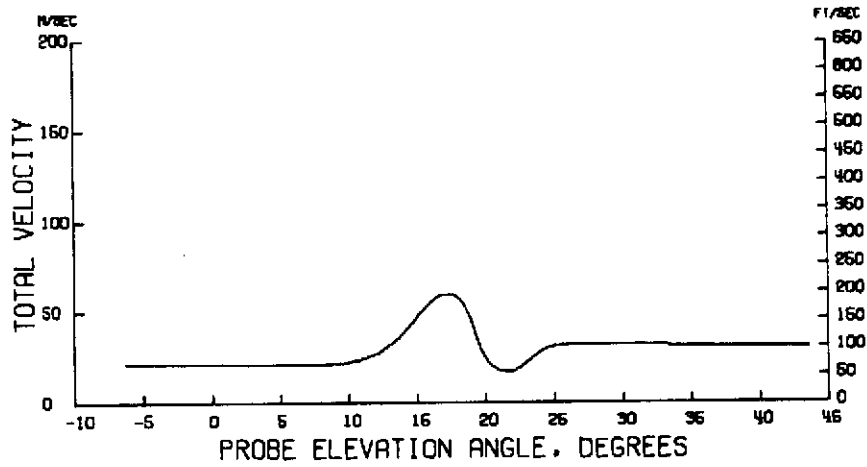(a) Streamwise velocity profile.
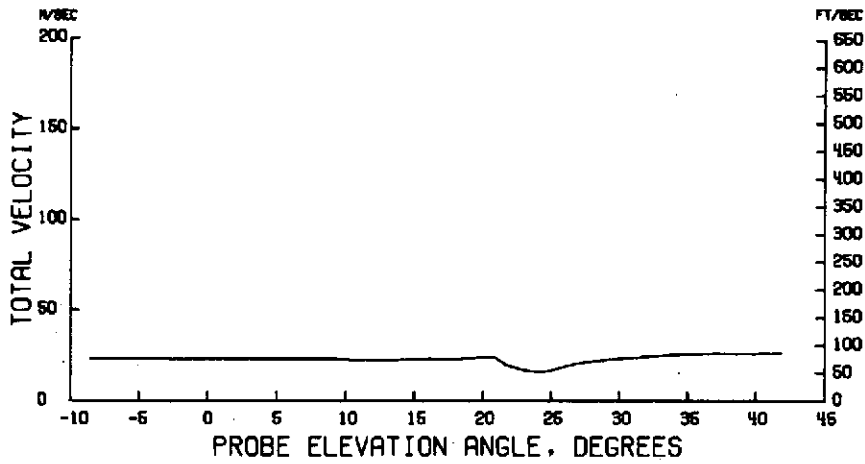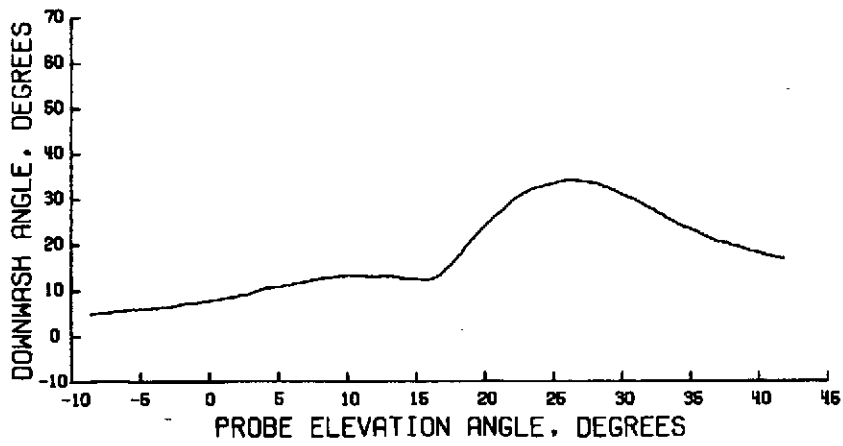


(b) Total velocity.



(c) Downwash angle.

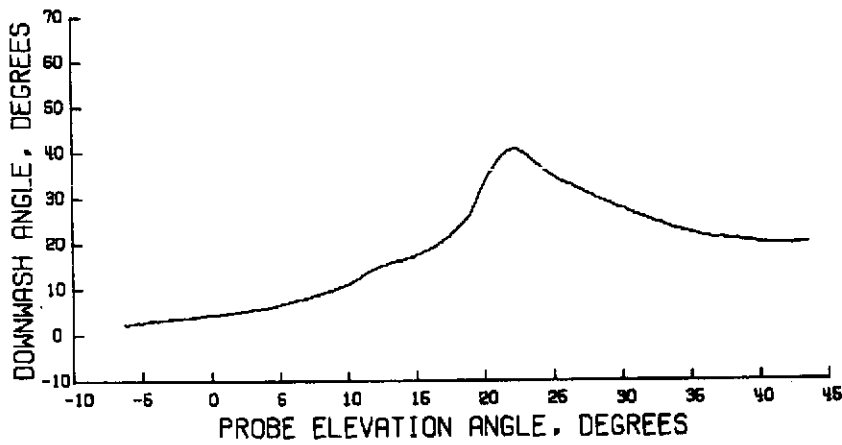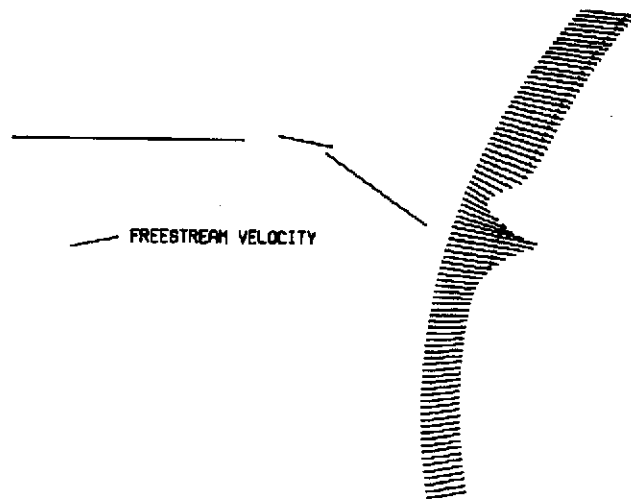Figure 28.- Wake survey results for $\eta = 0.161$; $\alpha = 8^{\circ}$; $C_T = 0$; $V_{\infty} = 25.29$ m/sec (82.98 ft/sec).

41
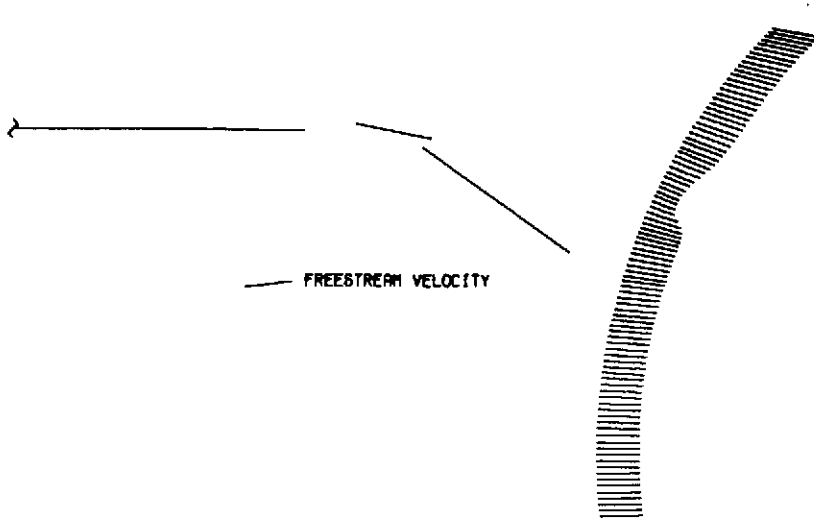
(a) Streamwise velocity profile.
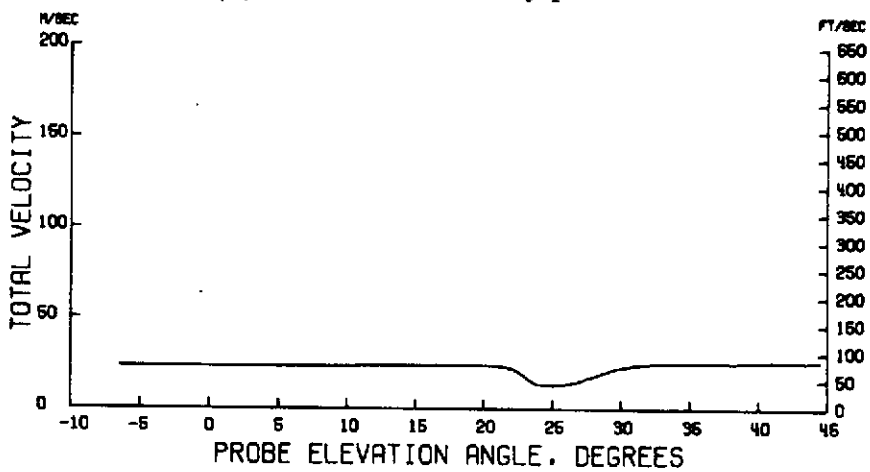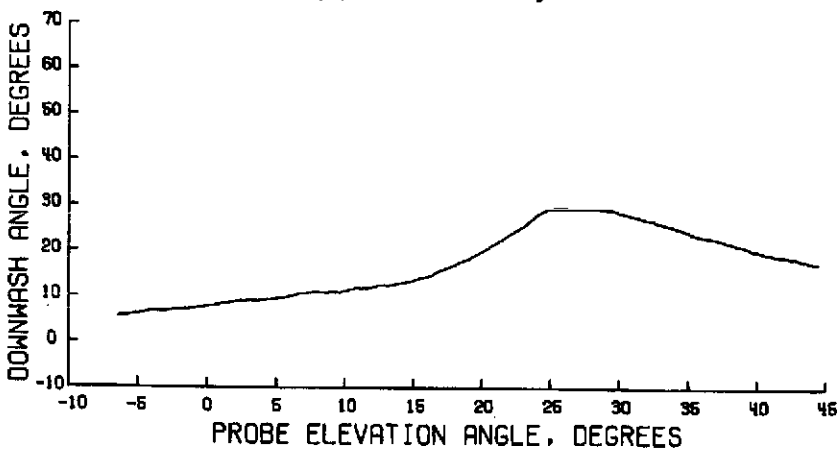


(b) Total velocity.



(c) Downwash angle.

Figure 29.- Wake survey results for $\eta = 0.201$; $\alpha = 8^O$; $C_T = 0$; $V_\infty = 25.40$ m/sec (83.33 ft/sec).
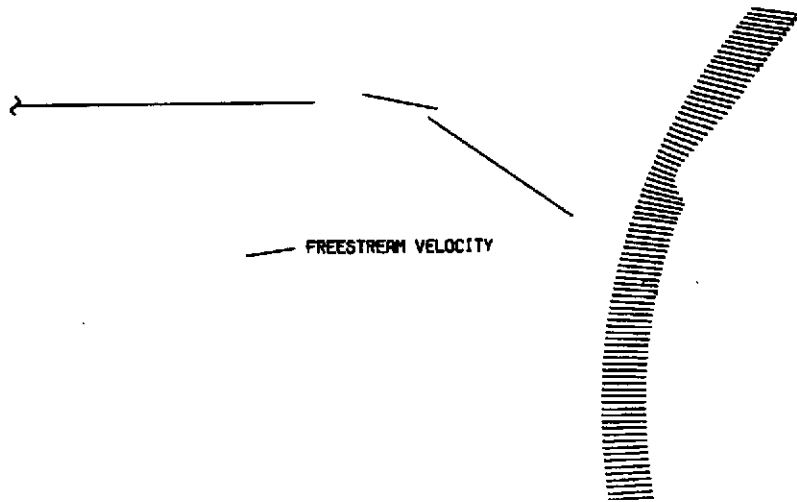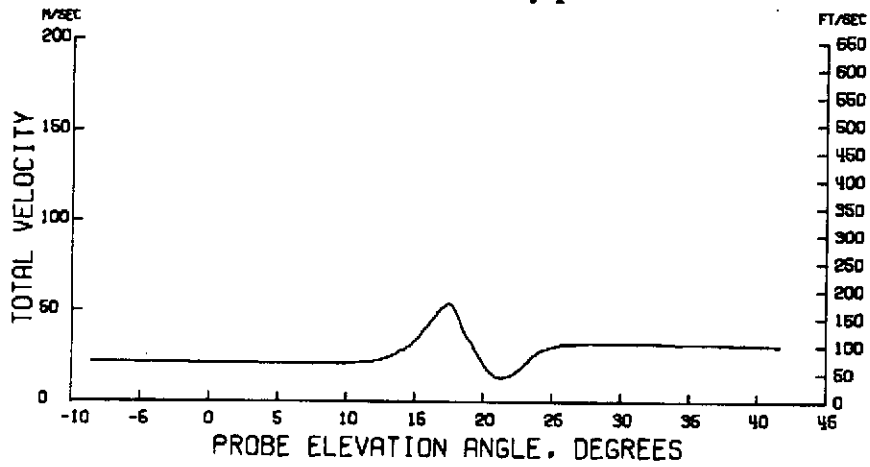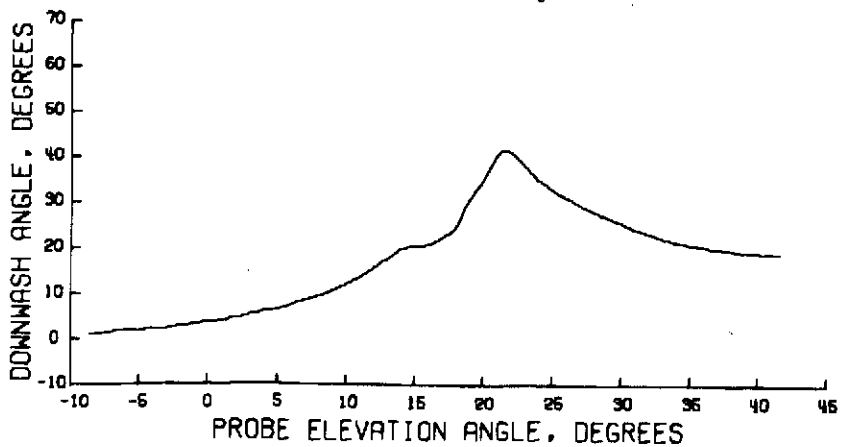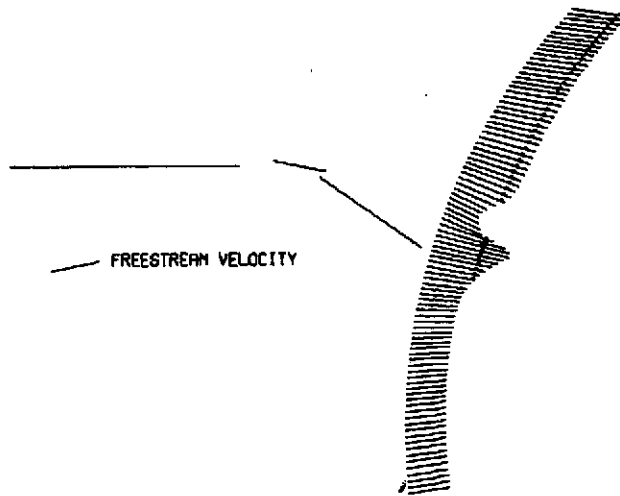
(a) Streamwise velocity profile.
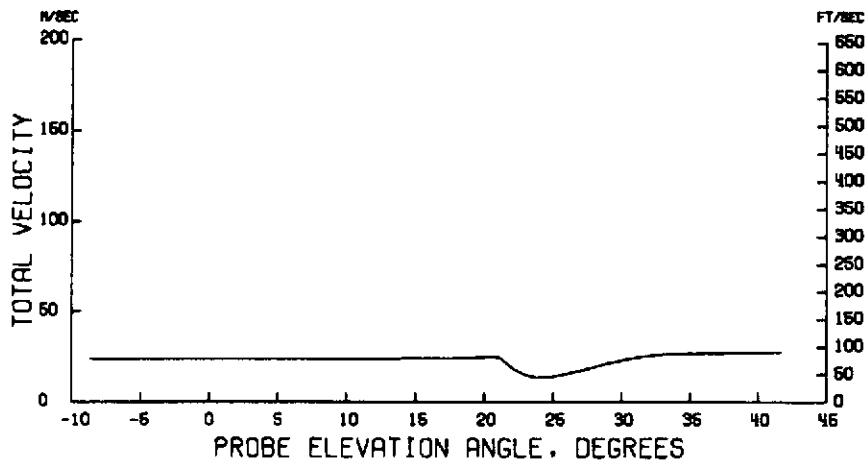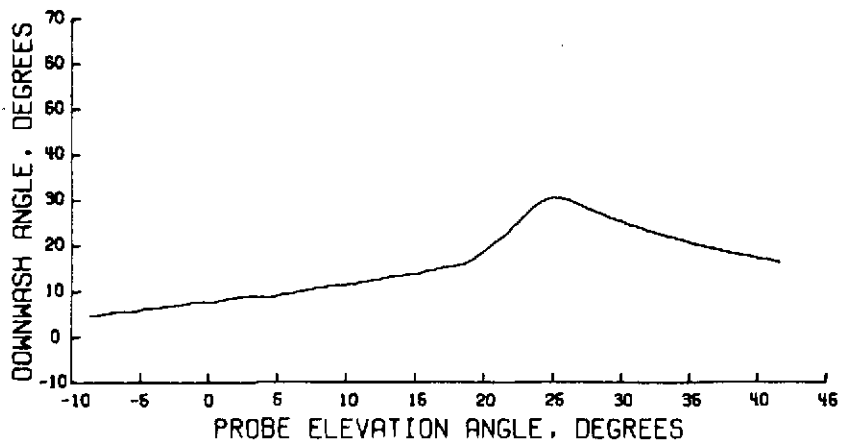


(b) Total velocity.



(c) Downwash angle.

Figure 30.- Wake survey results for $\eta = 0.227$; $\alpha = 8^O$; $C_T = 0$; $V_\infty = 25.48$ m/sec (83.59 ft/sec).
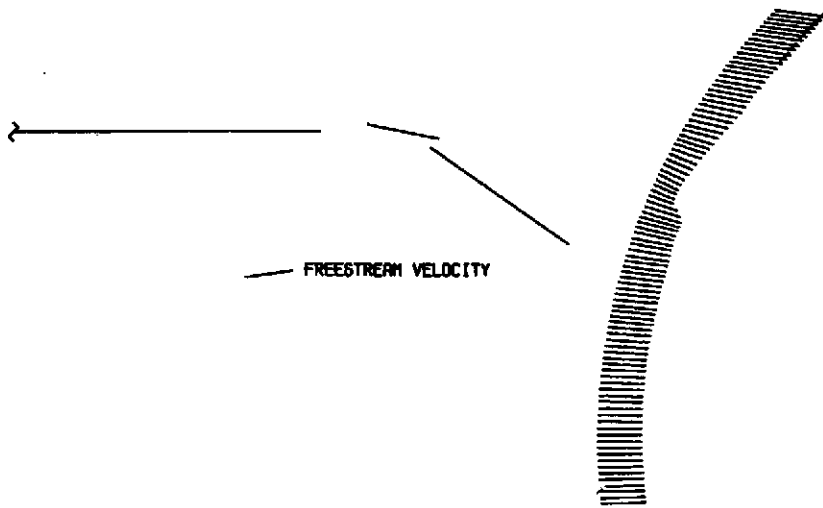
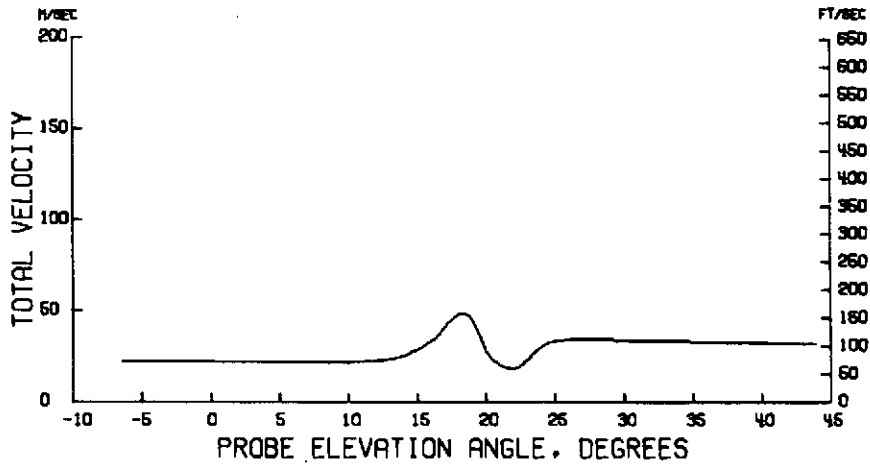(a) Streamwise velocity profile.
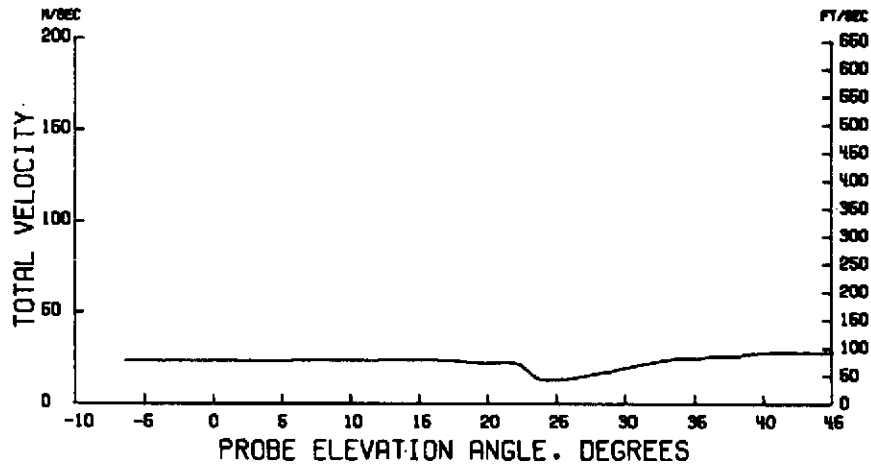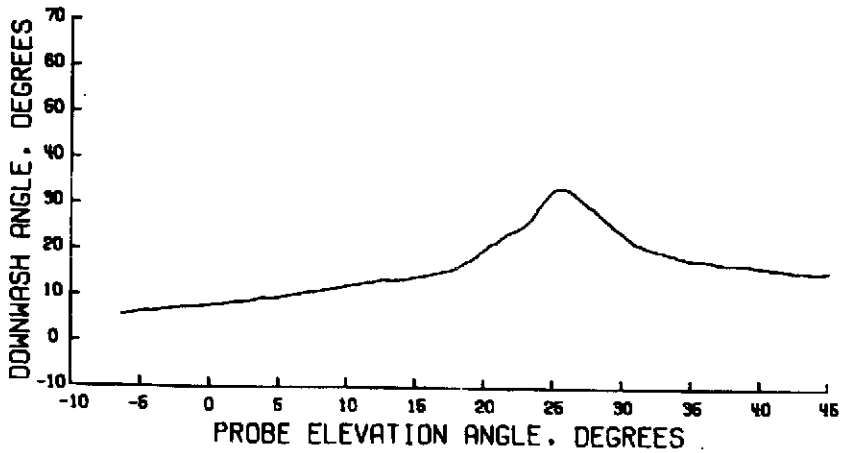


(b) Total velocity.



(c) Downwash angle.

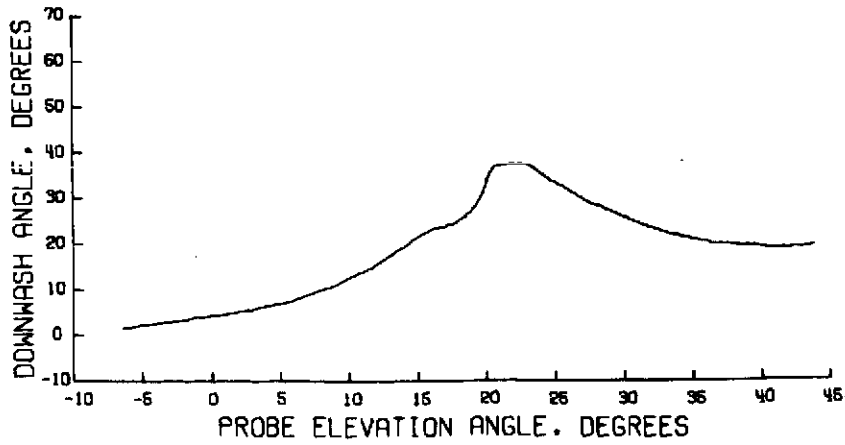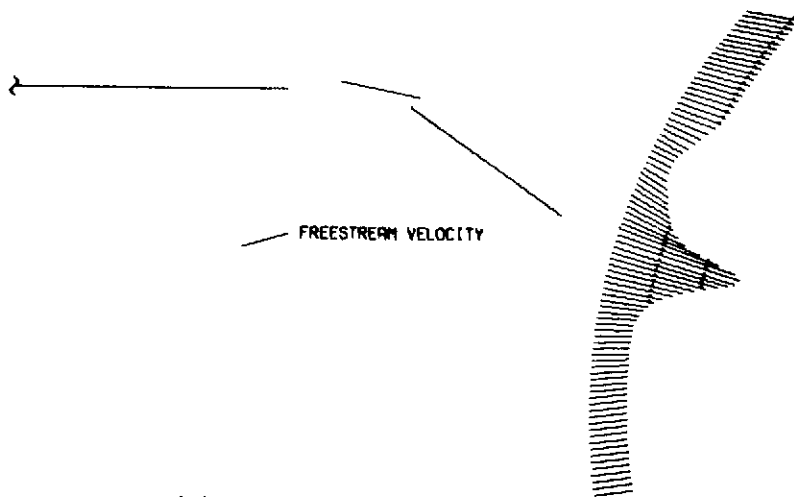Figure 31.- Wake survey results for $\eta = 0.254$; $\alpha = 8^{\circ}$; $C_T = 0$; $V_{\infty} = 25.41$ m/sec (83.37 ft/sec).
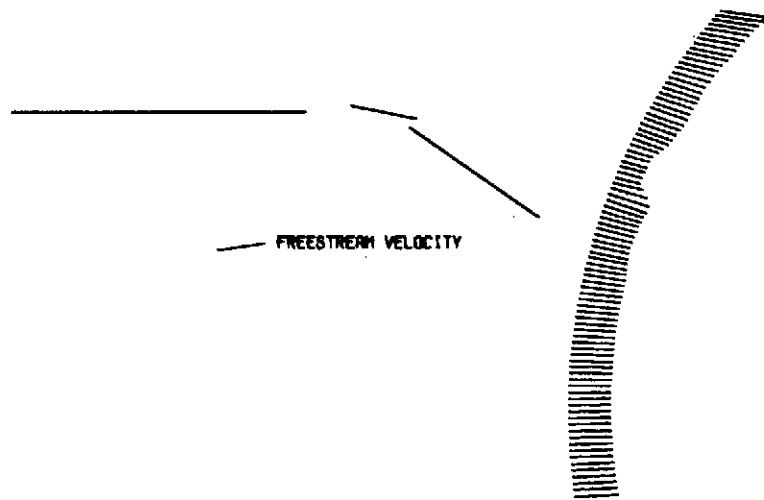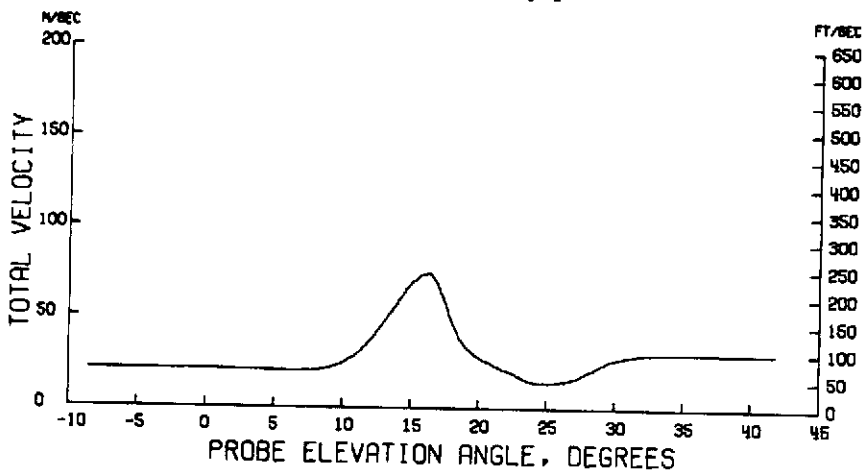
(a) Streamwise velocity profile.
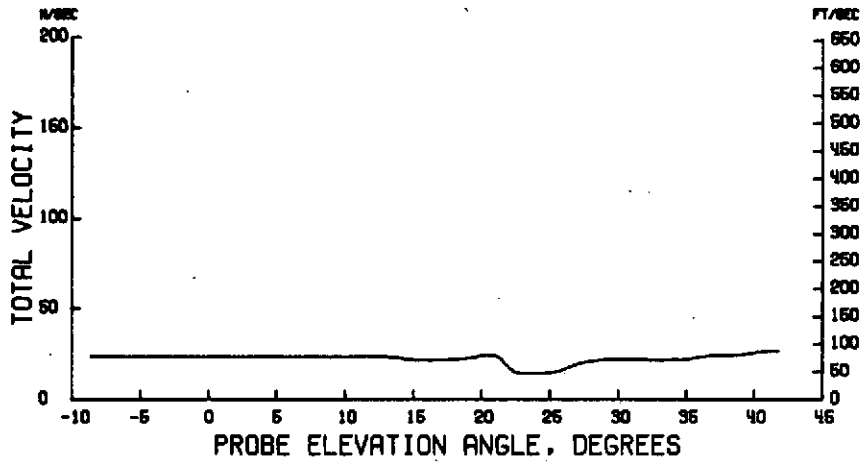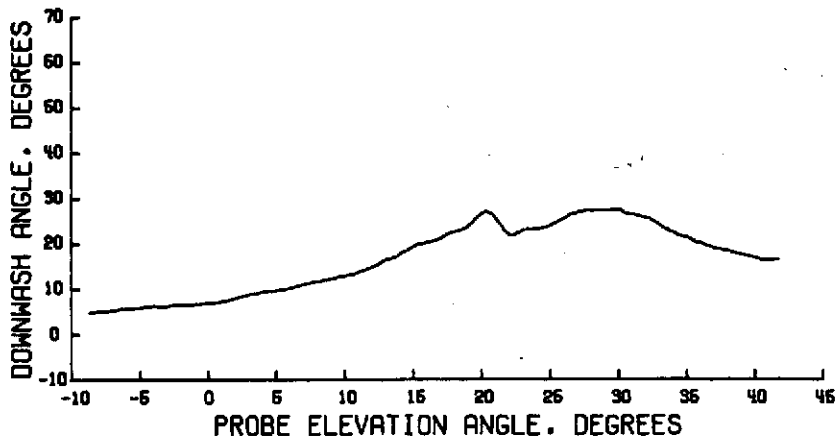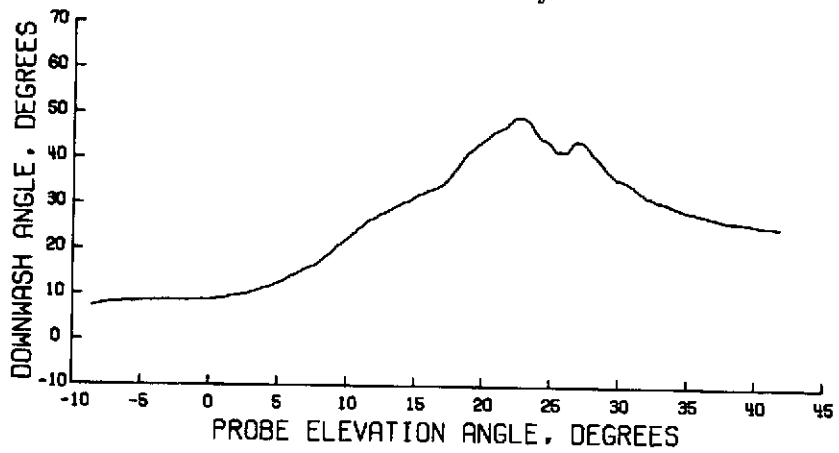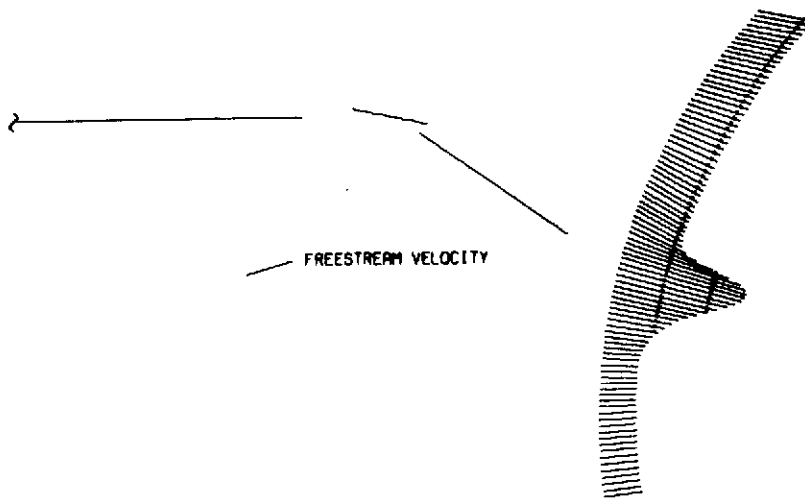


(b) Total velocity.



(c) Downwash angle.

Figure 32.- Wake survey results for  $\eta = 0.294$ ;   $\alpha = 8^{O}$ ;   $C_T = 0$ ;
$V_\infty = 25.43$  m/sec   (83.43 ft/sec).
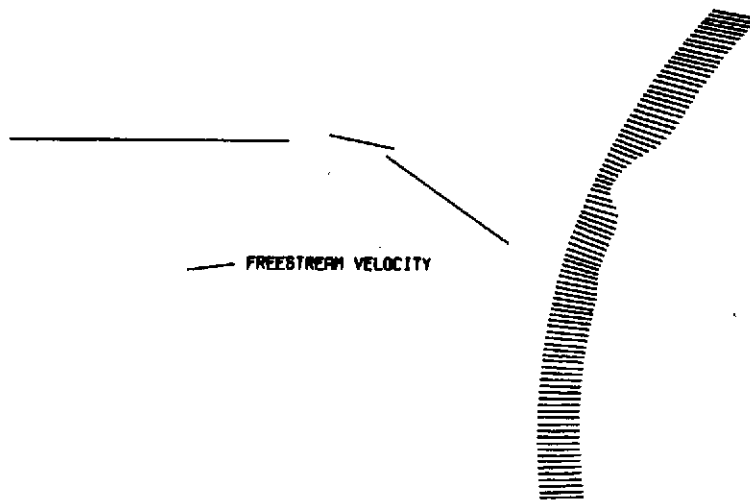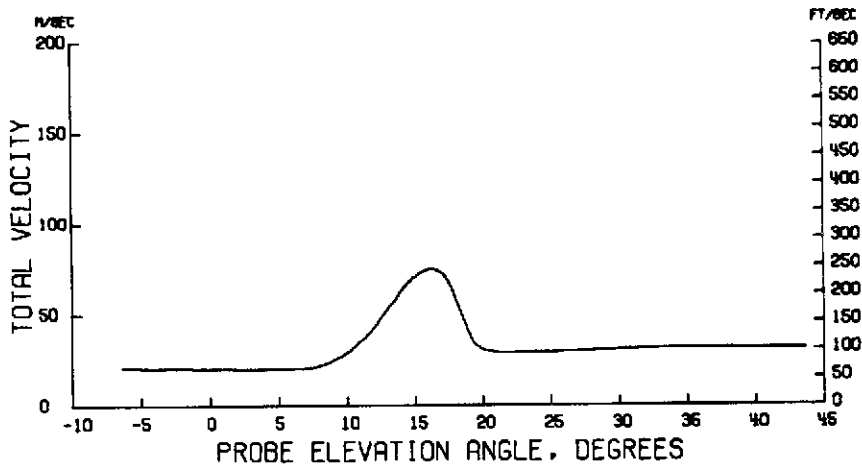
(a) Streamwise velocity profile.
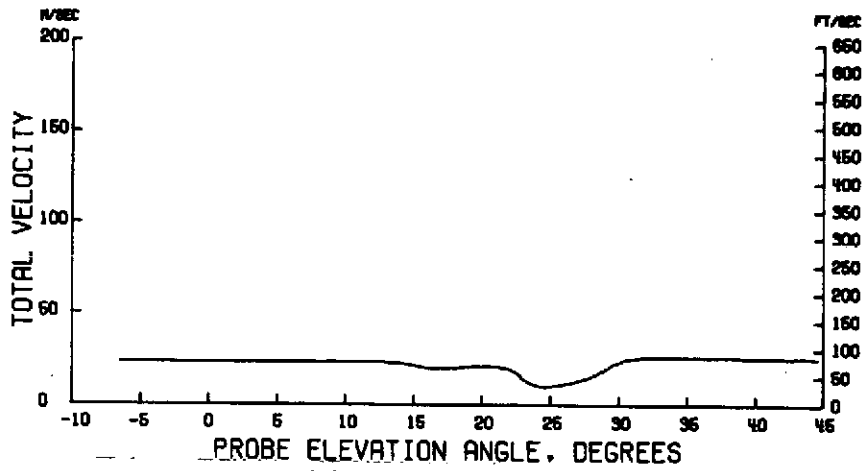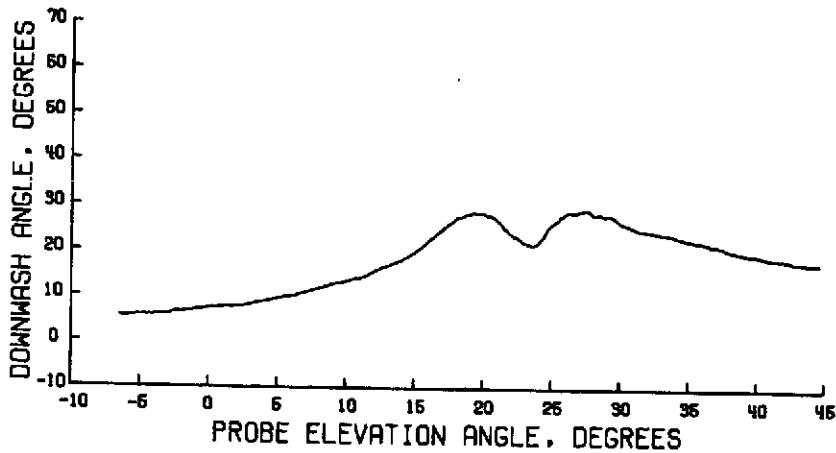


(b) Total velocity.



(c) Downwash angle.

Figure 33.- Wake survey results for $\eta = 0.335$; $\alpha = 8^O$; $C_T = 0$; $V_\infty = 25.34$ m/sec (83.16 ft/sec).
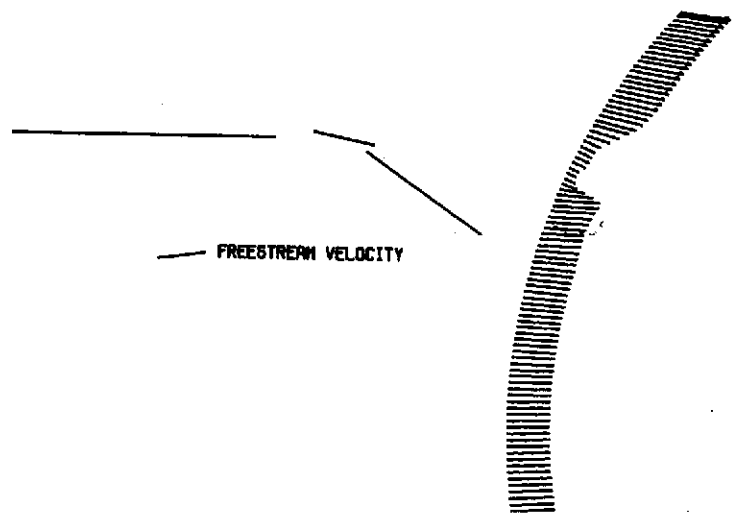
(a) Streamwise velocity profile.
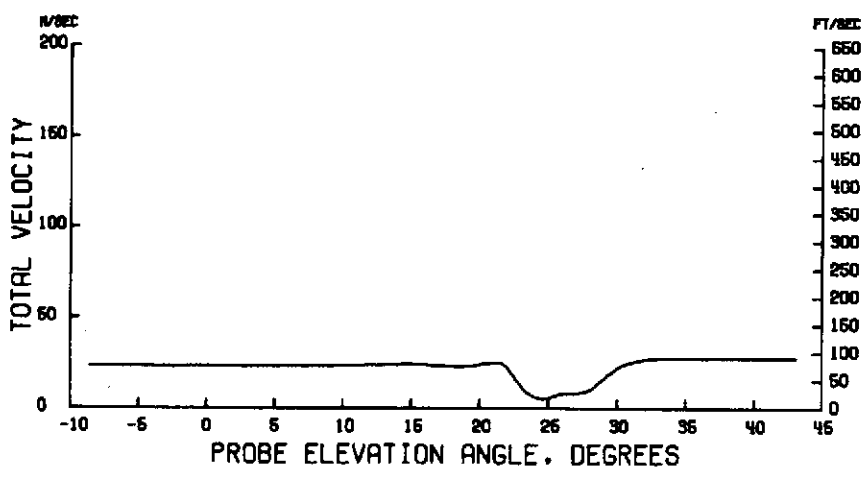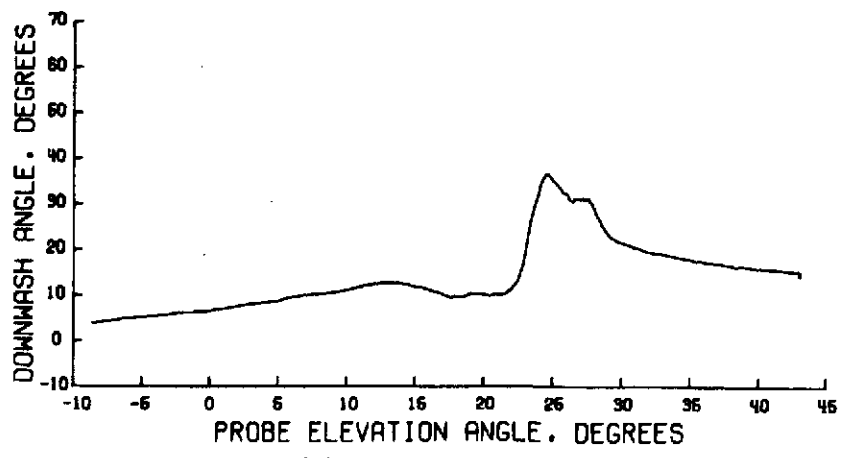


(b) Total velocity.



(c) Downwash angle.

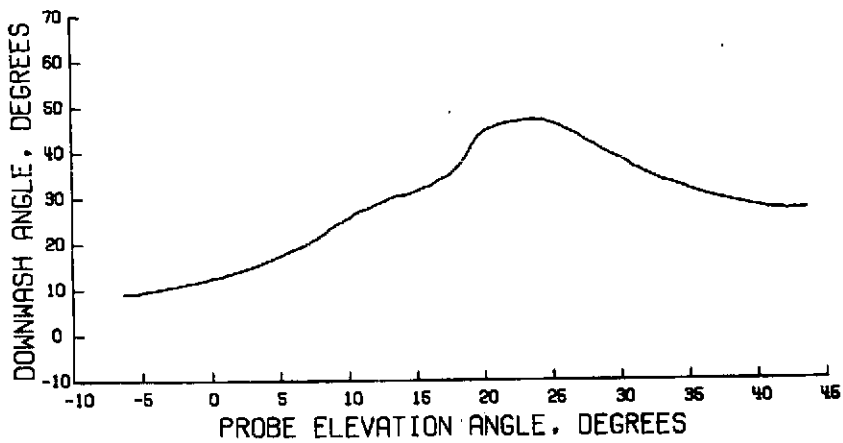Figure 34.- Wake survey results for $\eta = 0.375$; $\alpha = 8^O$; $C_T = 0$; $V_\infty = 25.32$ m/sec (83.08 ft/sec).
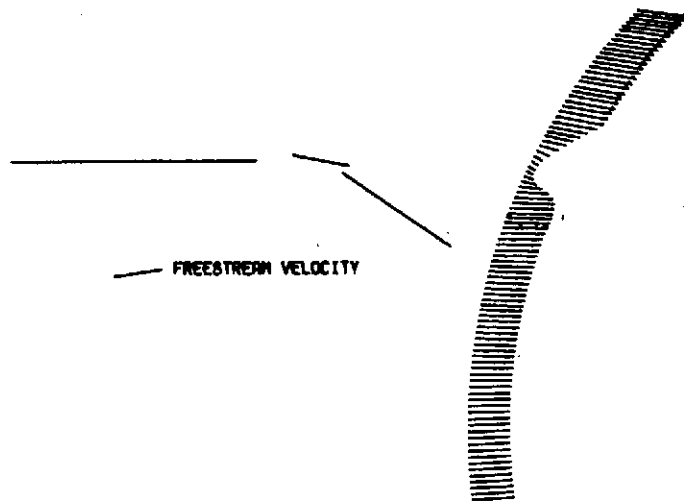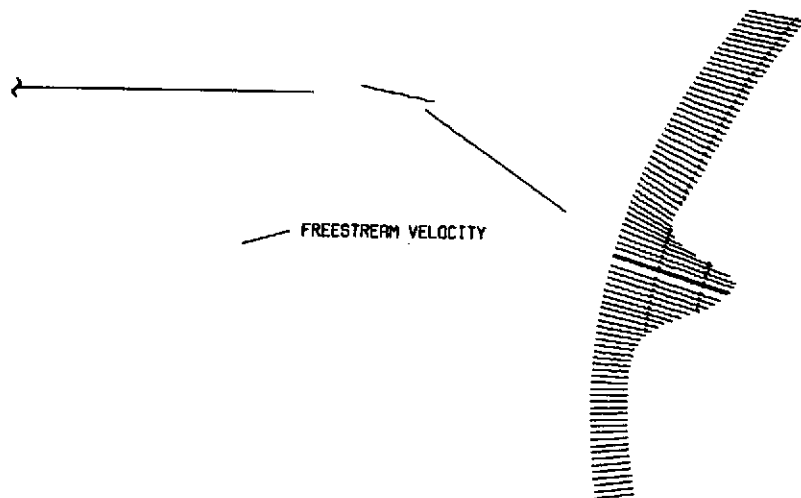
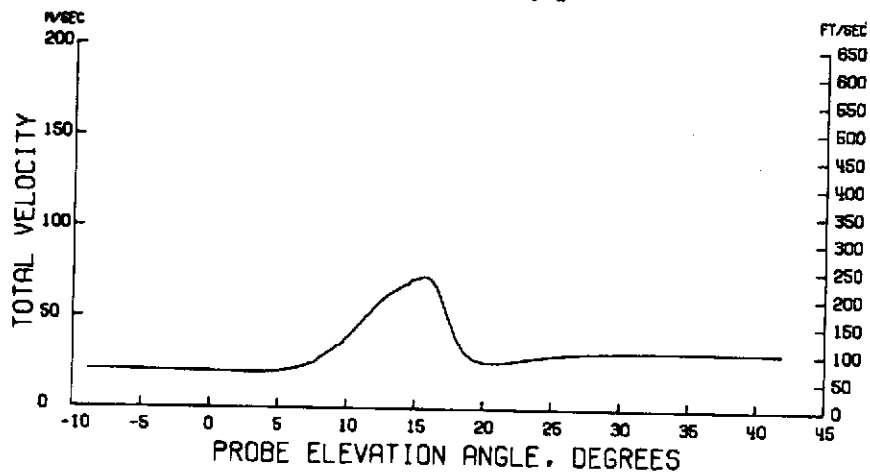(a) Streamwise velocity profile.
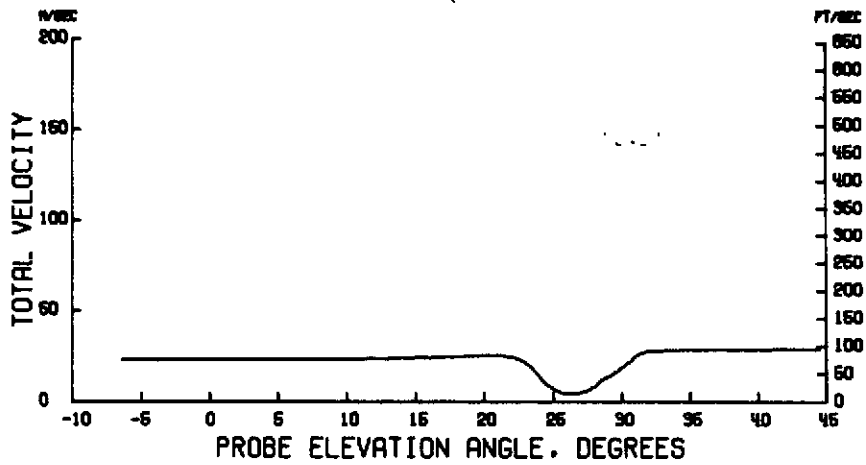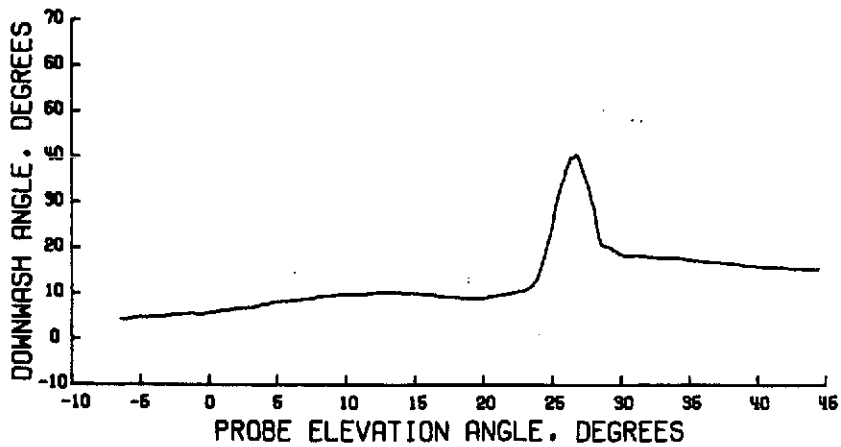


(b) Total velocity.



(c) Downwash angle.

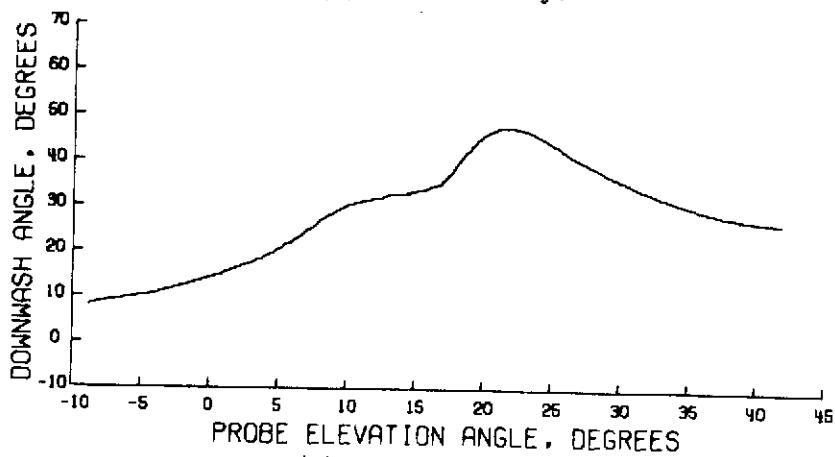Figure 35.- Wake survey results for $\eta = 0.417$; $\alpha = 8^O$; $C_T = 0$;

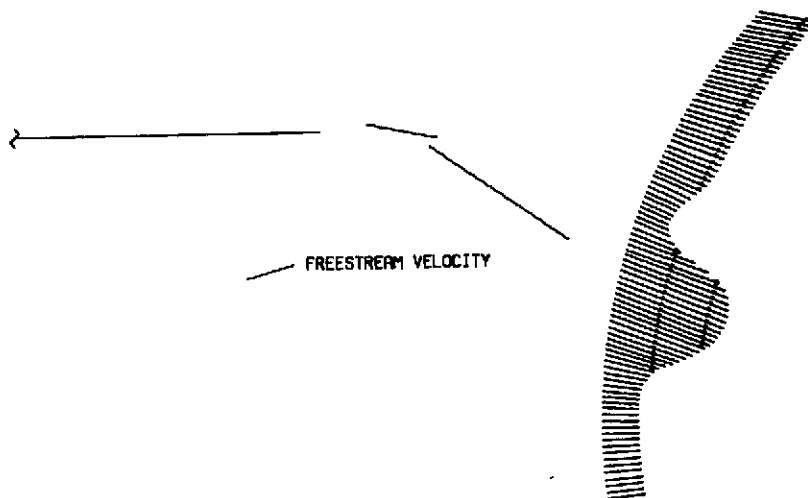$V_\infty = 25.41$ m/sec (83.39 ft/sec).
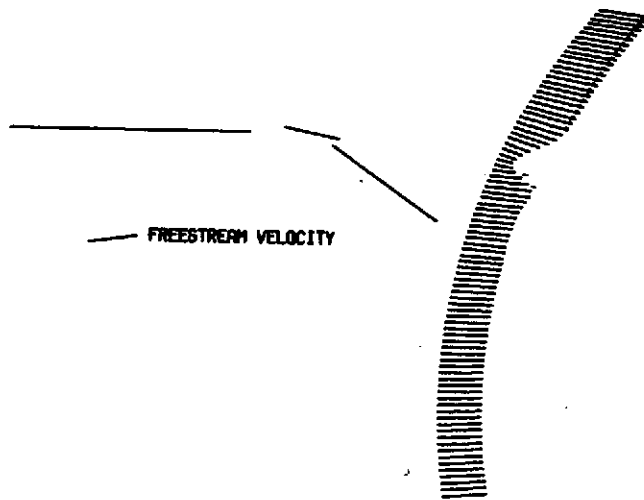
(a) Streamwise velocity profile.
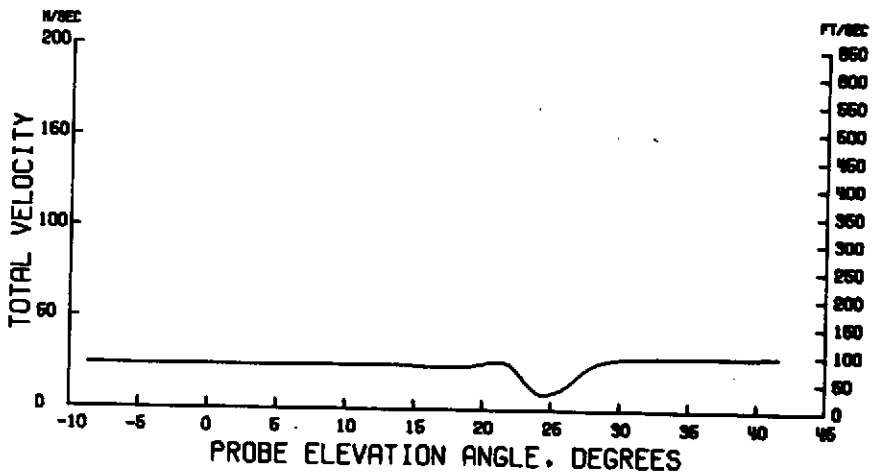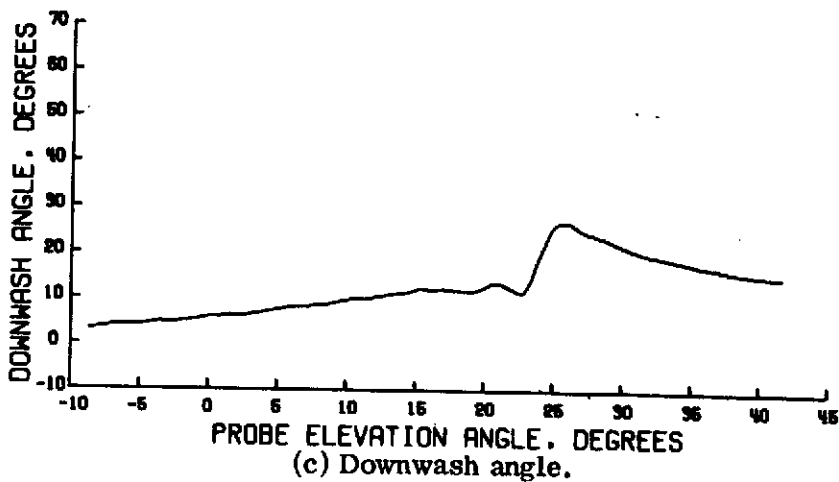


(b) Total velocity.



(c) Downwash angle.

Figure 36.- Wake survey results for $\eta = 0.442$; $\alpha = 8^\circ$; $C_T = 0$; $V_\infty = 25.49$ m/sec (83.63 ft/sec).
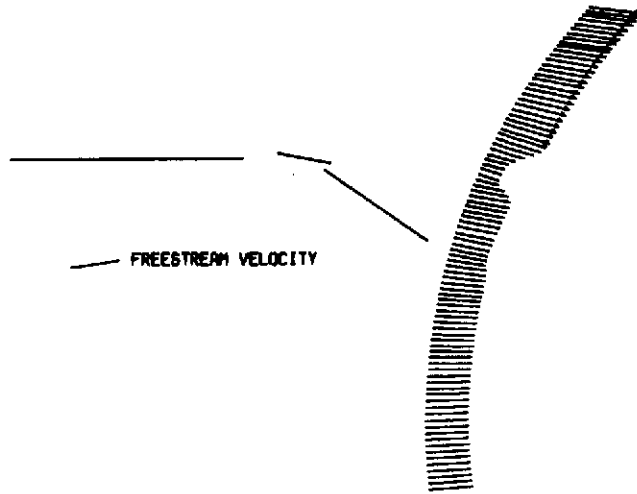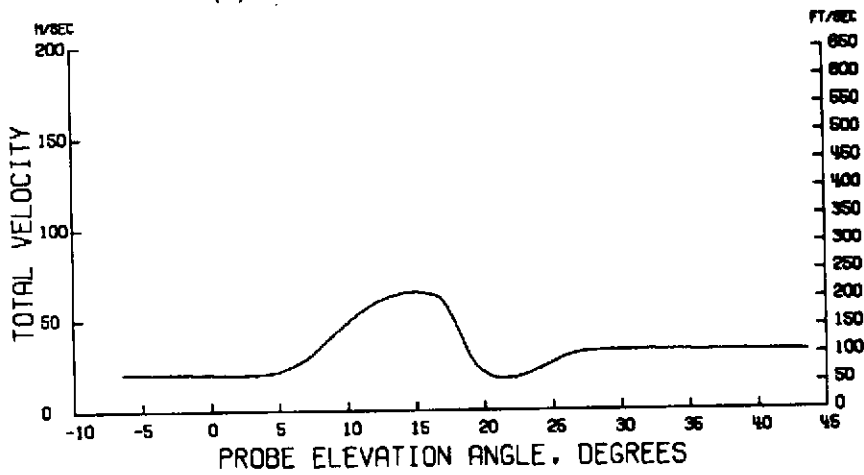
(a) Streamwise velocity profile.
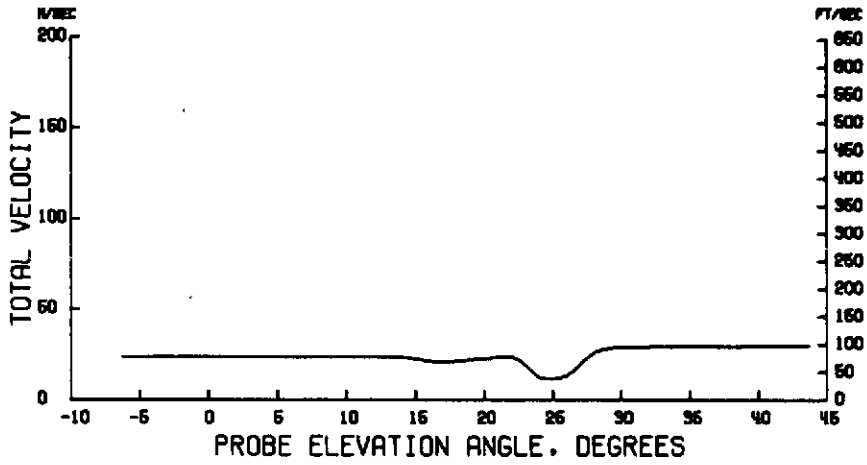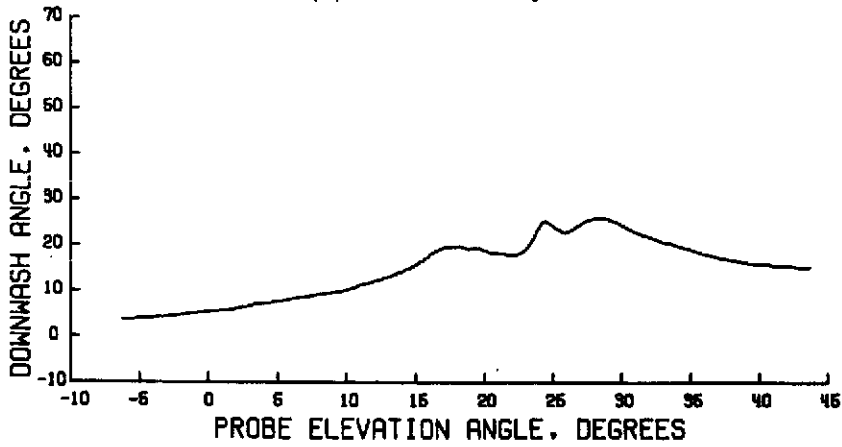


(b) Total velocity.



(c) Downwash angle.

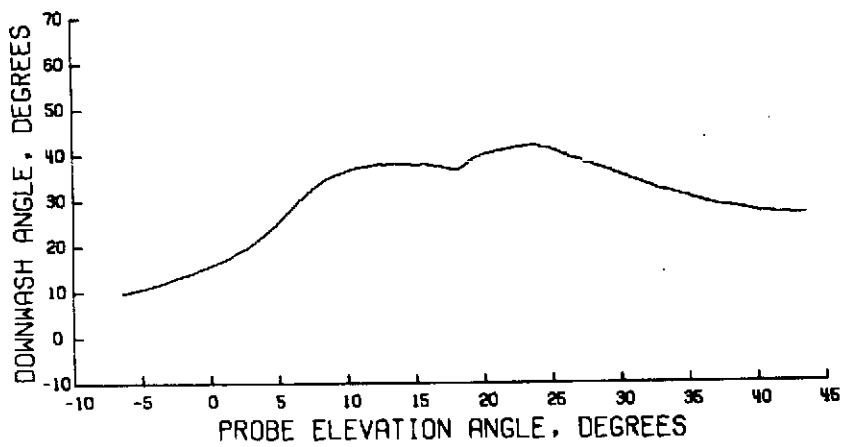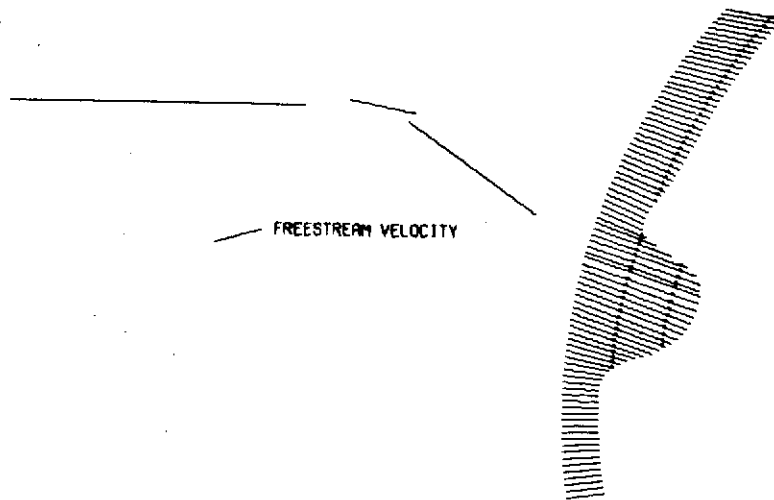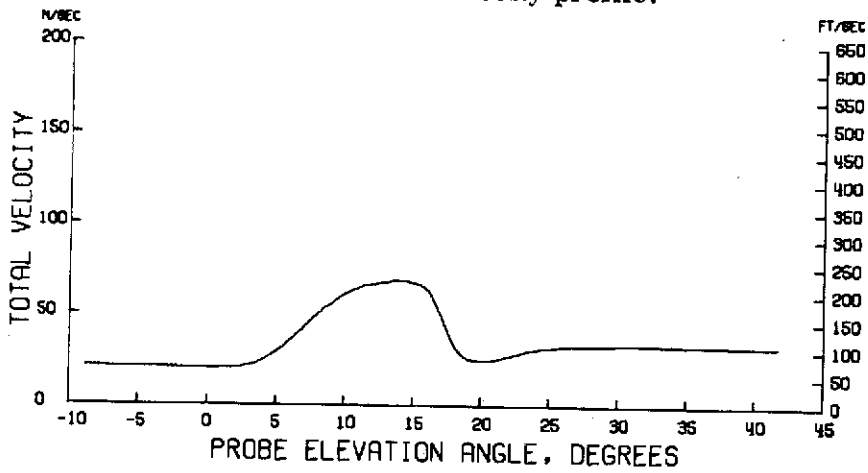Figure 37.- Wake survey results for $\eta = 0.469$; $\alpha = 8^O$; $C_T = 0$;
$V_\infty = 25.42$ m/sec (83.41 ft/sec).
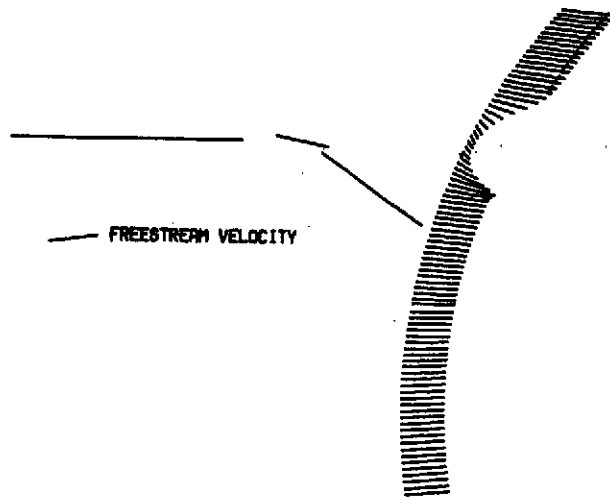
(a) Streamwise velocity profile.
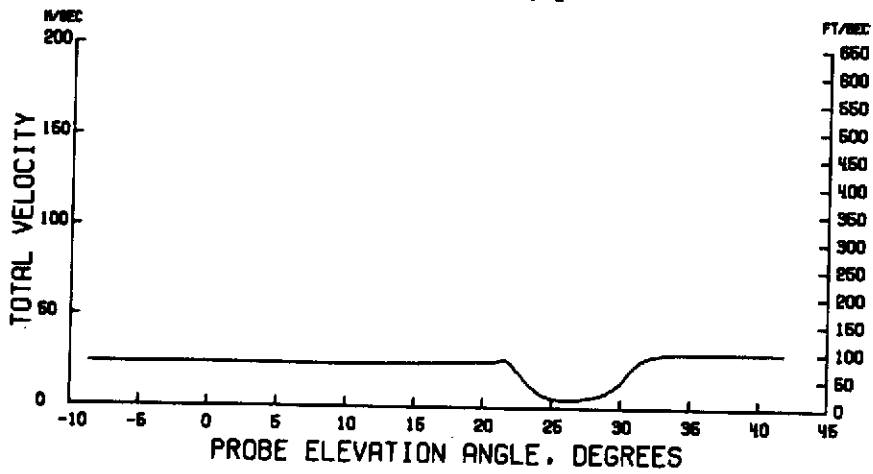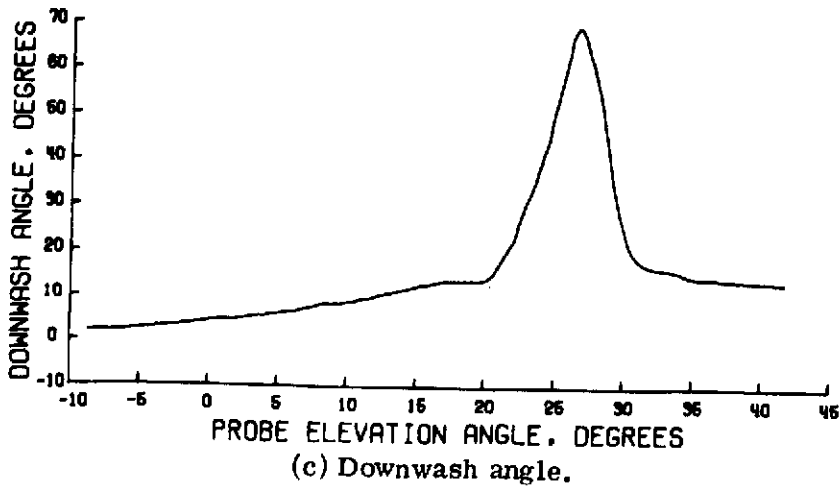


(b) Total velocity.



(c) Downwash angle.

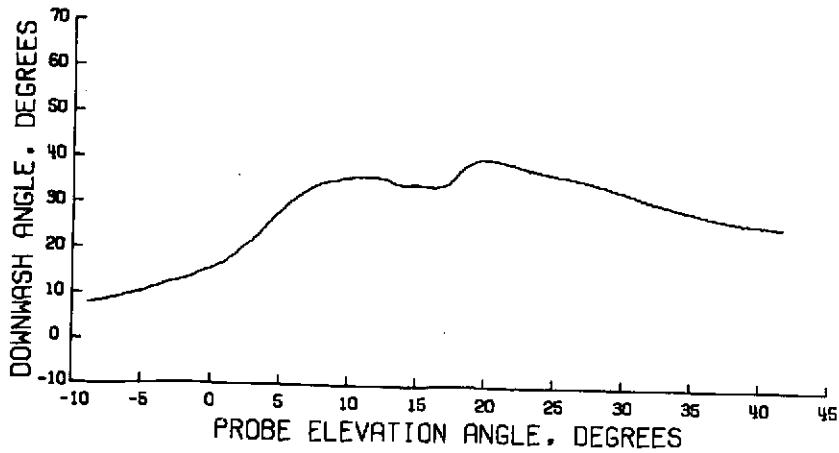Figure 38.- Wake survey results for $\eta = 0.562$; $\alpha = 8^{O}$; $C_T = 0$; $V_\infty = 25.49$ m/sec (83.64 ft/sec).
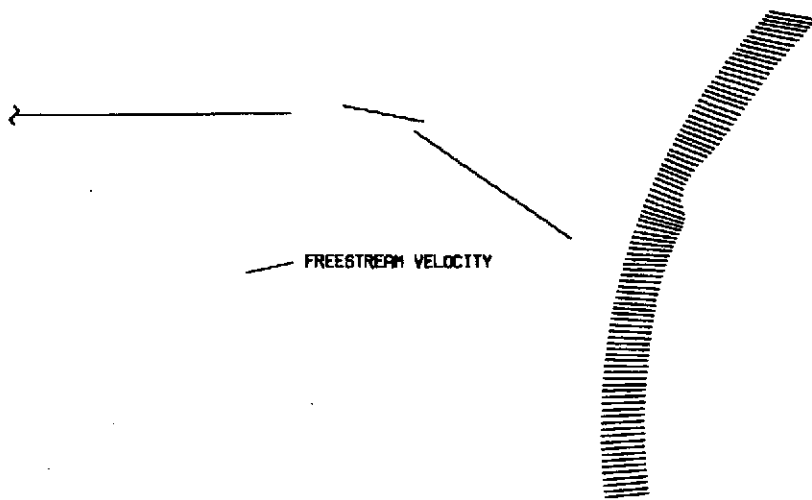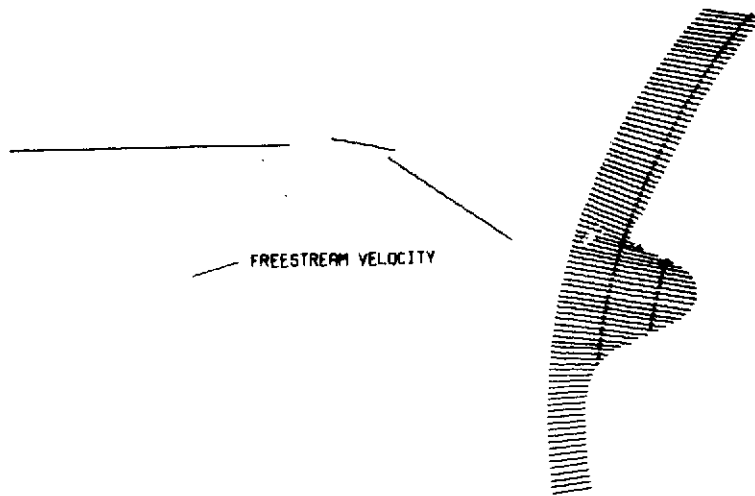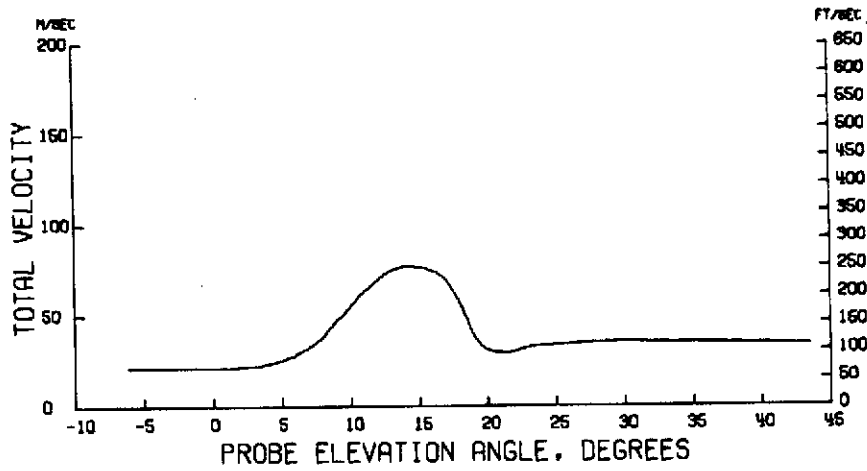
(a) Streamwise velocity profile.
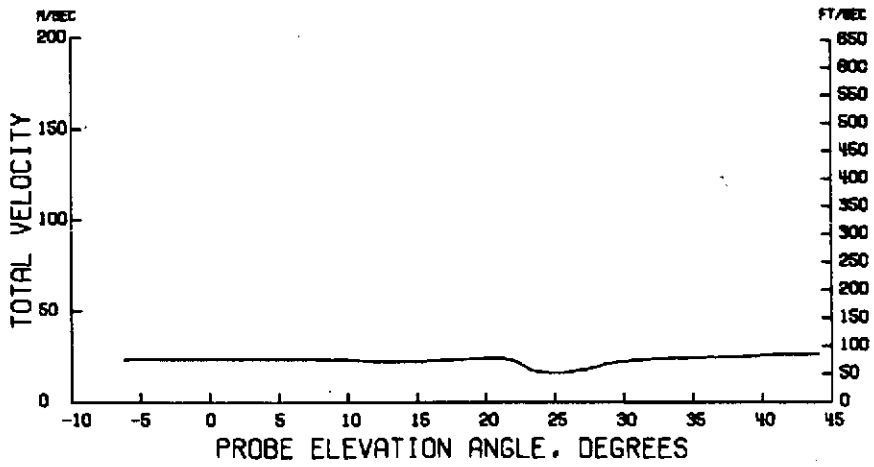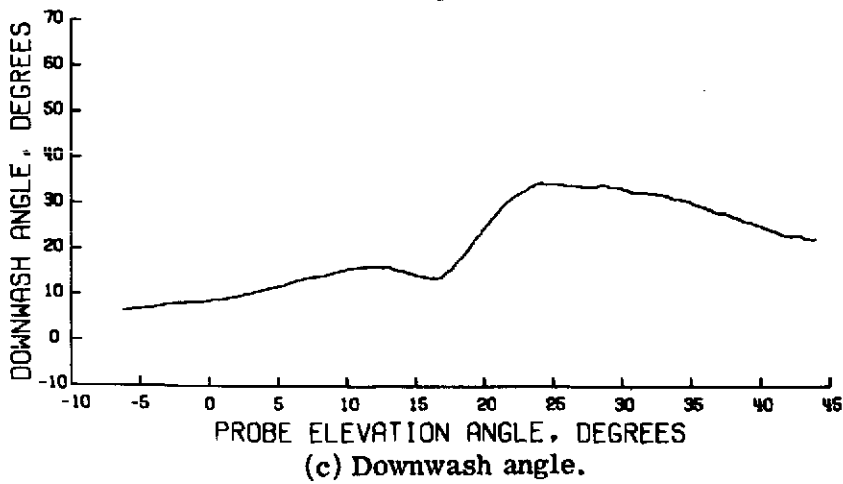


(b) Total velocity.



(c) Downwash angle.

Figure 39.- Wake survey results for $\eta = 0.162$; $\alpha = 12^{\circ}$; $C_T = 0$;
$V_{\infty} = 25.39$ m/sec (83.32 ft/sec).
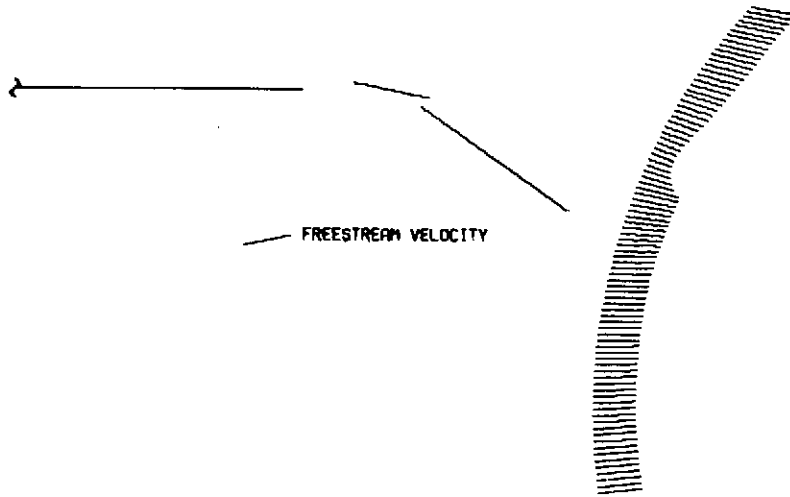
(a) Streamwise velocity profile.
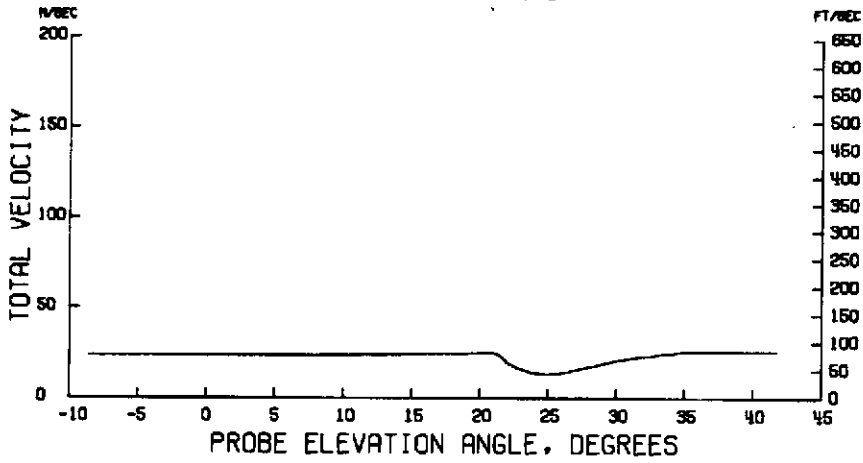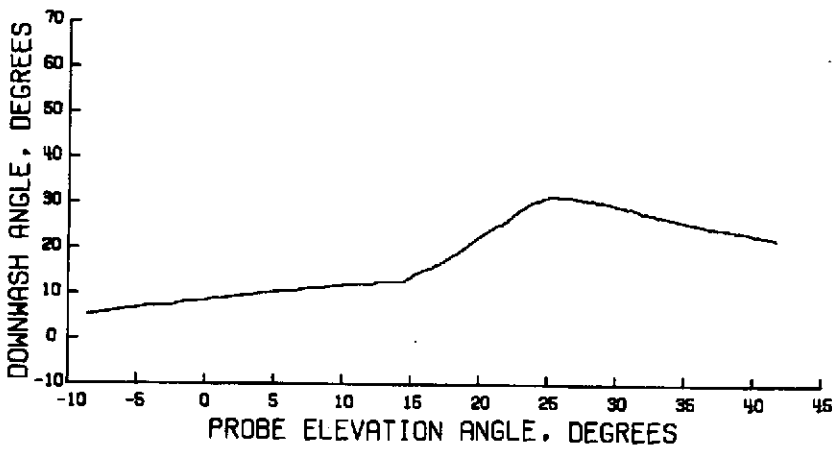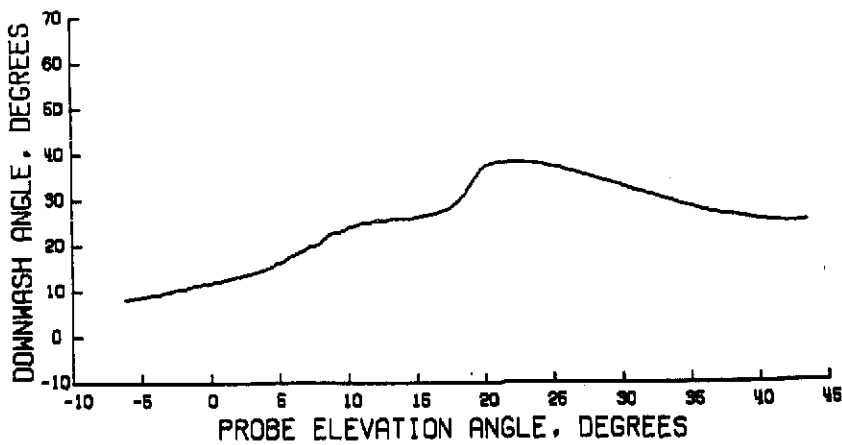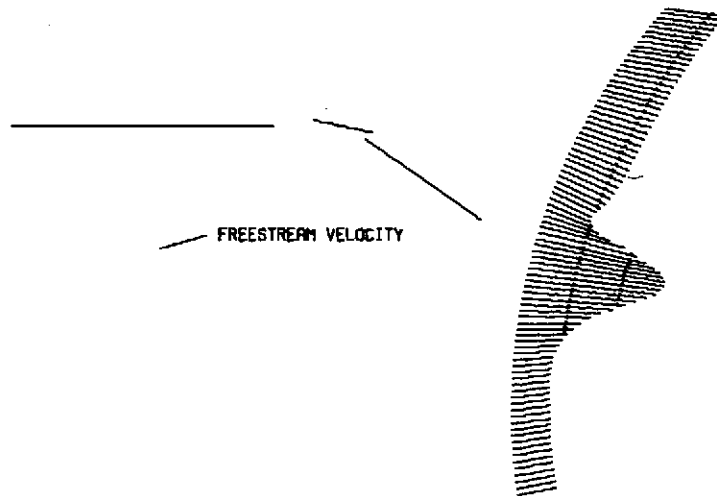


(b) Total velocity.



(c) Downwash angle.

Figure 40.- Wake survey results for $\eta = 0.201$; $\alpha = 12^O$; $C_T = 0$;
$V_\infty = 25.40$ m/sec (83.34 ft/sec).
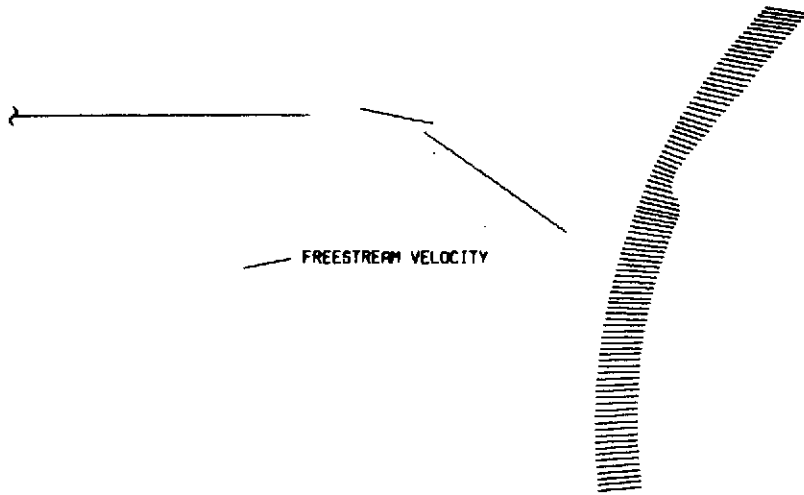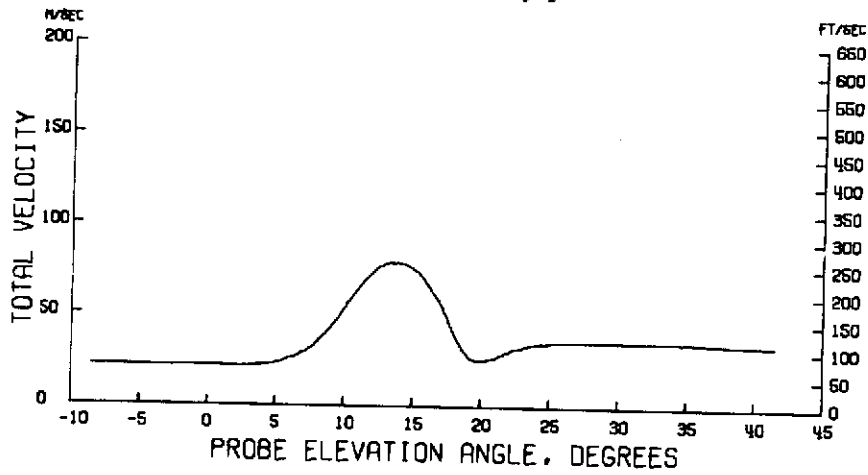
(a) Streamwise velocity profile.
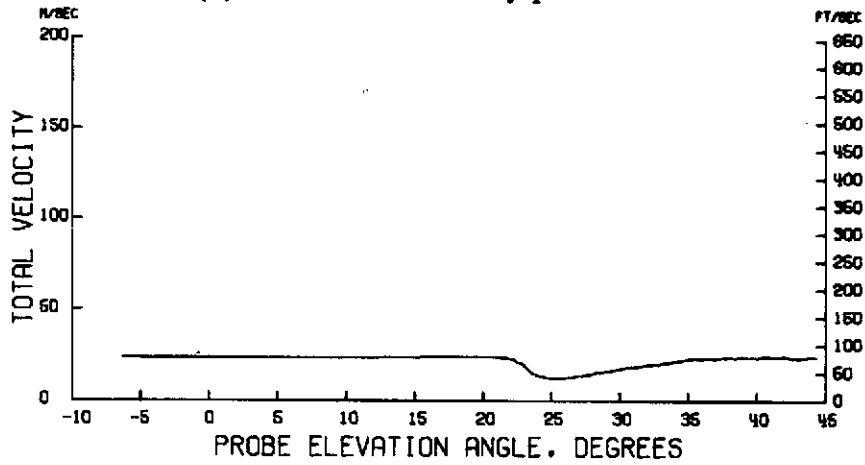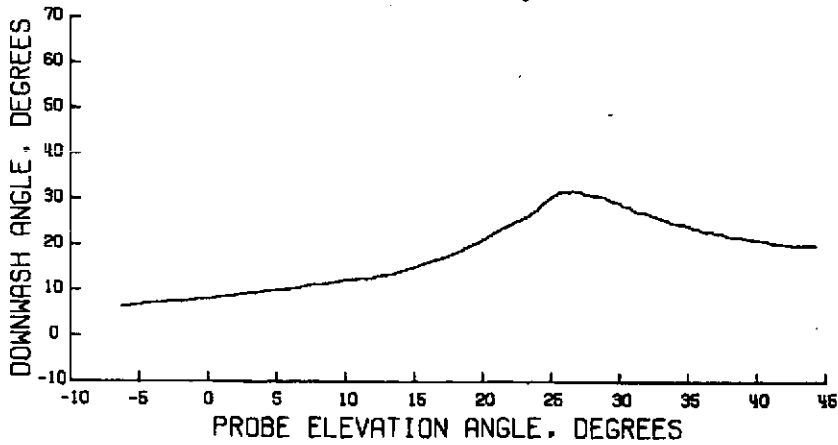


(b) Total velocity.



(c) Downwash angle.

Figure 41.- Wake survey results for $\eta = 0.227$; $\alpha = 12^{\circ}$; $C_T = 0$; $V_\infty = 25.44$ m/sec (83.49 ft/sec).
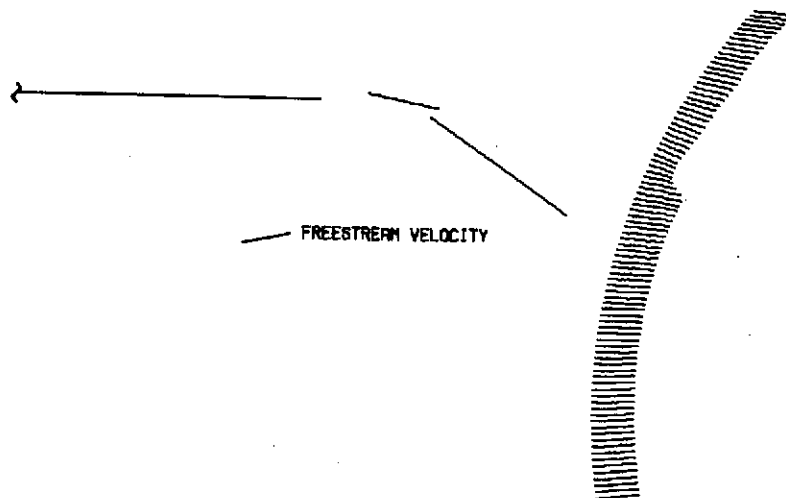
(a) Streamwise velocity profile.
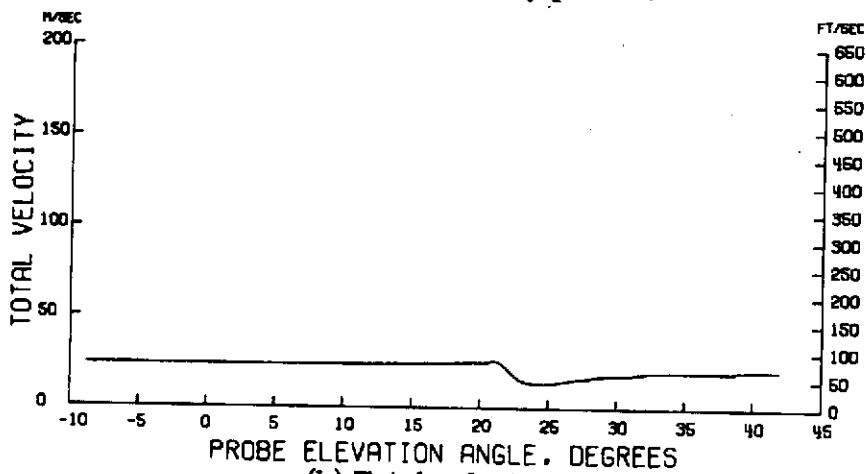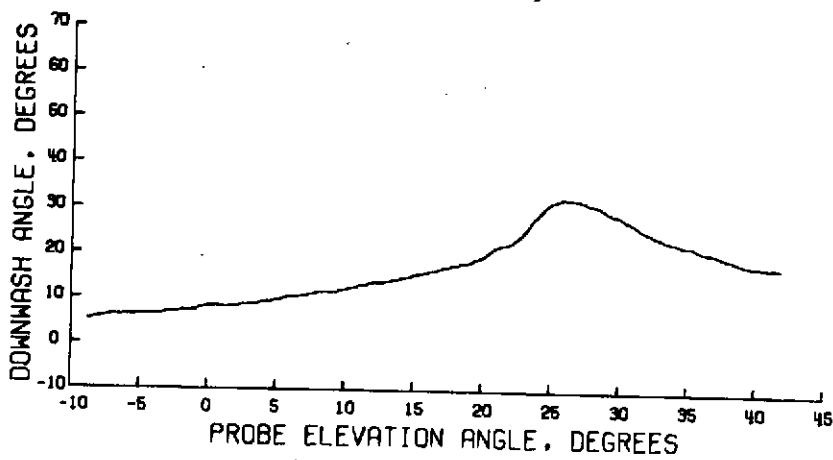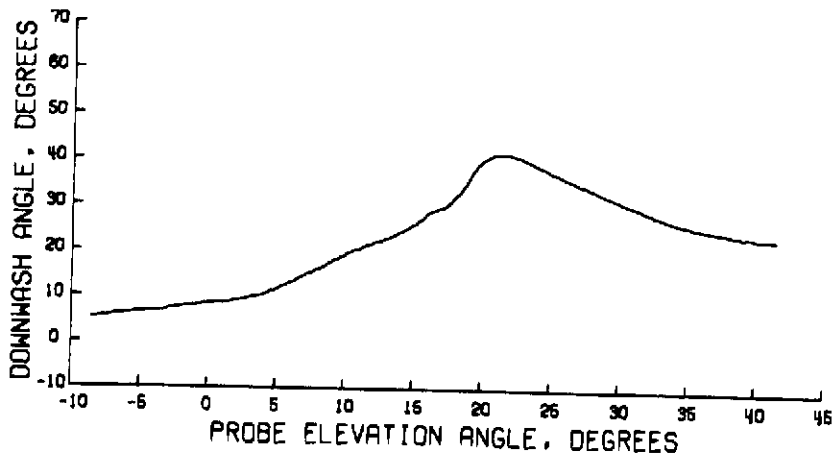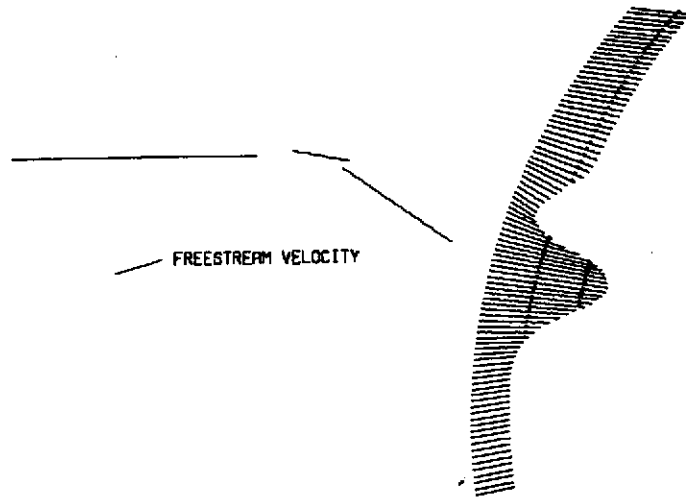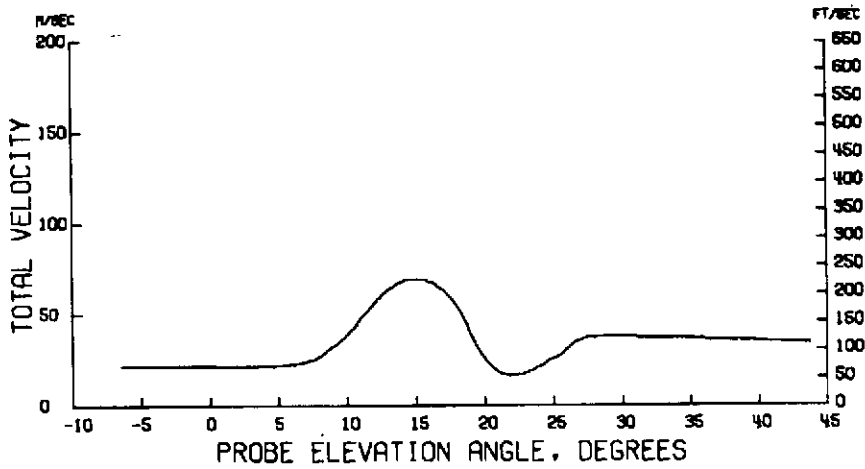


(b) Total velocity.



(c) Downwash angle.

Figure 42.- Wake survey results for $\eta = 0.254$; $\alpha = 12^O$; $C_T = 0$; $V_\infty = 25.45$ m/sec (83.50 ft/sec).

FREESTREAM VELOCITY
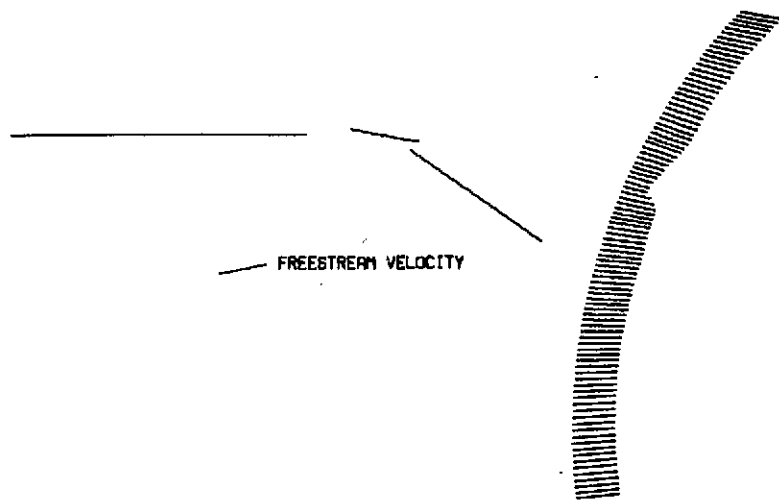
(a) Streamwise velocity profile.
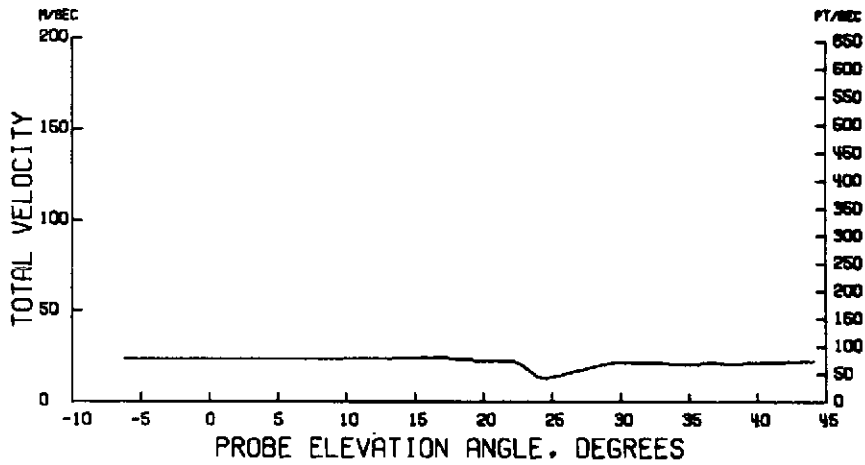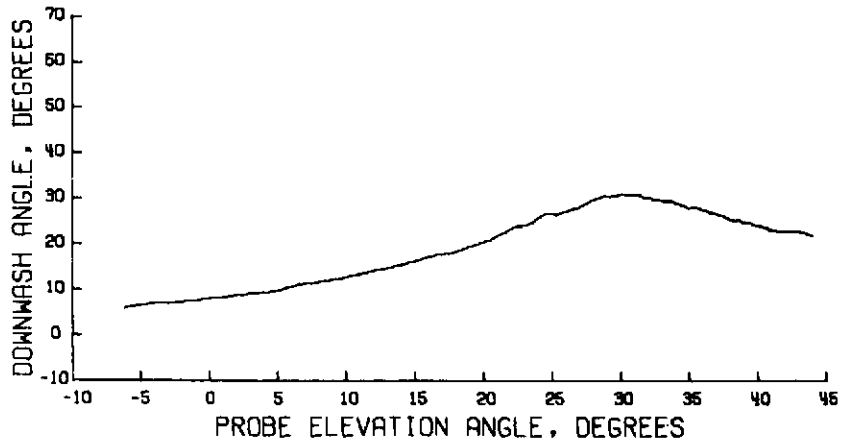


(b) Total velocity.



(c) Downwash angle.

Figure 43.- Wake survey results for $\eta = 0.294$; $\alpha = 12^O$; $C_T = 0$; $V_\infty = 25.46$ m/sec (83.55 ft/sec).
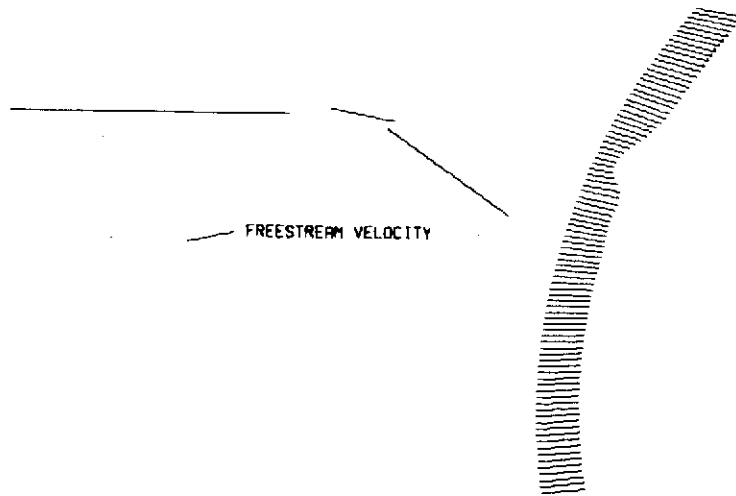
(a) Streamwise velocity profile.
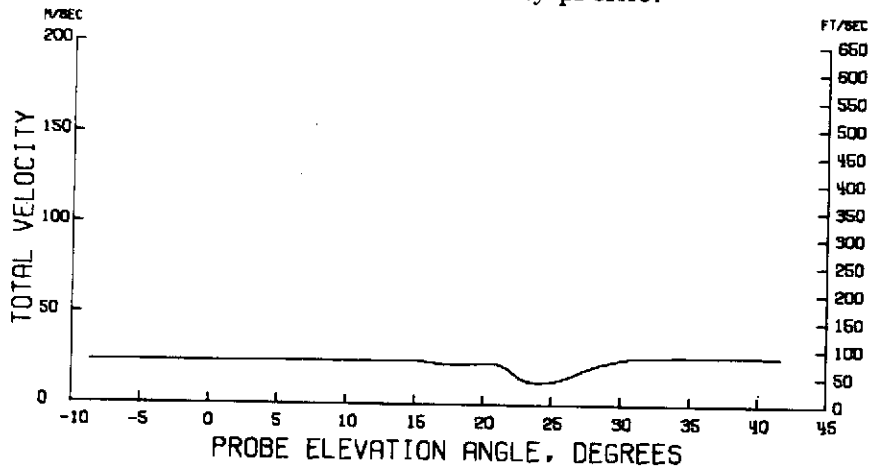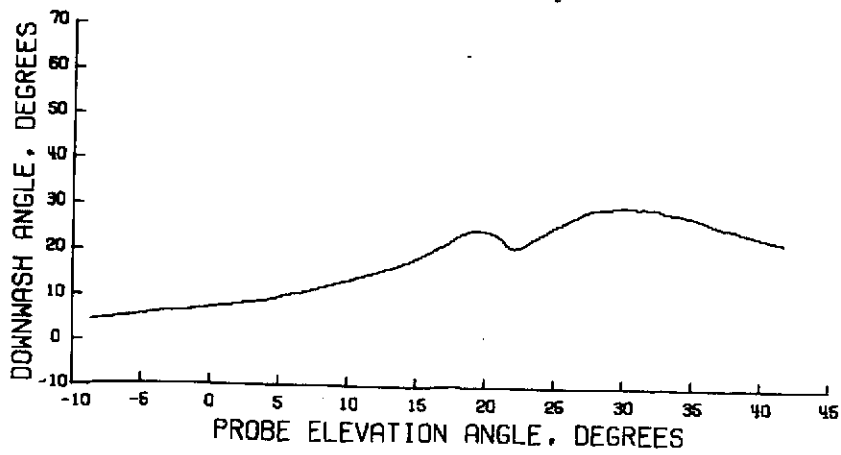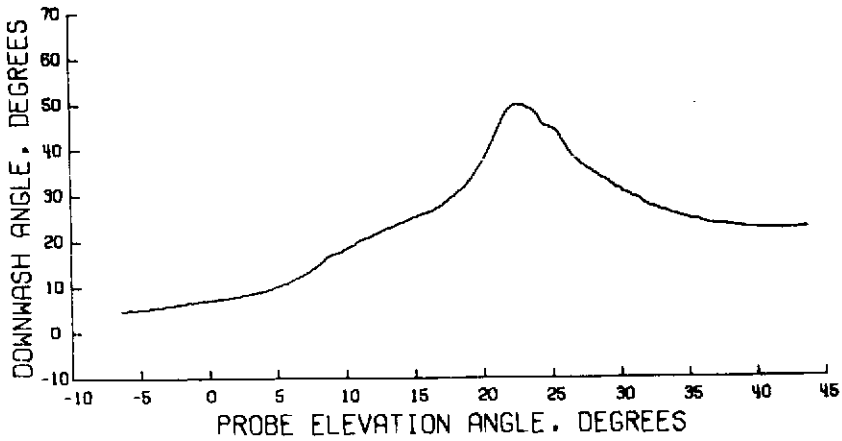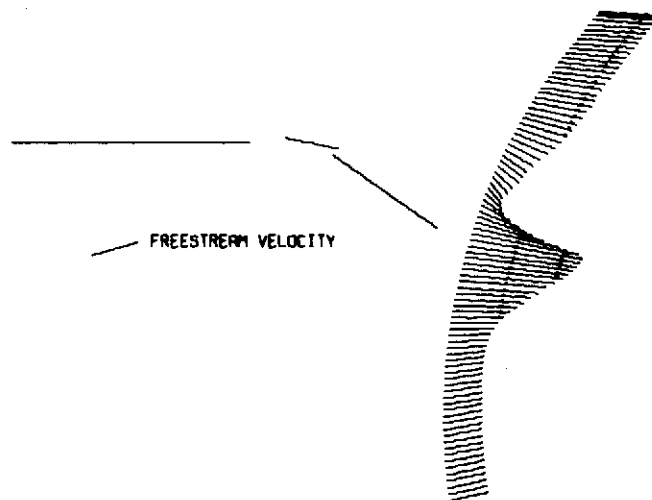


(b) Total velocity.



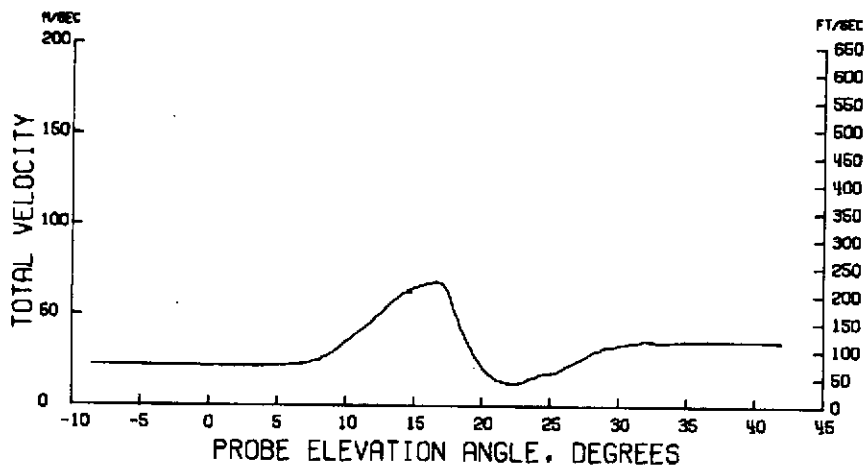(c) Downwash angle.

Figure 44.- Wake survey results for $\eta = 0.335$; $\alpha = 12^O$; $C_T = 0$; $V_\infty = 25.46$ m/sec (83.56 ft/sec).
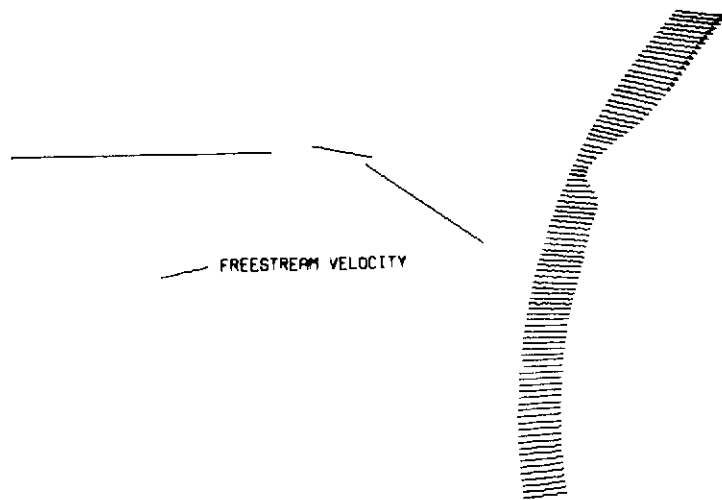
(a) Streamwise velocity profile.
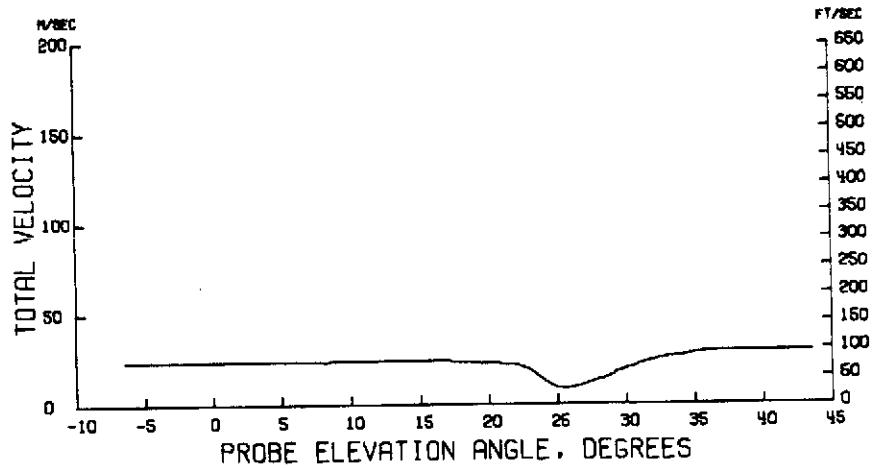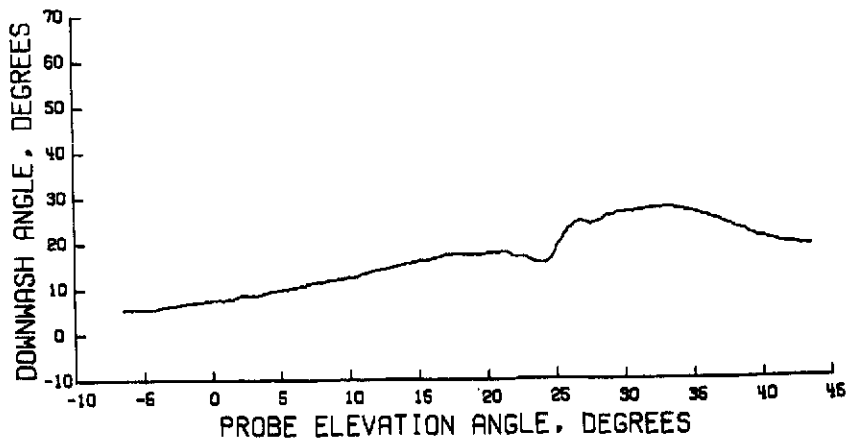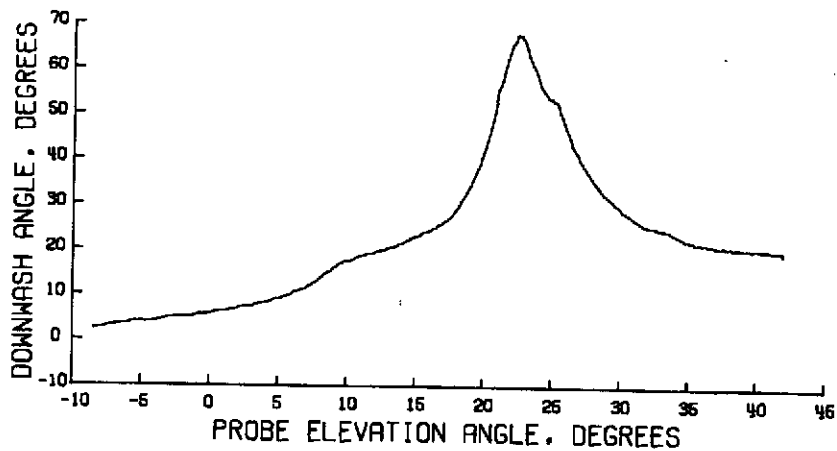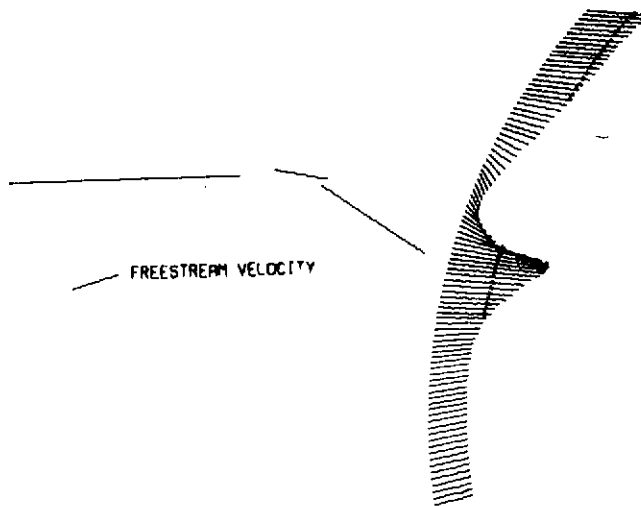


(b) Total velocity.



(c) Downwash angle.

Figure 45.- Wake survey results for $\eta = 0.376$; $\alpha = 12^{O}$; $C_T = 0$; $V_\infty = 25.66$ m/sec (84.20 ft/sec).
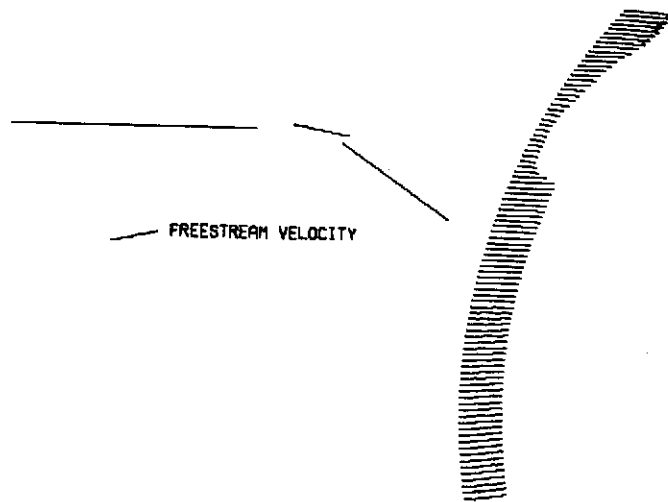
(a) Streamwise velocity profile.
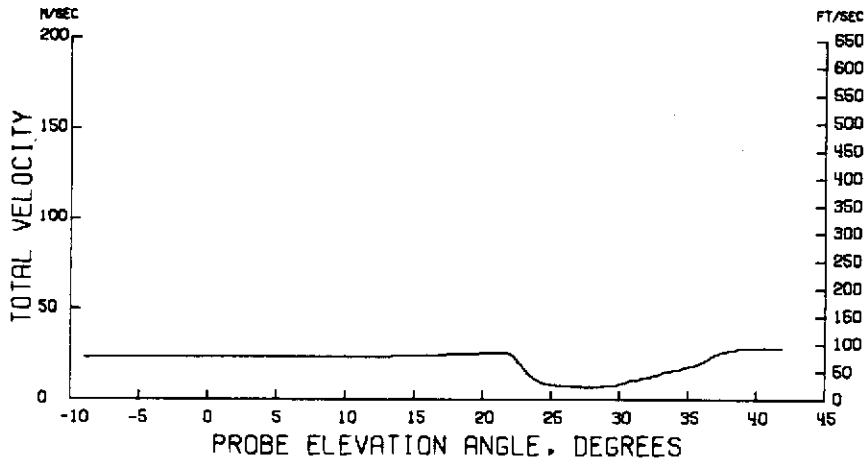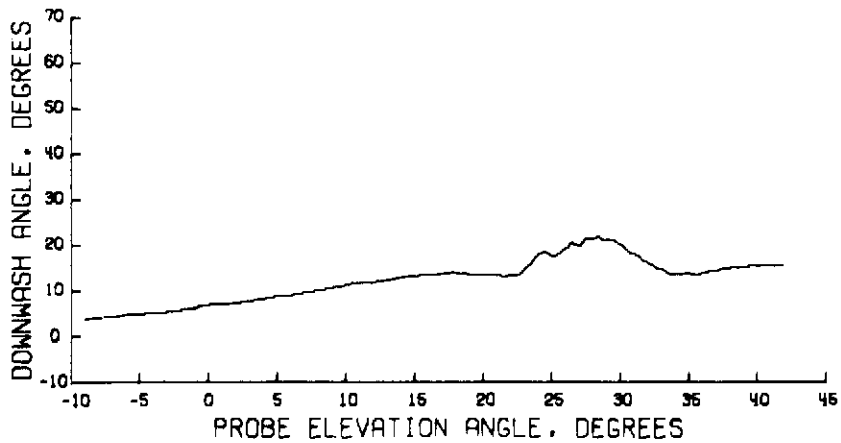


(b) Total velocity.



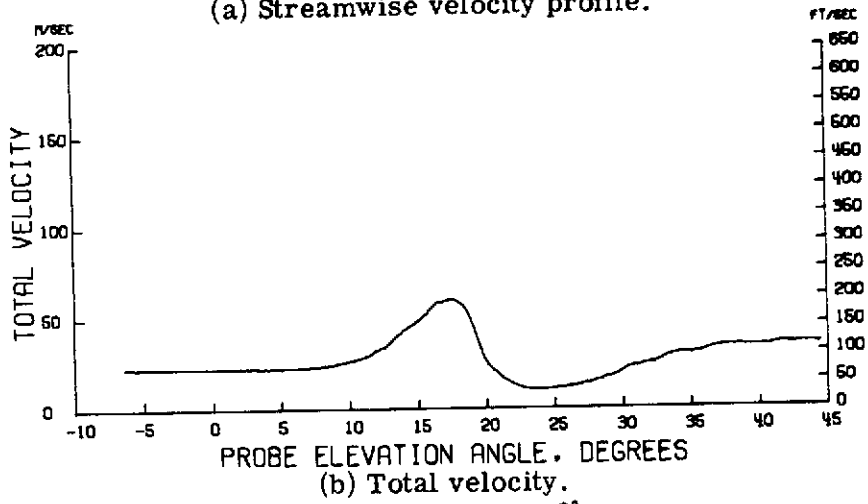(c) Downwash angle.

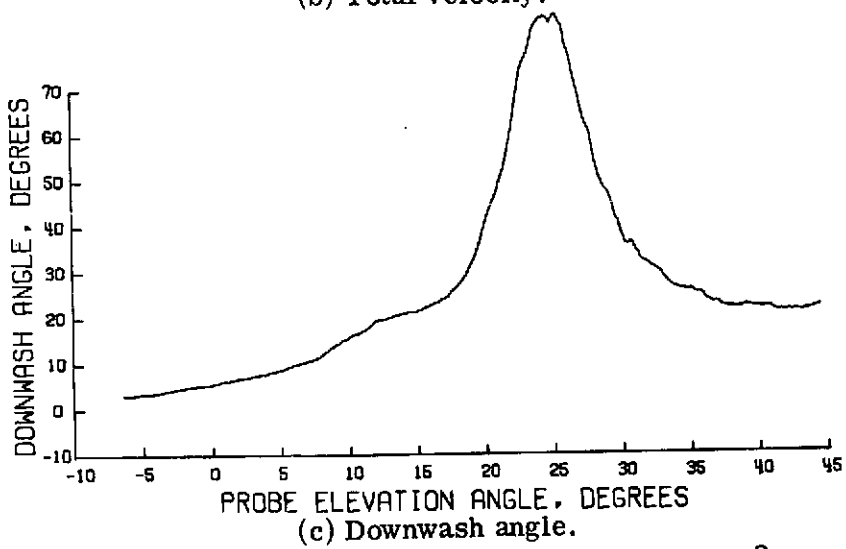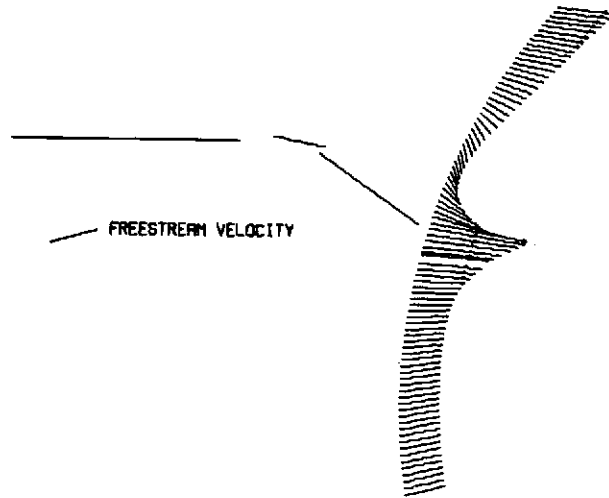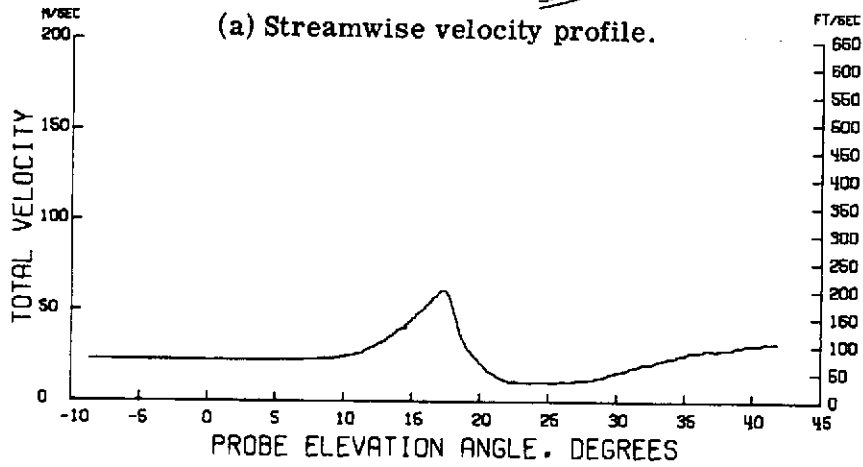Figure 46.- Wake survey results for $\eta = 0.416$; $\alpha = 12^O$; $C_T = 0$; $V_\infty = 25.38$ m/sec (83.27 ft/sec).
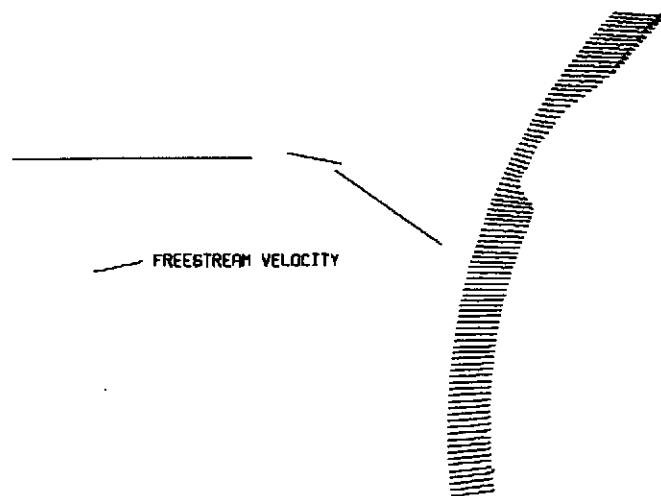
(a) Streamwise velocity profile.
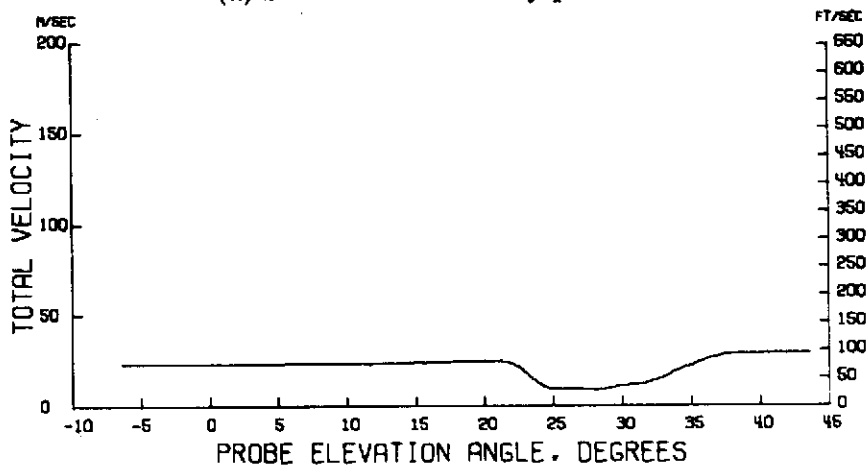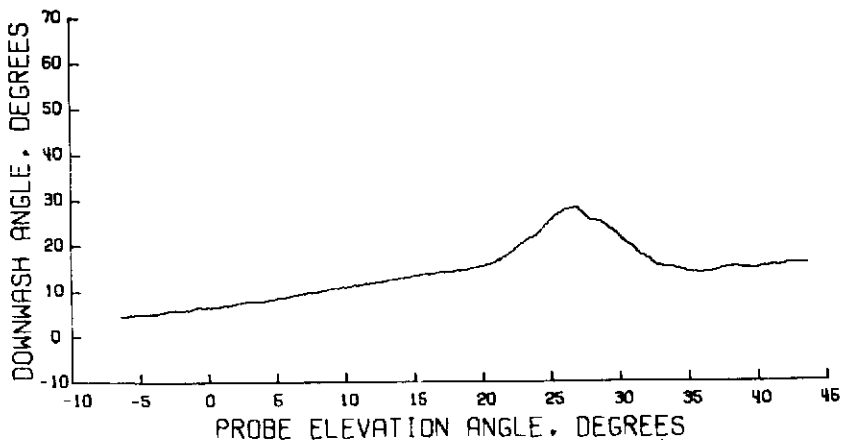


(b) Total velocity.



(c) Downwash angle.

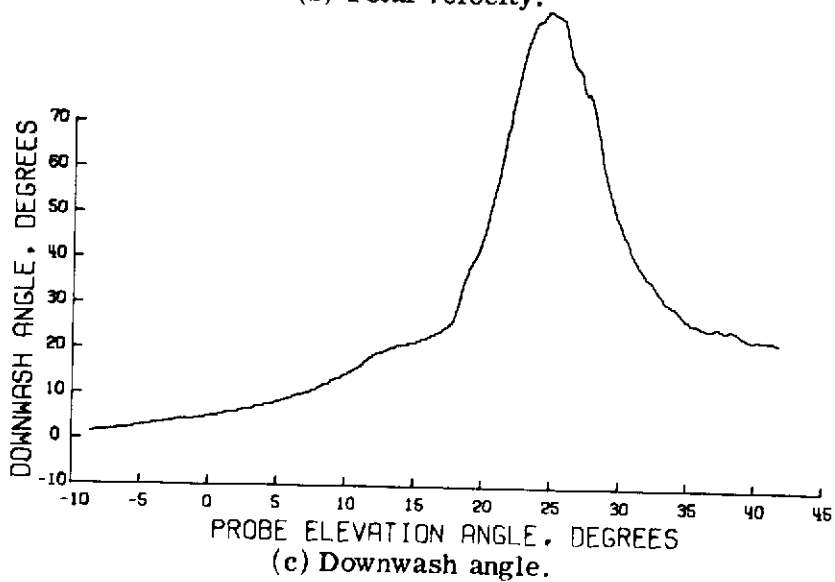Figure 47.- Wake survey results for $\eta = 0.443$; $\alpha = 12^O$; $C_T = 0$; $V_\infty = 25.44$ m/sec (83.46 ft/sec).
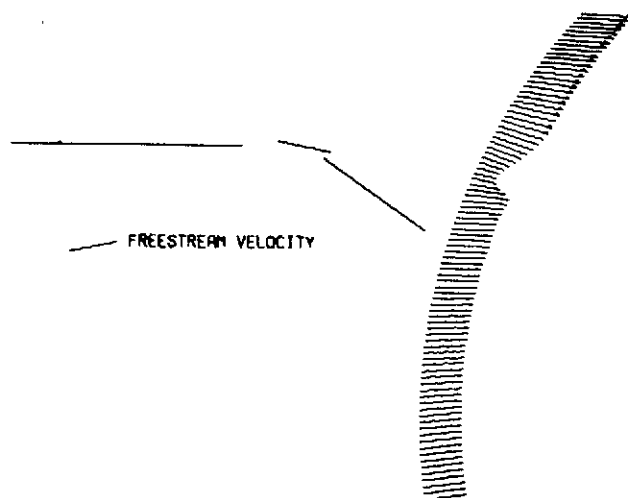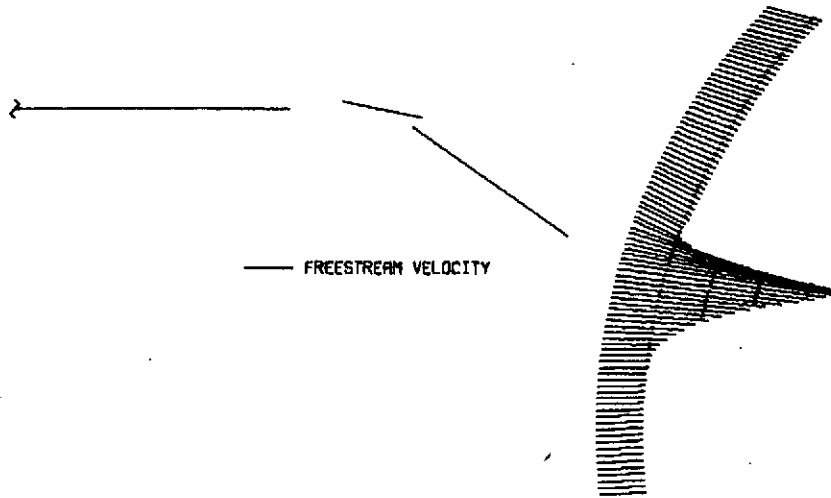
(a) Streamwise velocity profile.
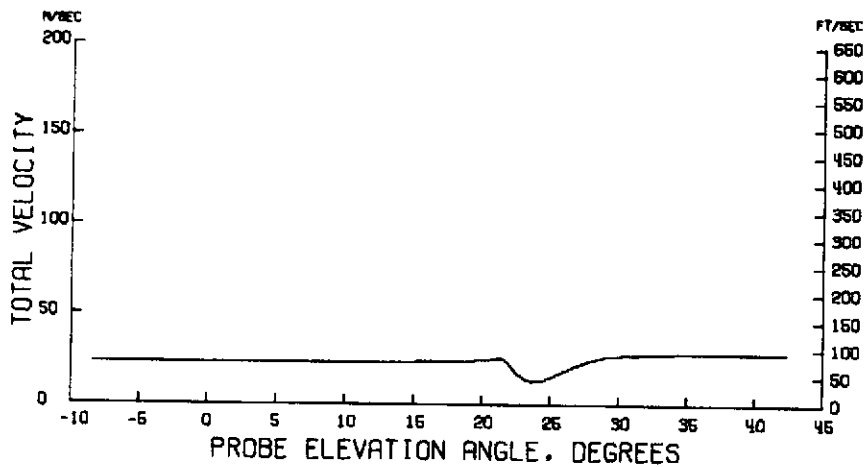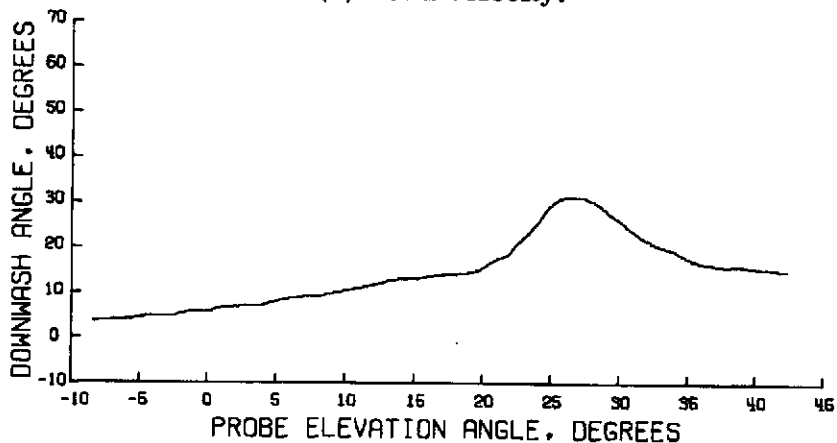


(b) Total velocity.



(c) Downwash angle.

Figure 48.- Wake survey results for $\eta = 0.470$; $\alpha = 12^O$; $C_T = 0$; $V_\infty = 25.44$ m/sec (83.48 ft/sec).
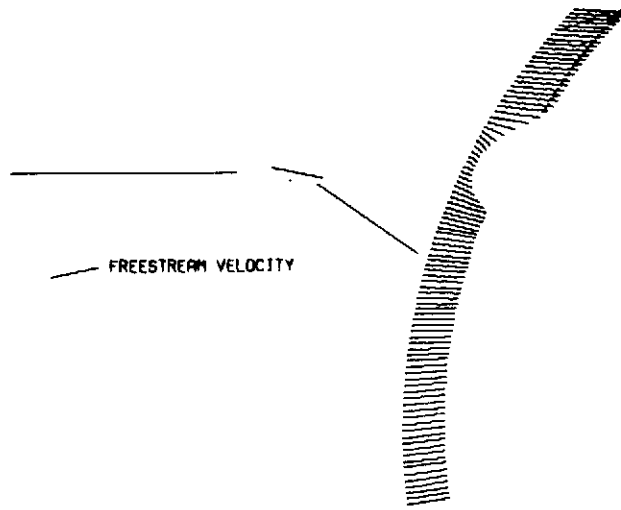
(a) Streamwise velocity profile.
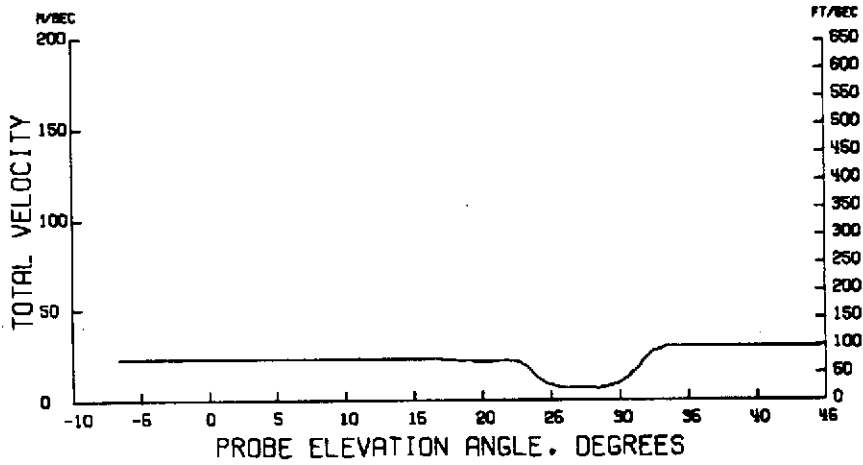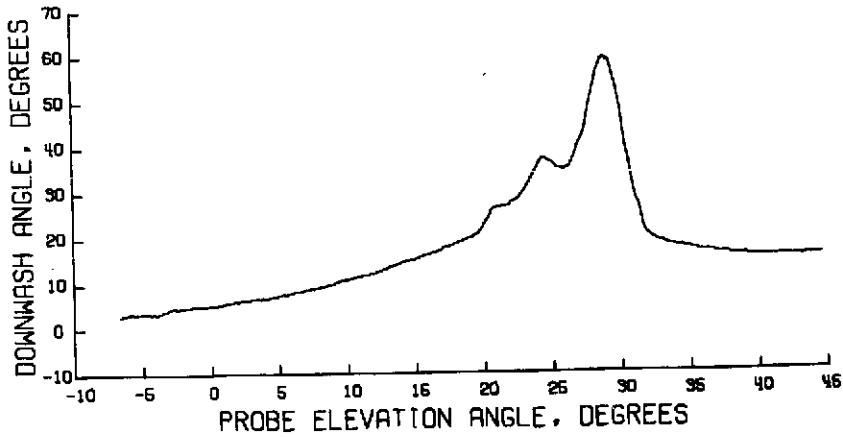


(b) Total velocity.



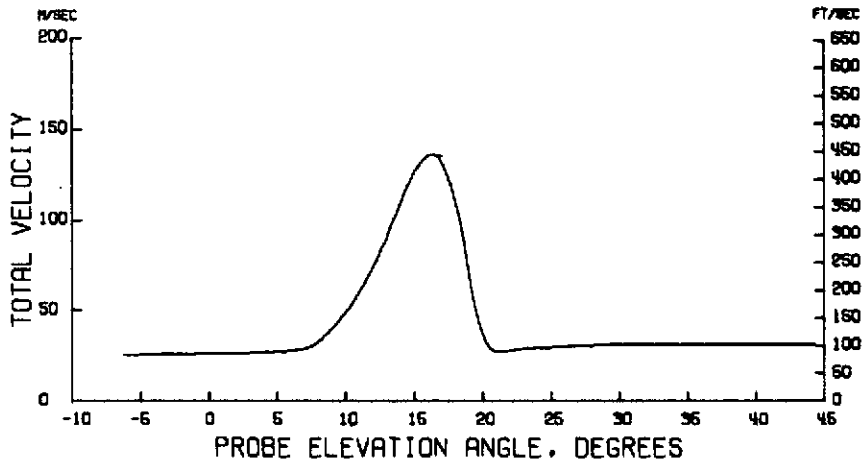(c) Downwash angle.

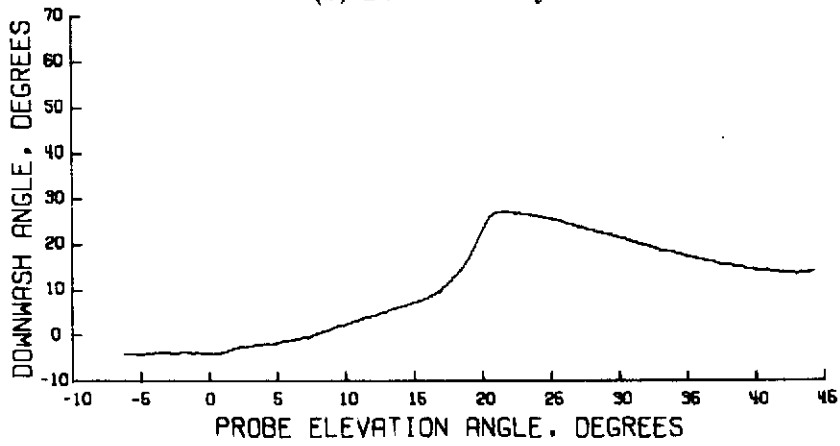Figure 49.- Wake survey results for $\eta = 0.562$; $\alpha = 12^O$; $C_T = 0$; $V_\infty = 25.34$ m/sec (83.16 ft/sec).
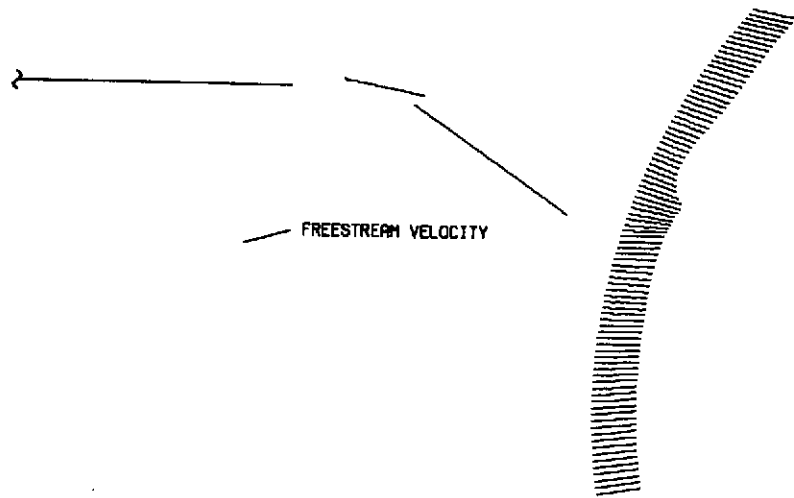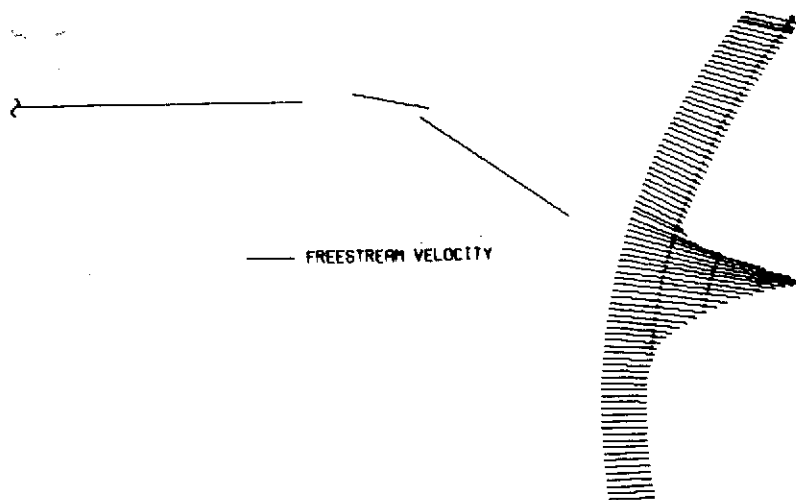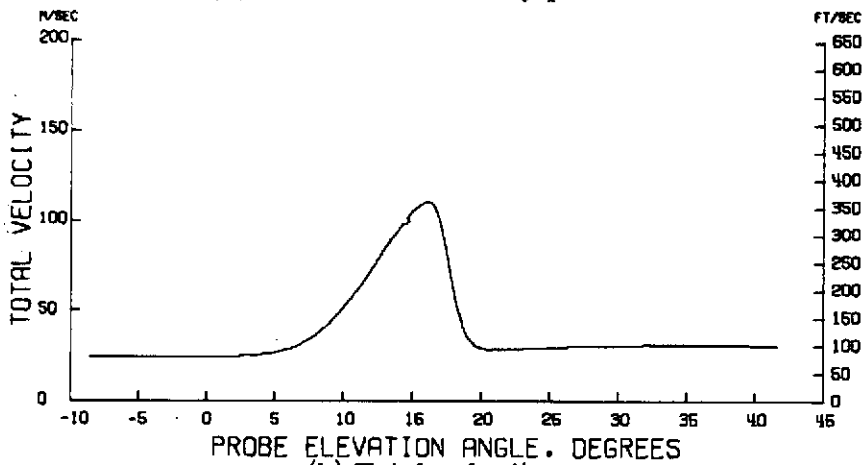
(a) Streamwise velocity profile.
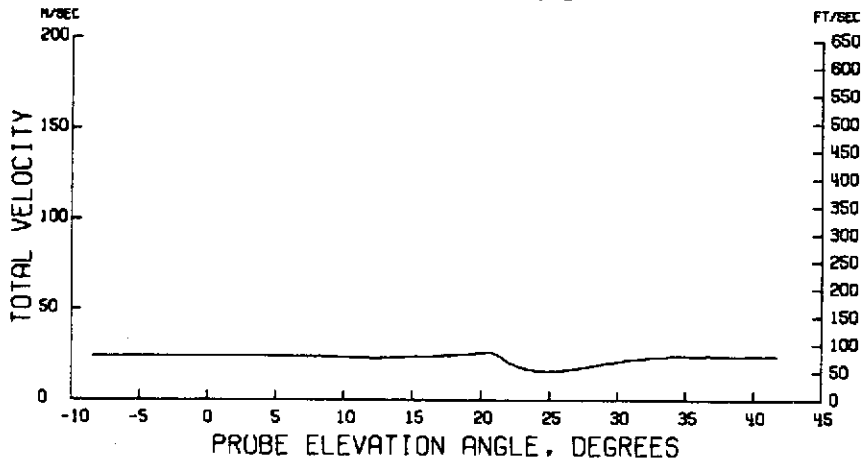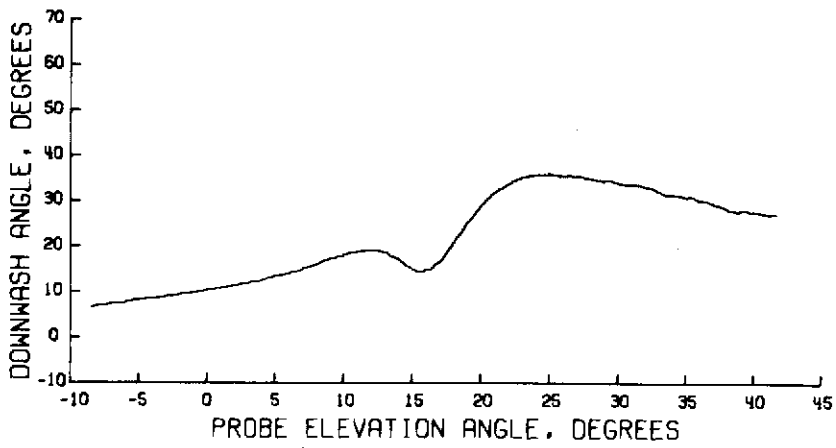


(b) Total velocity.



(c) Downwash angle.

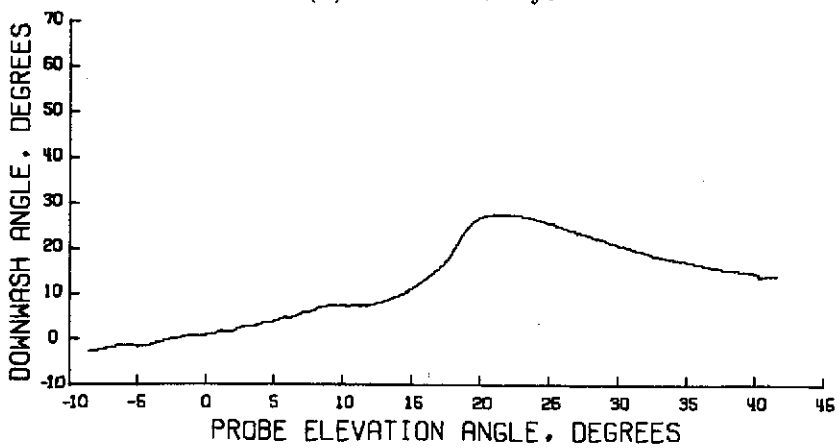Figure 50.- Wake survey results for $\eta = 0.162$; $\alpha = 16^O$; $C_T = 0$; $V_\infty = 25.50$ m/sec (83.69 ft/sec).
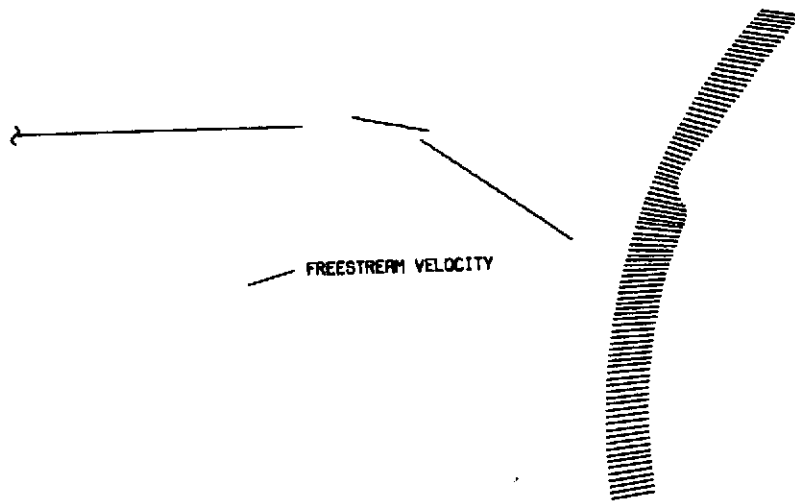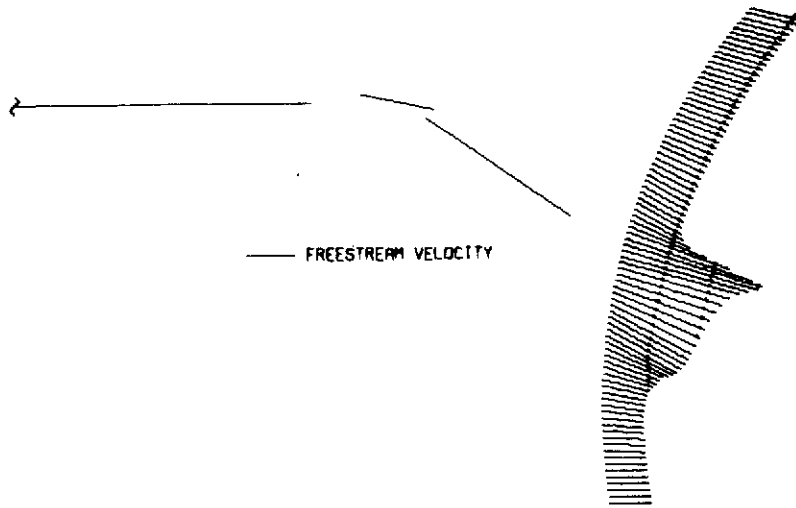
(a) Streamwise velocity profile.
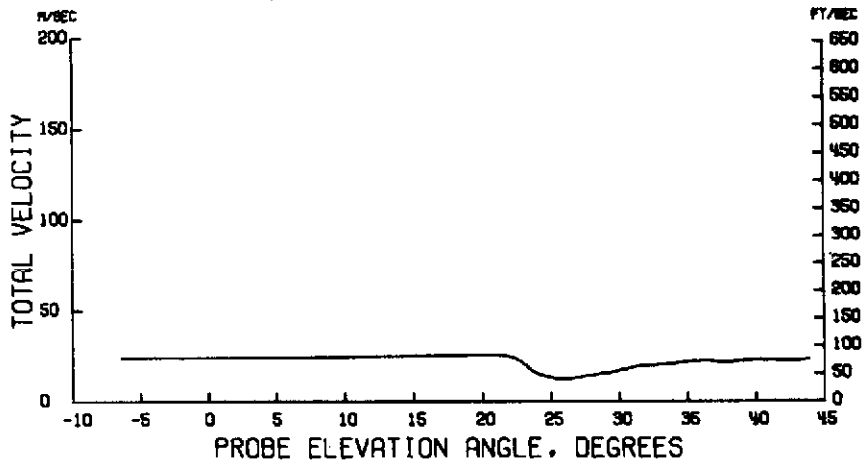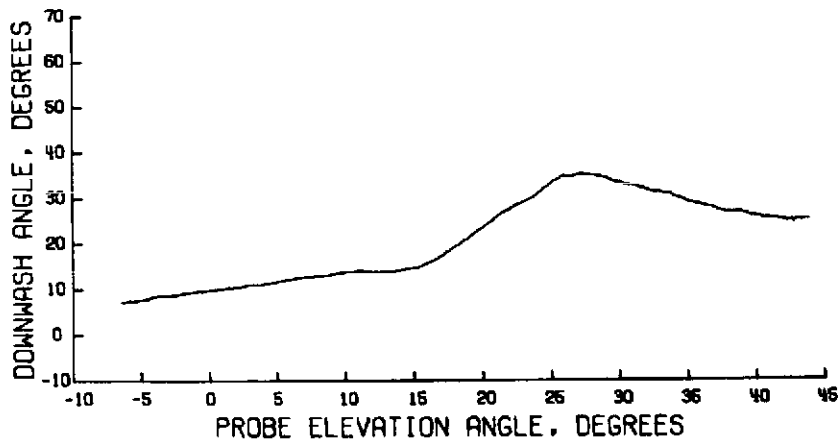


(b) Total velocity.



(c) Downwash angle.

Figure 51.- Wake survey results for $\eta = 0.201$; $\alpha = 16^O$; $C_T = 0$;
$V_\infty = 25.50$ m/sec (83.66 ft/sec).
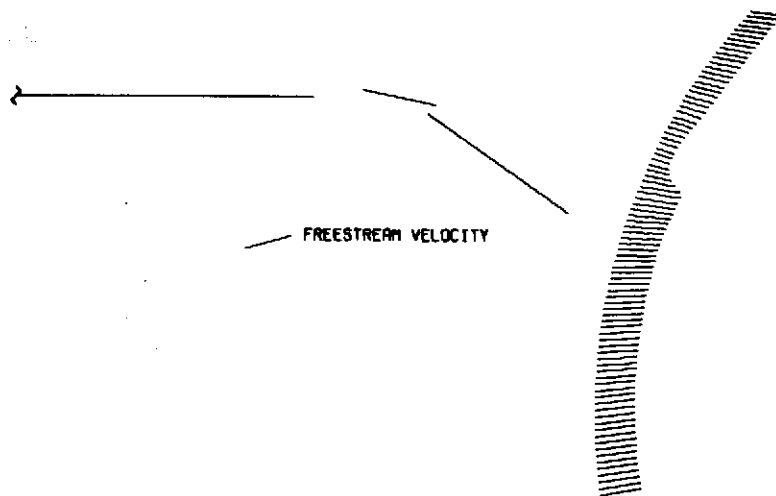
(a) Streamwise velocity profile.
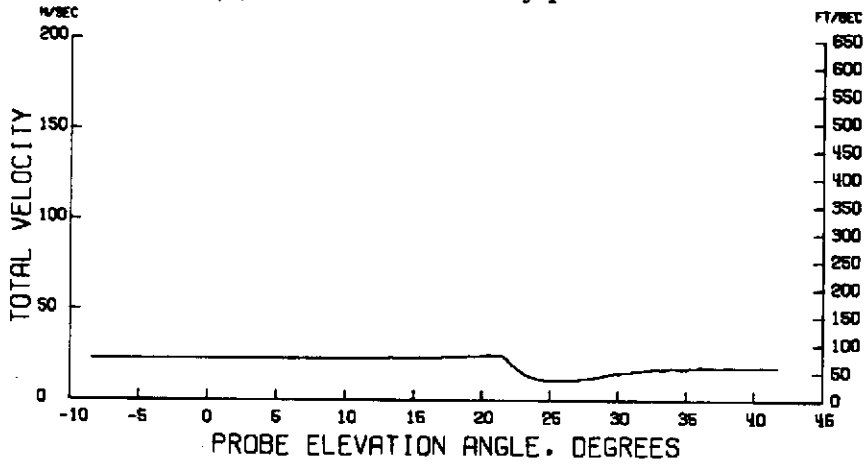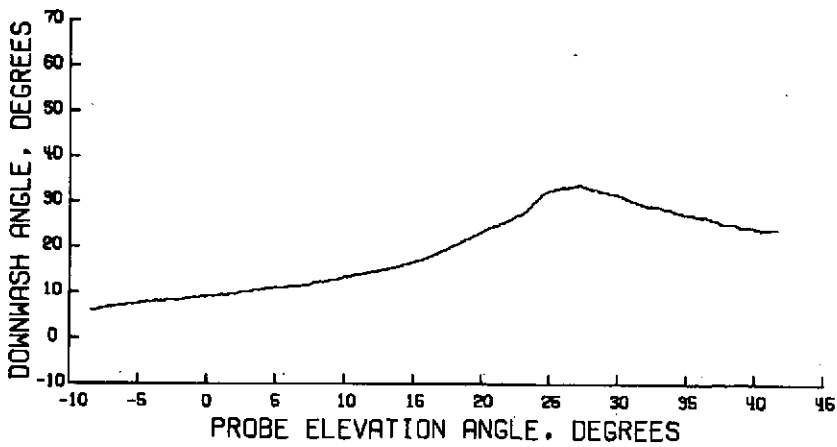


(b) Total velocity.



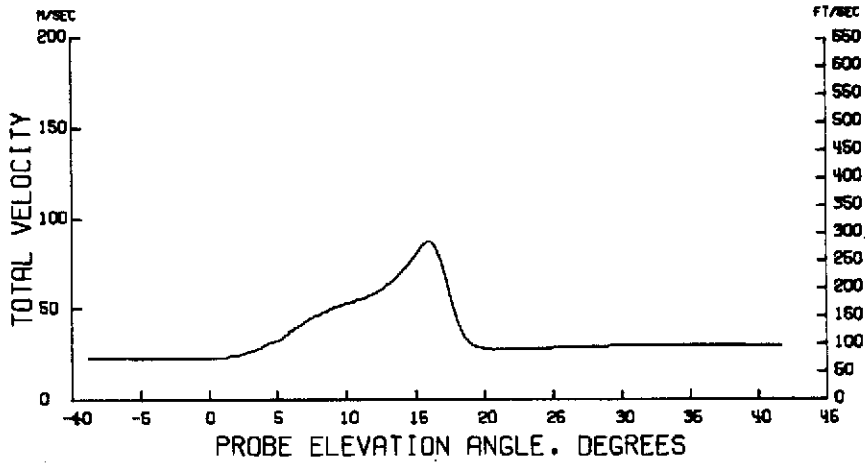(c) Downwash angle.

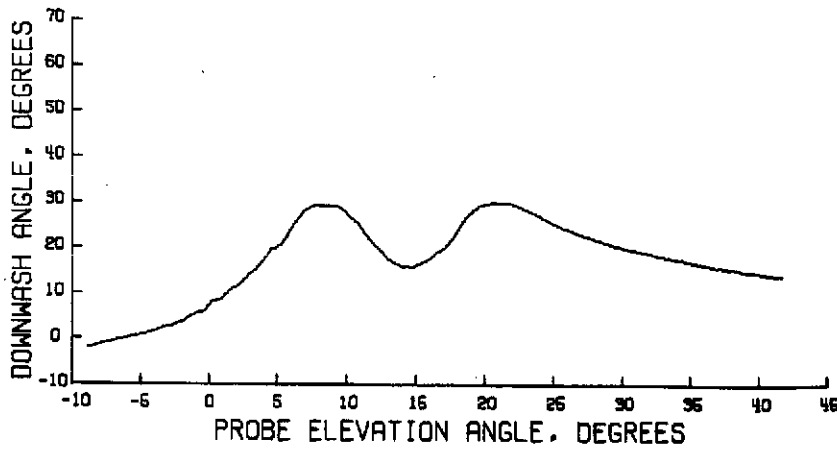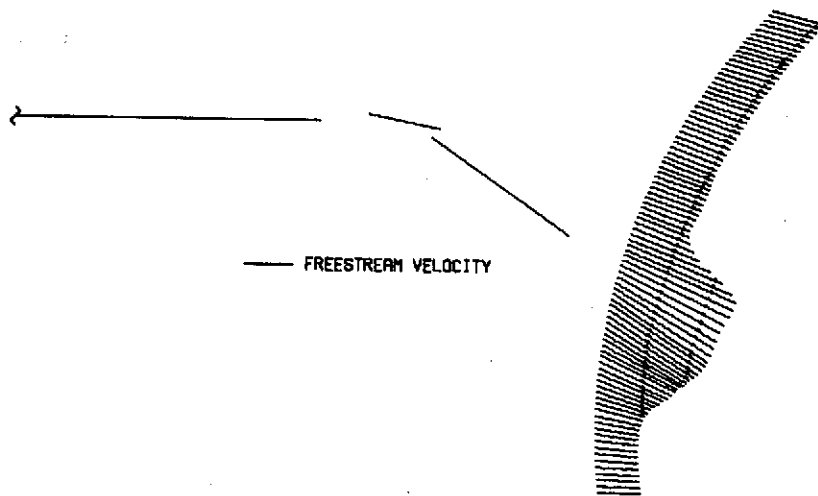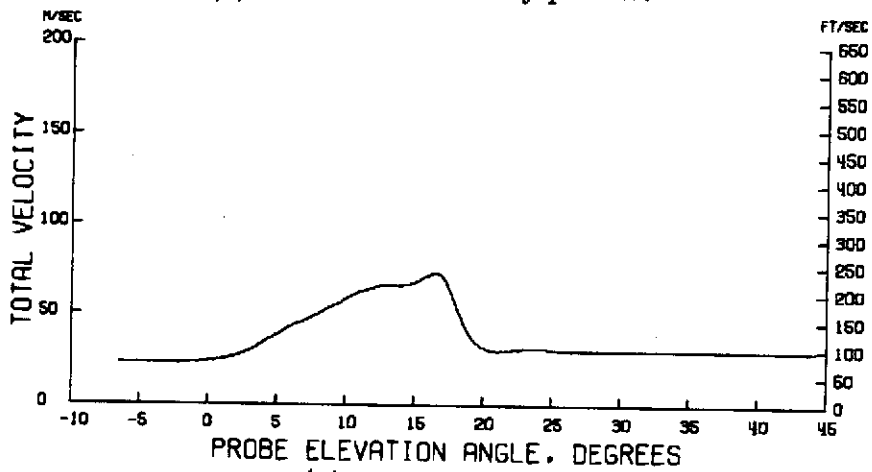Figure 52.- Wake survey results for $\eta = 0.227$; $\alpha = 16^O$; $C_T = 0$; $V_\infty = 25.17$ m/sec (82.58 ft/sec).
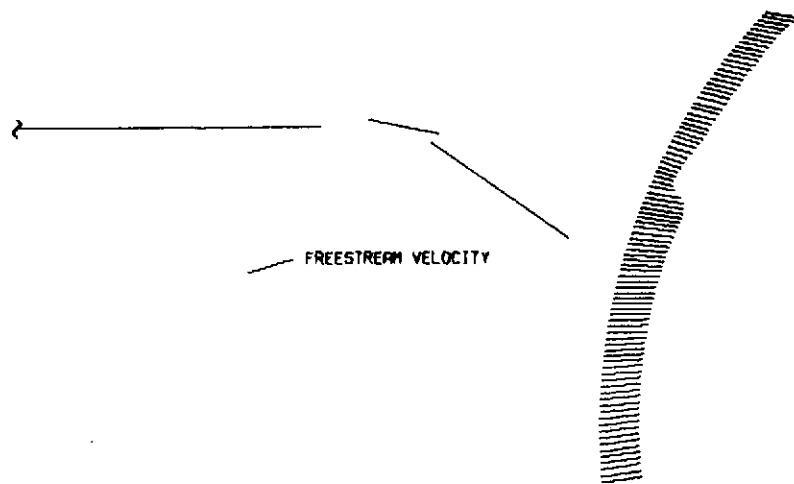
(a) Streamwise velocity profile.
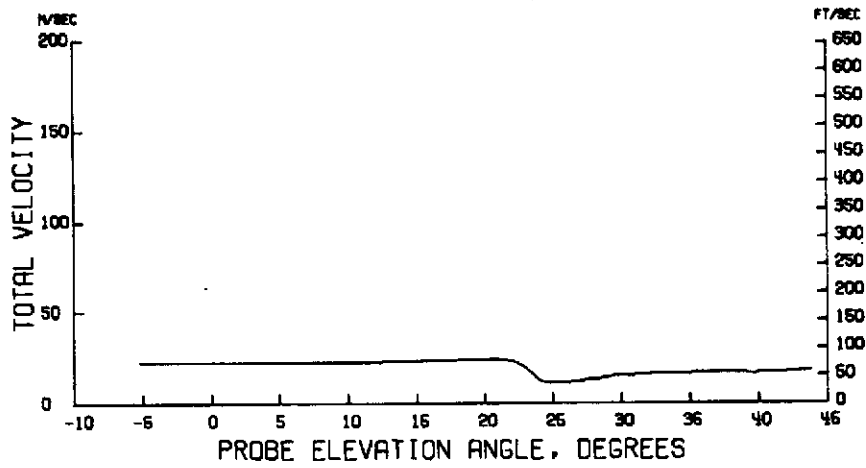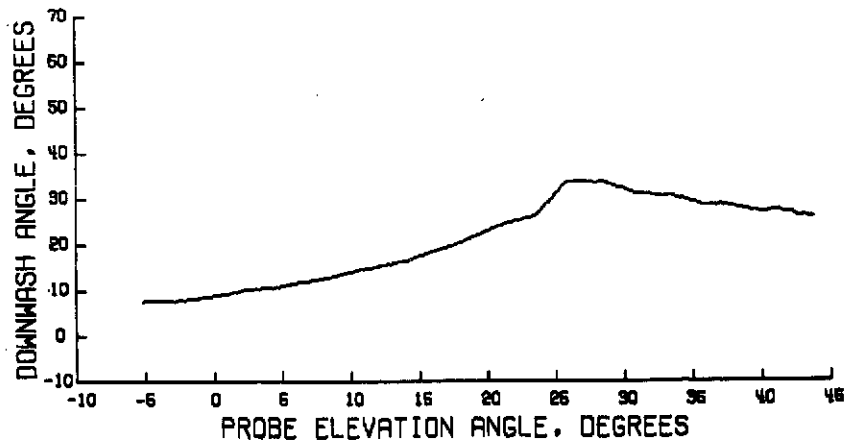


(b) Total velocity.



(c) Downwash angle.

Figure 53.- Wake survey results for $\eta = 0.254$; $\alpha = 16^{\circ}$; $C_T = 0$; $V_{\infty} = 25.34$ m/sec (83.14 ft/sec).

(a) Streamwise velocity profile.
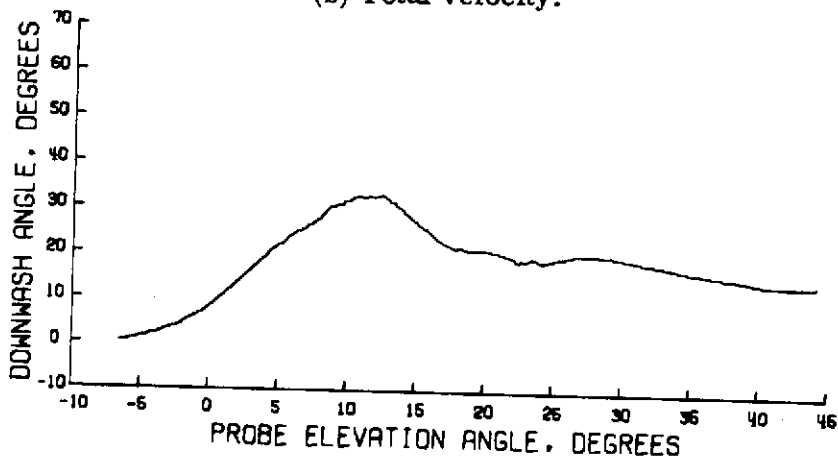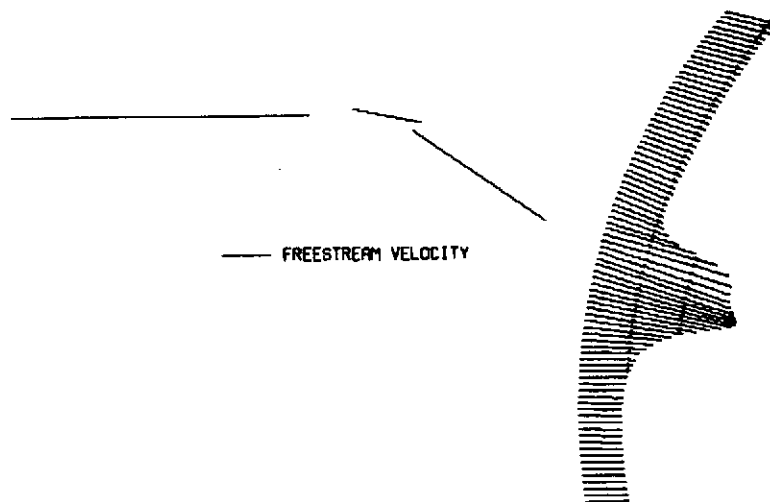


(b) Total velocity.



(c) Downwash angle.

Figure 54.- Wake survey results for $\eta = 0.294$; $\alpha = 16^O$; $C_T = 0$; $V_\infty = 25.49$ m/sec (83.65 ft/sec).
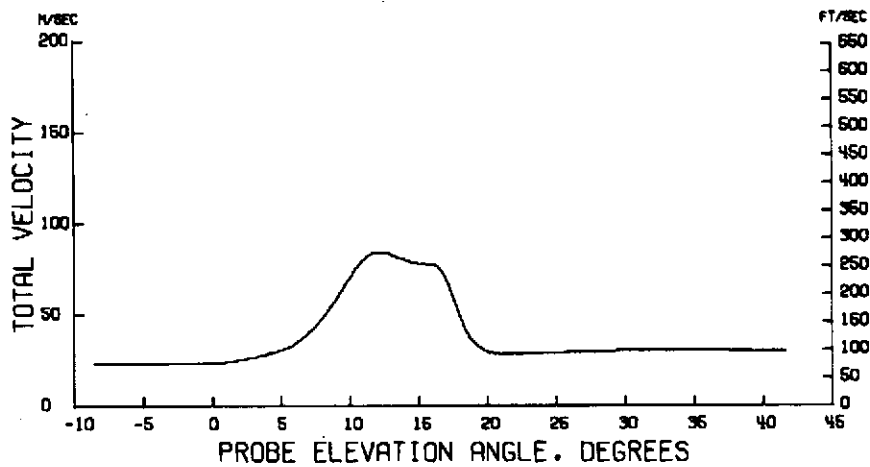
(a) Streamwise velocity profile.



(b) Total velocity.



(c) Downwash angle.

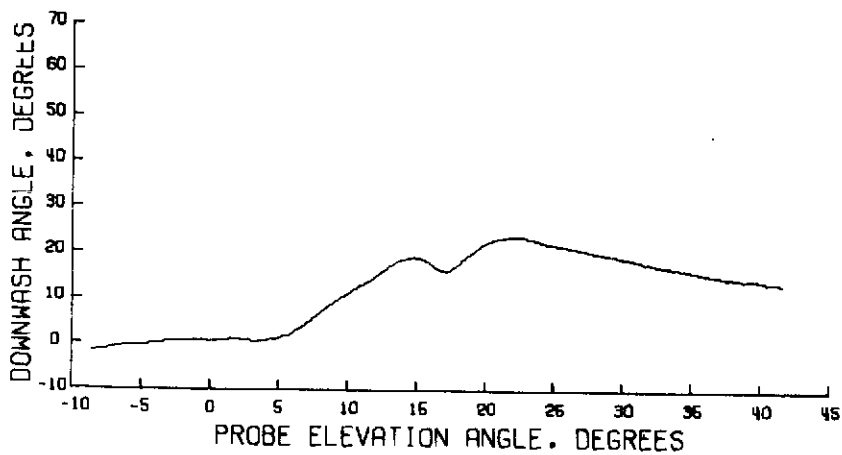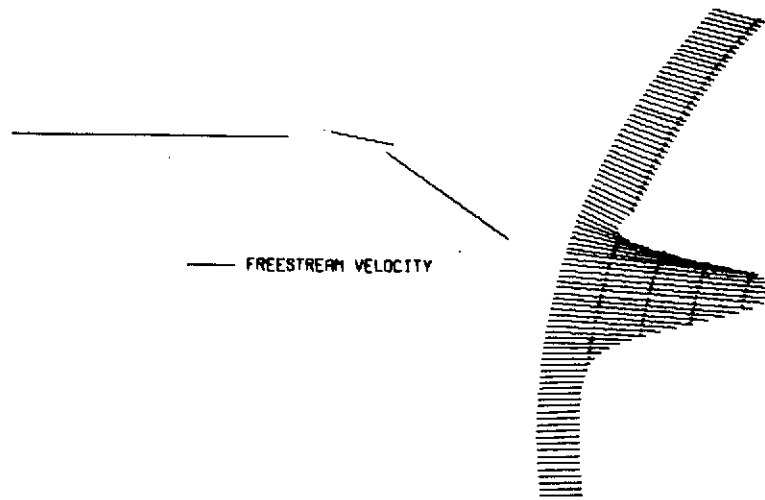Figure 55.- Wake survey results for $\eta = 0.335$; $\alpha = 16°$; $C_T = 0$; $V_\infty = 25.42$ m/sec (83.42 ft/sec).

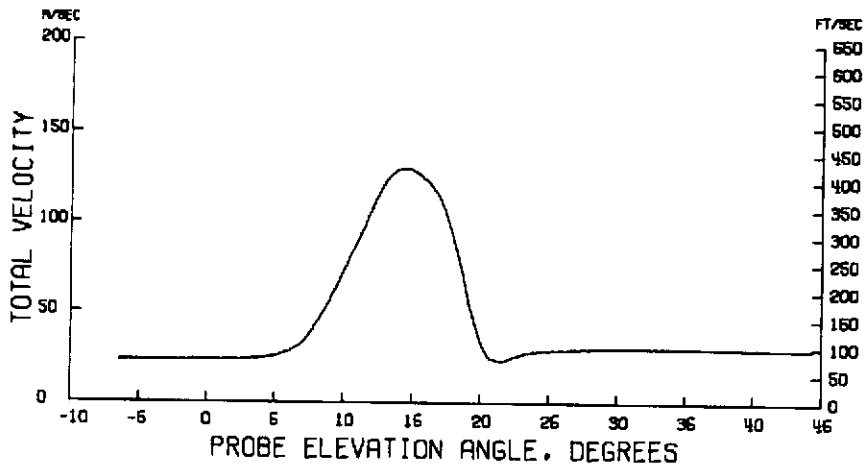(a) Streamwise velocity profile.



(b) Total velocity.



(c) Downwash angle.

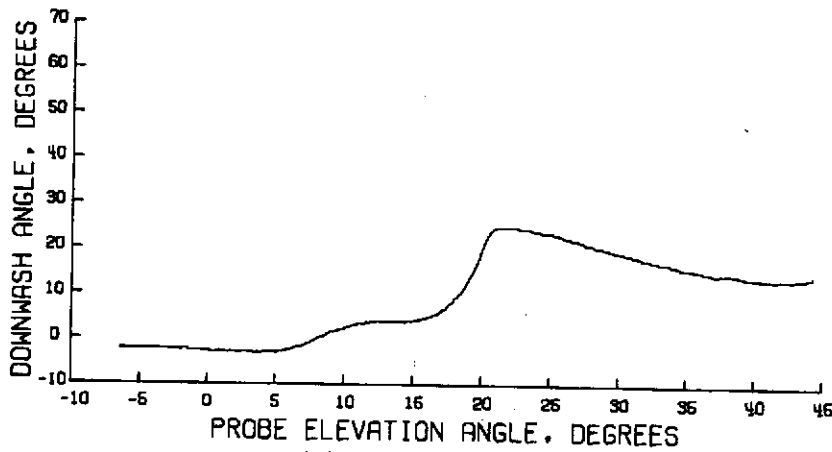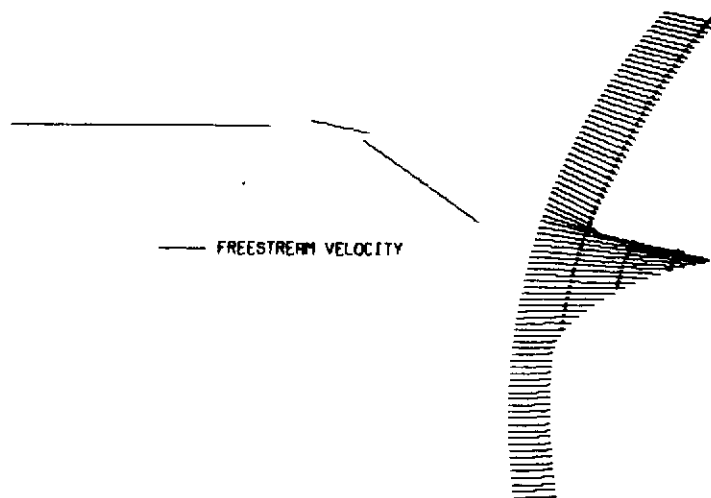Figure 56.- Wake survey results for $\eta = 0.375$; $\alpha = 16^{\circ}$; $C_T = 0$;
$V_\infty = 25.40$ m/sec (83.35 ft/sec).

FREESTREAM VELOCITY

(a) Streamwise velocity profile.



(b) Total velocity.
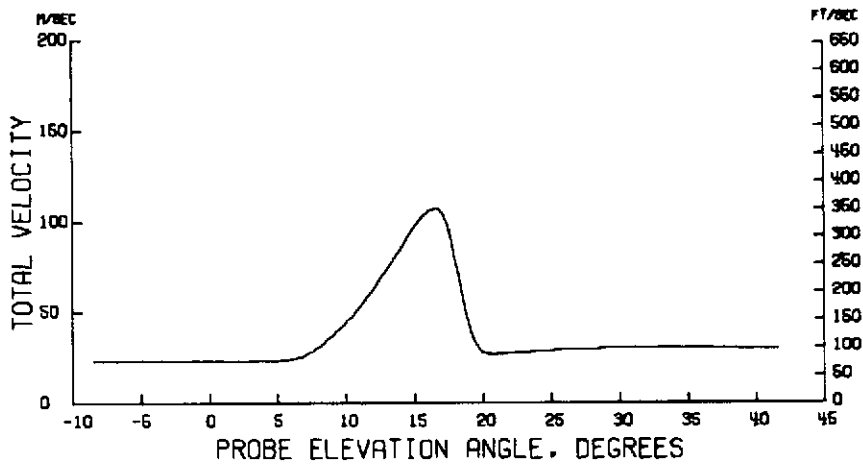


(c) Downwash angle.

Figure 57.- Wake survey results for $\eta = 0.416$; $\alpha = 16^O$; $C_T = 0$;
$V_\infty = 25.38$ m/sec (83.27 ft/sec).

(a) Streamwise velocity profile.



(b) Total velocity.



(c) Downwash angle.

Figure 58.- Wake survey results for $\eta = 0.442$; $\alpha = 16^O$; $C_T = 0$;
$V_\infty = 25.41$ m/sec (83.37 ft/sec).

(a) Streamwise velocity profile.
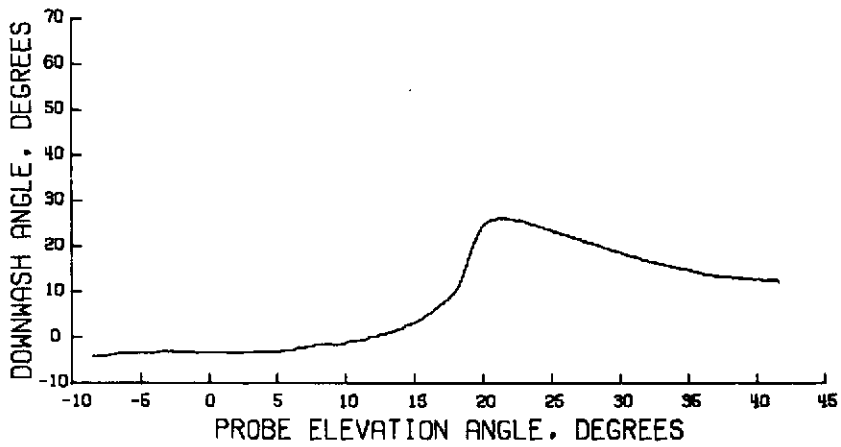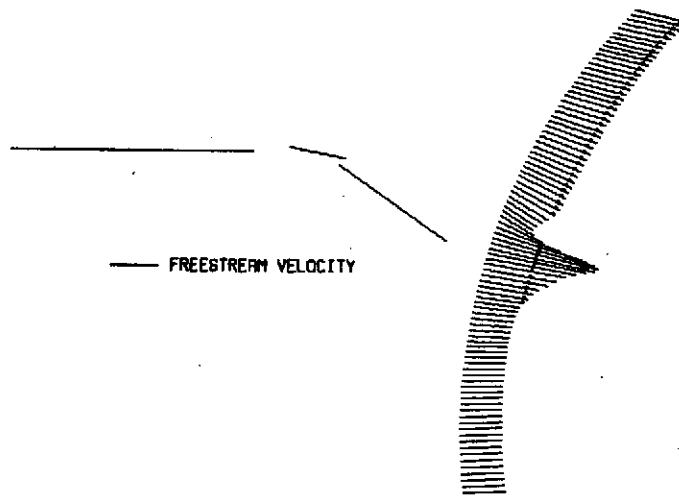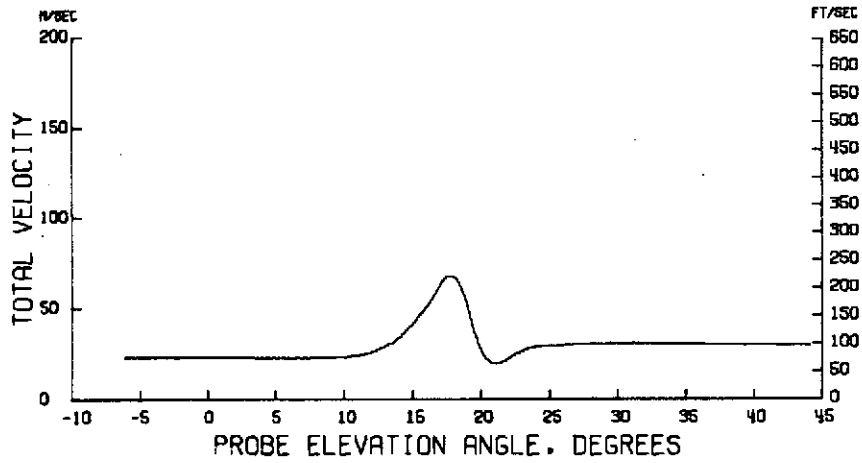


(b) Total velocity.



(c) Downwash angle.

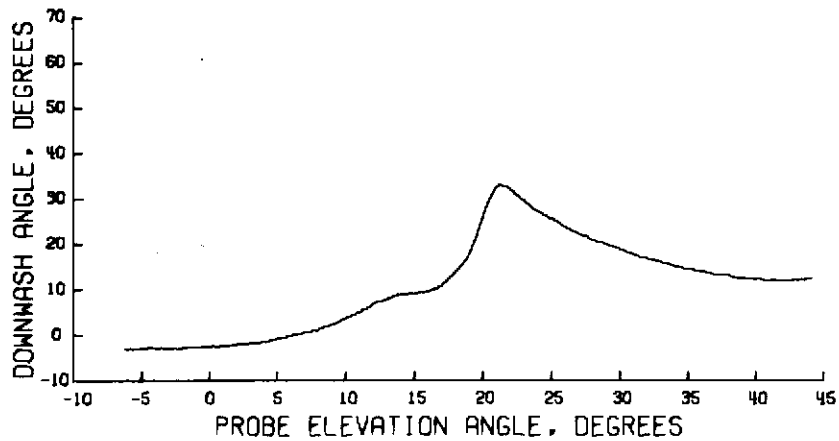Figure 59.- Wake survey results for $\eta = 0.469$; $\alpha = 16^{O}$; $C_T = 0$;
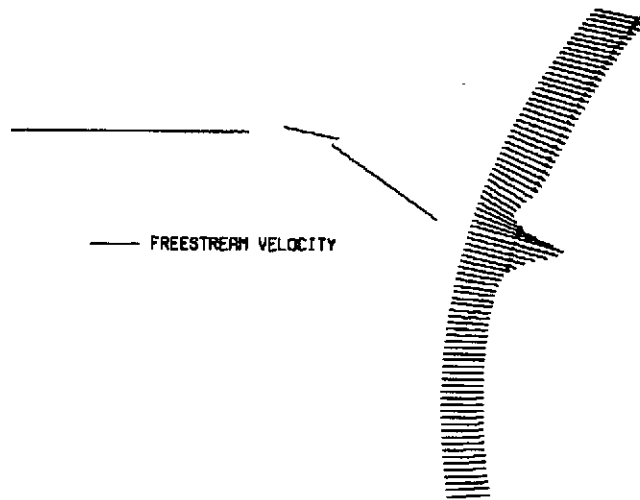$V_\infty = 25.52$ m/sec (83.75 ft/sec).
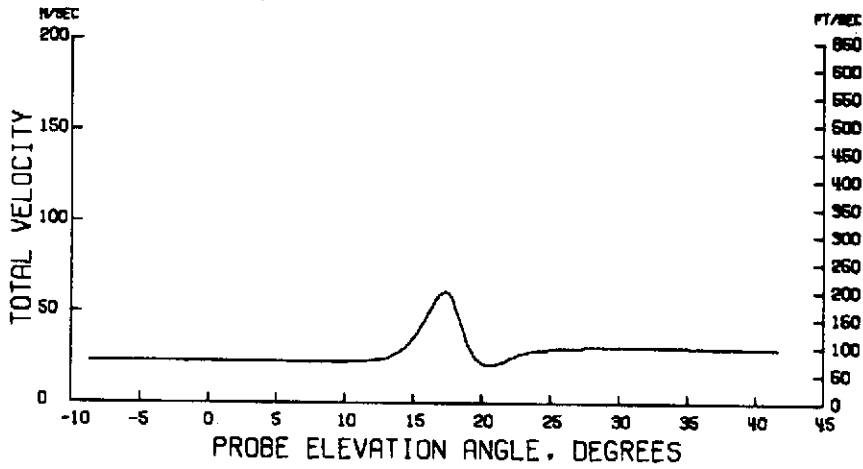
(a) Streamwise velocity profile.



(b) Total velocity.



(c) Downwash angle.

Figure 60.- Wake survey results for $\eta = 0.562$; $\alpha = 16^O$; $C_T = 0$; $V_\infty = 25.34$ m/sec (83.16 ft/sec).

(a) Streamwise velocity profile.



(b) Total velocity.



(c) Downwash angle.

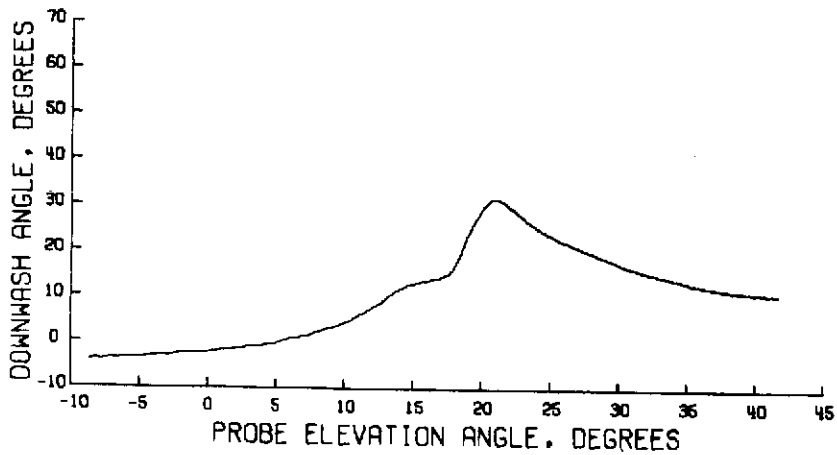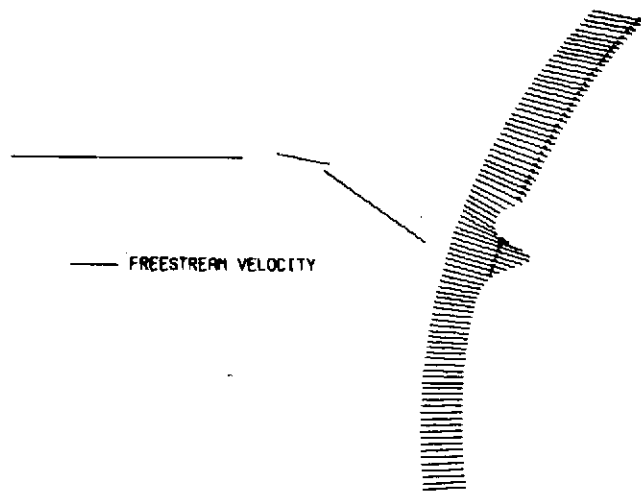Figure 61.- Wake survey results for $\eta = 0.162$; $\alpha = 12^O$; $C_T = 1.0$; $V_\infty = 25.49$ m/sec (83.66 ft/sec).
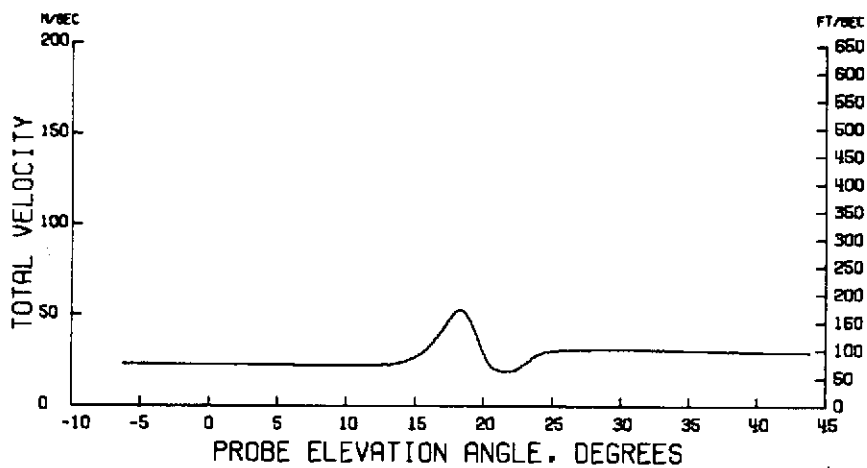
(a) Streamwise velocity profile.



(b) Total velocity.



(c) Downwash angle.

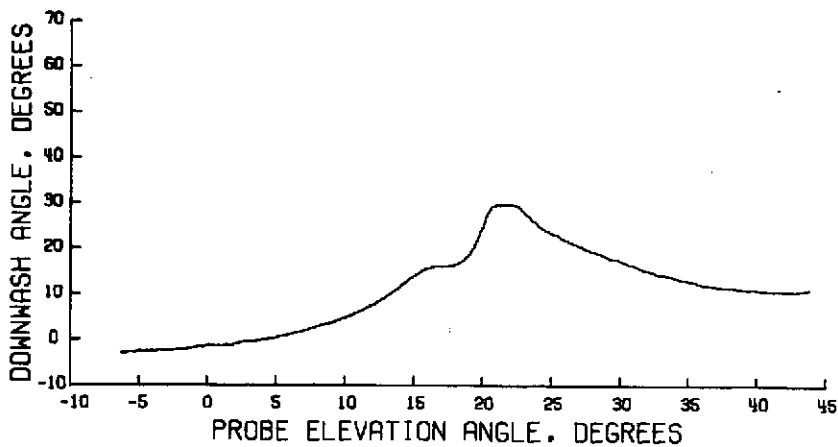Figure 62.- Wake survey results for $\eta = 0.201$; $\alpha = 12^O$; $C_T = 1.0$;
$V_\infty = 25.66$ m/sec   (84.19 ft/sec).
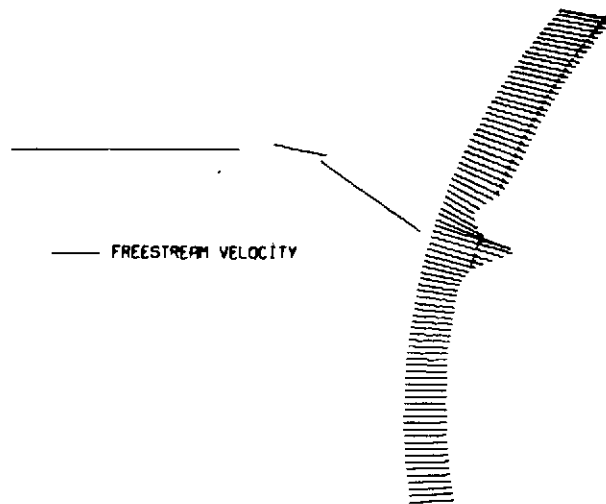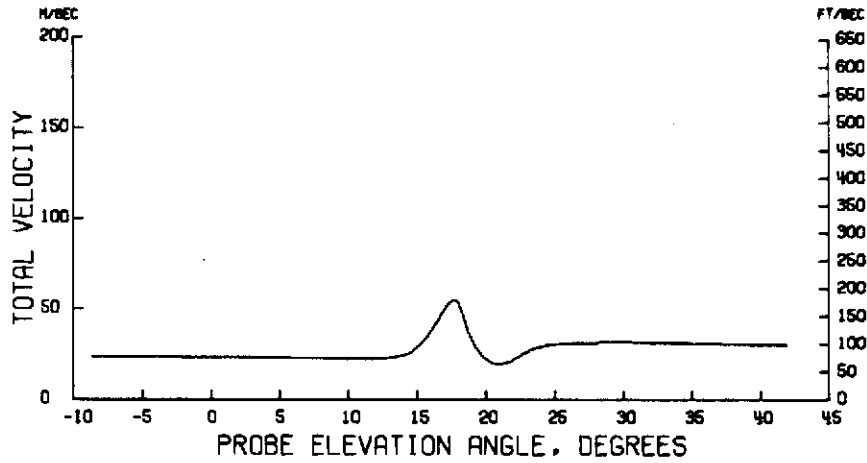
(a) Streamwise velocity profile.



(b) Total velocity.



(c) Downwash angle.

Figure 63.- Wake survey results for $\eta = 0.227$; $\alpha = 12°$; $C_T = 1.0$; $V_\infty = 25.60$ m/sec (84.00 ft/sec).

(a) Streamwise velocity profile.
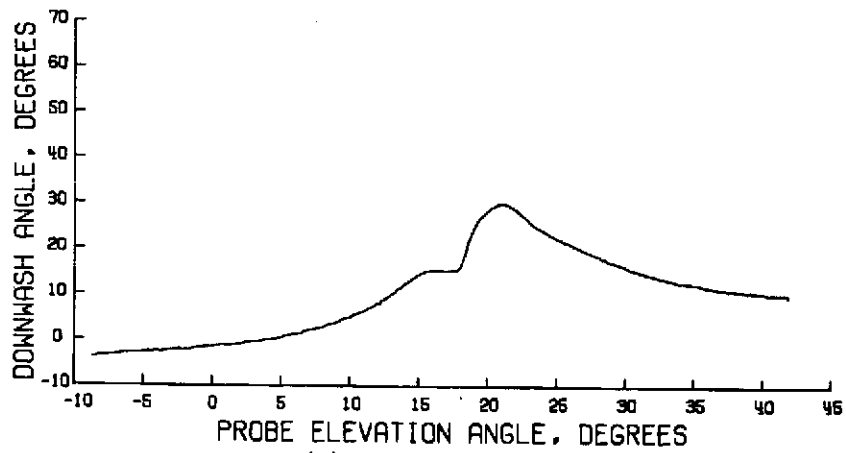


(b) Total velocity.



(c) Downwash angle.

Figure 64.- Wake survey results for $\eta = 0.254$; $\alpha = 12^O$; $C_T = 1.0$; $V_\infty = 25.64$ m/sec (84.13 ft/sec).
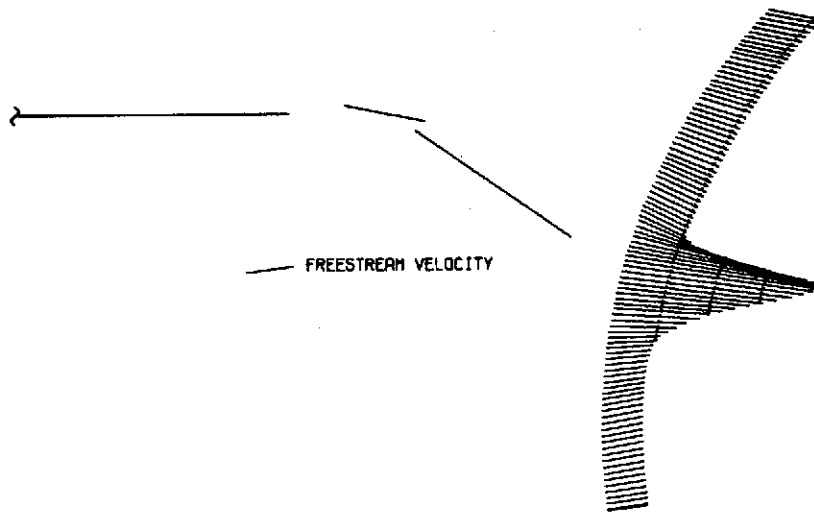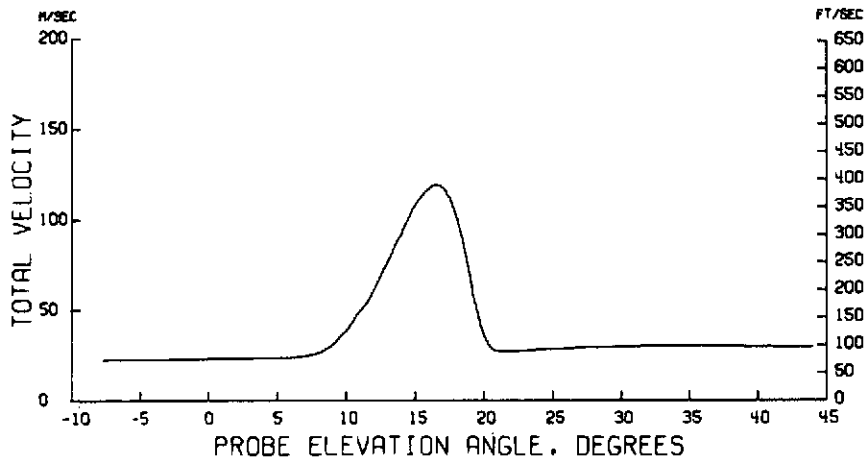
(a) Streamwise velocity profile.
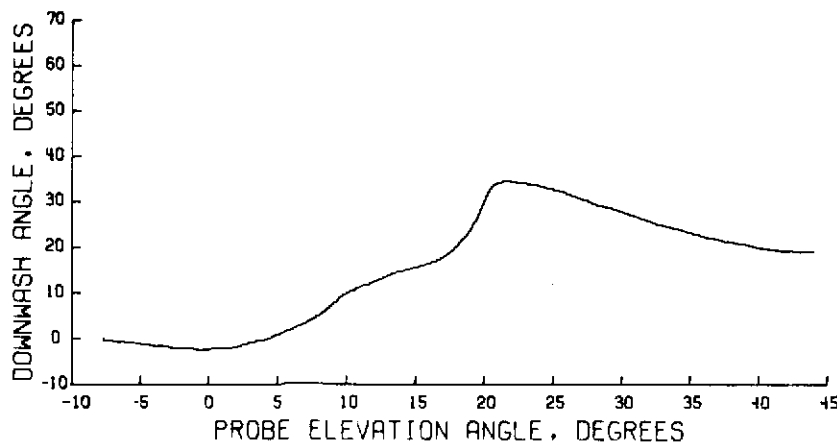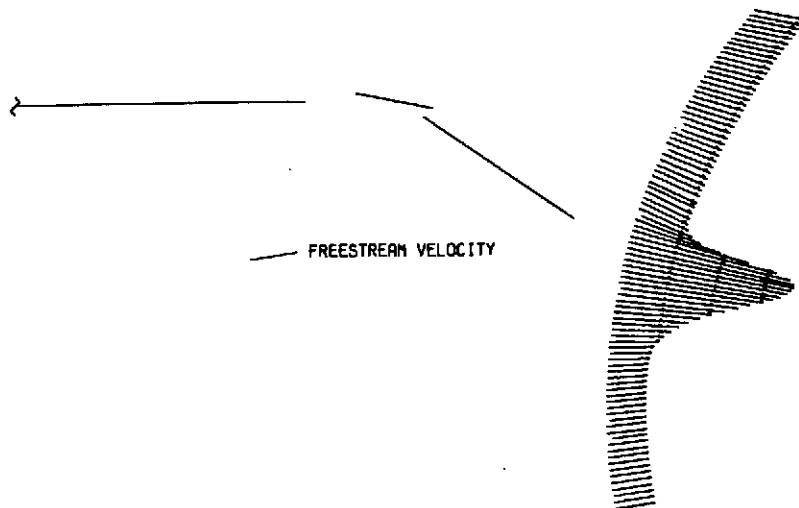


(b) Total velocity.



(c) Downwash angle.

Figure 65.- Wake survey results for $\eta = 0.294$; $\alpha = 12^O$; $C_T = 1.0$; $V_\infty = 25.55$ m/sec (83.85 ft/sec).

FREESTREAM VELOCITY

(a) Streamwise velocity profile.



(b) Total velocity.



(c) Downwash angle.

Figure 66.- Wake survey results for $\eta = 0.335$; $\alpha = 12^O$; $C_T = 1.0$; $V_\infty = 25.46$ m/sec (83.55 ft/sec).
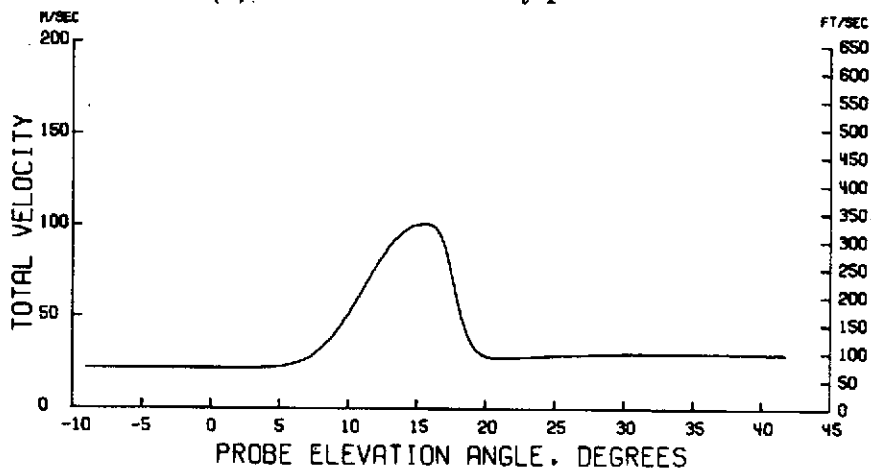
(a) Streamwise velocity profile.



(b) Total velocity.



(c) Downwash angle.

Figure 67.- Wake survey results for $\eta = 0.375$; $\alpha = 12^O$; $C_T = 1.0$;
$V_\infty = 25.47$ m/sec (83.67 ft/sec).

(a) Streamwise velocity profile.
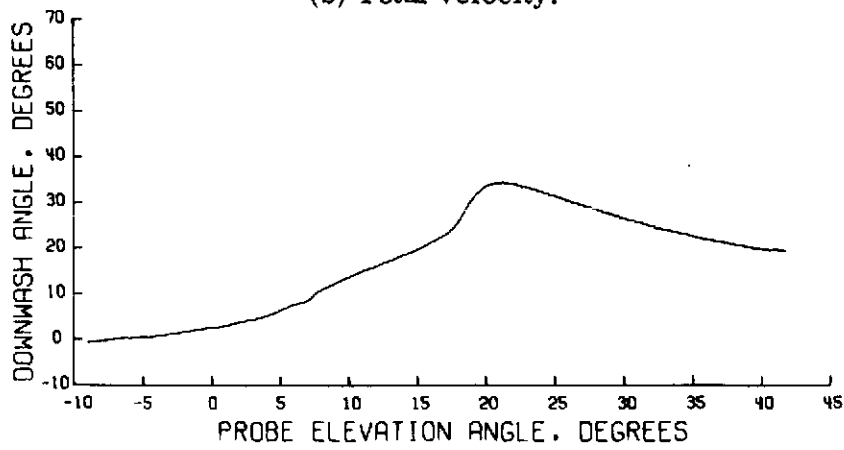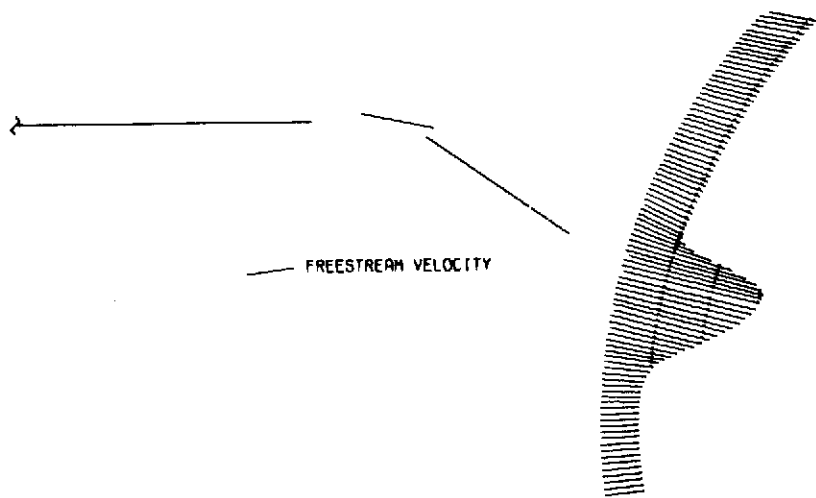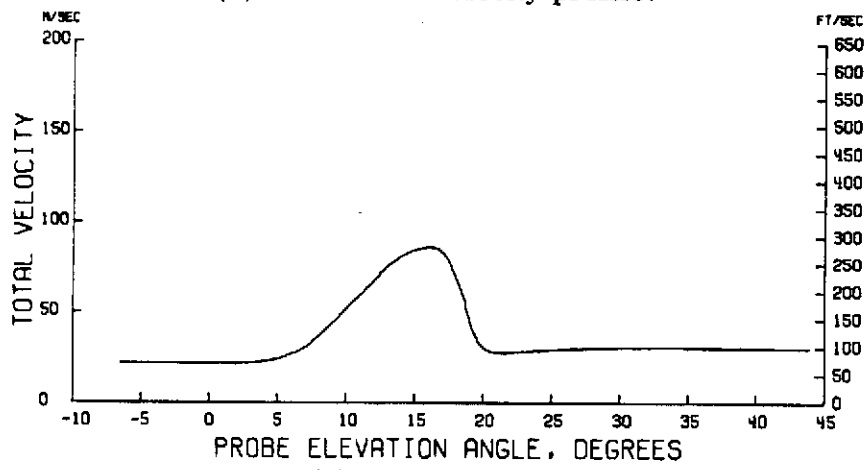


(b) Total velocity.



(c) Downwash angle.

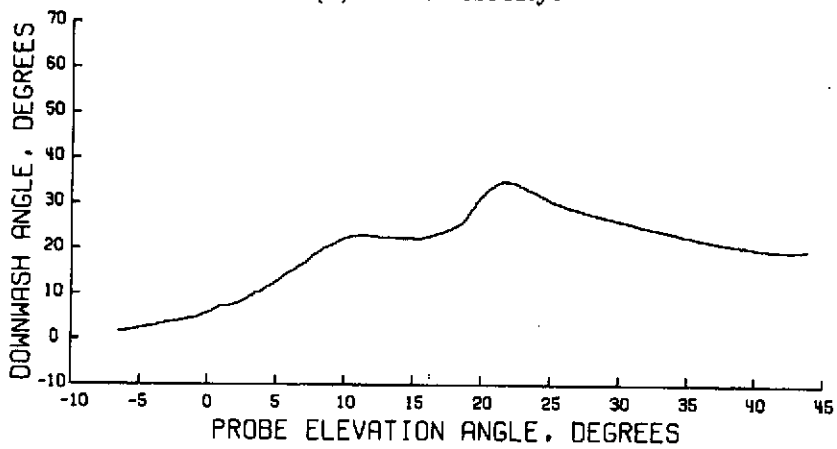Figure 68.- Wake survey results for $\eta = 0.415$; $\alpha = 12^O$; $C_T = 1.0$; $V_\infty = 25.39$ m/sec (83.30 ft/sec).
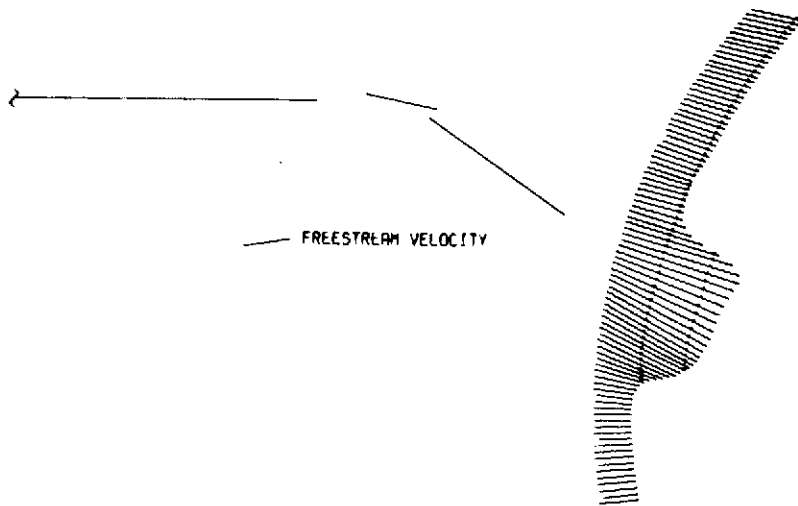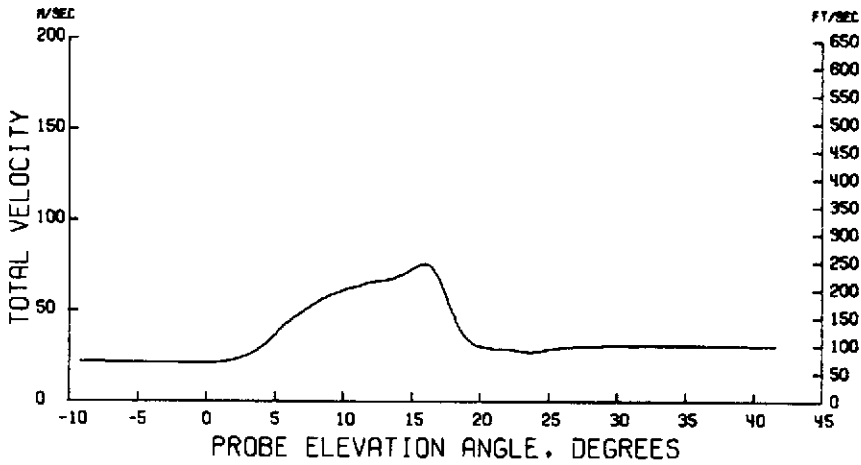
(a) Streamwise velocity profile.



(b) Total velocity.



(c) Downwash angle.

Figure 69.- Wake survey results for $\eta = 0.443$; $\alpha = 12^O$; $C_T = 1.0$; $V_\infty = 25.31$ m/sec (83.05 ft/sec).

(a) Streamwise velocity profile.



(b) Total velocity.



(c) Downwash angle.

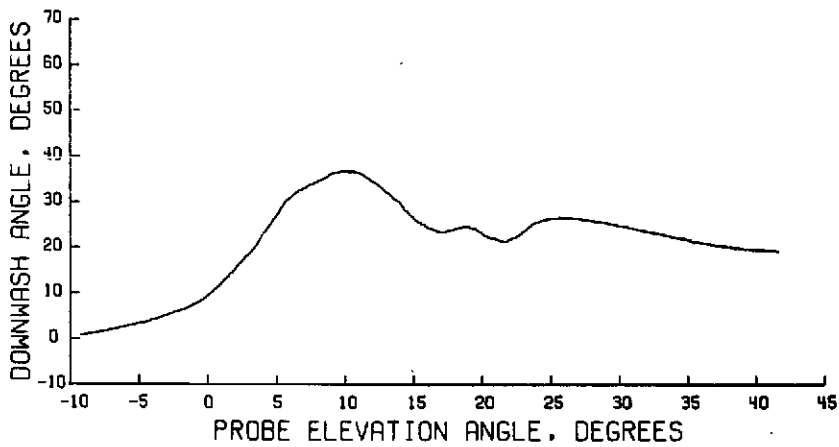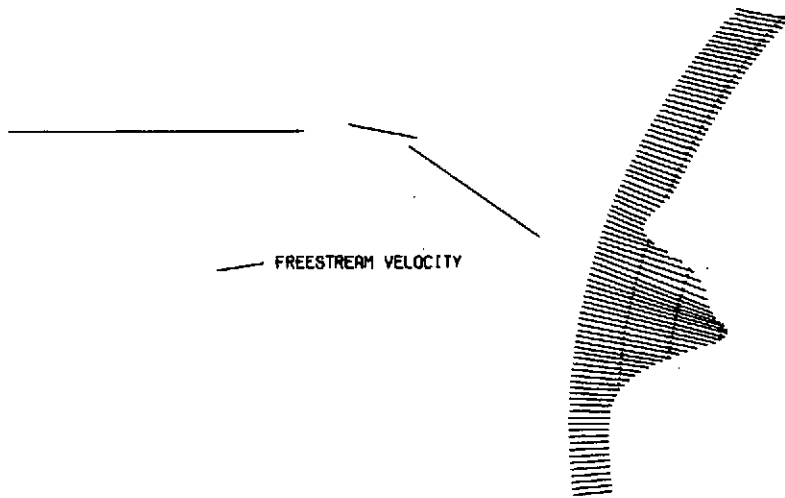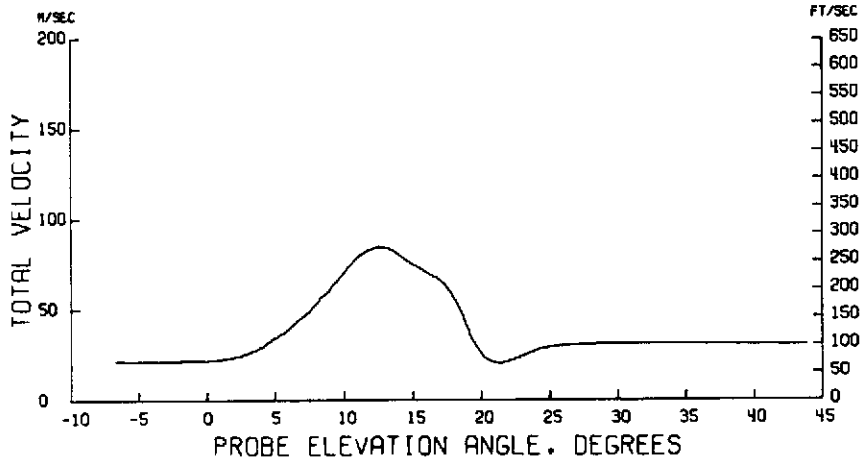Figure 70.- Wake survey results for $\eta = 0.469$; $\alpha = 12^O$; $C_T = 1.0$; $V_\infty = 25.38$ m/sec (83.27 ft/sec).

(a) Streamwise velocity profile.



(b) Total velocity.



(c) Downwash angle.

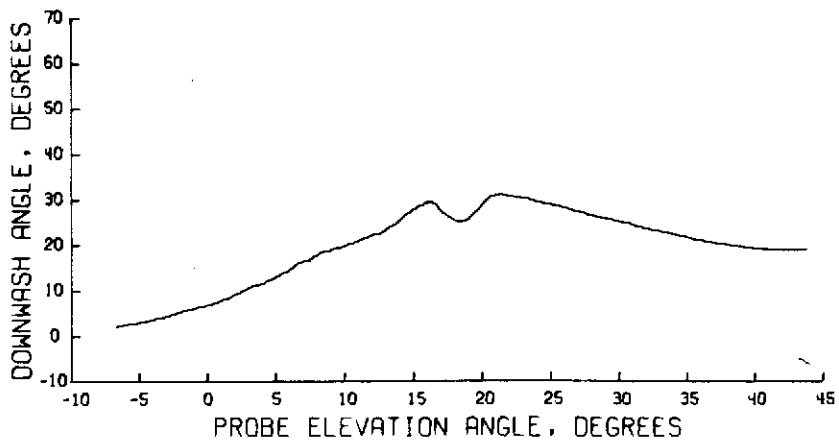Figure 71.- Wake survey results for $\eta = 0.481$; $\alpha = 12^O$; $C_T = 1.0$; $V_\infty = 25.60$ m/sec (84.01 ft/sec).
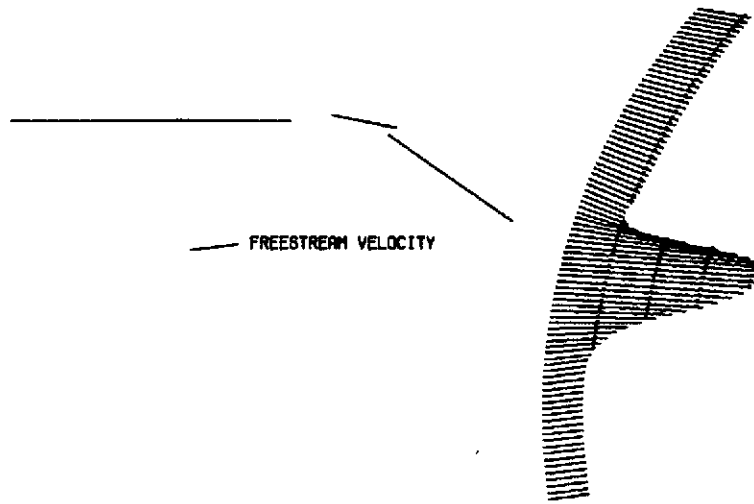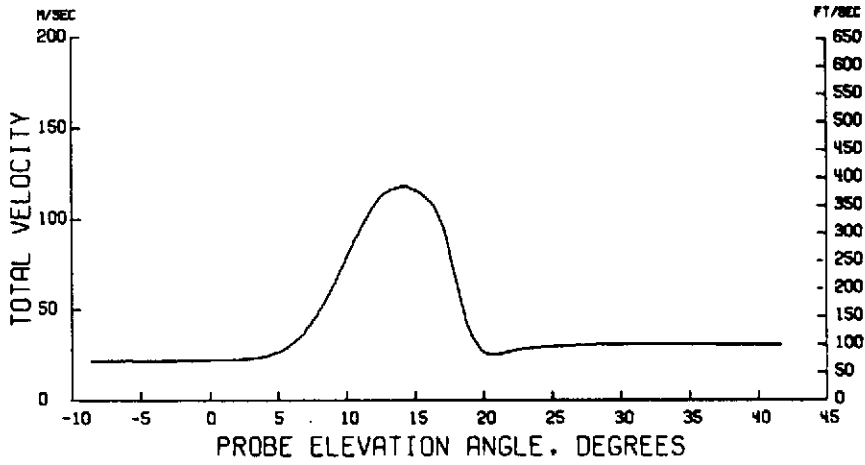
(a) Streamwise velocity profile.
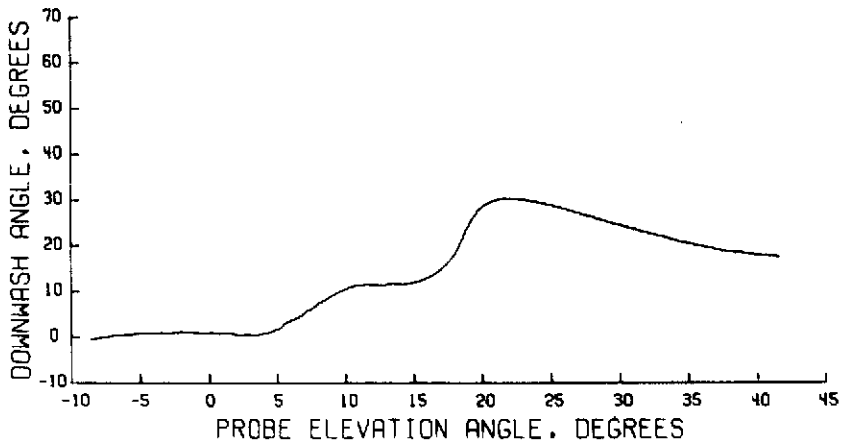


(b) Total velocity.



(c) Downwash angle.

Figure 72.- Wake survey results for $\eta = 0.163$; $\alpha = 16^O$; $C_T = 1.0$; $V_\infty = 25.46$ m/sec (83.54 ft/sec).
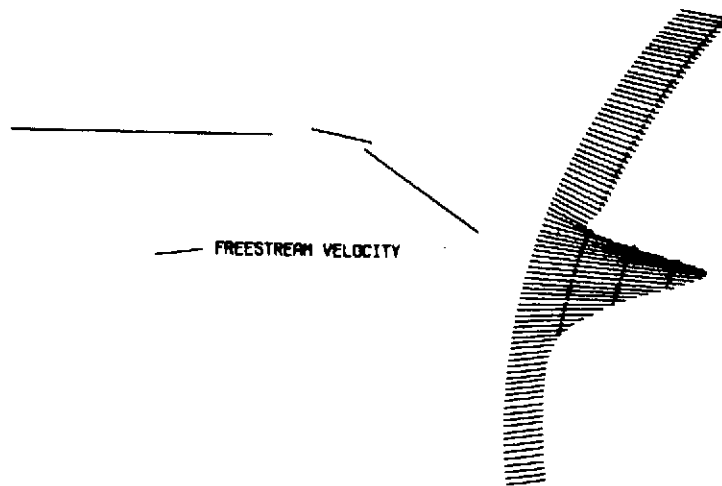
(a) Streamwise velocity profile.



(b) Total velocity.



(c) Downwash angle.

Figure 73.- Wake survey results for $\eta = 0.201$; $\alpha = 16^{\circ}$; $C_T = 1.0$; $V_\infty = 25.48$ m/sec (83.61 ft/sec).
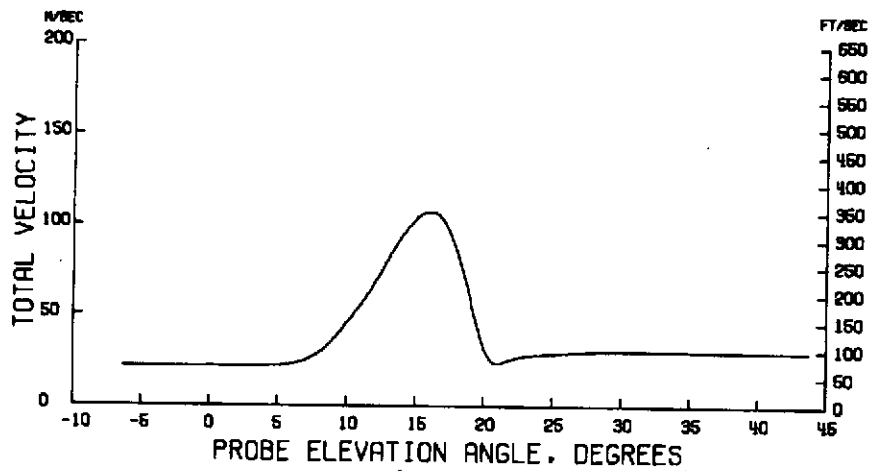
(a) Streamwise velocity profile.
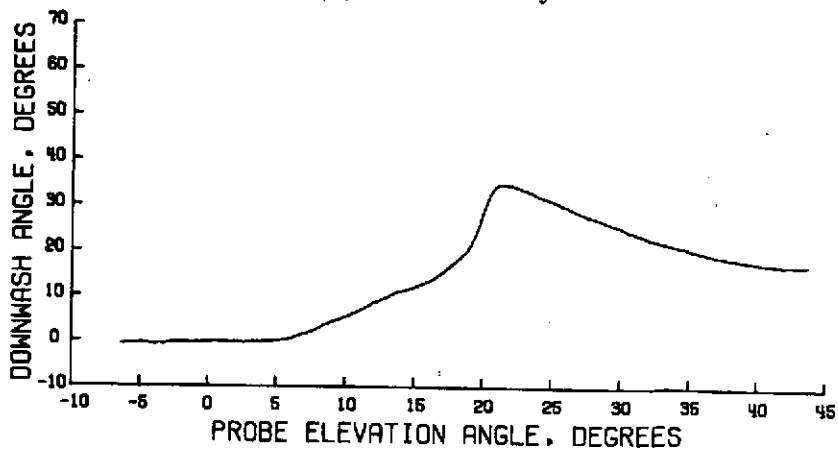


(b) Total velocity.



(c) Downwash angle.

Figure 74.- Wake survey results for $\eta = 0.227$; $\alpha = 16^O$; $C_T = 1.0$; $V_\infty = 25.47$ m/sec (83.58 ft/sec).
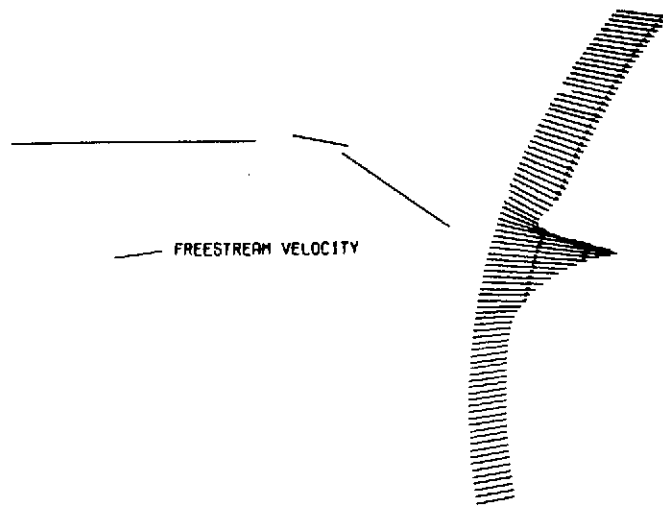
(a) Streamwise velocity profile.



(b) Total velocity.



(c) Downwash angle.

Figure 75.- Wake survey results for $\eta = 0.254$; $\alpha = 16^O$; $C_T = 1.0$; $V_\infty = 25.49$ m/sec (83.65 ft/sec).

(a) Streamwise velocity profile.



(b) Total velocity.



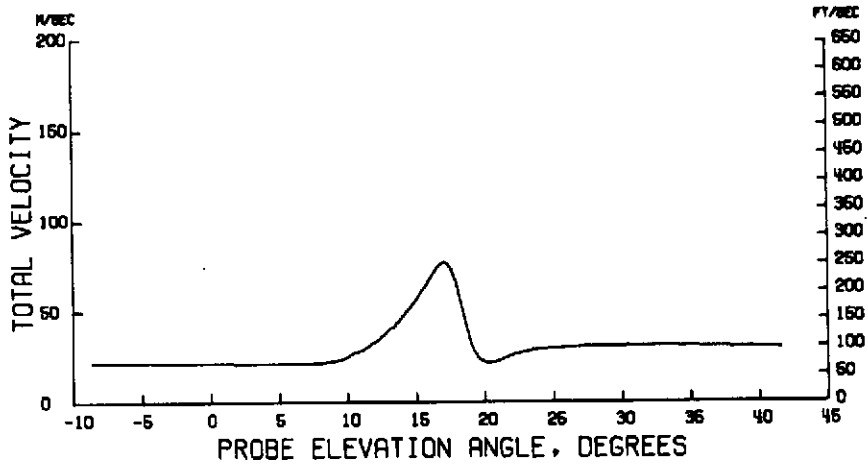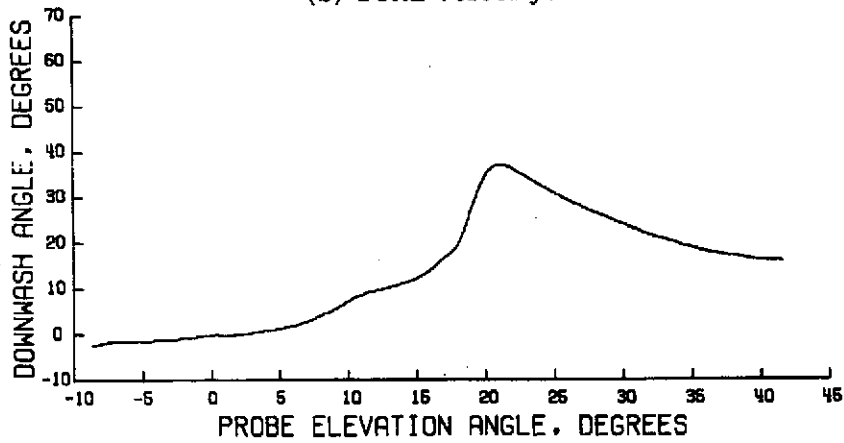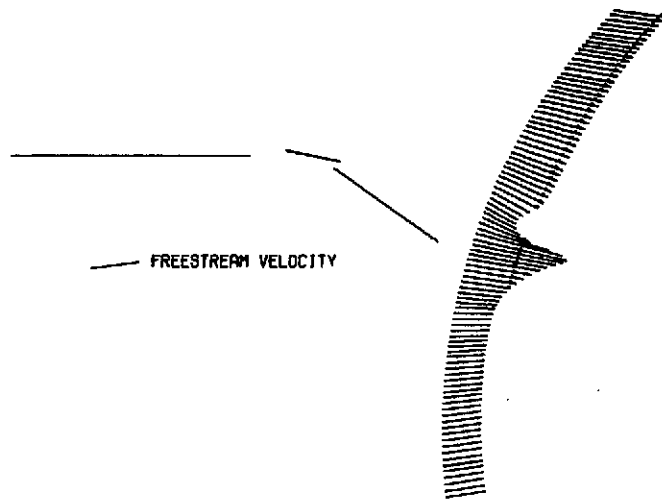(c) Downwash angle.

Figure 76.- Wake survey results for $\eta = 0.294$; $\alpha = 16^O$; $C_T = 1.0$; $V_\infty = 25.52$ m/sec (83.75 ft/sec).
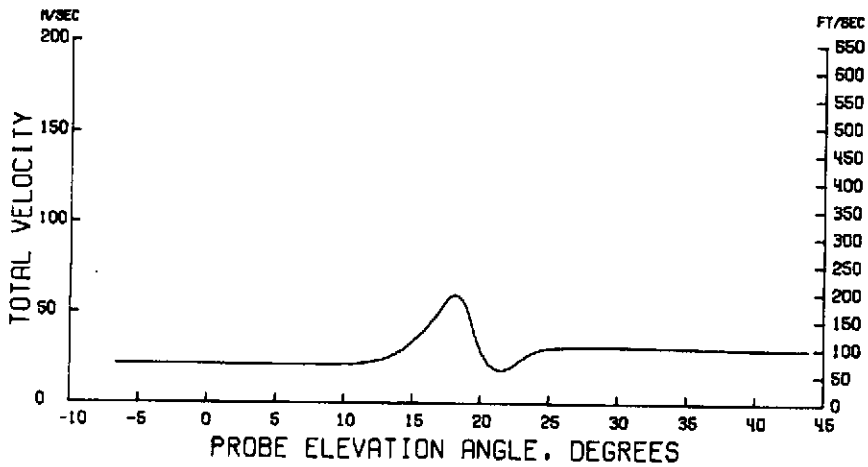
(a) Streamwise velocity profile.



(b) Total velocity.



(c) Downwash angle.

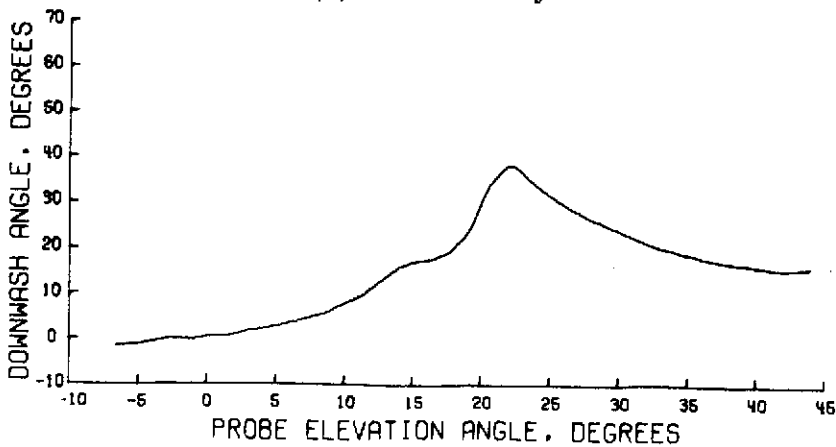Figure 77.- Wake survey results for $\eta = 0.335$; $\alpha = 16^O$; $C_T = 1.0$;
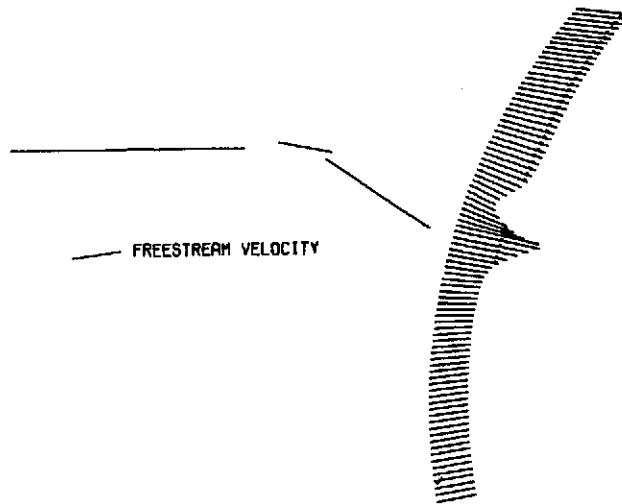$V_\infty = 25.53$ m/sec (83.76 ft/sec).
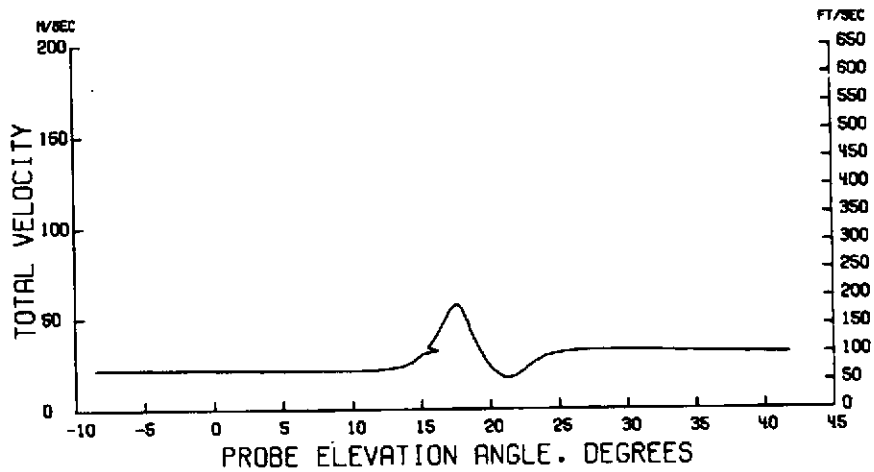
(a) Streamwise velocity profile.



(b) Total velocity.



(c) Downwash angle.

Figure 78.- Wake survey results for $\eta = 0.376$; $\alpha = 16^O$; $C_T = 1.0$; $V_\infty = 25.47$ m/sec (83.57 ft/sec).

(a) Streamwise velocity profile.



(b) Total velocity.



(c) Downwash angle.

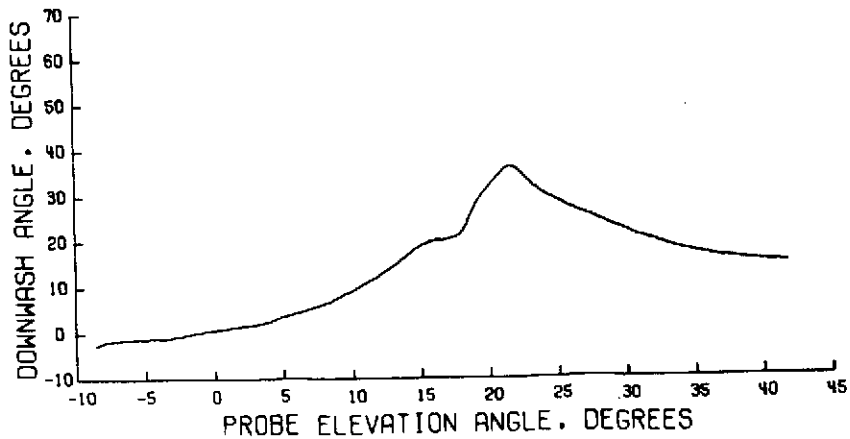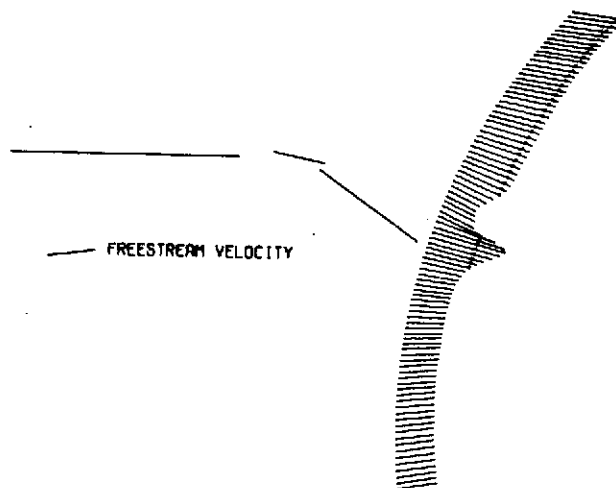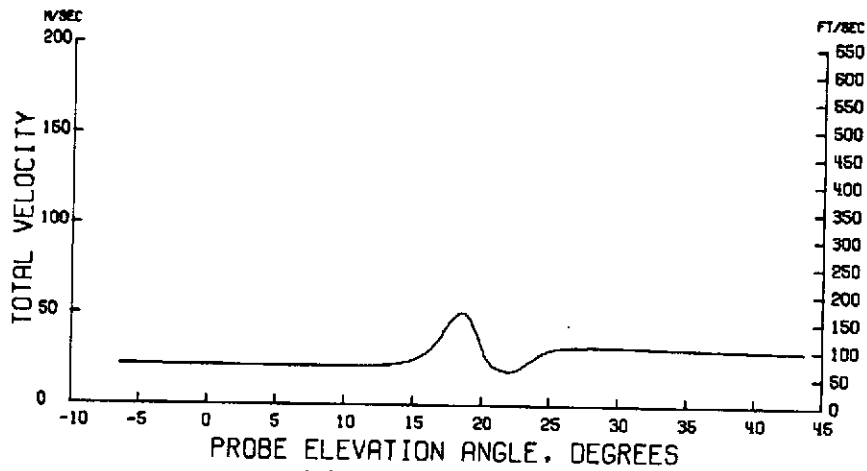Figure 79.- Wake survey results for $\eta = 0.415$; $\alpha = 16^{O}$; $C_T = 1.0$;
$V_\infty = 25.44$ m/sec (83.48 ft/sec).

FREESTREAM VELOCITY

(a) Streamwise velocity profile.



(b) Total velocity.



(c) Downwash angle.

Figure 80.- Wake survey results for $\eta = 0.443$; $\alpha = 16^O$; $C_T = 1.0$;
$V_\infty = 25.45$ m/sec (83.51 ft/sec).

(a) Streamwise velocity profile.
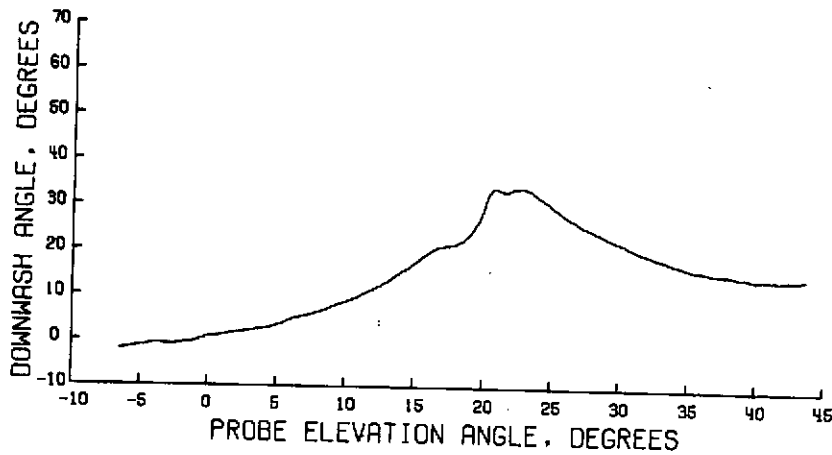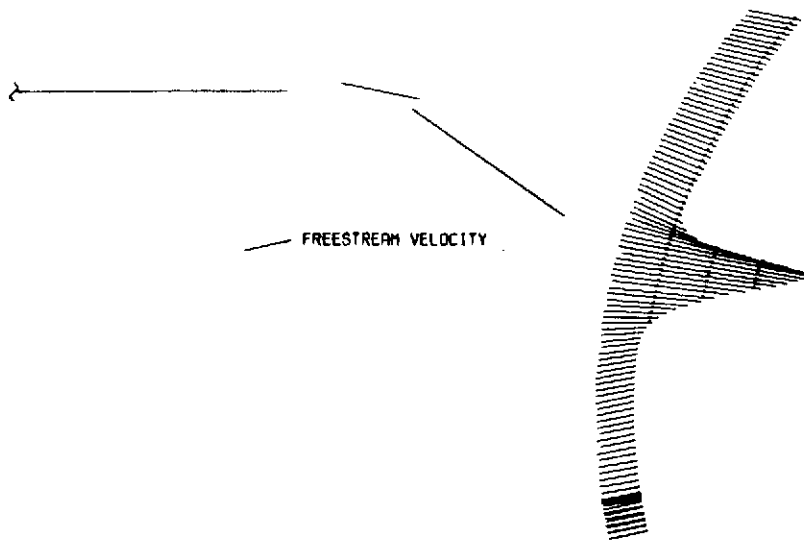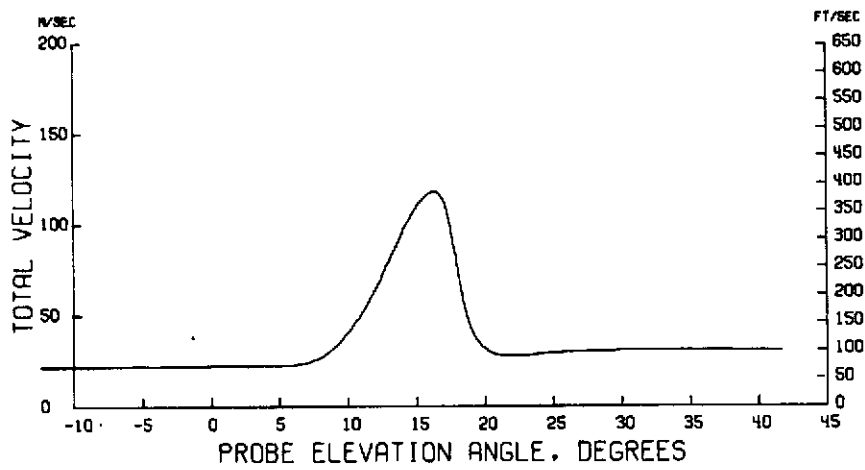


(b) Total velocity.



(c) Downwash angle.

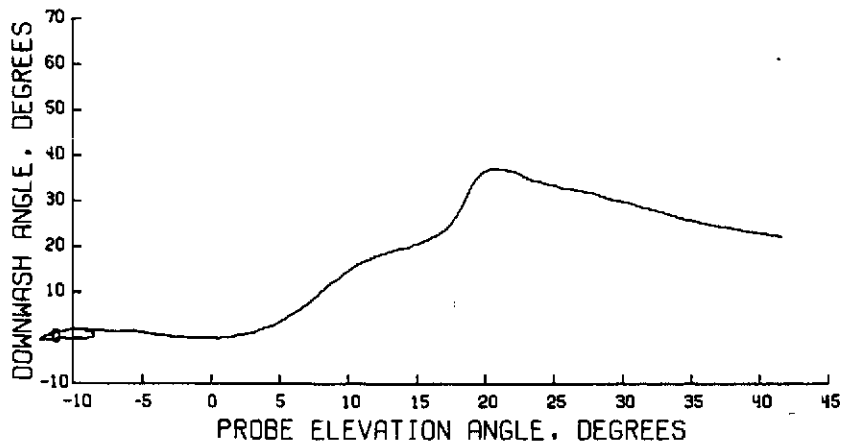Figure 81.- Wake survey results for $\eta = 0.469$; $\alpha = 16^{\circ}$; $C_T = 1.0$;
$V_{\infty} = 25.45$ m/sec (83.52 ft/sec).
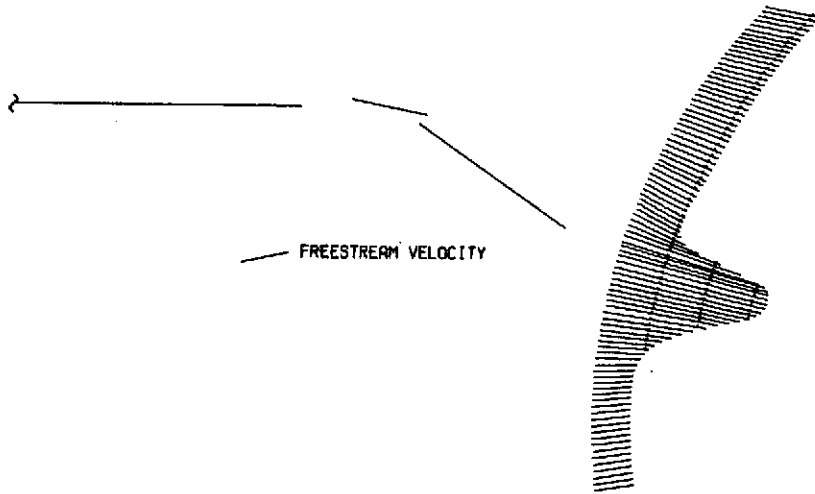
FREESTREAM VELOCITY

(a) Streamwise velocity profile.



(b) Total velocity.



(c) Downwash angle.

Figure 82.- Wake survey results for $\eta = 0.483$; $\alpha = 16^O$; $C_T = 1.0$;
$V_\infty = 25.52$ m/sec (83.73 ft/sec).

(a) Streamwise velocity profile.



(b) Total velocity.



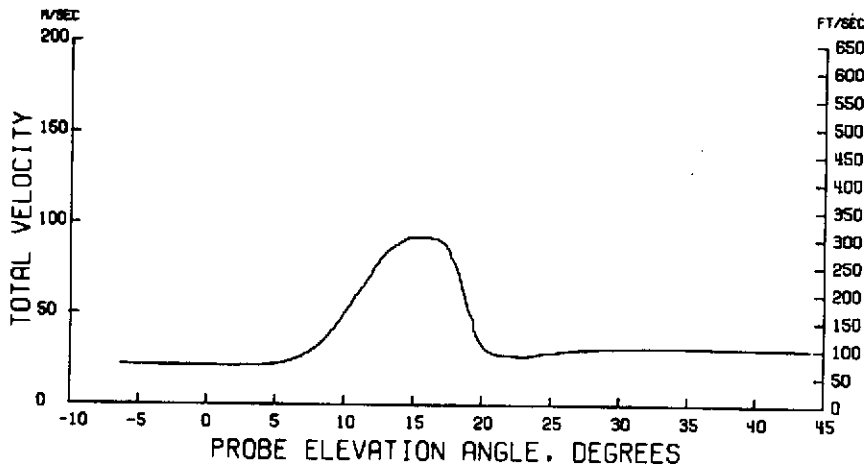(c) Downwash angle.

Figure 83.- Wake survey results for $\eta = 0.163$; $\alpha = 0^O$; $C_T = 2.0$;
$V_\infty = 25.56$ m/sec (83.86 ft/sec).

(a) Streamwise velocity profile.
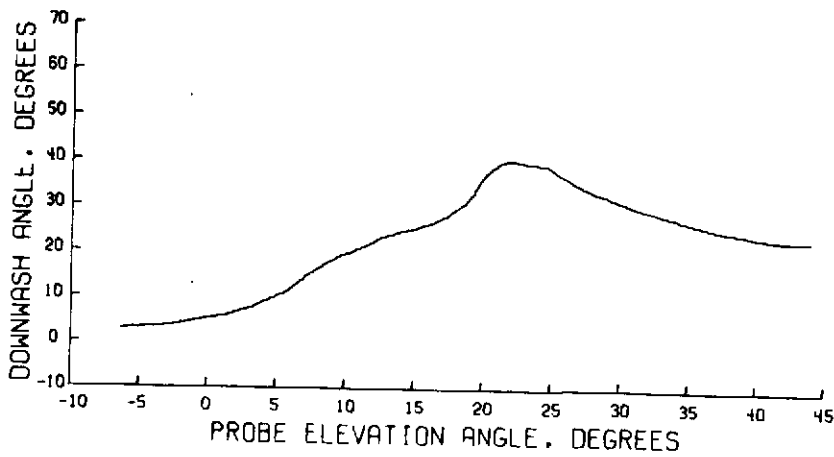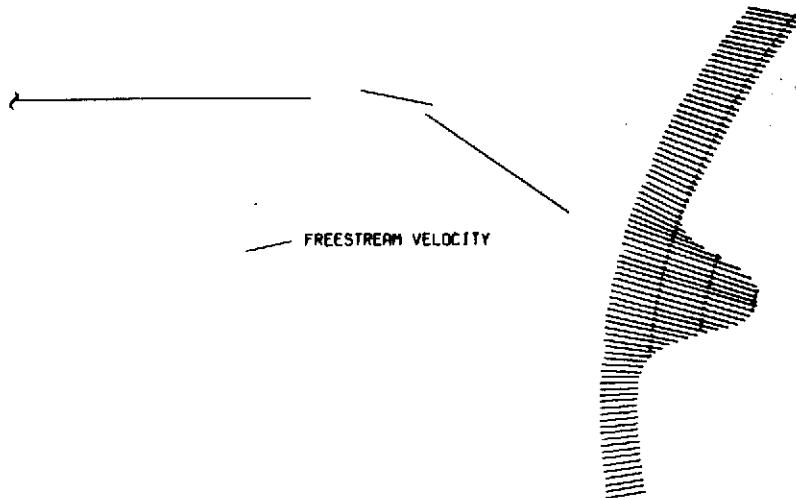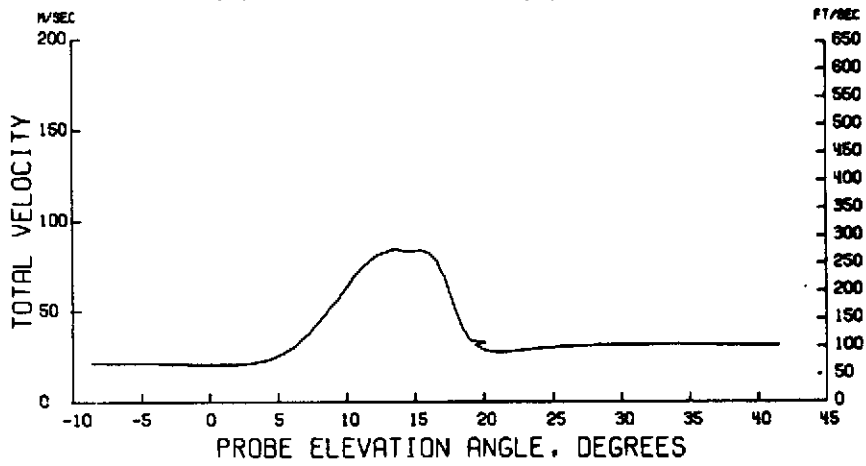


(b) Total velocity.



(c) Downwash angle.

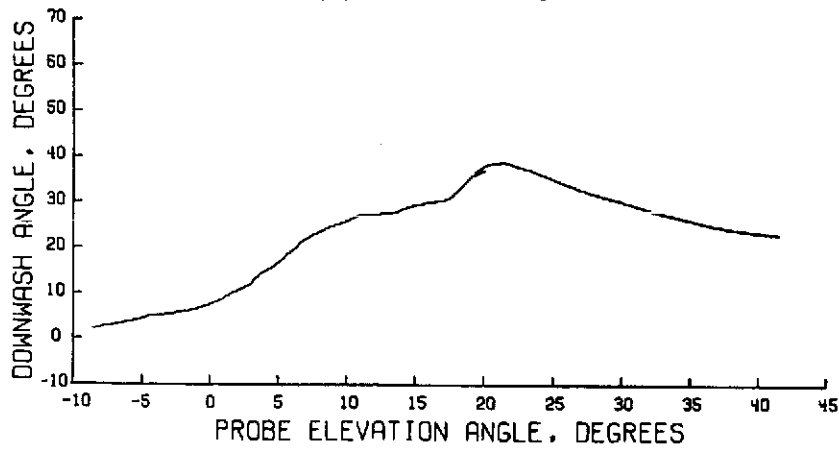Figure 84.- Wake survey results for $\eta = 0.200$; $\alpha = 0^O$; $C_T = 2.0$;
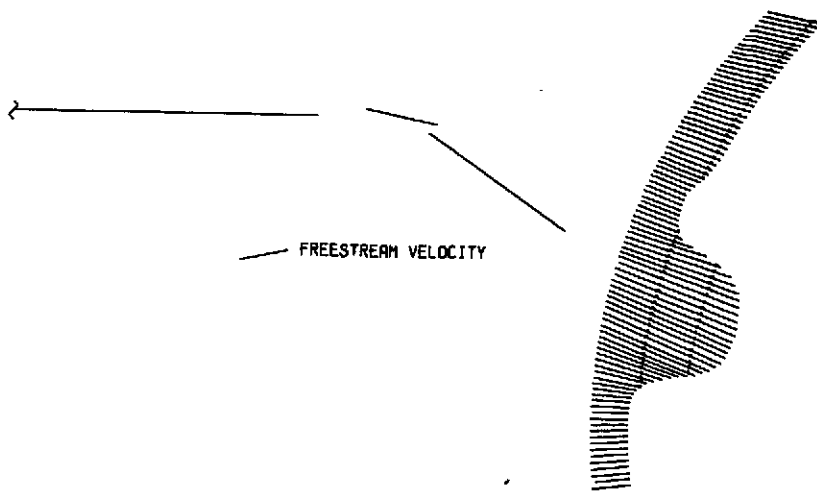$V_\infty = 25.53$ m/sec (83.76 ft/sec).

(a) Streamwise velocity profile.



(b) Total velocity.


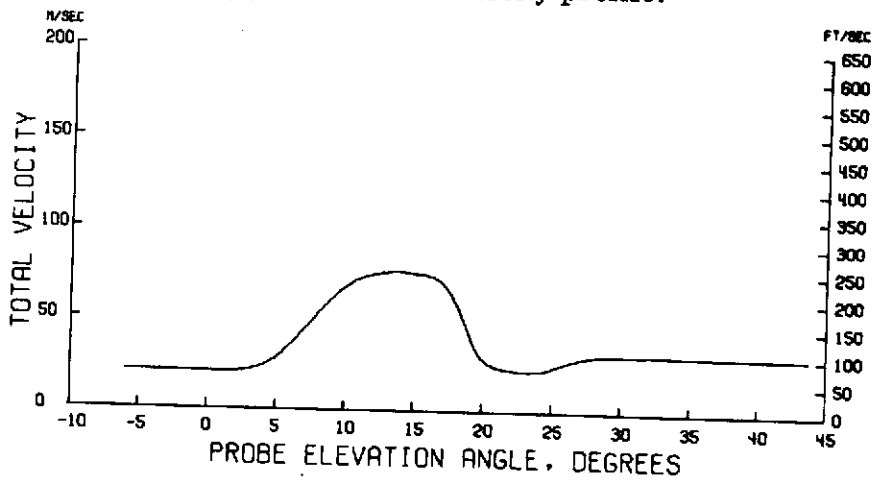
(c) Downwash angle.

Figure 85.- Wake survey results for $\eta = 0.227$; $\alpha = 0^O$; $C_T = 2.0$; $V_\infty = 25.28$ m/sec (82.95 ft/sec).

(a) Streamwise velocity profile.



(b) Total velocity.



(c) Downwash angle.

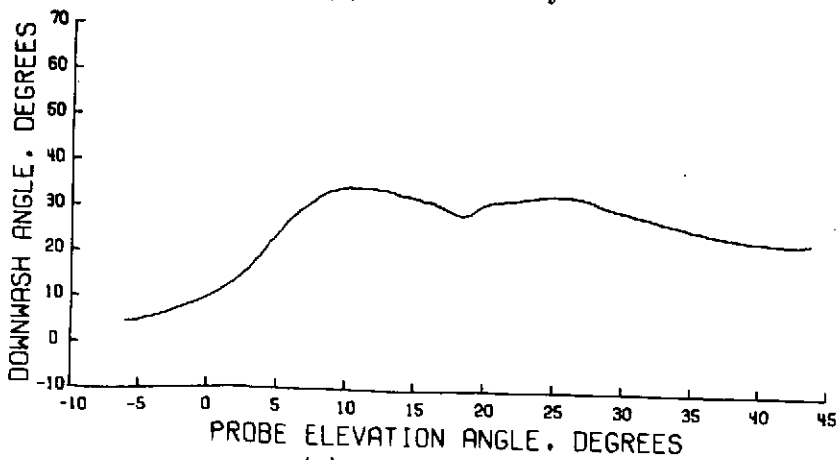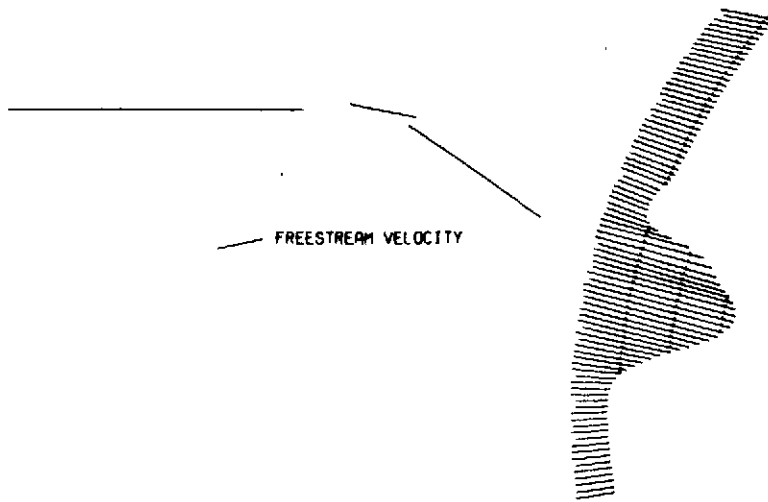Figure 86.- Wake survey results for $\eta = 0.255$; $\alpha = 0°$; $C_T = 2.0$; $V_\infty = 25.53$ m/sec (83.78 ft/sec).
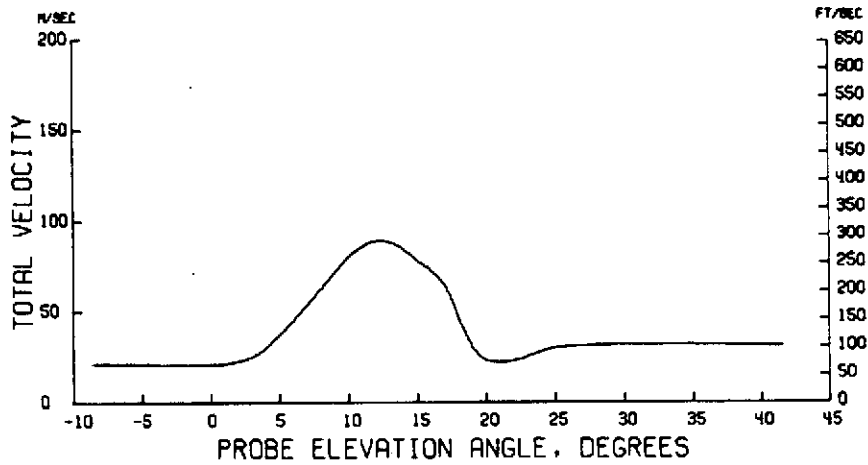
(a) Streamwise velocity profile.



(b) Total velocity.



(c) Downwash angle.

Figure 87.- Wake survey results for $\eta = 0.295$; $\alpha = 0^{\circ}$; $C_T = 2.0$; $V_\infty = 25.50$ m/sec (83.66 ft/sec).

(a) Streamwise velocity profile.
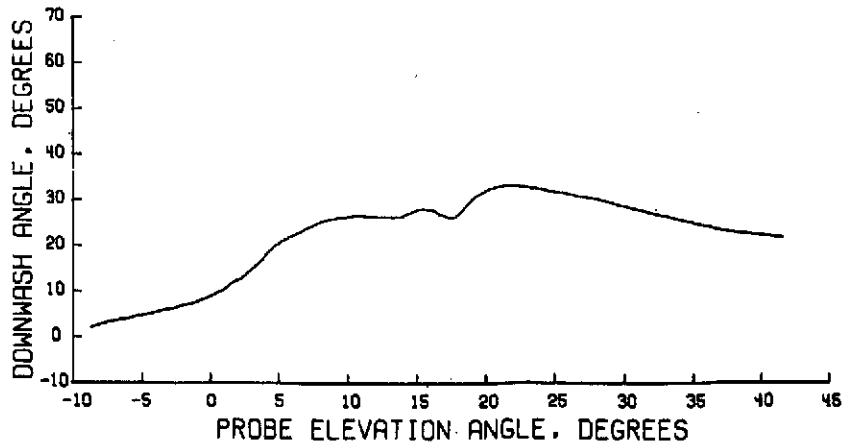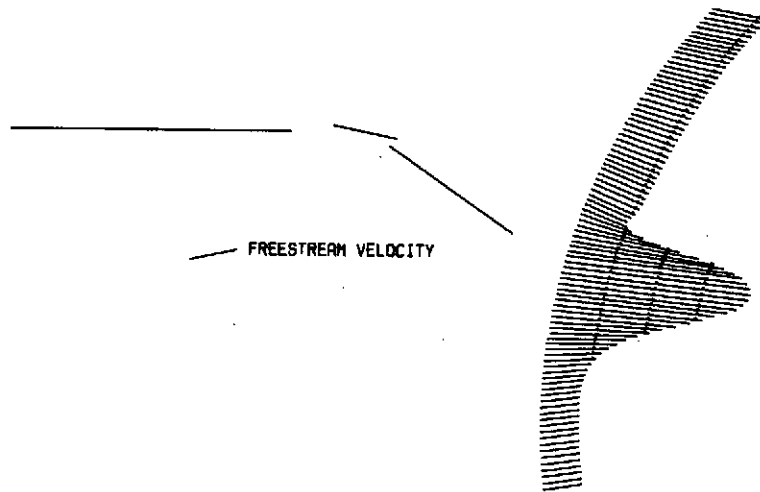


(b) Total velocity.



(c) Downwash angle.

Figure 88.- Wake survey results for $\eta = 0.335$; $\alpha = 0^\circ$; $C_T = 2.0$;
$V_\infty = 25.35$ m/sec (83.20 ft/sec).
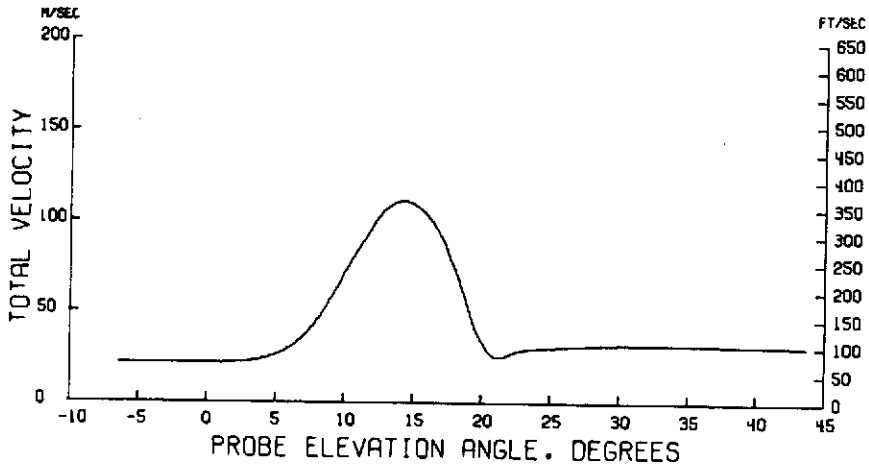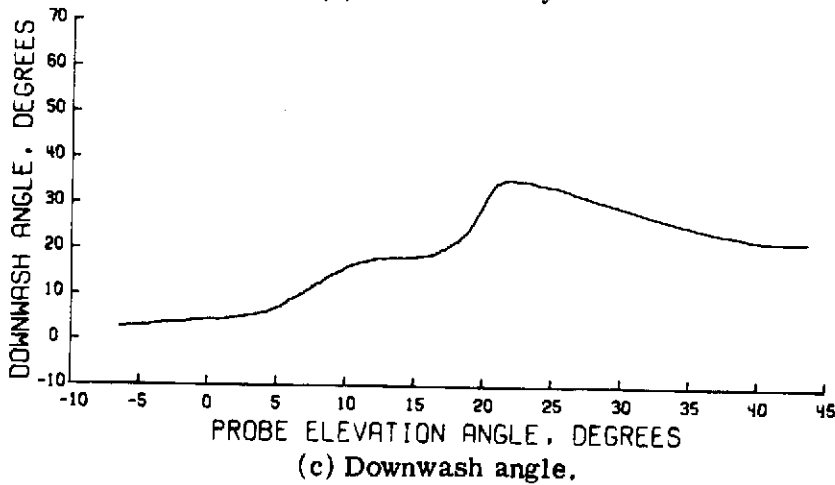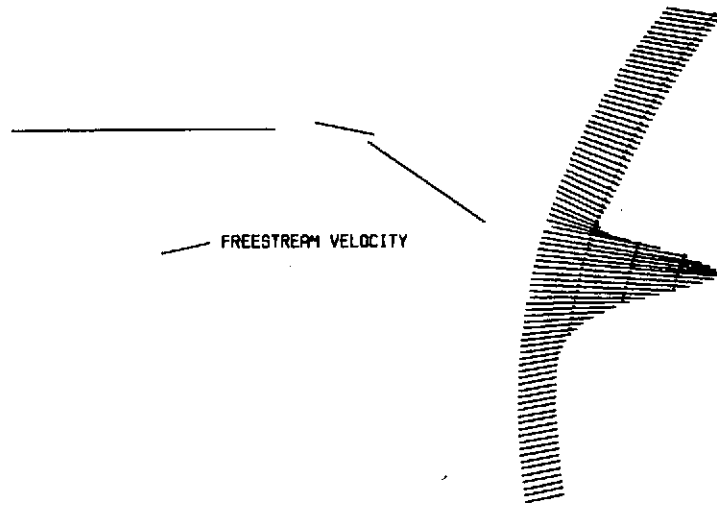
(a) Streamwise velocity profile.



(b) Total velocity.



(c) Downwash angle.

Figure 89.- Wake survey results for $\eta = 0.376$; $\alpha = 0^{\circ}$; $C_T = 2.0$; $V_\infty = 25.45$ m/sec (83.51 ft/sec).
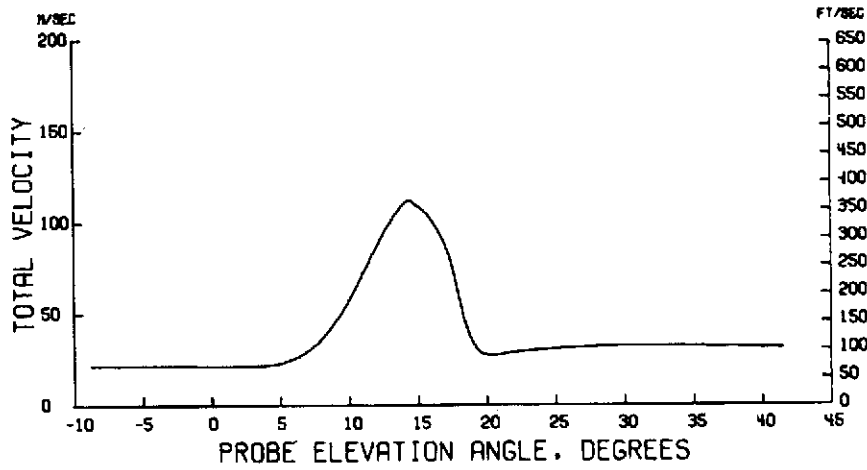
(a) Streamwise velocity profile.
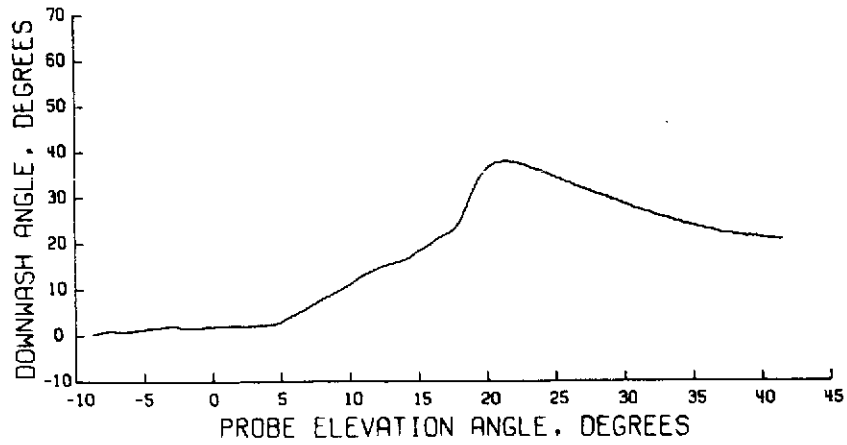


(b) Total velocity.



(c) Downwash angle.

Figure 90.- Wake survey results for $\eta = 0.416$; $\alpha = 0°$; $C_T = 2.0$; $V_\infty = 25.43$ m/sec (83.44 ft/sec).
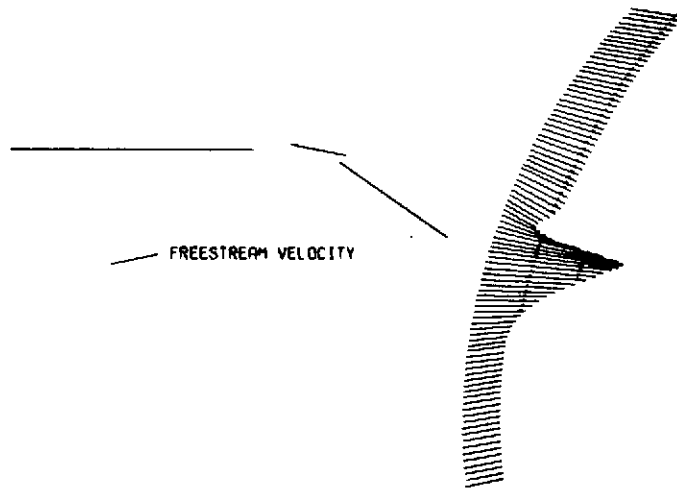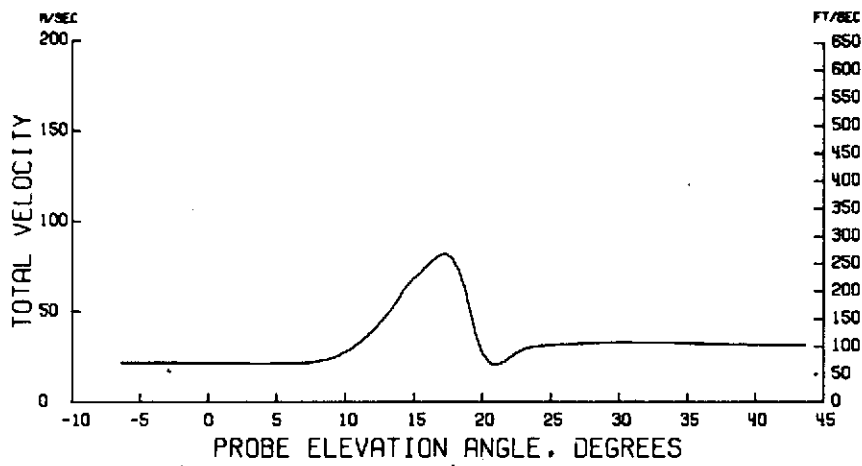
(a) Streamwise velocity profile.



(b) Total velocity.



(c) Downwash angle.

Figure 91.- Wake survey results for $\eta = 0.443$; $\alpha = 0^O$; $C_T = 2.0$; $V_\infty = 25.44$ m/sec (83.46 ft/sec).

(a) Streamwise velocity profile.



(b) Total velocity.



(c) Downwash angle.

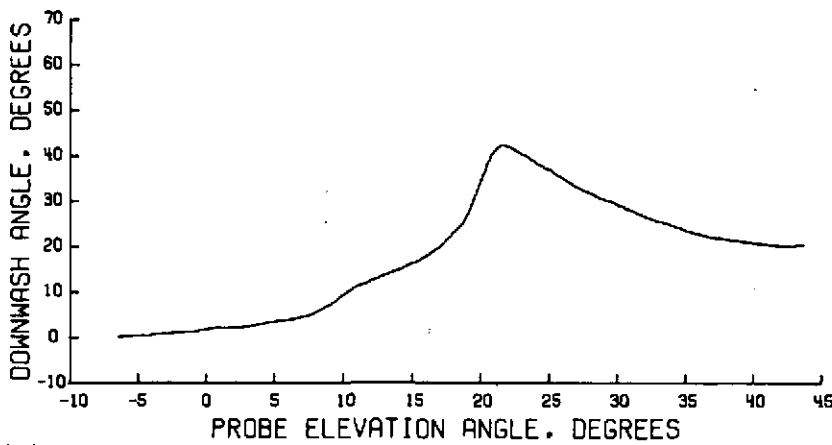Figure 92.- Wake survey results for  $\eta = 0.470$;  $\alpha = 0^O$;  $C_T = 2.0$;
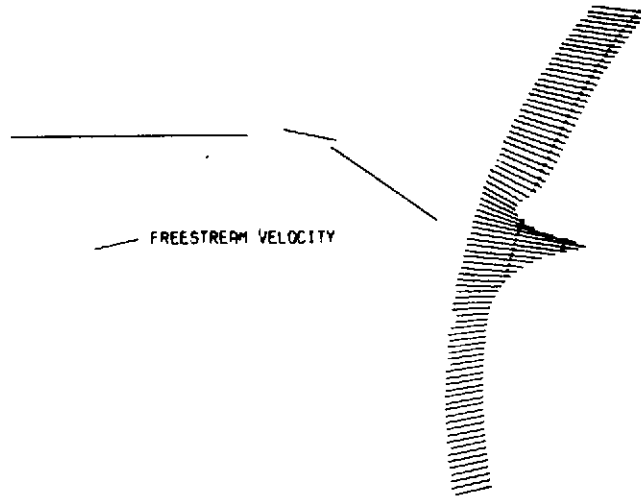$V_\infty = 25.39$ m/sec  (83.31 ft/sec).
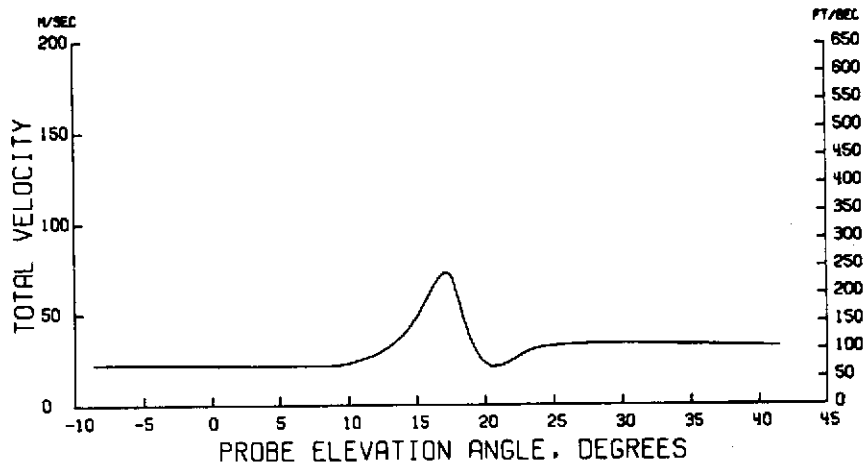
(a) Streamwise velocity profile.



(b) Total velocity.



(c) Downwash angle.

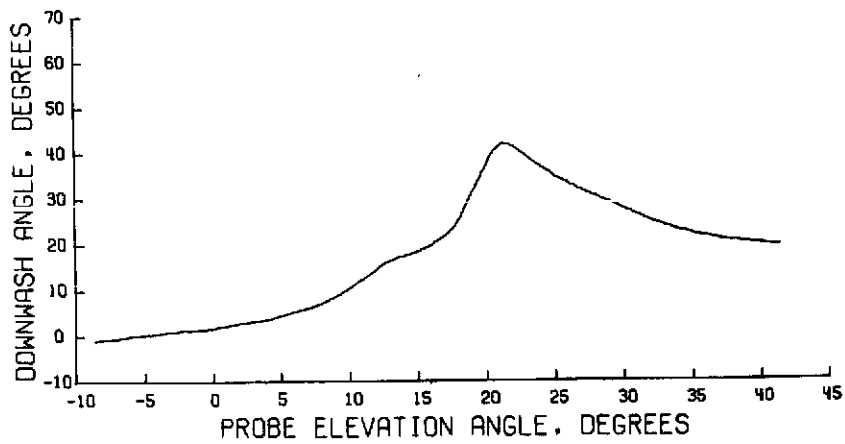Figure 93.- Wake survey results for $\eta = 0.482$; $\alpha = 0^O$; $C_T = 2.0$; $V_\infty = 25.47$ m/sec (83.56 ft/sec).
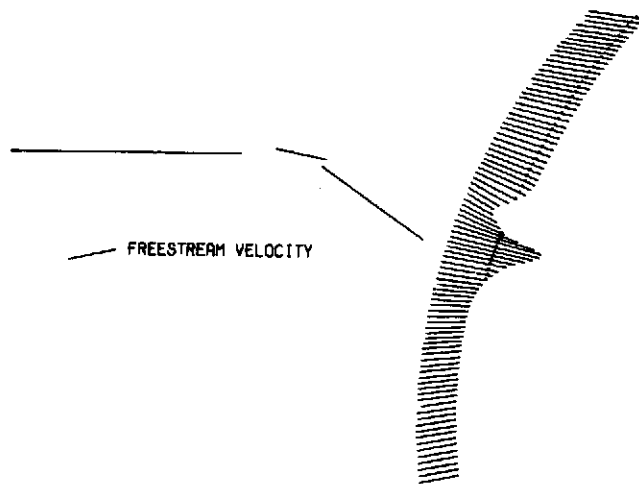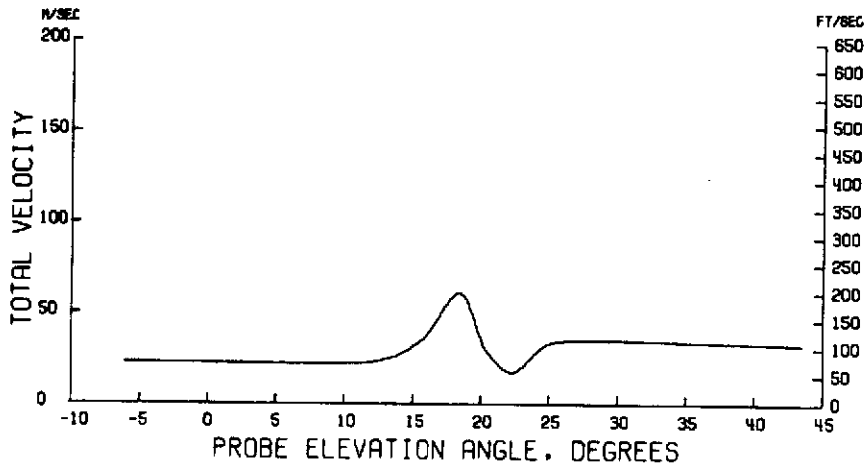
(a) Streamwise velocity profile.
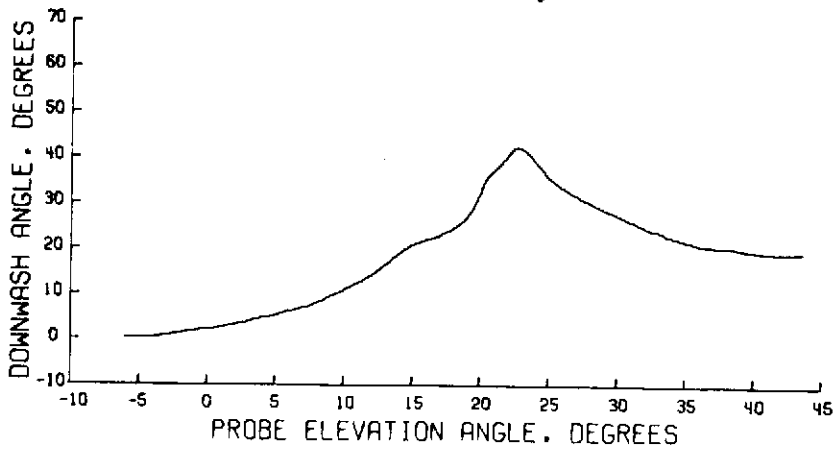


(b) Total velocity.



(c) Downwash angle.

Figure 94.- Wake survey results for $\eta = 0.162$; $\alpha = 8^O$; $C_T = 2.0$; $V_\infty = 25.35$ m/sec (83.19 ft/sec).
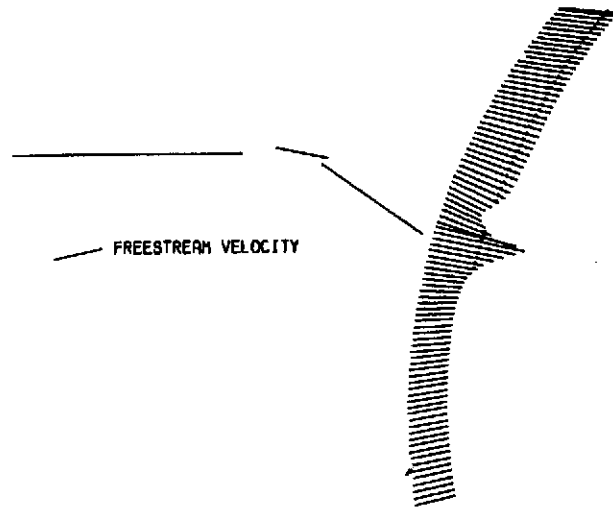
(a) Streamwise velocity profile.



(b) Total velocity.



(c) Downwash angle.

Figure 95.- Wake survey results for $\eta = 0.201$; $\alpha = 8^\circ$; $C_T = 2.0$; $V_\infty = 25.41$ m/sec (83.38 ft/sec).
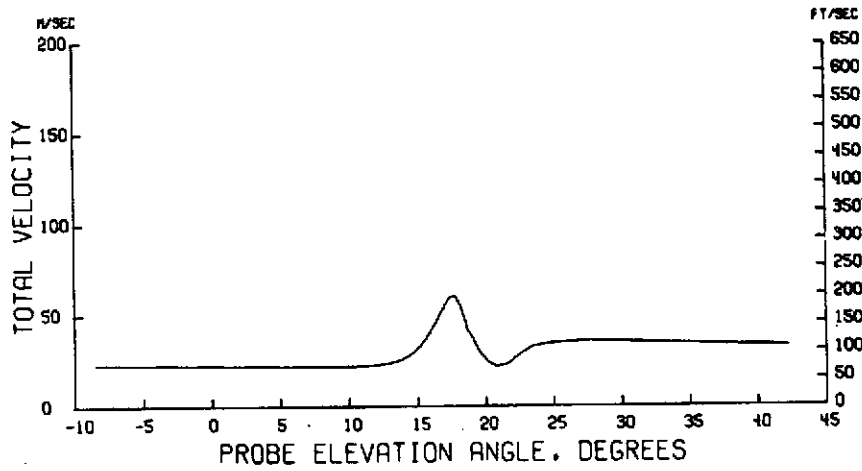
(a) Streamwise velocity profile.



(b) Total velocity.



(c) Downwash angle.

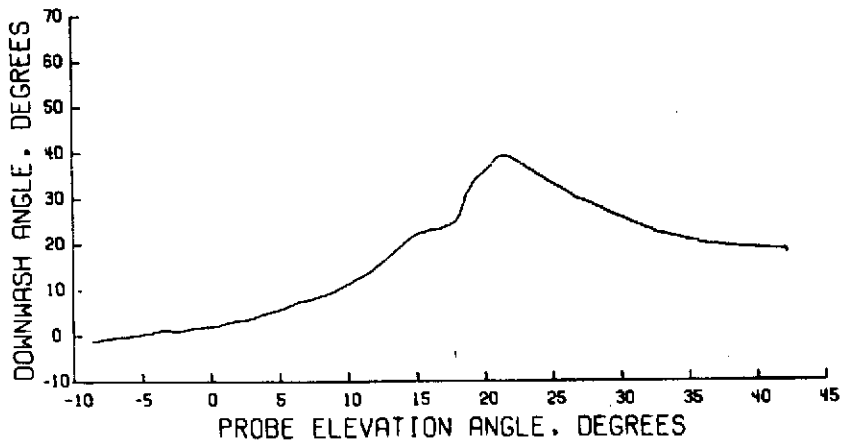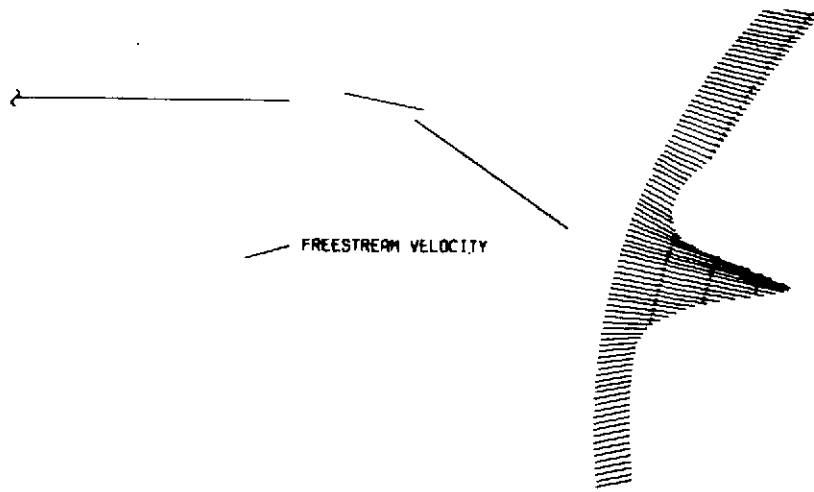Figure 96.- Wake survey results for $\eta = 0.227$; $\alpha = 8^{O}$; $C_T = 2.0$;
$V_\infty = 25.40$ m/sec   (83.34 ft/sec).

(a) Streamwise velocity profile.


(b) Total velocity.


(c) Downwash angle.

Figure 97.- Wake survey results for $\eta = 0.254$; $\alpha = 8^{O}$; $C_T = 2.0$; $V_{\infty} = 25.42$ m/sec (83.40 ft/sec).
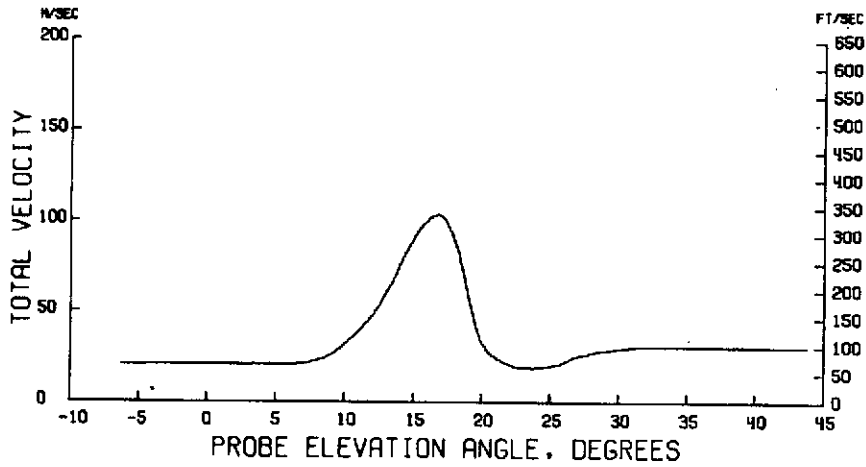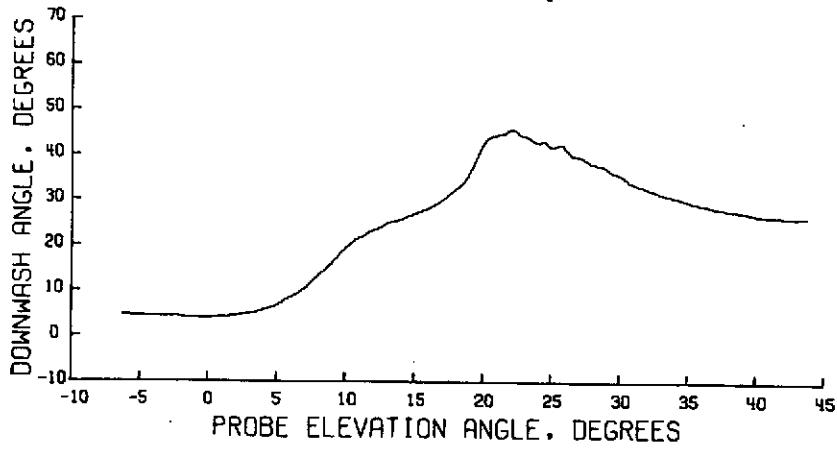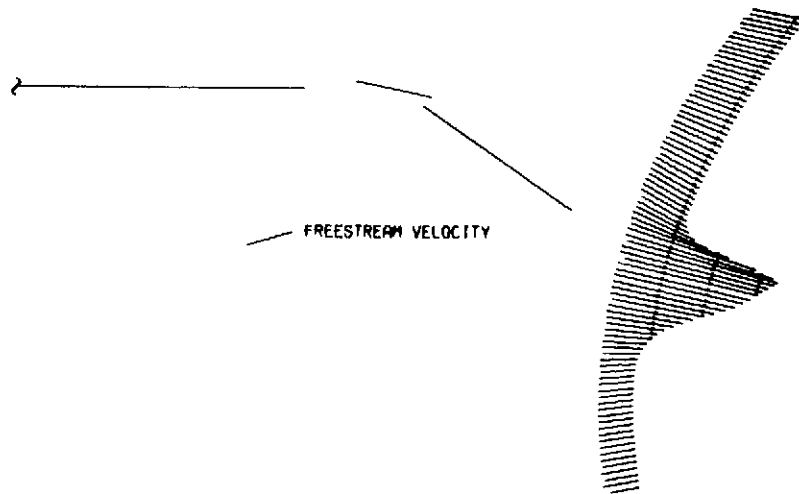
(a) Streamwise velocity profile.



(b) Total velocity.



(c) Downwash angle.

Figure 98.- Wake survey results for  $\eta = 0.295$;  $\alpha = 8^{\circ}$;  $C_T = 2.0$;
$V_\infty = 25.42$ m/sec   (83.42 ft/sec).
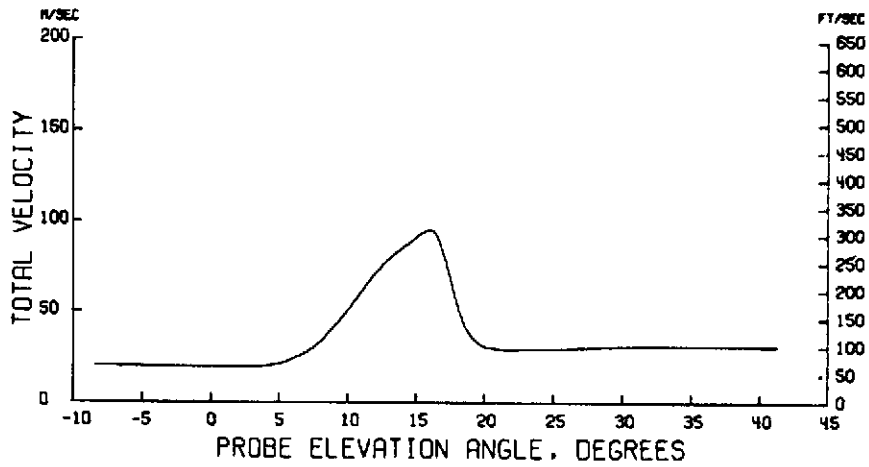
(a) Streamwise velocity profile.



(b) Total velocity.



(c) Downwash angle.
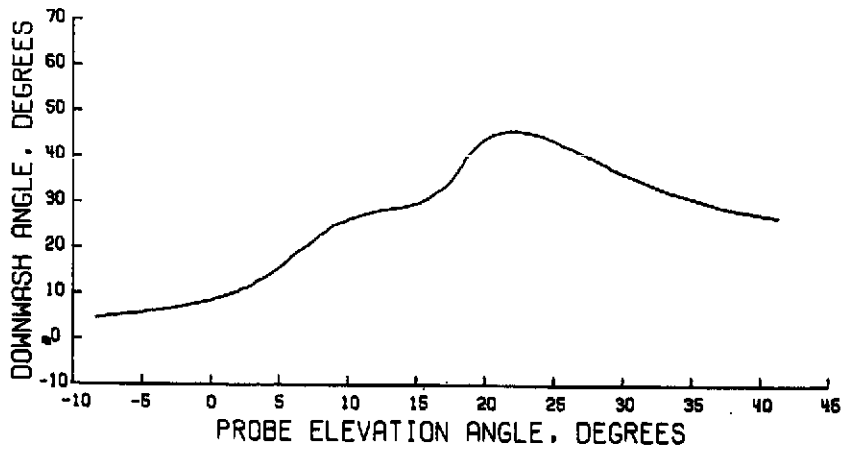
Figure 99.- Wake survey results for $\eta = 0.335$; $\alpha = 8^{O}$; $C_T = 2.0$; $V_\infty = 25.40$ m/sec (83.34 ft/sec).
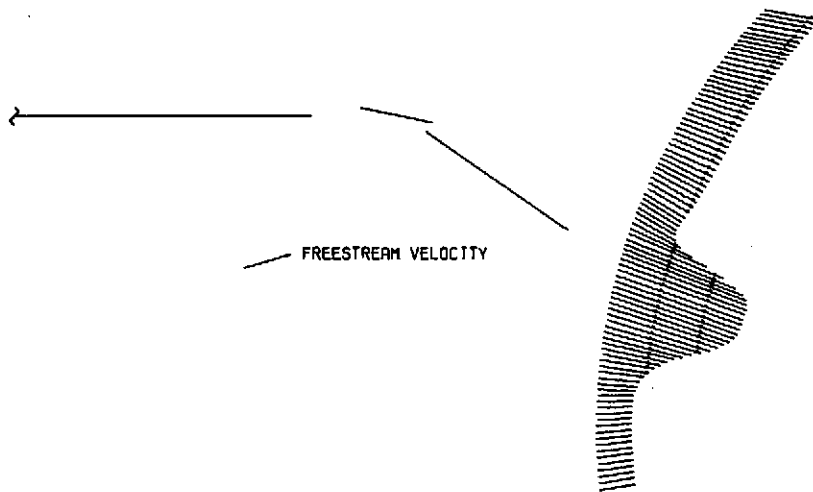
(a) Streamwise velocity profile.



(b) Total velocity.



(c) Downwash angle.

Figure 100.- Wake survey results for $\eta = 0.375$; $\alpha = 8°$; $C_T = 2.0$; $V_\infty = 25.35$ m/sec (83.19 ft/sec).
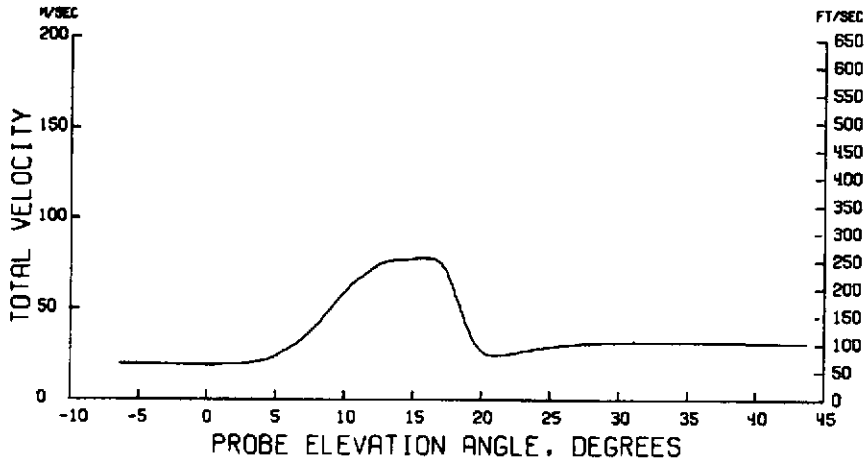
(a) Streamwise velocity profile.



(b) Total velocity.



(c) Downwash angle.

Figure 101.- Wake survey results for $\eta = 0.415$; $\alpha = 8^{\circ}$; $C_T = 2.0$; $V_{\infty} = 25.35$ m/sec (83.17 ft/sec).

(a) Streamwise velocity profile.



(b) Total velocity.



(c) Downwash angle.
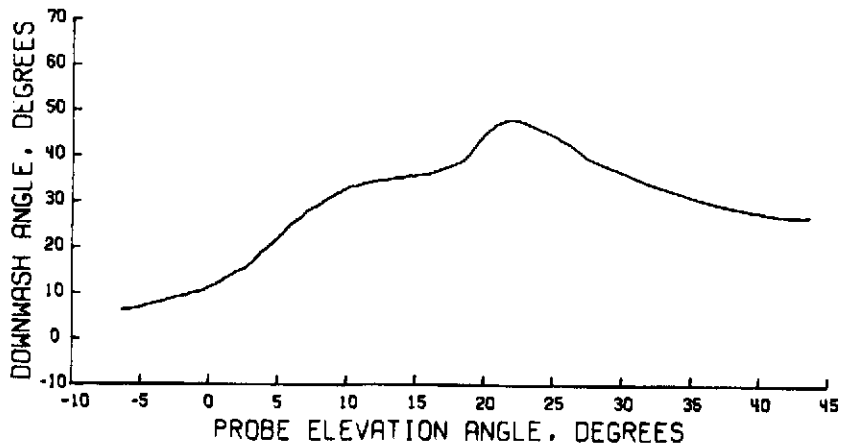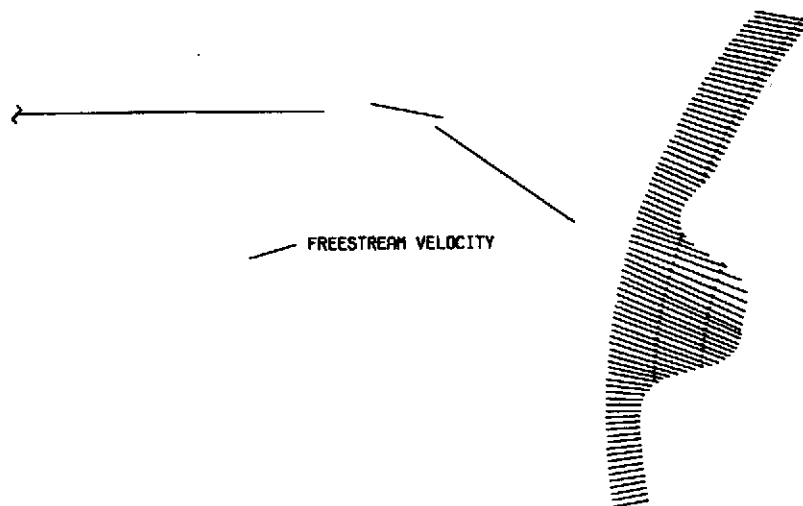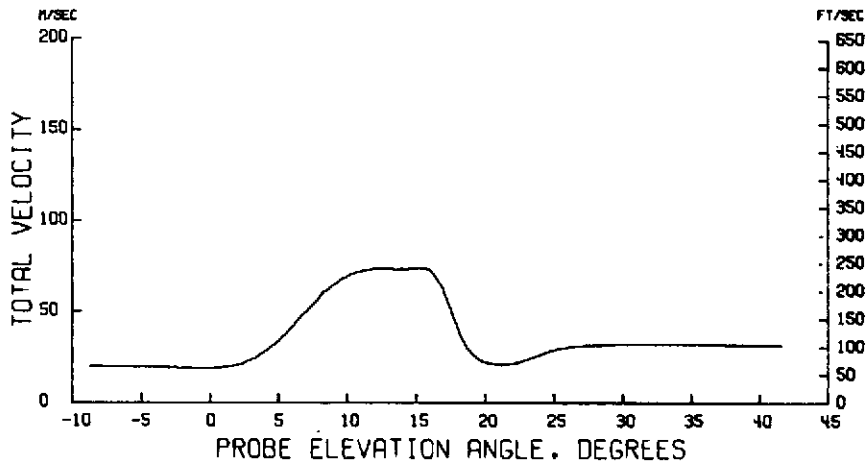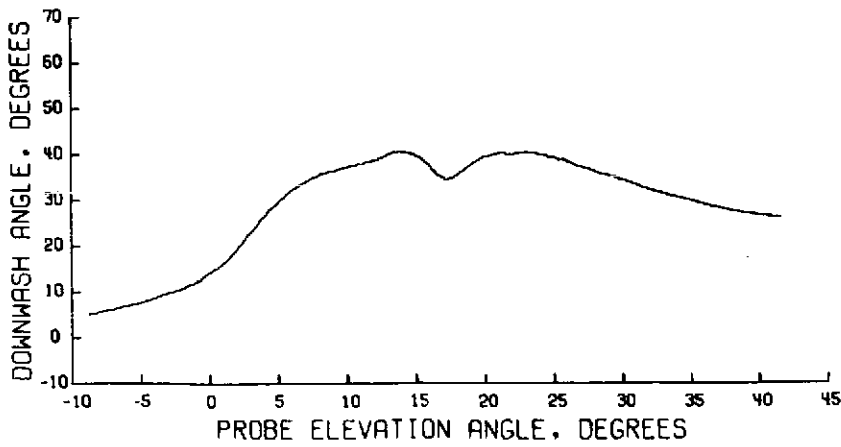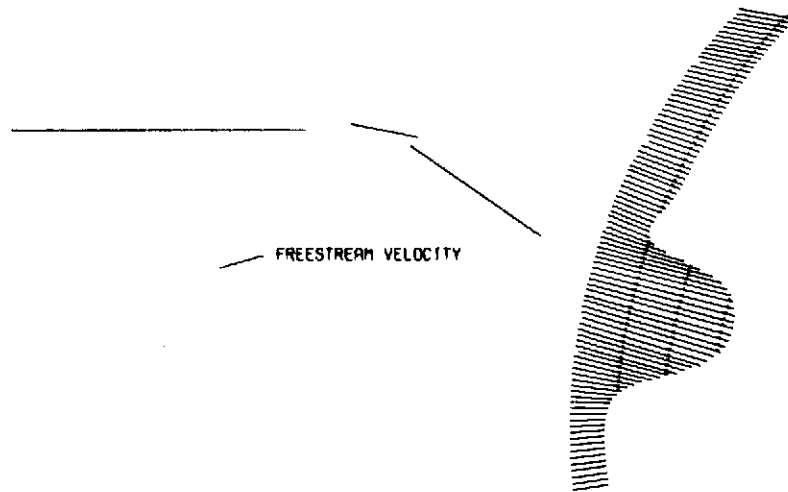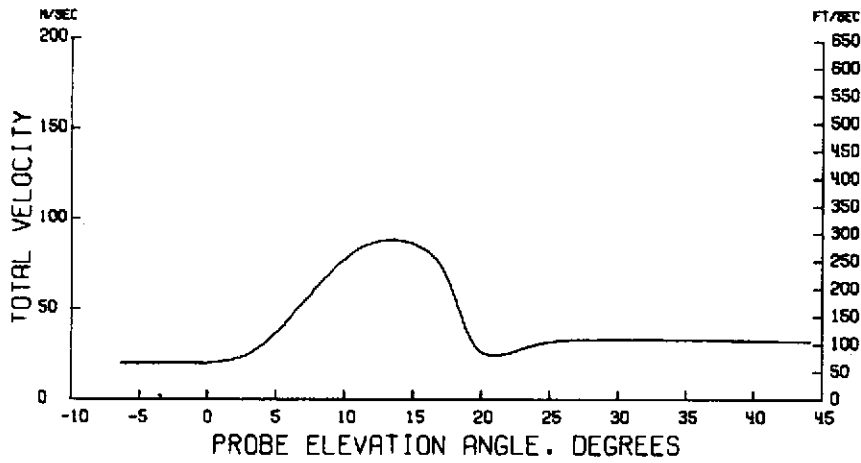
Figure 102.- Wake survey results for $\eta = 0.443$; $\alpha = 8^{\circ}$; $C_T = 2.0$; $V_{\infty} = 25.33$ m/sec (83.12 ft/sec).

(a) Streamwise velocity profile.



(b) Total velocity.



(c) Downwash angle.

Figure 103.- Wake survey results for $\eta = 0.470$; $\alpha = 8^O$; $C_T = 2.0$; $V_\infty = 25.35$ m/sec (83.17 ft/sec).

(a) Streamwise velocity profile.



(b) Total velocity.



(c) Downwash angle.

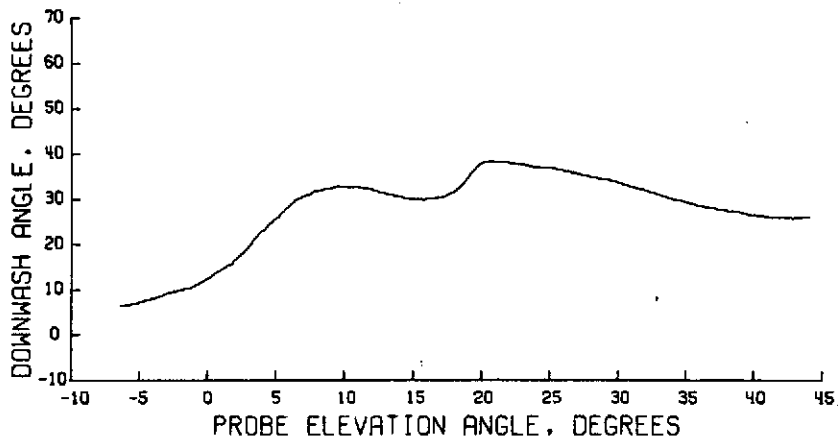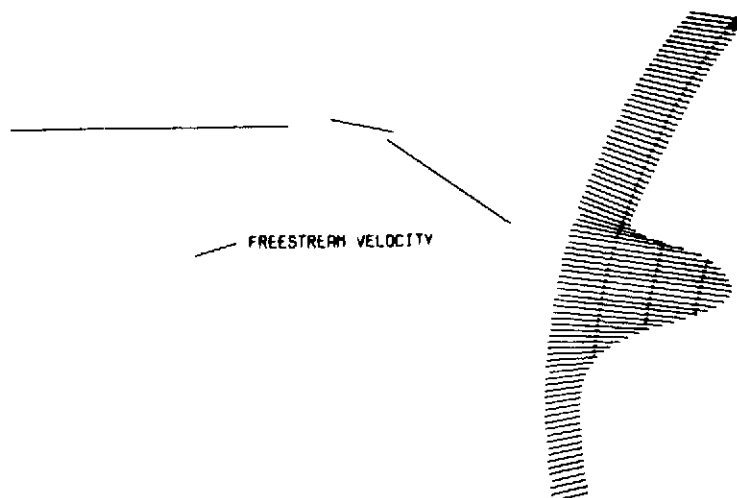Figure 104.- Wake survey results for $\eta = 0.482$; $\alpha = 8^{\circ}$; $C_T = 2.0$;
$V_\infty = 25.26$ m/sec (82.90 ft/sec).
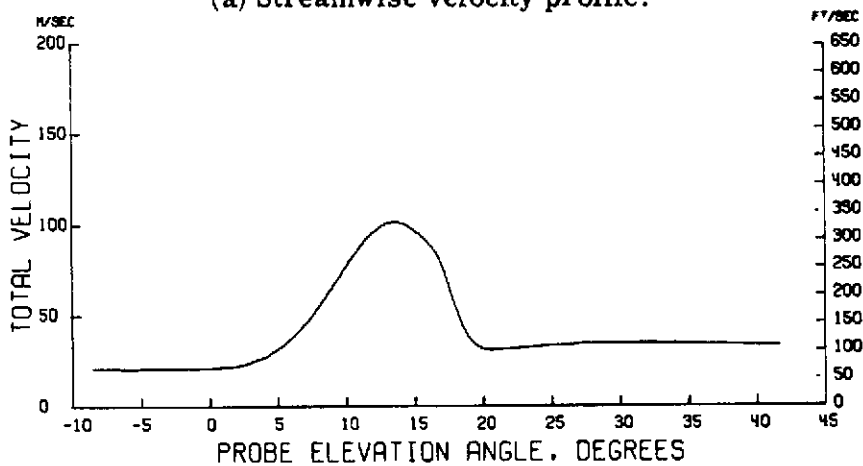
(a) Streamwise velocity profile.
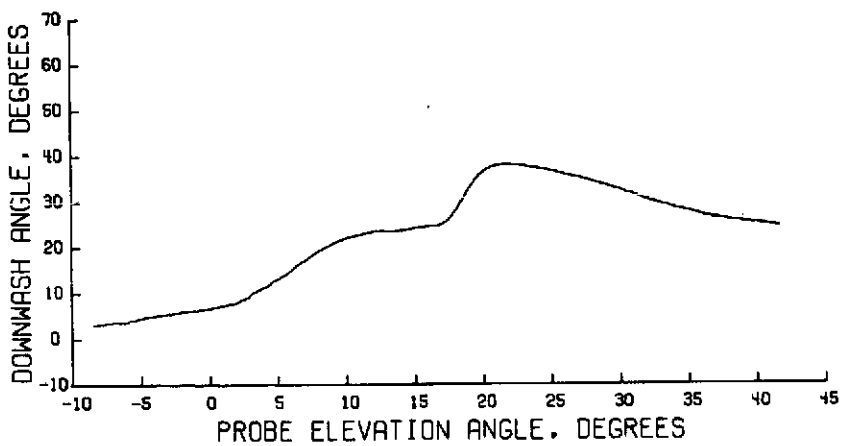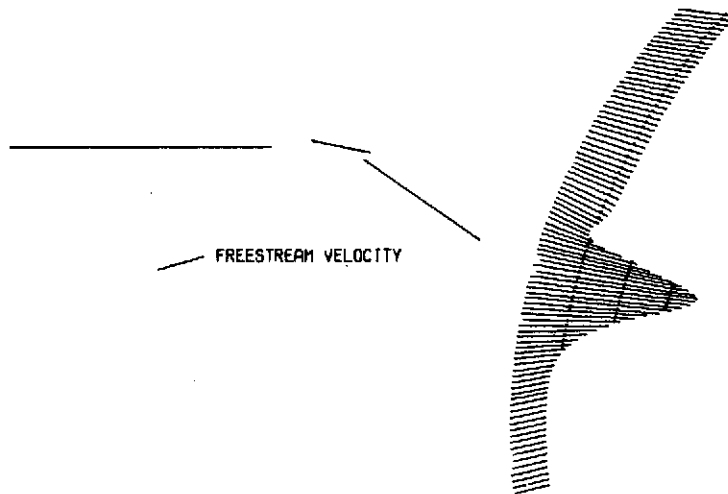


(b) Total velocity.



(c) Downwash angle.

Figure 105.- Wake survey results for $\eta = 0.163$; $\alpha = 12^O$; $C_T = 2.0$;
$V_\infty = 25.42$ m/sec (83.40 ft/sec).

(a) Streamwise velocity profile.



(b) Total velocity.
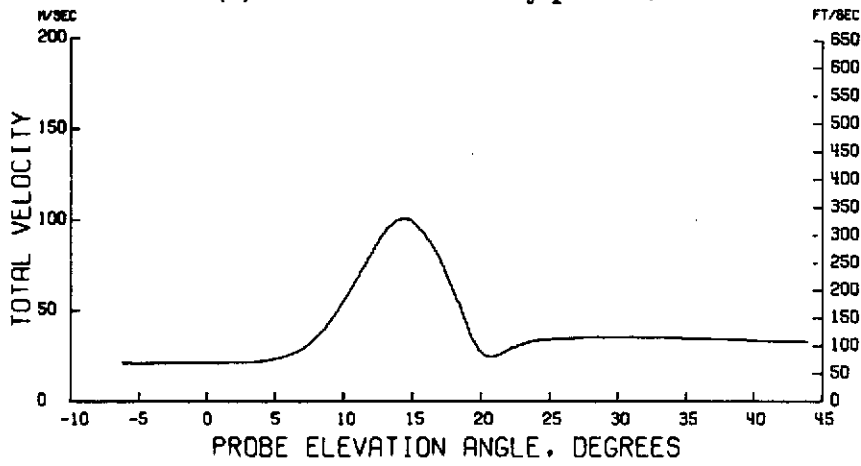


(c) Downwash angle.

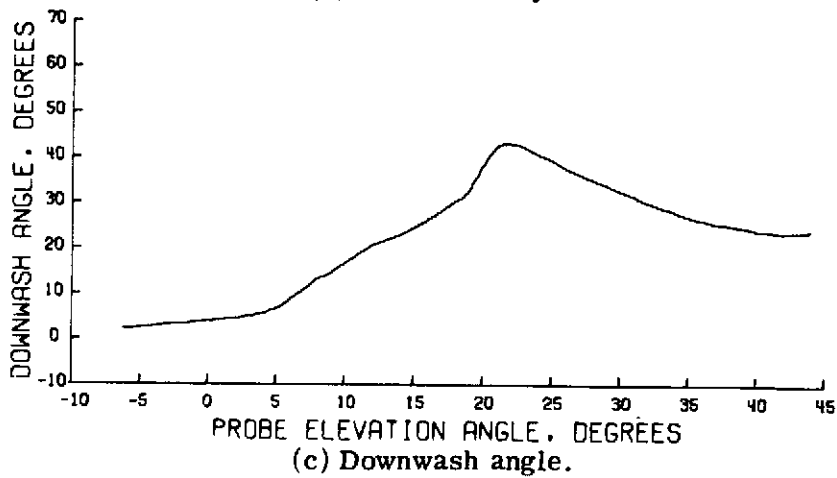Figure 106.- Wake survey results for $\eta = 0.200$; $\alpha = 12^O$; $C_T = 2.0$; $V_\infty = 25.49$ m/sec (83.63 ft/sec).
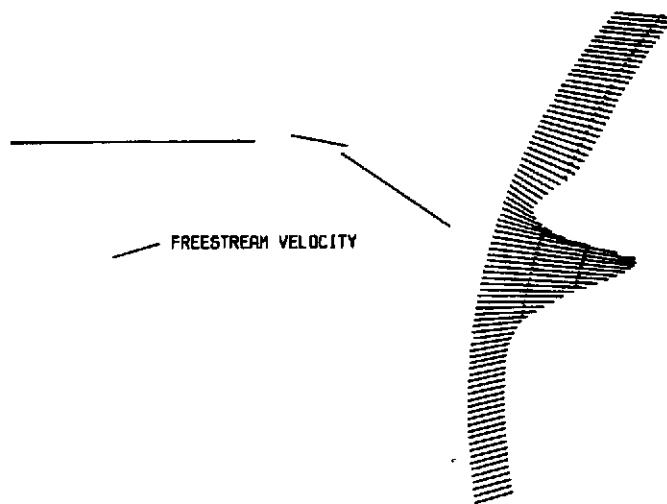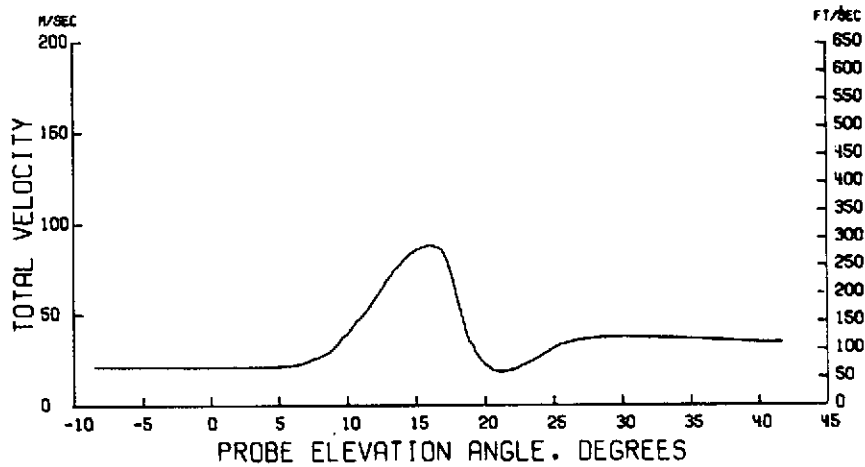
(a) Streamwise velocity profile.



(b) Total velocity.



(c) Downwash angle.

Figure 107.- Wake survey results for $\eta = 0.227$; $\alpha = 12^O$; $C_T = 2.0$; $V_\infty = 25.52$ m/sec (83.74 ft/sec).

(a) Streamwise velocity profile.
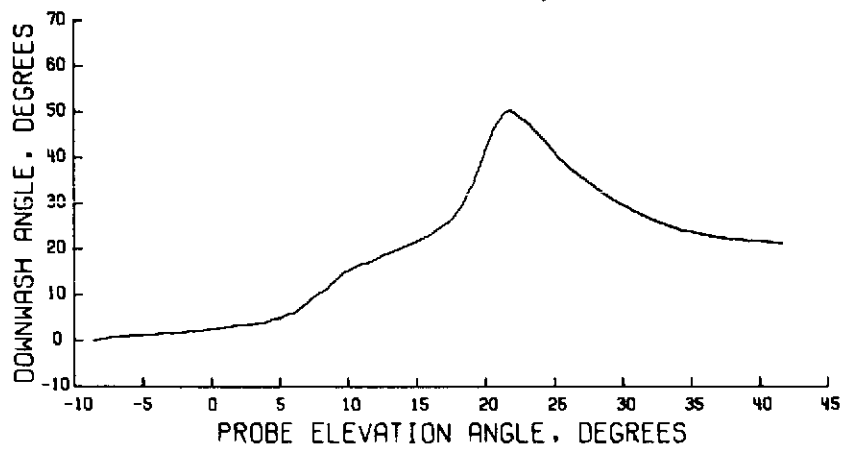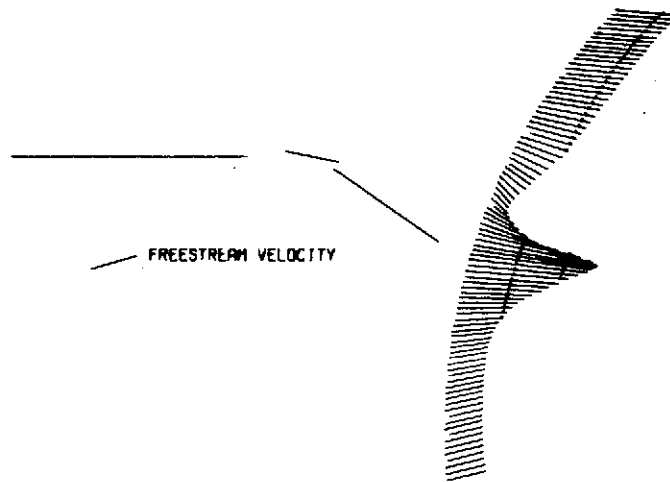


(b) Total velocity.



(c) Downwash angle.

Figure 108.- Wake survey results for $\eta = 0.254$; $\alpha = 12^{O}$; $C_T = 2.0$; $V_\infty = 25.48$ m/sec (83.61 ft/sec).
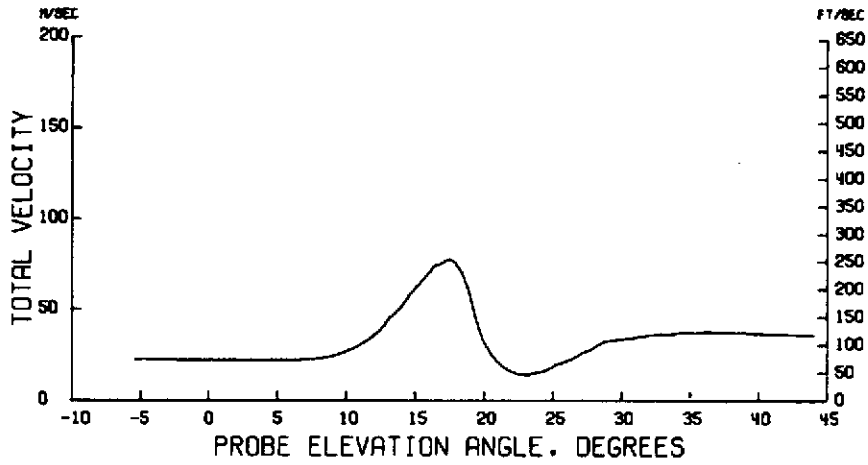
(a) Streamwise velocity profile.



(b) Total velocity.



(c) Downwash angle.

Figure 109.- Wake survey results for $\eta = 0.294$; $\alpha = 12^{O}$; $C_T = 2.0$; $V_\infty = 25.49$ m/sec (83.64 ft/sec).

(a) Streamwise velocity profile.



(b) Total velocity.



(c) Downwash angle.

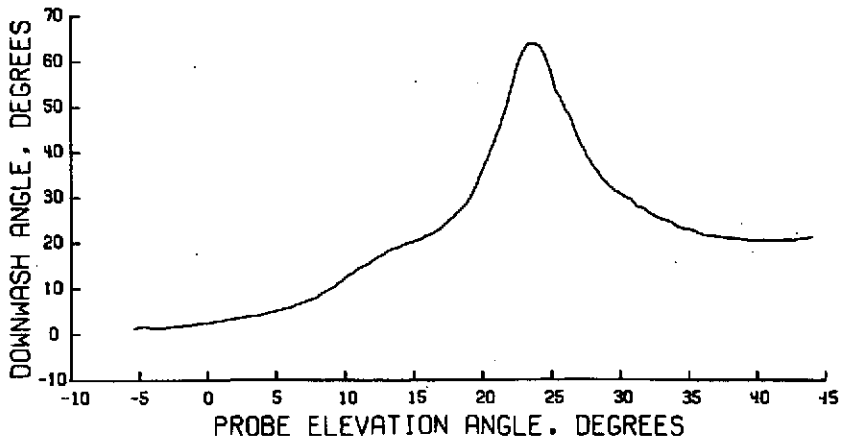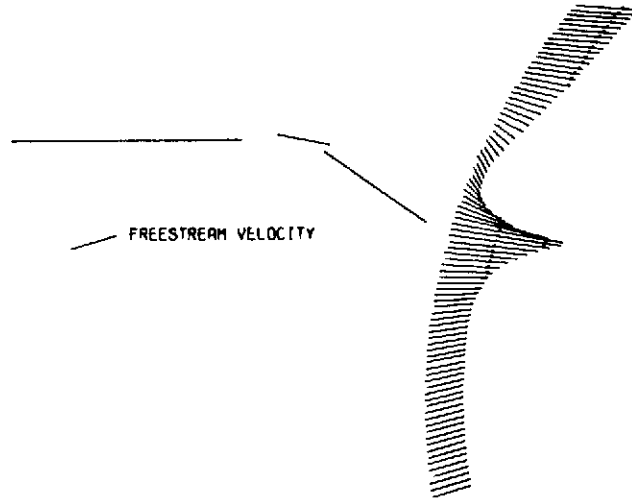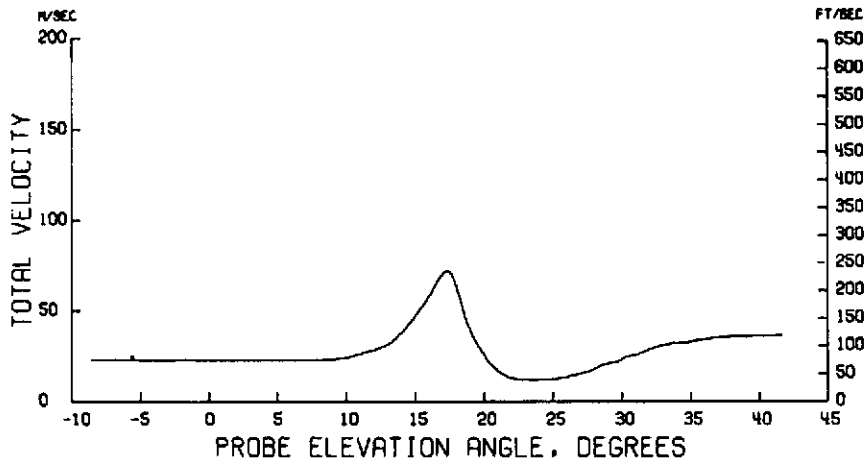Figure 110.- Wake survey results for $\eta = 0.335$; $\alpha = 12^O$; $C_T = 2.0$; $V_\infty = 25.43$ m/sec (83.45 ft/sec).

FREESTREAM VELOCITY

(a) Streamwise velocity profile.



(b) Total velocity.



(c) Downwash angle.

Figure 111.- Wake survey results for $\eta = 0.376$; $\alpha = 12^{O}$; $C_T = 2.0$; $V_\infty = 25.42$ m/sec (83.42 ft/sec).

(a) Streamwise velocity profile.
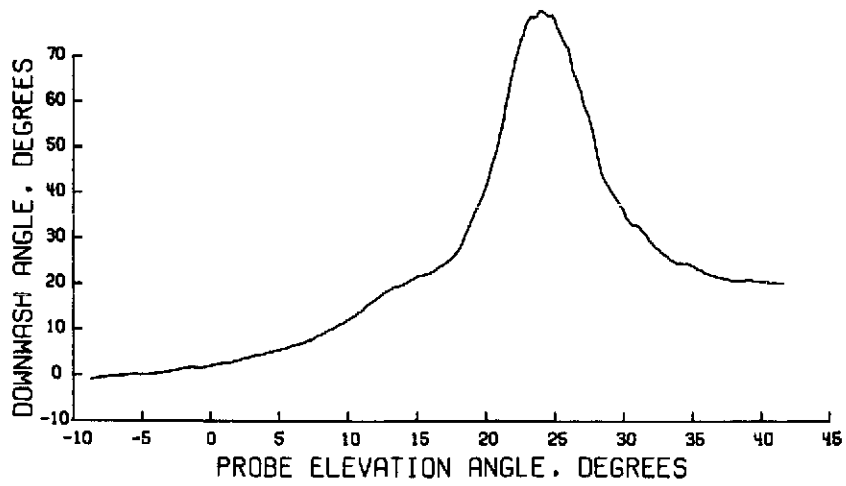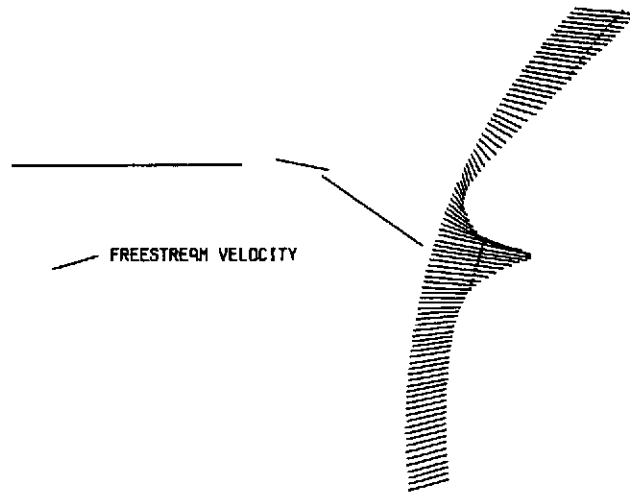


(b) Total velocity.



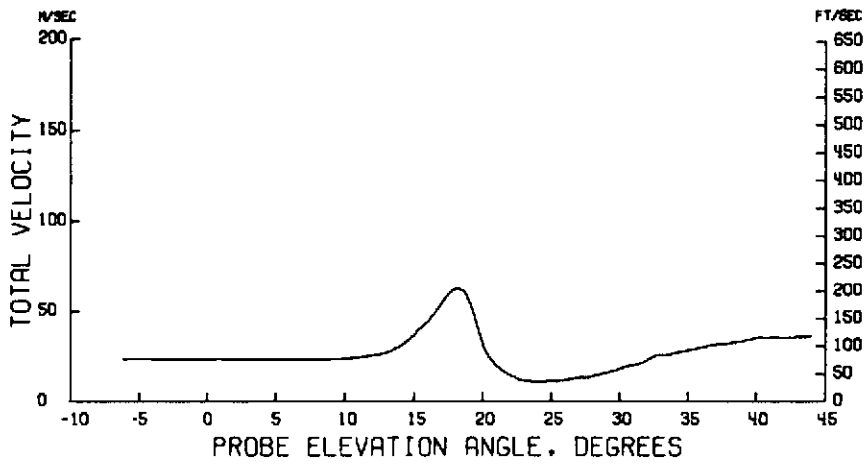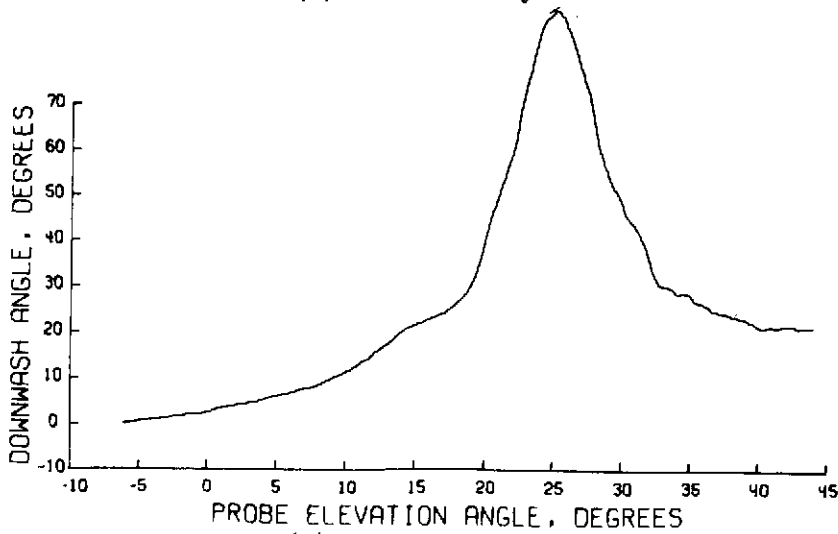(c) Downwash angle.

Figure 112.- Wake survey results for $\eta = 0.416$; $\alpha = 12^O$; $C_T = 2.0$; $V_\infty = 25.41$ m/sec (83.38 ft/sec).
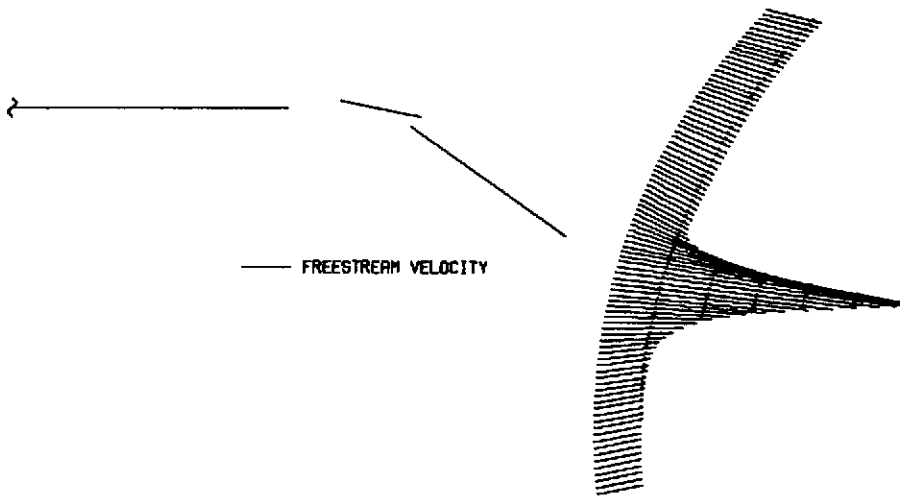
(a) Streamwise velocity profile.



(b) Total velocity.



(c) Downwash angle.

Figure 113.- Wake survey results for $\eta = 0.443$; $\alpha = 12^{\circ}$; $C_T = 2.0$;
$V_{\infty} = 25.44$ m/sec (83.48 ft/sec).
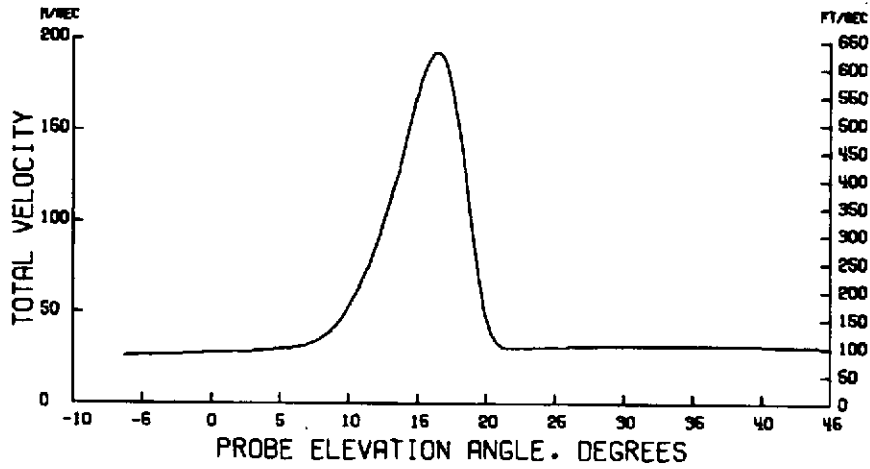
(a) Streamwise velocity profile.
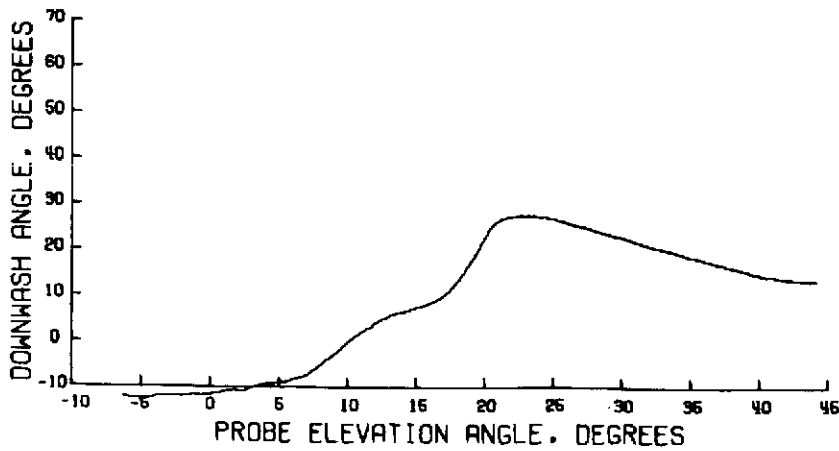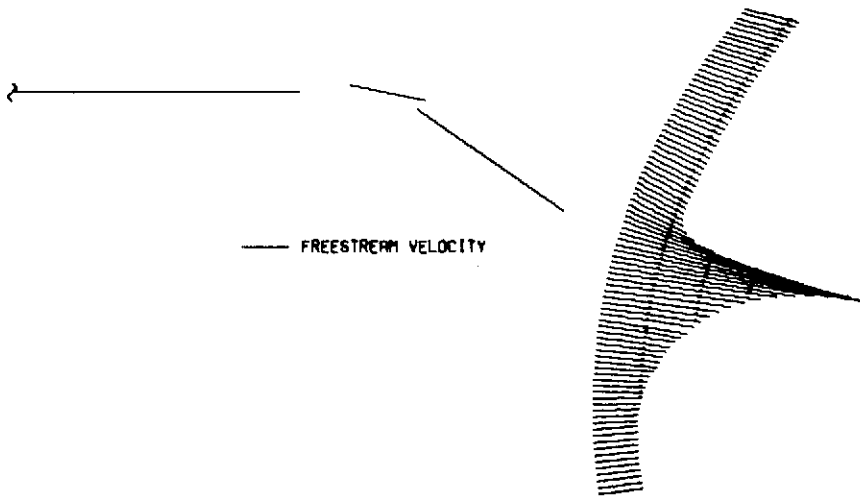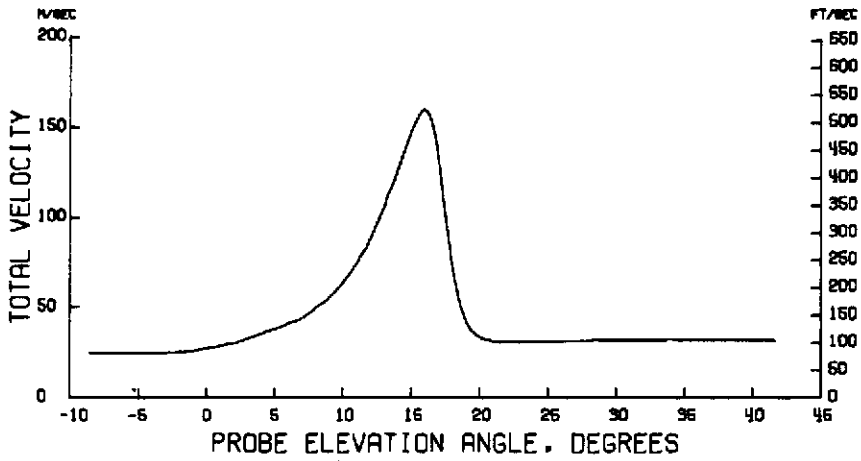


(b) Total velocity.



(c) Downwash angle.

Figure 114.- Wake survey results for $\eta = 0.470$; $\alpha = 12^O$; $C_T = 2.0$; $V_\infty = 25.50$ m/sec (83.68 ft/sec).

FREESTREAM VELOCITY

(a) Streamwise velocity profile.



(b) Total velocity.



(c) Downwash angle.

Figure 115.- Wake survey results for $\eta = 0.482$; $\alpha = 12^O$; $C_T = 2.0$;
$V_\infty = 25.47$ m/sec (83.57 ft/sec).

(a) Streamwise velocity profile.
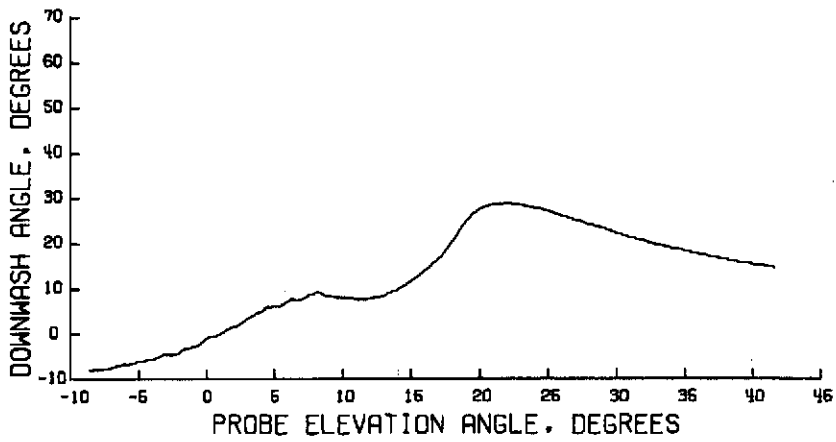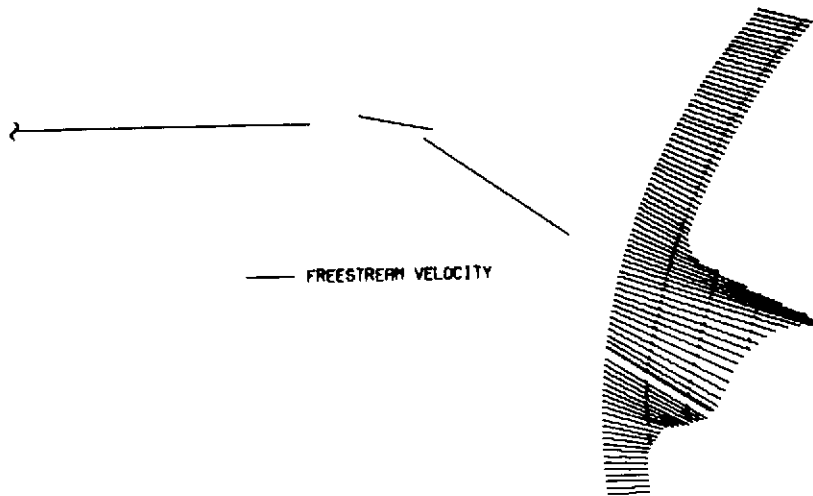


(b) Total velocity.



(c) Downwash angle.

Figure 116.- Wake survey results for $\eta = 0.162$; $\alpha = 16^{\circ}$; $C_T = 2.0$;
$V_{\infty} = 25.32$ m/sec (83.07 ft/sec).

129
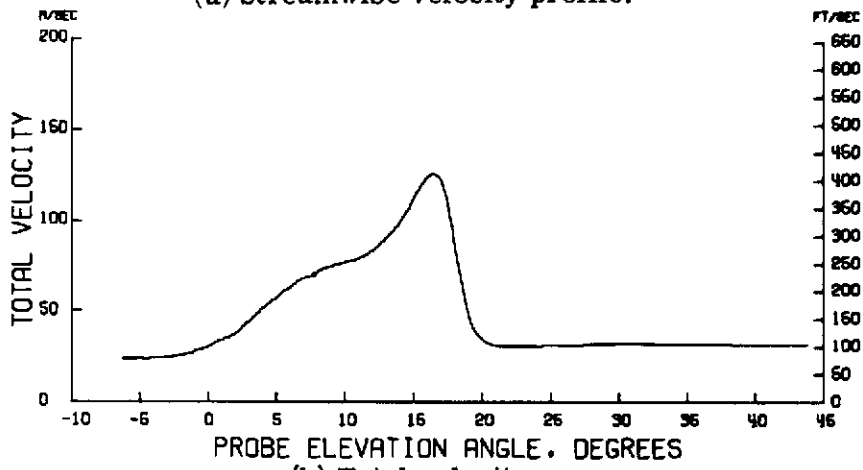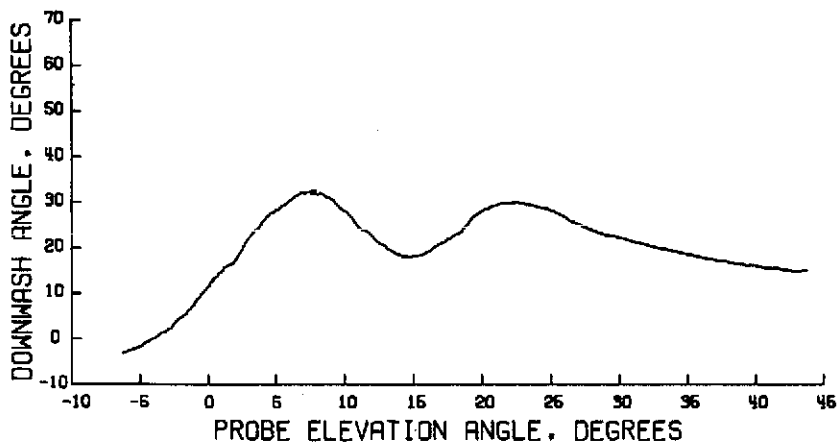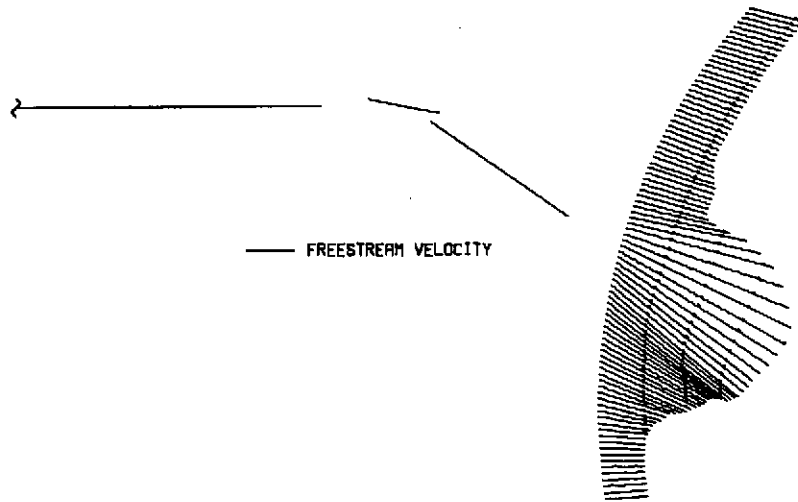
(a) Streamwise velocity profile.



(b) Total velocity.



(c) Downwash angle.

Figure 117.- Wake survey results for $\eta = 0.201$; $\alpha = 16^O$; $C_T = 2.0$; $V_\infty = 25.35$ m/sec (83.18 ft/sec).
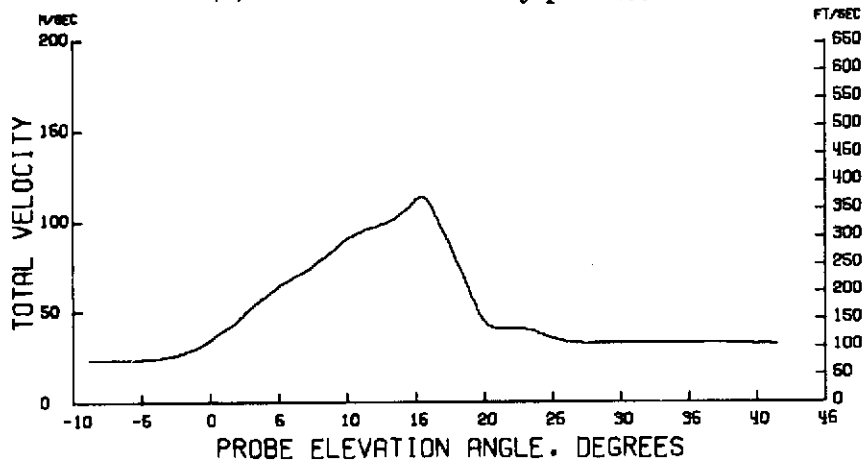
(a) Streamwise velocity profile.



(b) Total velocity.



(c) Downwash angle.

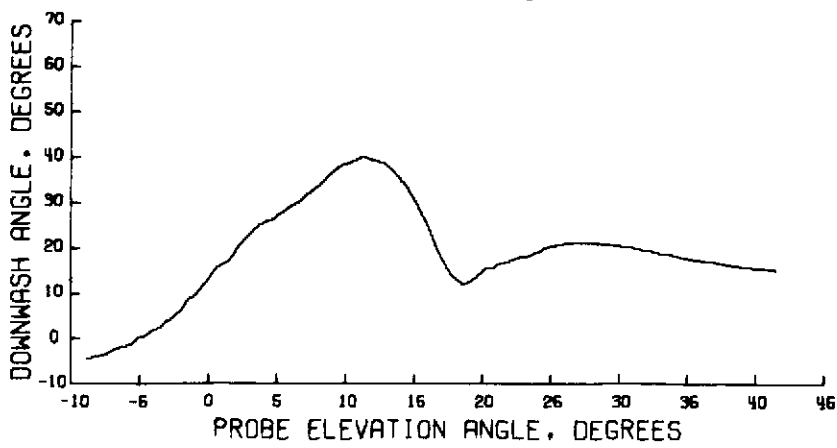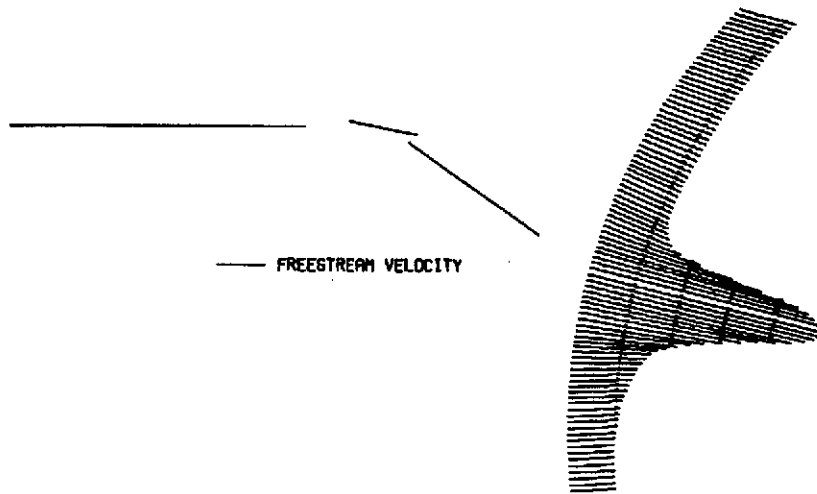Figure 118.- Wake survey results for $\eta = 0.227$; $\alpha = 16^O$; $C_T = 2.0$;
$V_\infty = 25.34$ m/sec (83.16 ft/sec).

131

(a) Streamwise velocity profile.



(b) Total velocity.



(c) Downwash angle.

Figure 119.- Wake survey results for $\eta = 0.253$; $\alpha = 16^{O}$; $C_T = 2.0$; $V_\infty = 25.36$ m/sec (83.20 ft/sec).
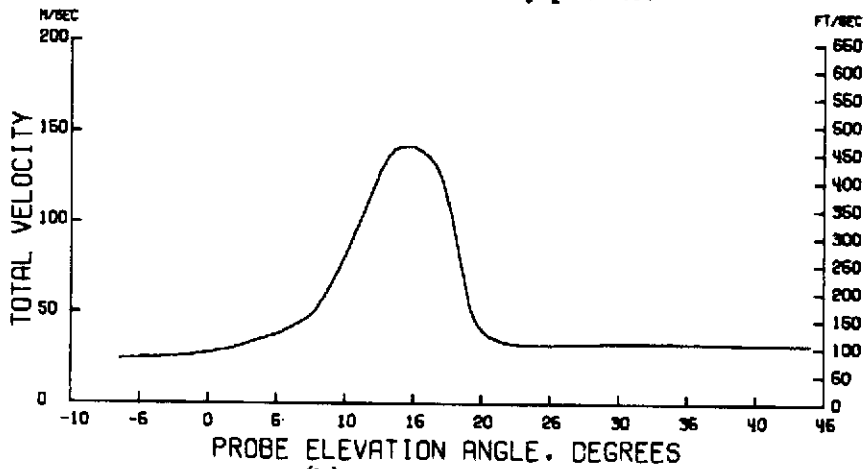
(a) Streamwise velocity profile.



(b) Total velocity.



(c) Downwash angle.

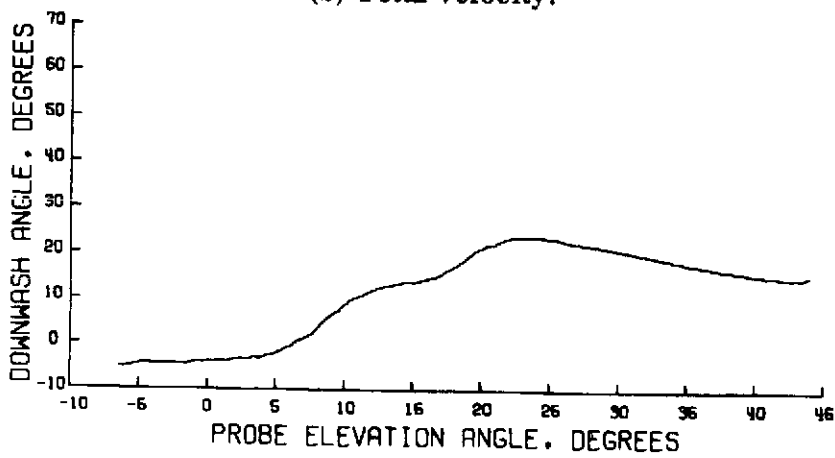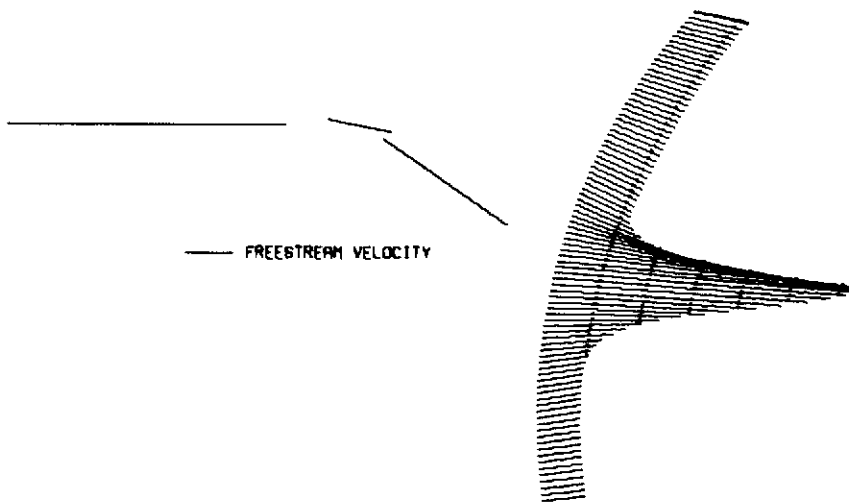Figure 120.- Wake survey results for $\eta = 0.294$; $\alpha = 16^{O}$; $C_T = 2.0$; $V_\infty = 25.36$ m/sec (83.23 ft/sec).

133

(a) Streamwise velocity profile.



(b) Total velocity.



(c) Downwash angle.

Figure 121.- Wake survey results for $\eta = 0.335$; $\alpha = 16^O$; $C_T = 2.0$; $V_\infty = 25.39$ m/sec (83.30 ft/sec).
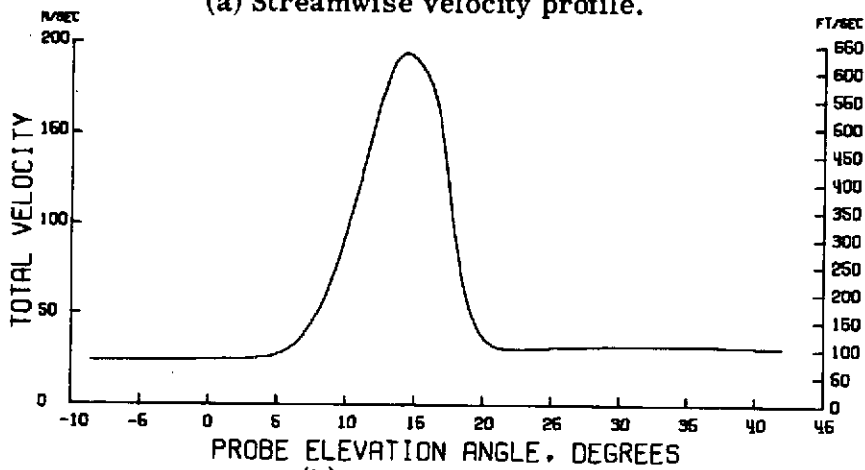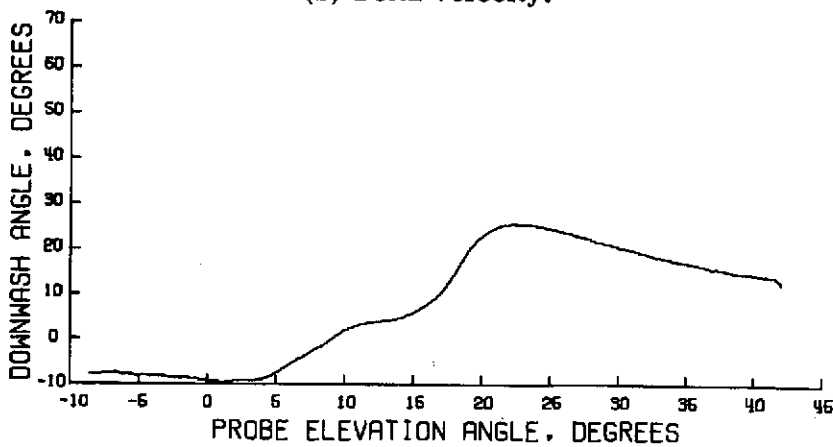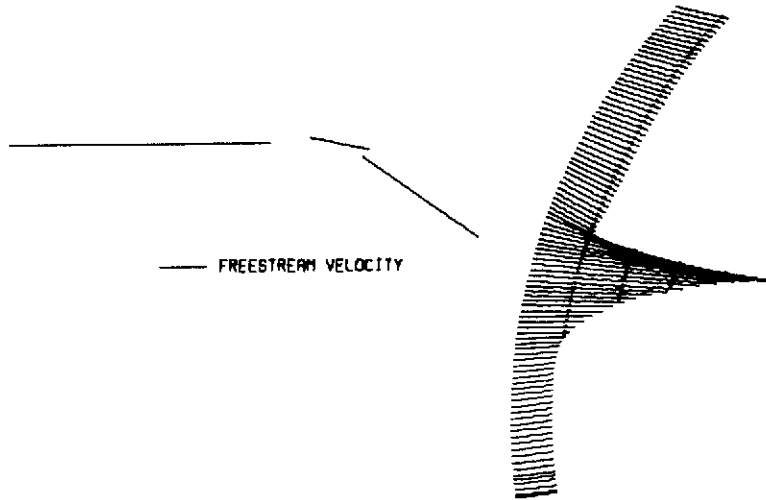
(a) Streamwise velocity profile.



(b) Total velocity.
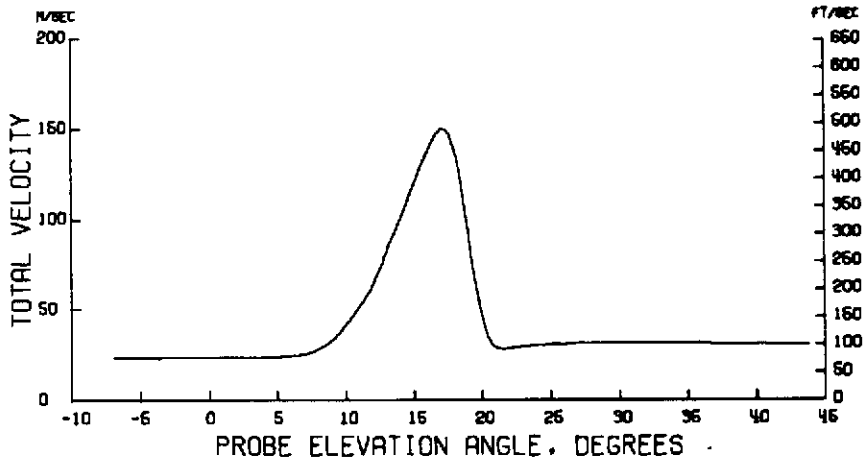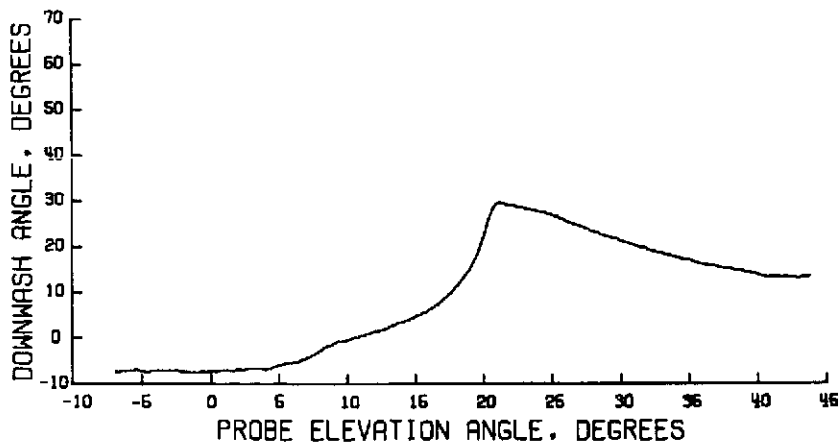


(c) Downwash angle.

Figure 122.- Wake survey results for $\eta = 0.375$; $\alpha = 16^{O}$; $C_T = 2.0$; $V_{\infty} = 25.32$ m/sec (83.08 ft/sec).
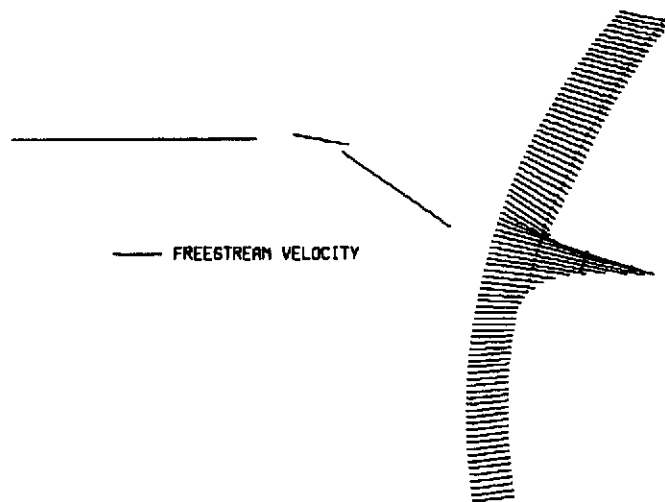
135

(a) Streamwise velocity profile.
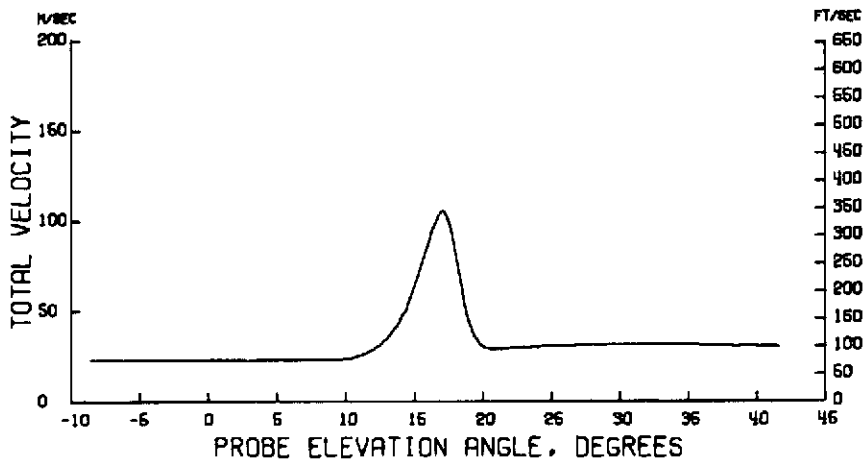


(b) Total velocity.



(c) Downwash angle.

Figure 123.- Wake survey results for $\eta = 0.416$; $\alpha = 16^O$; $C_T = 2.0$; $V_\infty = 25.32$ m/sec (83.07 ft/sec).

136

(a) Streamwise velocity profile.
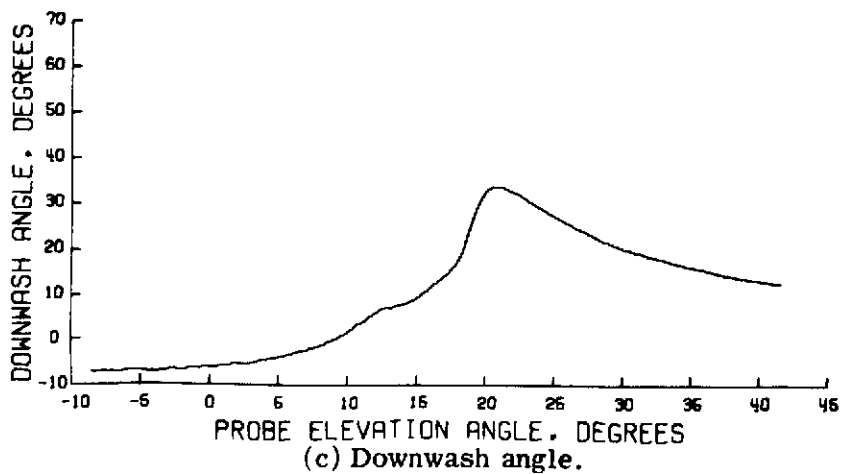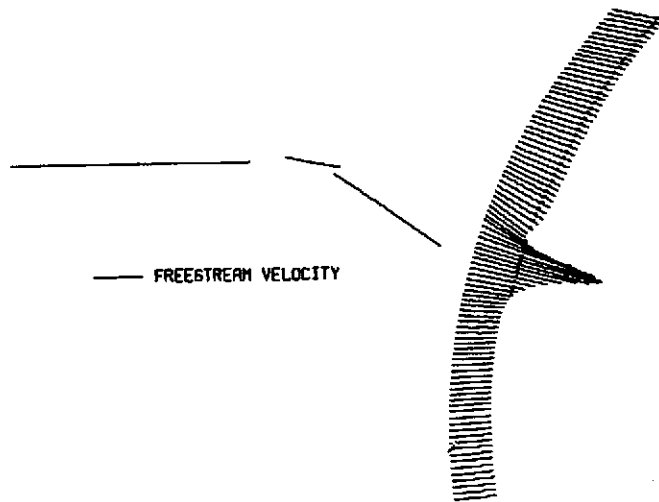


(b) Total velocity.



(c) Downwash angle.

Figure 124.- Wake survey results for $\eta = 0.443$; $\alpha = 16^O$; $C_T = 2.0$; $V_\infty = 25.36$ m/sec (83.22 ft/sec).
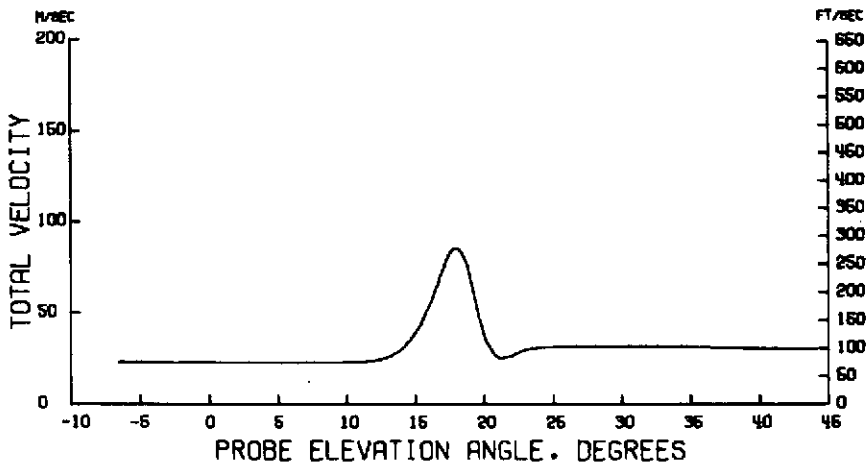
137

(a) Streamwise velocity profile.



(b) Total velocity.



(c) Downwash angle.

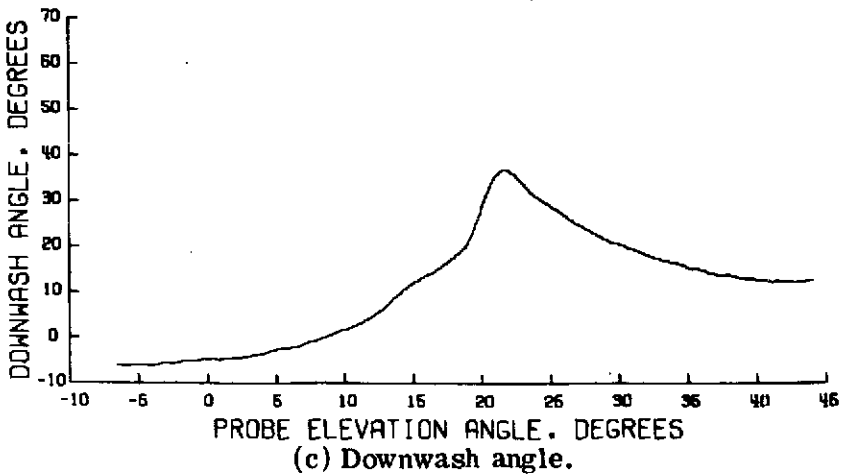Figure 125.- Wake survey results for $\eta = 0.469$; $\alpha = 16^O$; $C_T = 2.0$;
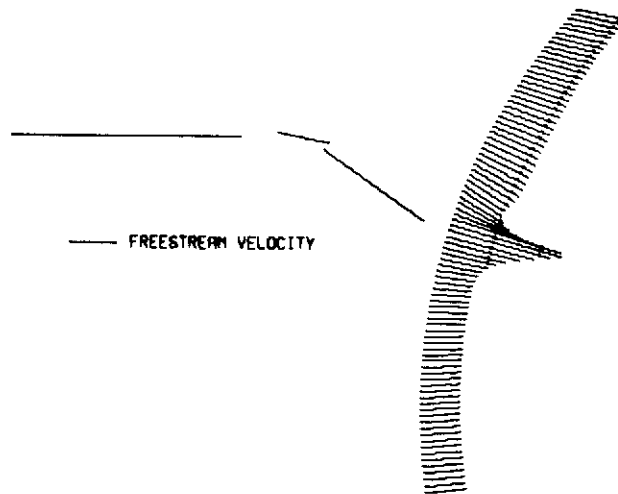$V_\infty = 25.41$ m/sec (83.39 ft/sec).
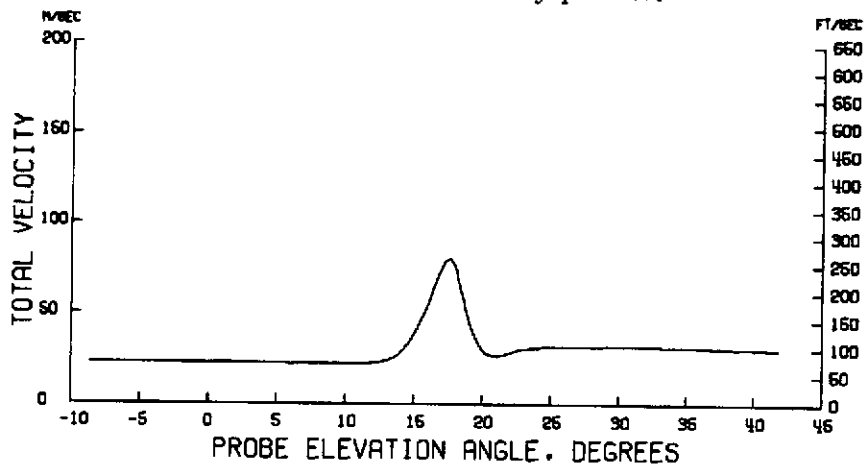
(a) Streamwise velocity profile.



(b) Total velocity.



(c) Downwash angle.

Figure 126.- Wake survey results for $\eta = 0.483$; $\alpha = 16^O$; $C_T = 2.0$; $V_\infty = 25.37$ m/sec (83.25 ft/sec).

(a) Streamwise velocity profile.



(b) Total velocity.



(c) Downwash angle.

Figure 127.- Wake survey results for $\eta = 0.162$; $\alpha = 0^{\circ}$; $C_T = 4.0$; $V_{\infty} = 25.51$ m/sec (83.72 ft/sec).

(a) Streamwise velocity profile.
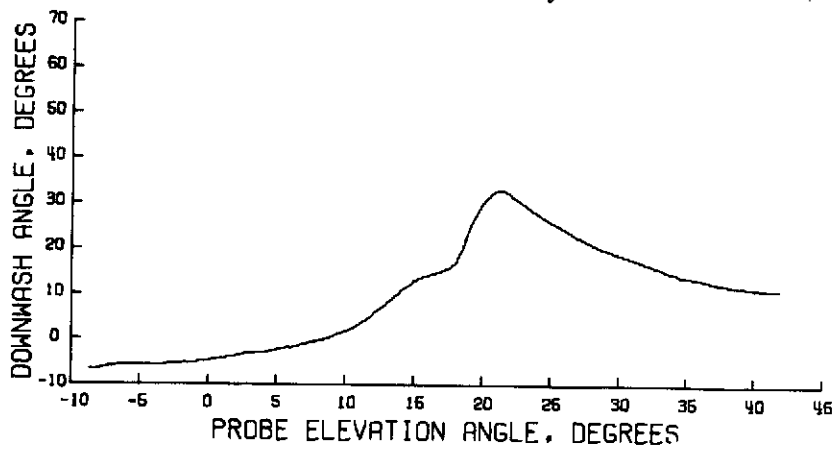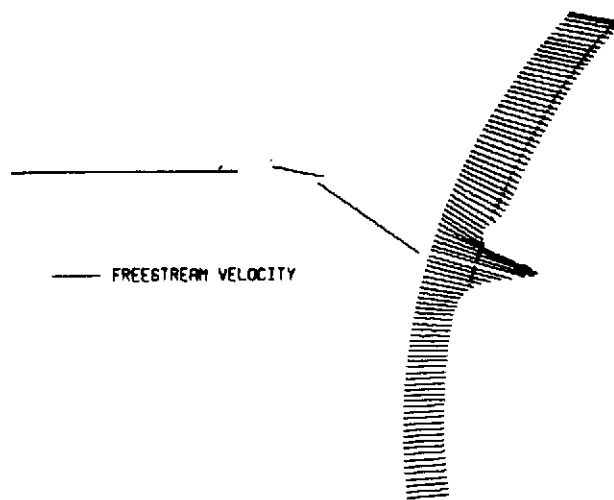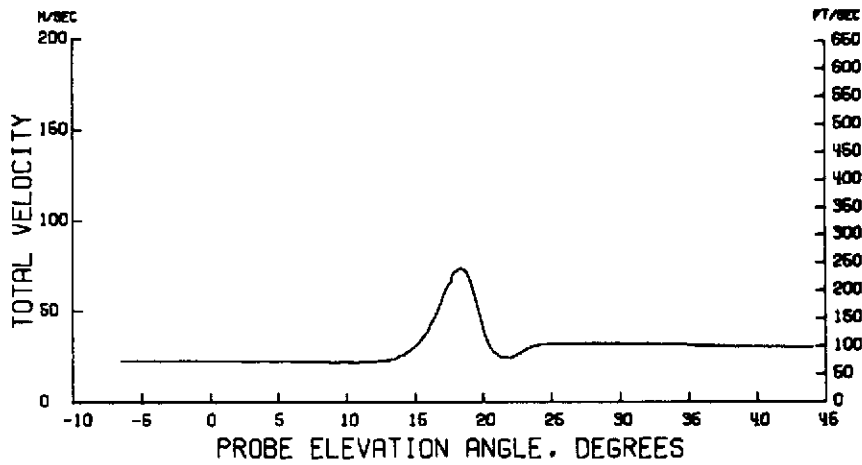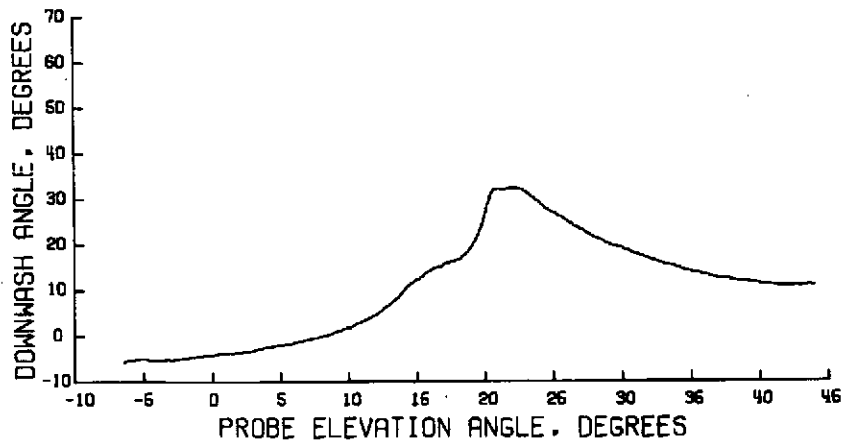


(b) Total velocity.



(c) Downwash angle.

Figure 128.- Wake survey results for $\eta = 0.200$; $\alpha = 0°$; $C_T = 4.0$; $V_\infty = 25.52$ m/sec (83.74 ft/sec).

(a) Streamwise velocity profile.



(b) Total velocity.



(c) Downwash angle.

Figure 129.- Wake survey results for $\eta = 0.227$; $\alpha = 0°$; $C_T = 4.0$; $V_\infty = 25.53$ m/sec (83.76 ft/sec).
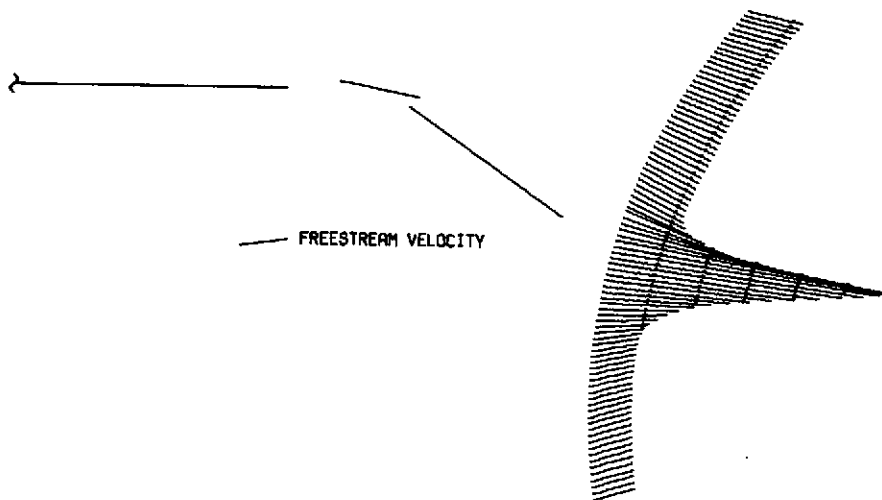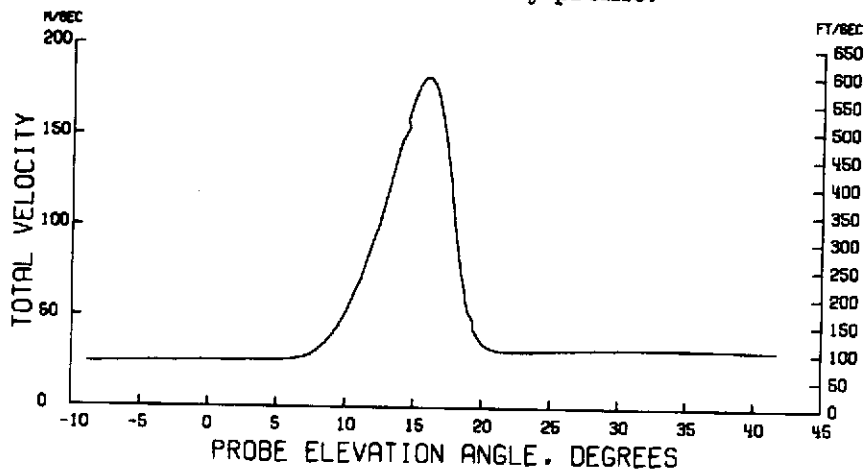
(a) Streamwise velocity profile.



(b) Total velocity.



(c) Downwash angle.
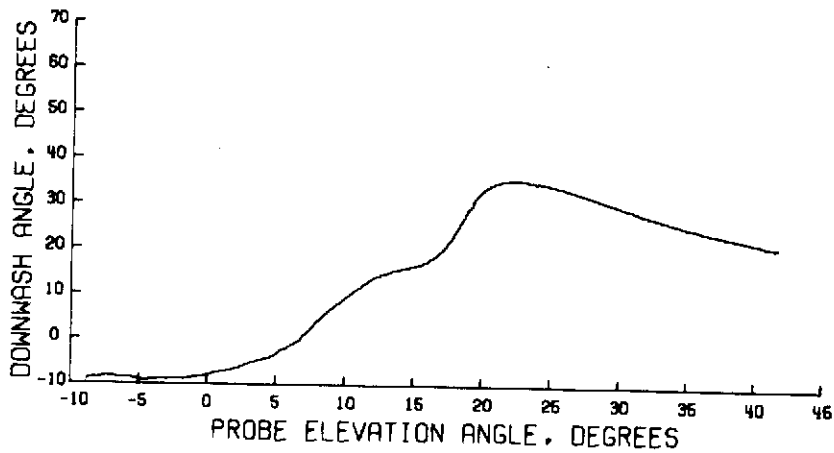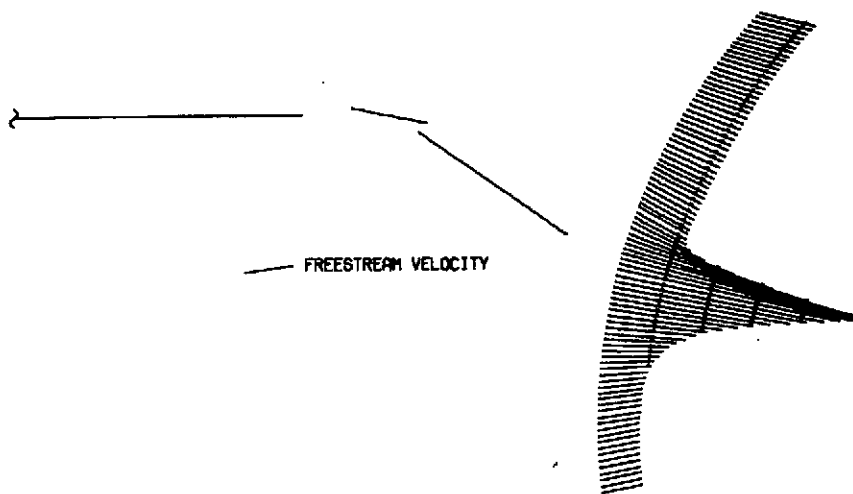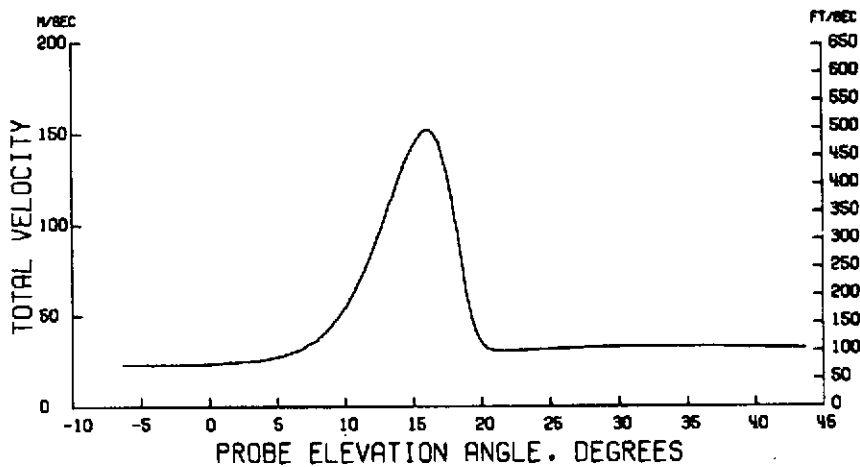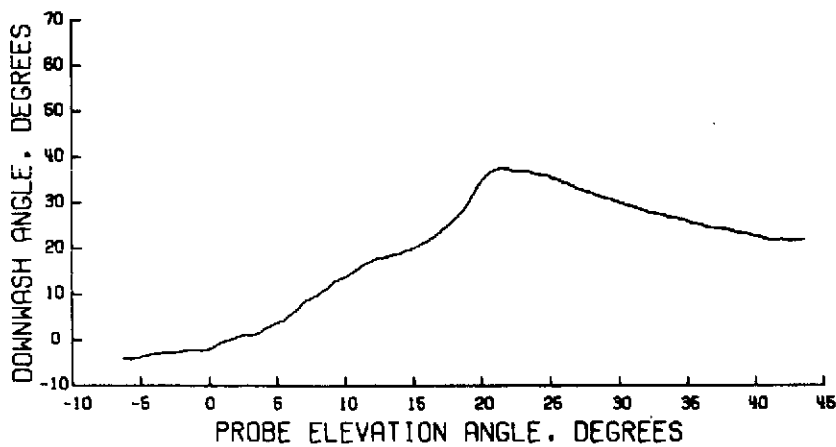
Figure 130.- Wake survey results for $\eta = 0.254$; $\alpha = 0^O$; $C_T = 4.0$;
$V_\infty = 25.54$ m/sec (83.81 ft/sec).
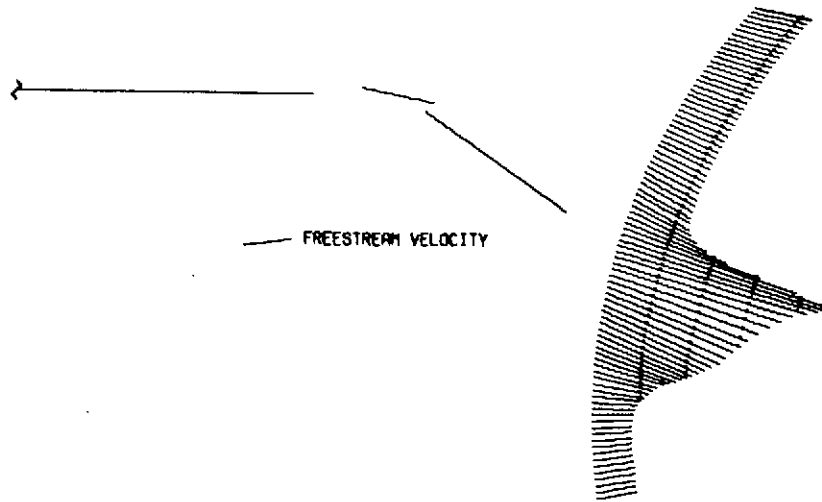
— FREESTREAM VELOCITY

(a) Streamwise velocity profile.



(b) Total velocity.



(c) Downwash angle.

Figure 131.- Wake survey results for $\eta = 0.294$; $\alpha = 0^O$; $C_T = 4.0$;
$V_\infty = 25.60$ m/sec (84.01 ft/sec).

— FREESTREAM VELOCITY

(a) Streamwise velocity profile.



(b) Total velocity.



(c) Downwash angle.

Figure 132.- Wake survey results for $\eta = 0.335$; $\alpha = 0^O$; $C_T = 4.0$; $V_\infty = 25.55$ m/sec (83.83 ft/sec).

(a) Streamwise velocity profile.



(b) Total velocity.



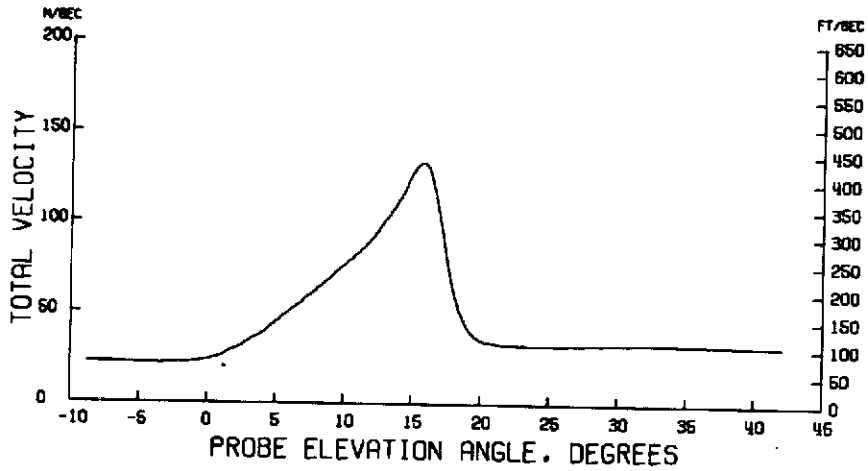(c) Downwash angle.

Figure 133.- Wake survey results for $\eta = 0.376$; $\alpha = 0^{\circ}$; $C_T = 4.0$; $V_{\infty} = 25.44$ m/sec (83.47 ft/sec).

(a) Streamwise velocity profile.
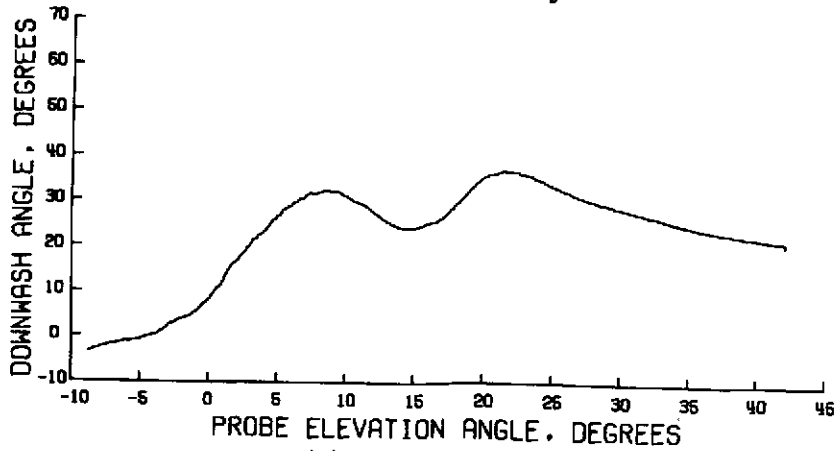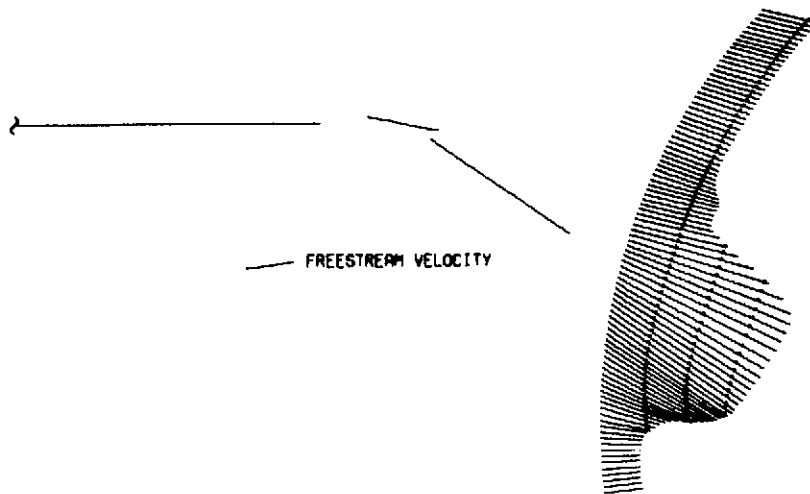


(b) Total velocity.



(c) Downwash angle.

Figure 134.- Wake survey results for $\eta = 0.416$; $\alpha = 0^O$; $C_T = 4.0$;
$V_\infty = 25.40$ m/sec (83.34 ft/sec).
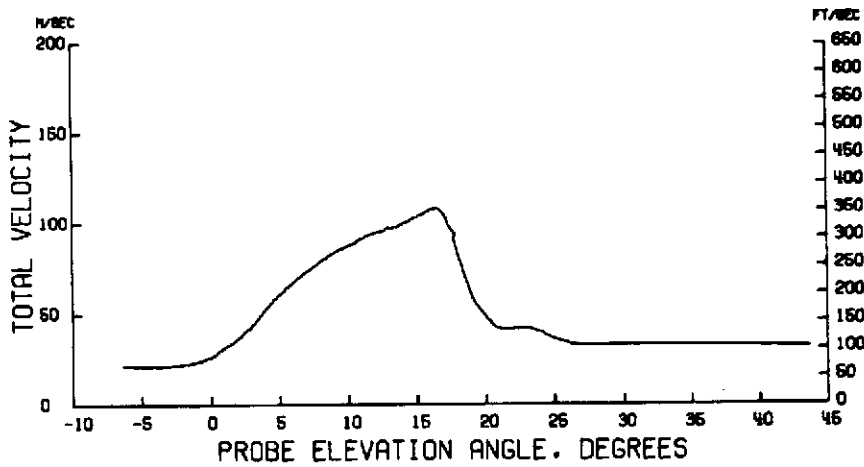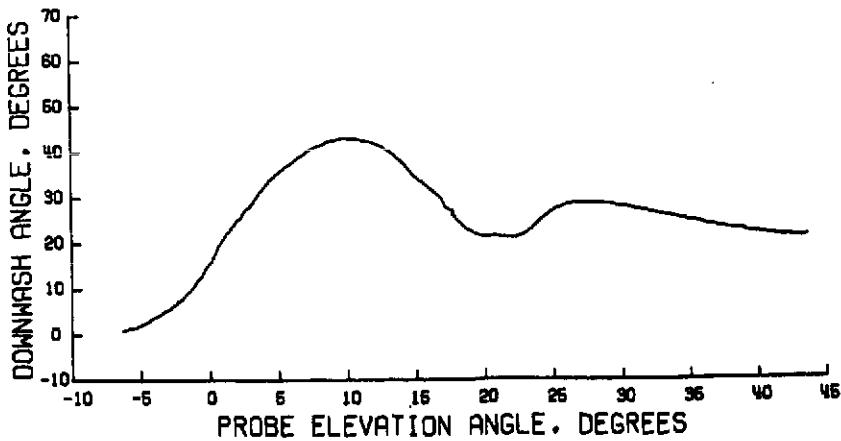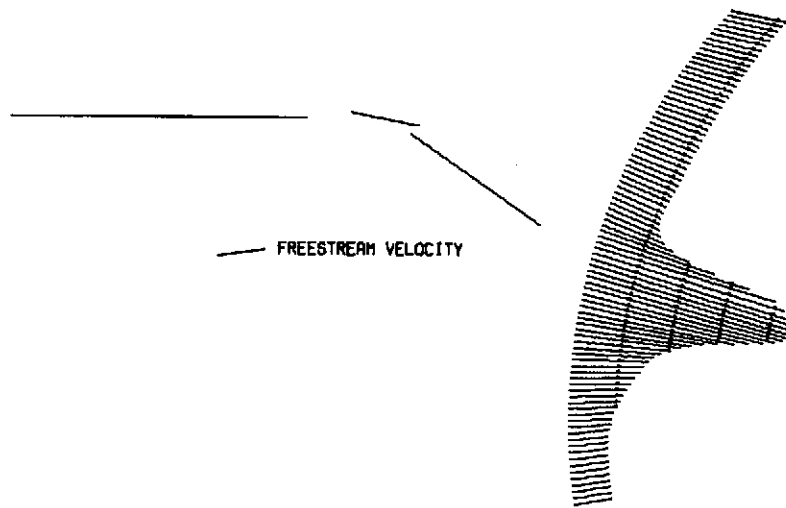
(a) Streamwise velocity profile.



(b) Total velocity.



(c) Downwash angle.

Figure 135.- Wake survey results for $\eta = 0.443$; $\alpha = 0^O$; $C_T = 4.0$; $V_\infty = 25.37$ m/sec (83.24 ft/sec).

(a) Streamwise velocity profile.



(b) Total velocity.



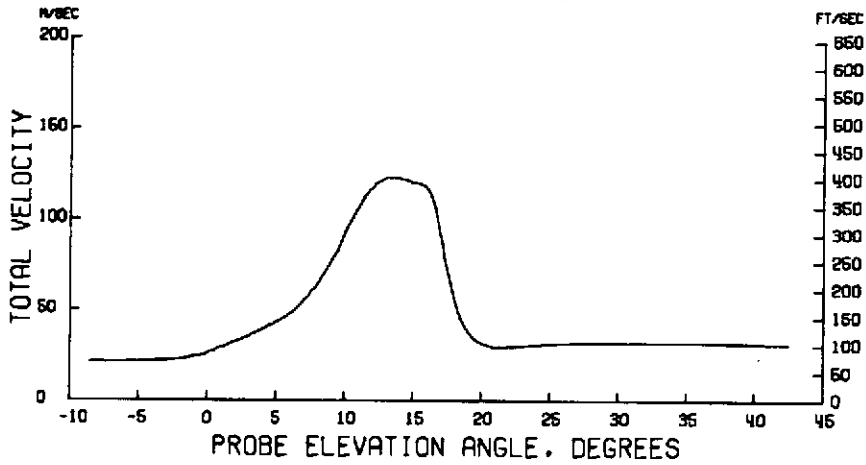(c) Downwash angle.

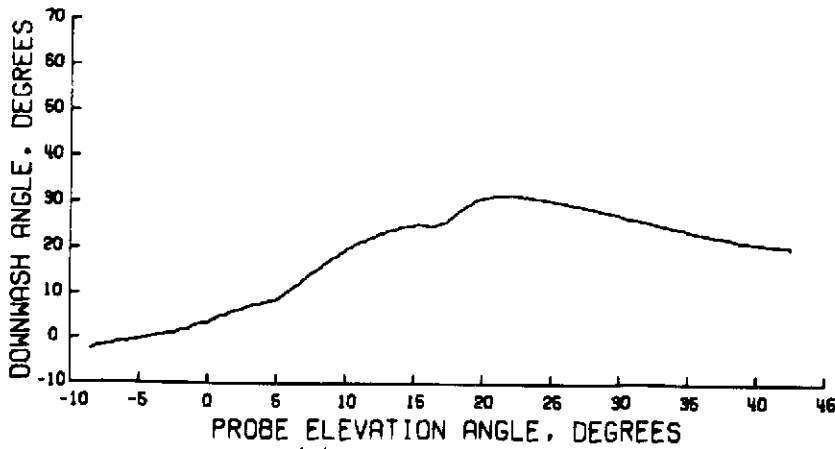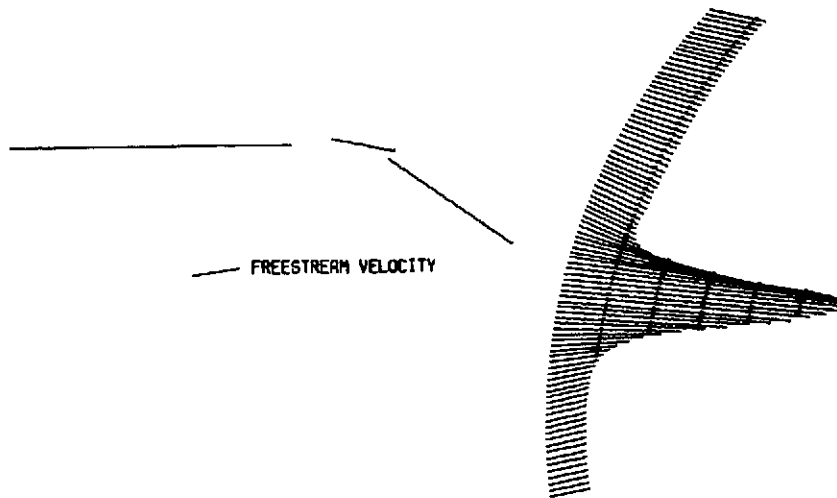Figure 136.- Wake survey results for $\eta = 0.469$; $\alpha = 0^O$; $C_T = 4.0$; $V_\infty = 25.39$ m/sec (83.31 ft/sec).
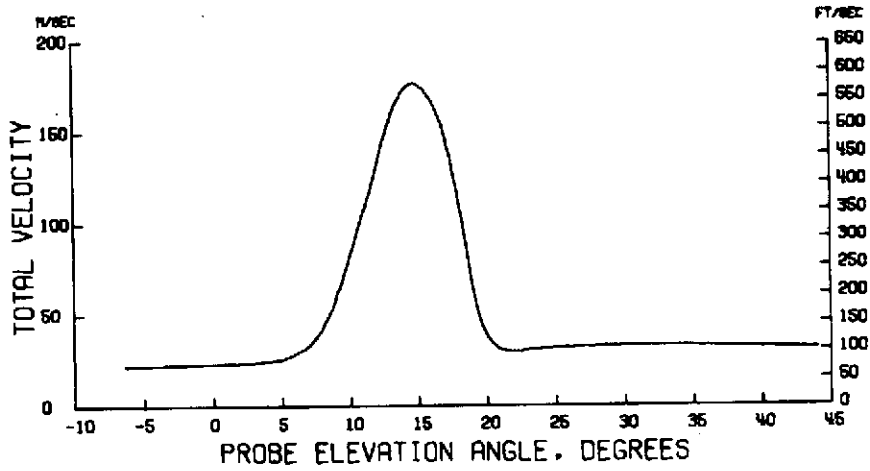
(a) Streamwise velocity profile.



(b) Total velocity.



(c) Downwash angle.

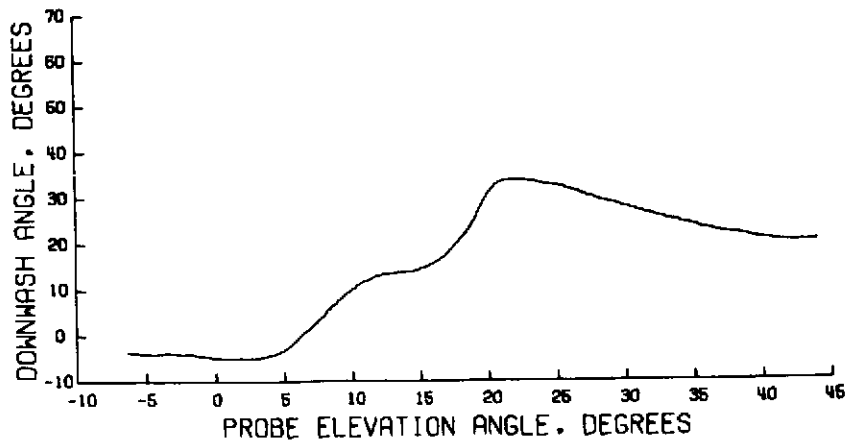Figure 137.- Wake survey results for $\eta = 0.481$; $\alpha = 0^O$; $C_T = 4.0$; $V_\infty = 25.37$ m/sec (83.23 ft/sec).
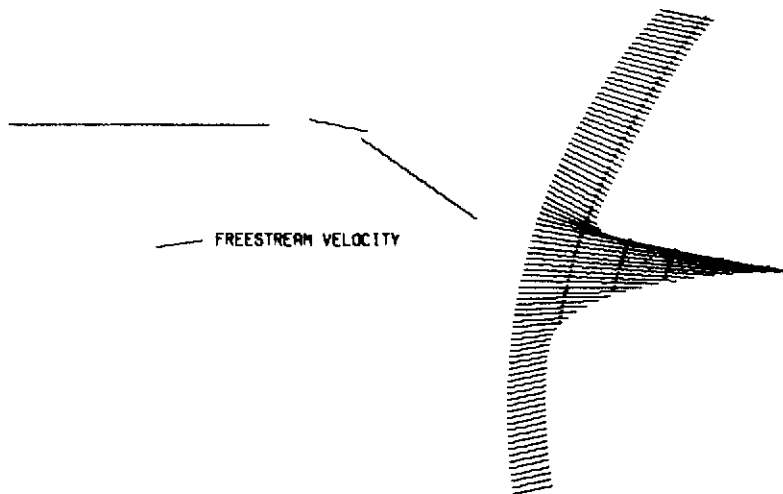
(a) Streamwise velocity profile.



(b) Total velocity.

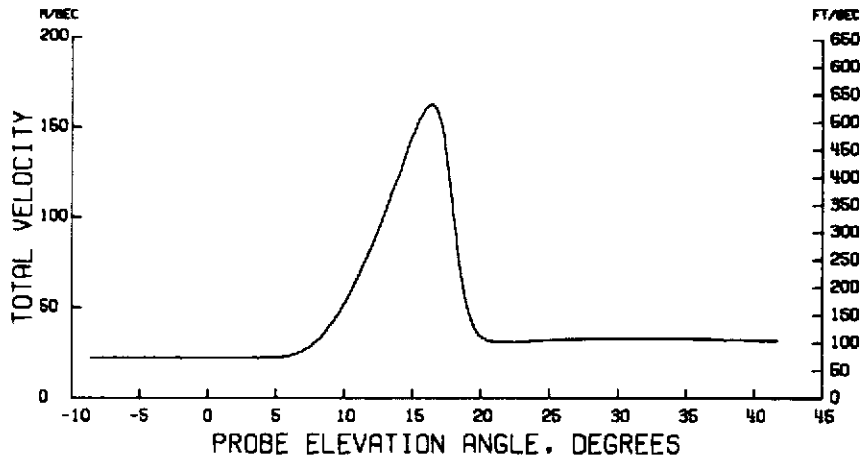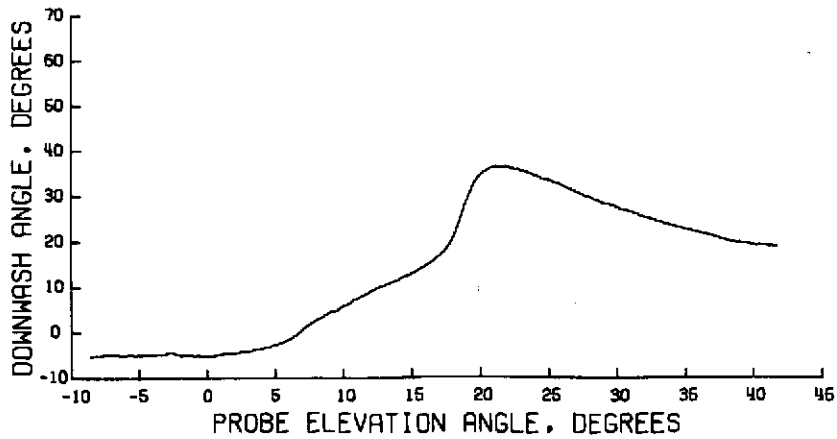

(c) Downwash angle.

Figure 138.- Wake survey results for $\eta = 0.162$; $\alpha = 8^O$; $C_T = 4.0$;
$V_\infty = 25.46$ m/sec (83.55 ft/sec).

FREESTREAM VELOCITY

(a) Streamwise velocity profile.



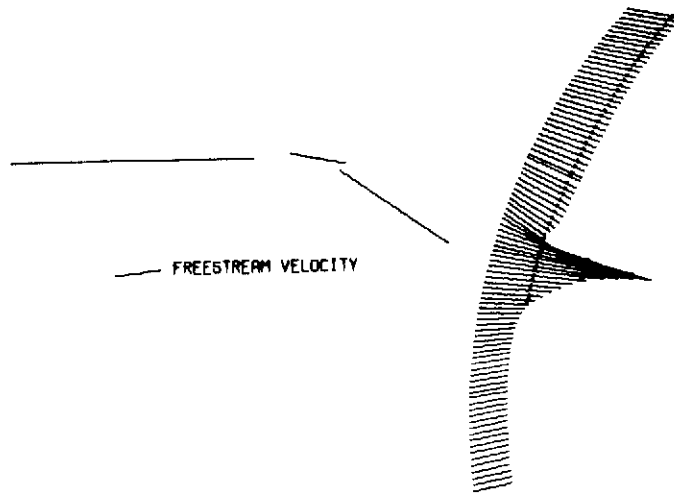(b) Total velocity.



(c) Downwash angle.

Figure 139.- Wake survey results for $\eta = 0.201$; $\alpha = 8^{\circ}$; $C_T = 4.0$; $V_{\infty} = 25.49$ m/sec (83.65 ft/sec).
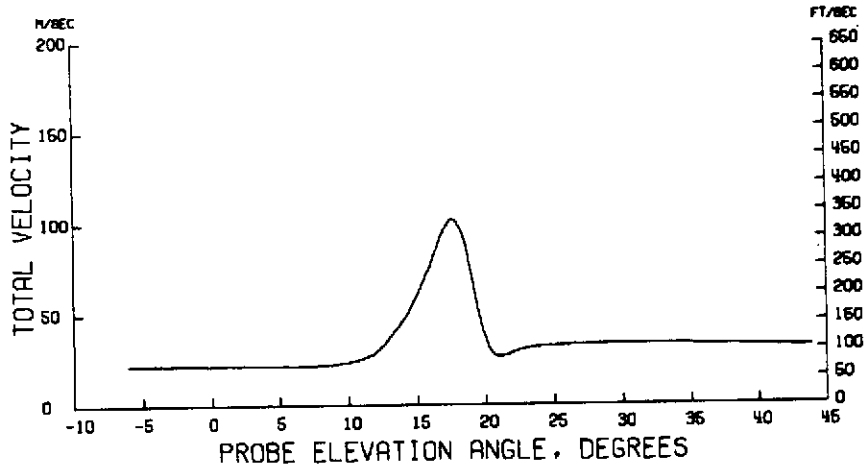
(a) Streamwise velocity profile.
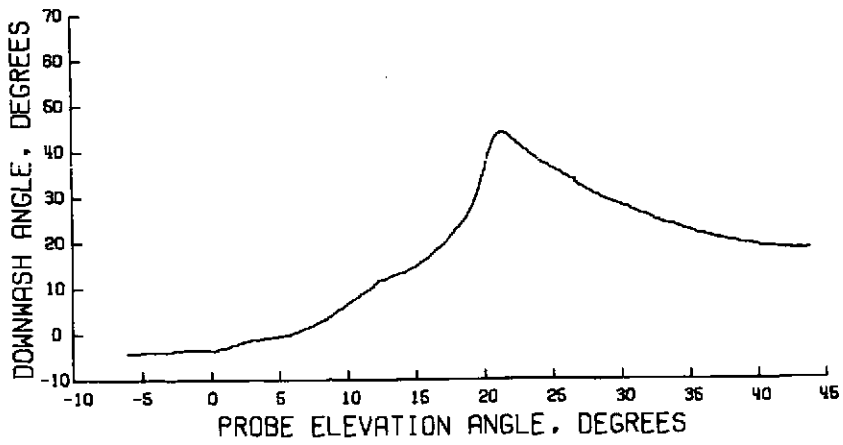


(b) Total velocity.



(c) Downwash angle.

Figure 140.- Wake survey results for $\eta = 0.227$; $\alpha = 8^{o}$; $C_T = 4.0$; $V_{\infty} = 25.51$ m/sec (83.72 ft/sec).
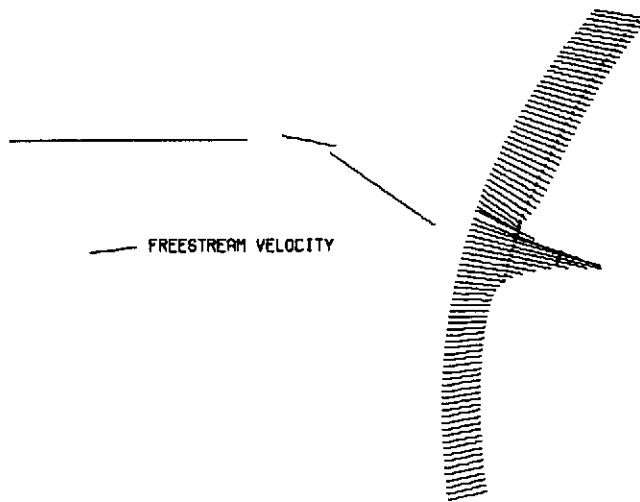
(a) Streamwise velocity profile.



(b) Total velocity.



(c) Downwash angle.

Figure 141.- Wake survey results for $\eta = 0.254$; $\alpha = 8^O$; $C_T = 4.0$; $V_\infty = 25.45$ m/sec (83.49 ft/sec).
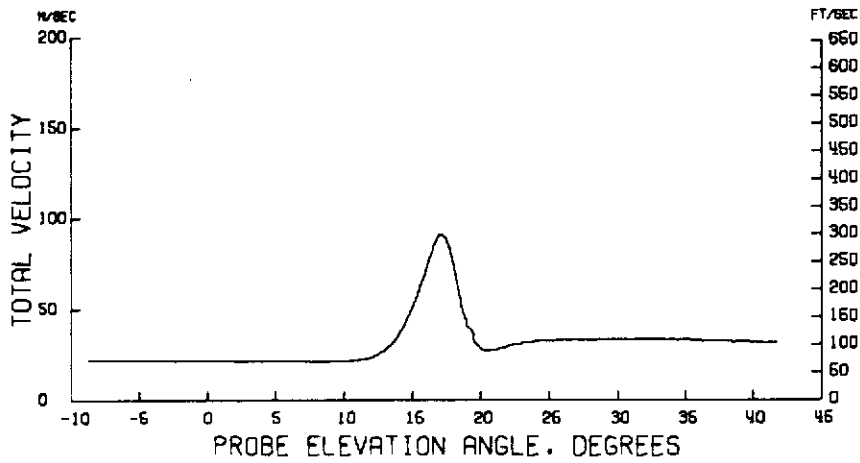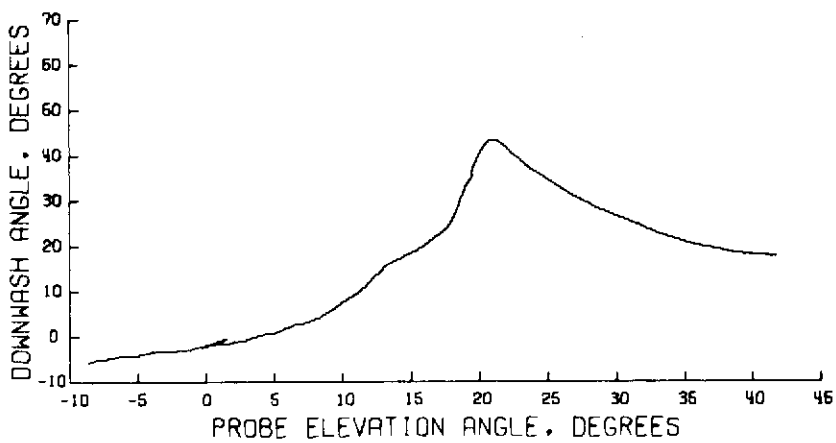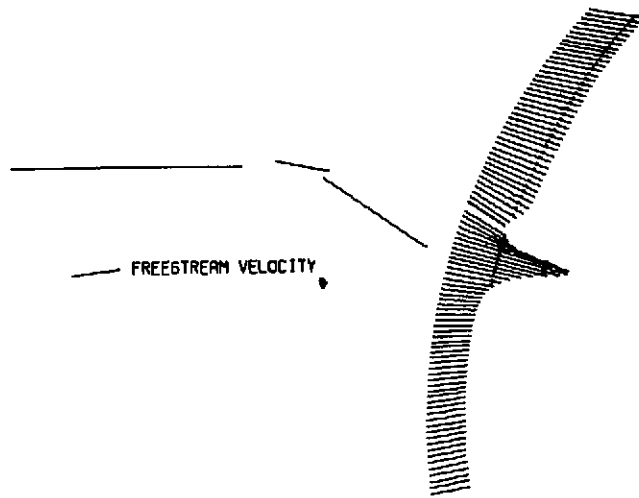
(a) Streamwise velocity profile.



(b) Total velocity.



(c) Downwash angle.

Figure 142.- Wake survey results for $\eta = 0.294$; $\alpha = 8^{\circ}$; $C_T = 4.0$; $V_{\infty} = 25.44$ m/sec (83.48 ft/sec).
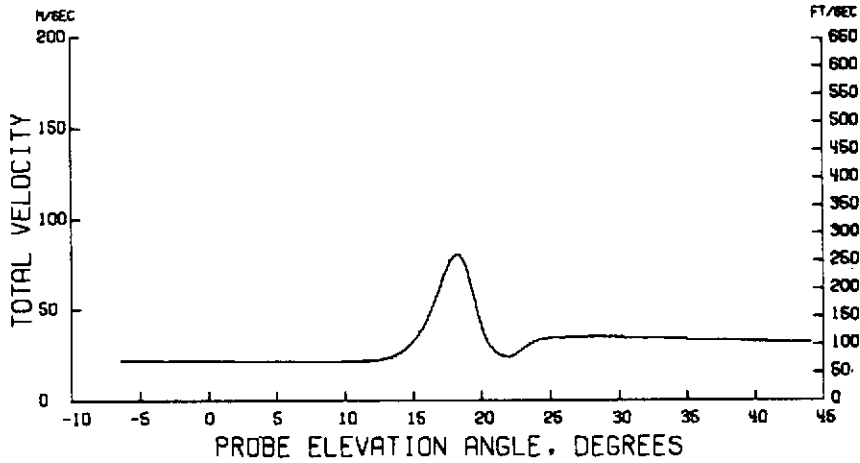
(a) Streamwise velocity profile.
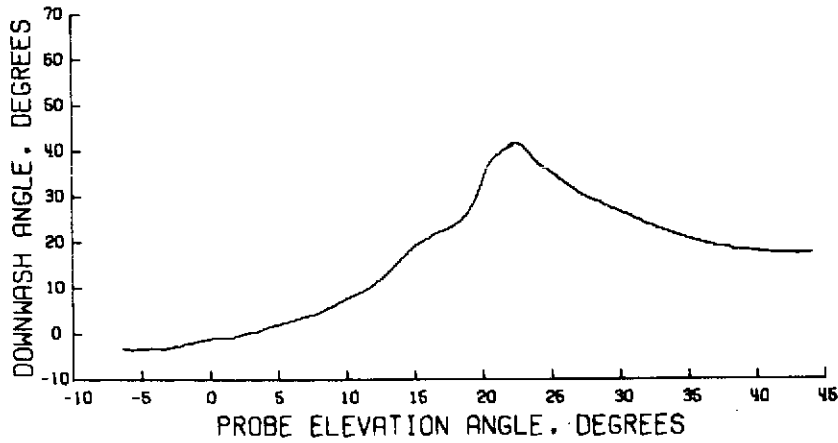


(b) Total velocity.



(c) Downwash angle.

Figure 143.- Wake survey results for $\eta = 0.335$; $\alpha = 8^{O}$; $C_T = 4.0$;
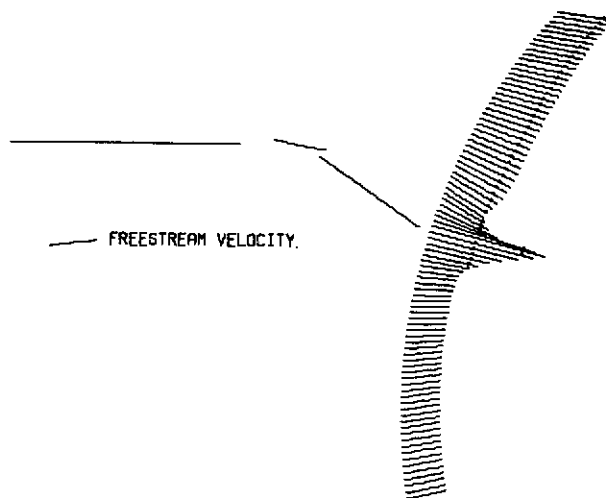$V_\infty = 25.45$ m/sec (83.51 ft/sec).

(a) Streamwise velocity profile.



(b) Total velocity.



(c) Downwash angle.

Figure 144.- Wake survey results for $\eta = 0.375$; $\alpha = 8^O$; $C_T = 4.0$; $V_\infty = 25.42$ m/sec (83.41 ft/sec).

(a) Streamwise velocity profile.



(b) Total velocity.



(c) Downwash angle.

Figure 145.- Wake survey results for $\eta = 0.417$; $\alpha = 8^O$; $C_T = 4.0$; $V_\infty = 25.23$ m/sec (82.77 ft/sec).

FREESTREAM VELOCITY

(a) Streamwise velocity profile.



(b) Total velocity.



(c) Downwash angle.

Figure 146.- Wake survey results for $\eta = 0.443$; $\alpha = 8^O$; $C_T = 4.0$;
$V_\infty = 25.21$ m/sec (82.72 ft/sec).

(a) Streamwise velocity profile.



(b) Total velocity.



(c) Downwash angle.

Figure 147.- Wake survey results for $\eta = 0.469$; $\alpha = 8^O$; $C_T = 4.0$; $V_\infty = 25.23$ m/sec (82.80 ft/sec).

(a) Streamwise velocity profile.
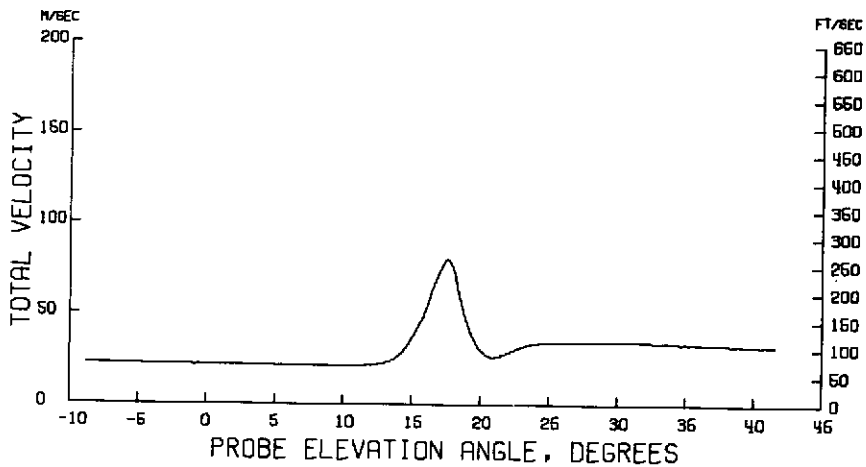


(b) Total velocity.
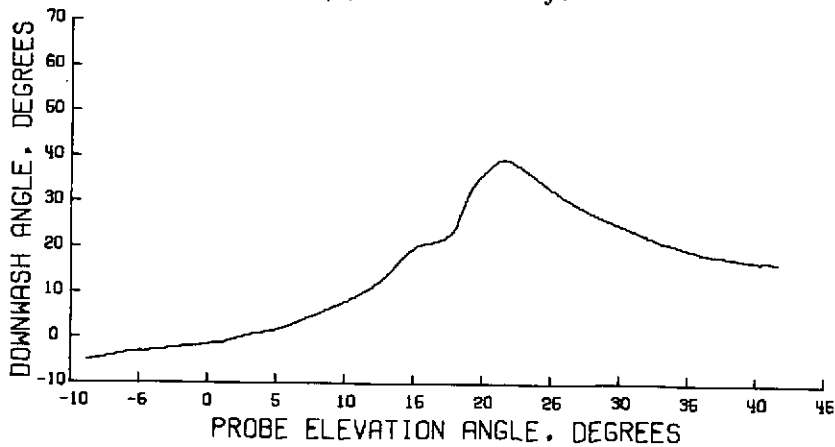


(c) Downwash angle.

Figure 148.- Wake survey results for $\eta = 0.481$; $\alpha = 8^{\circ}$; $C_T = 4.0$;
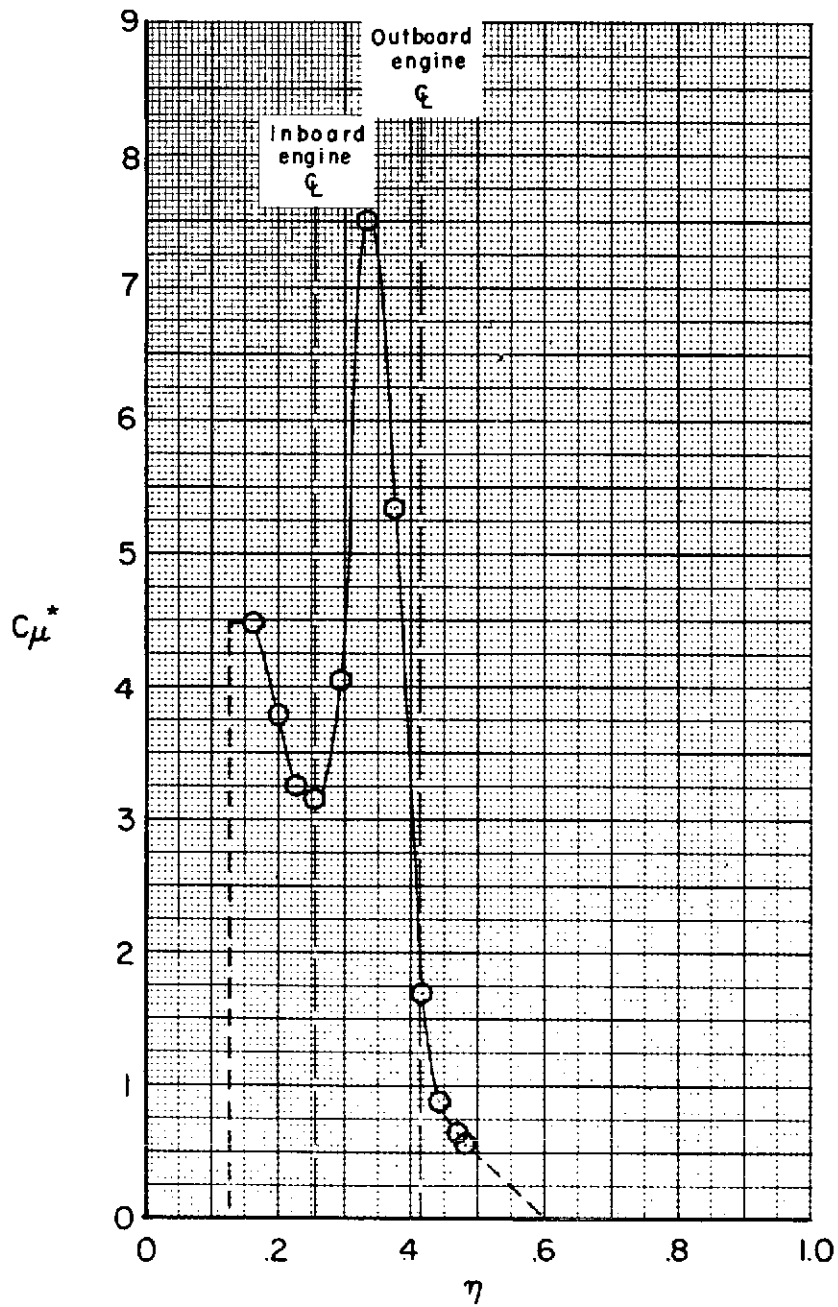$V_{\infty} = 25.28$ m/sec (82.96 ft/sec).
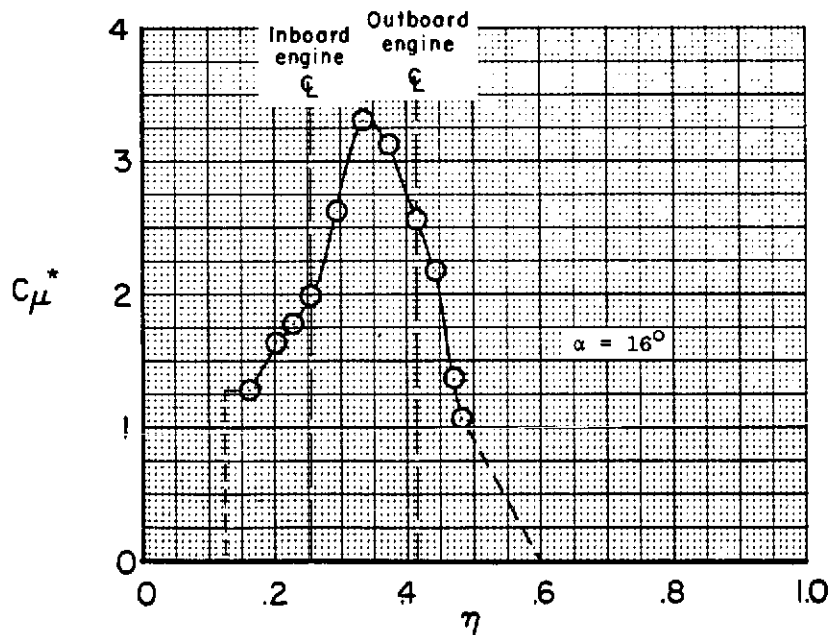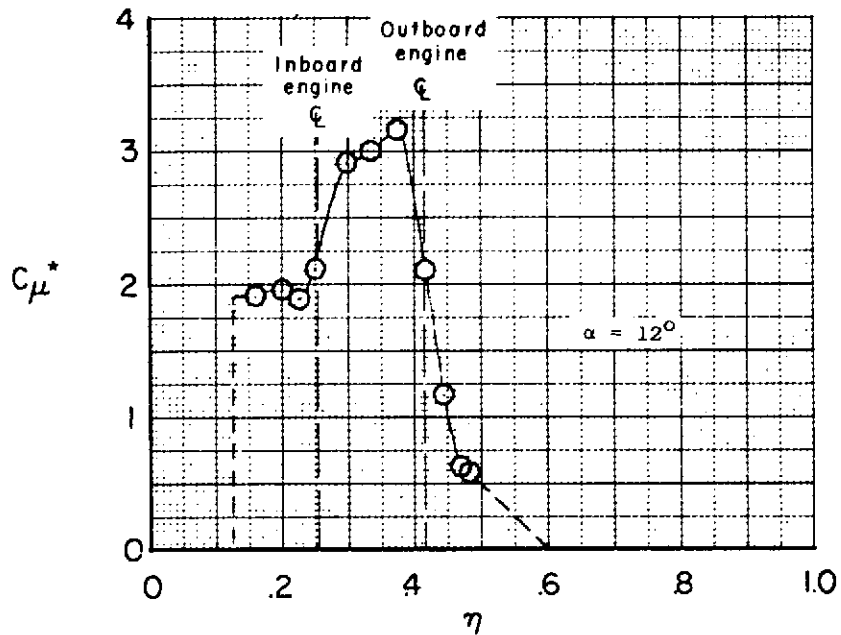
Figure 149.- Experimental momentum coefficient distribution for a thrust coefficient of 1.0.

(a)  $\alpha = 0^{o}$.
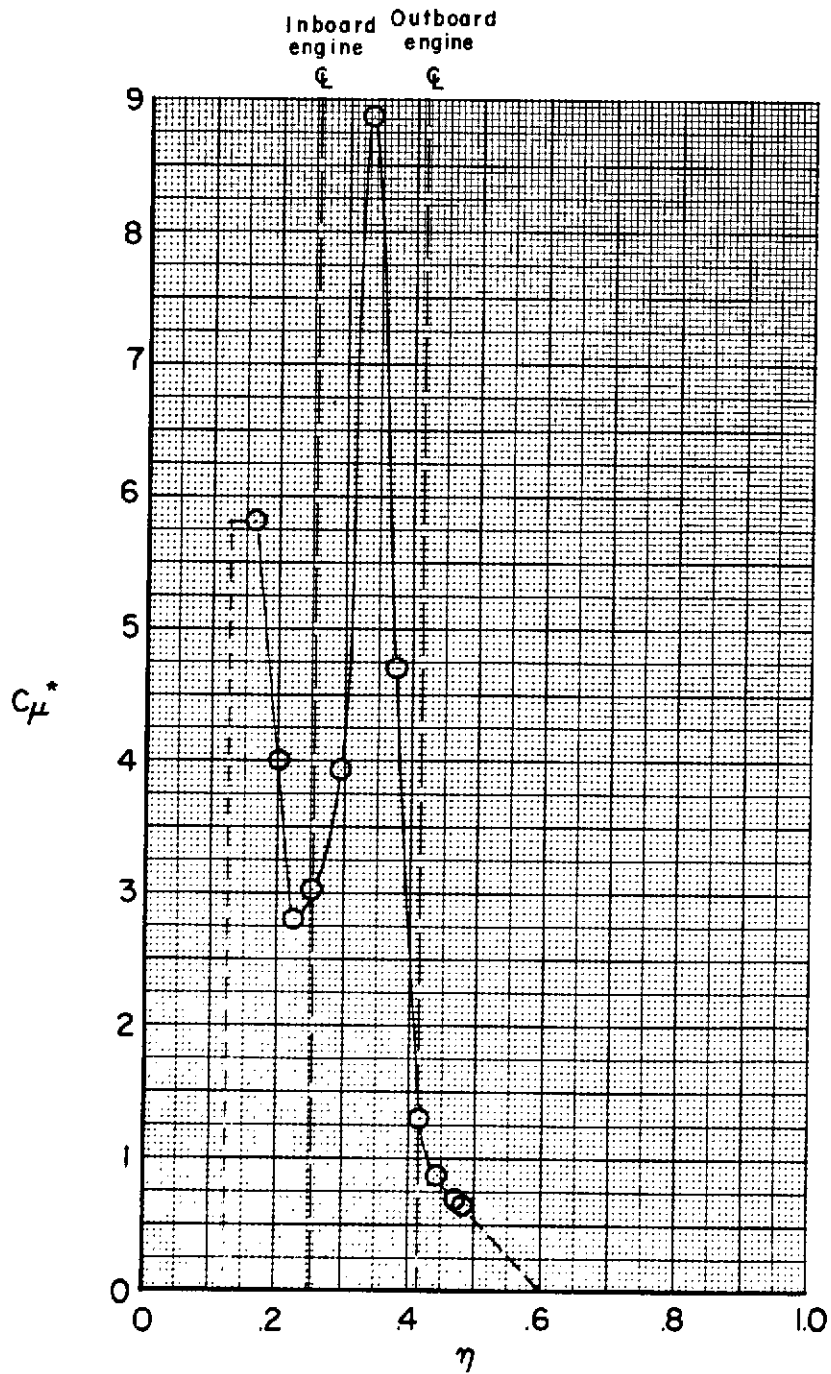
Figure 150.- Experimental momentum coefficient distribution for a
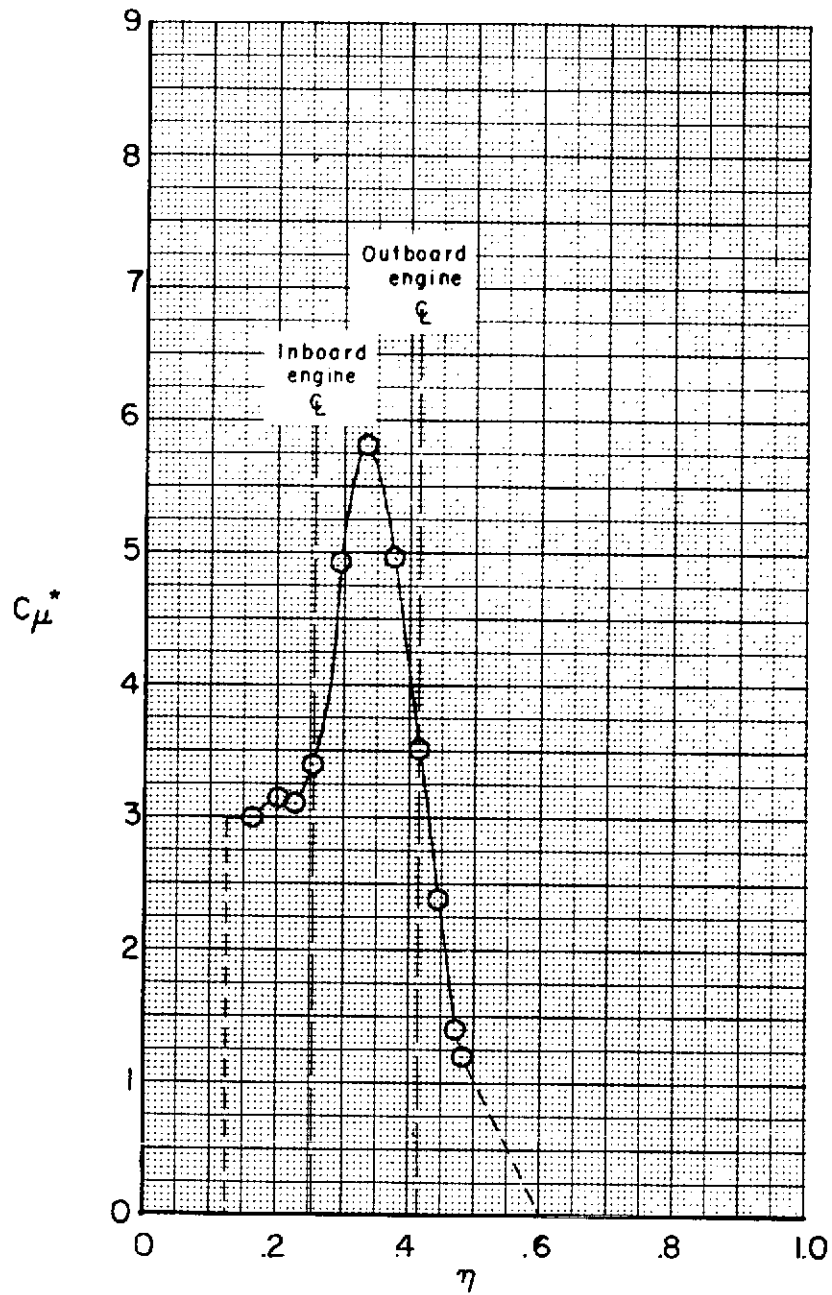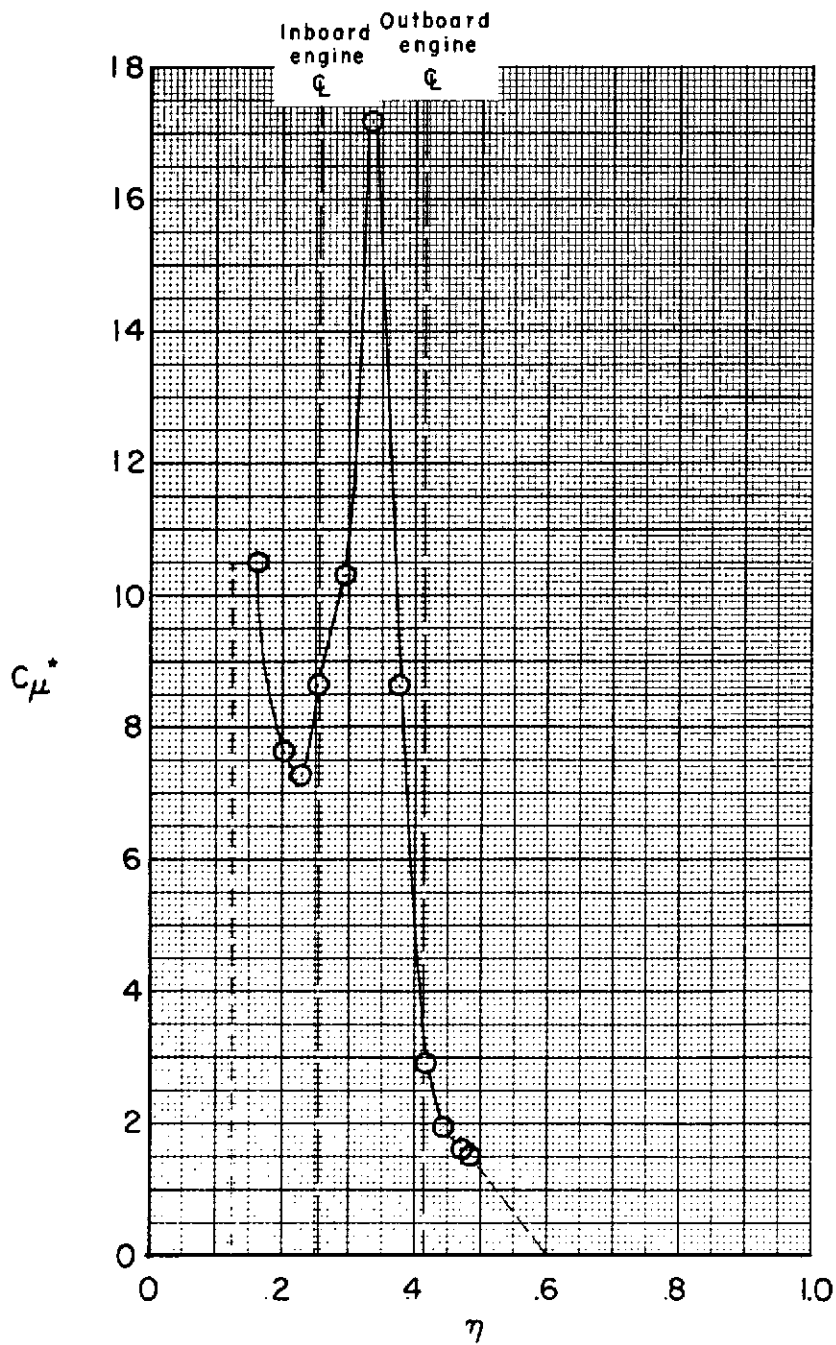thrust coefficient of 1.95.

(b) $\alpha = 8^{\circ}$.

Figure 150.- Continued.
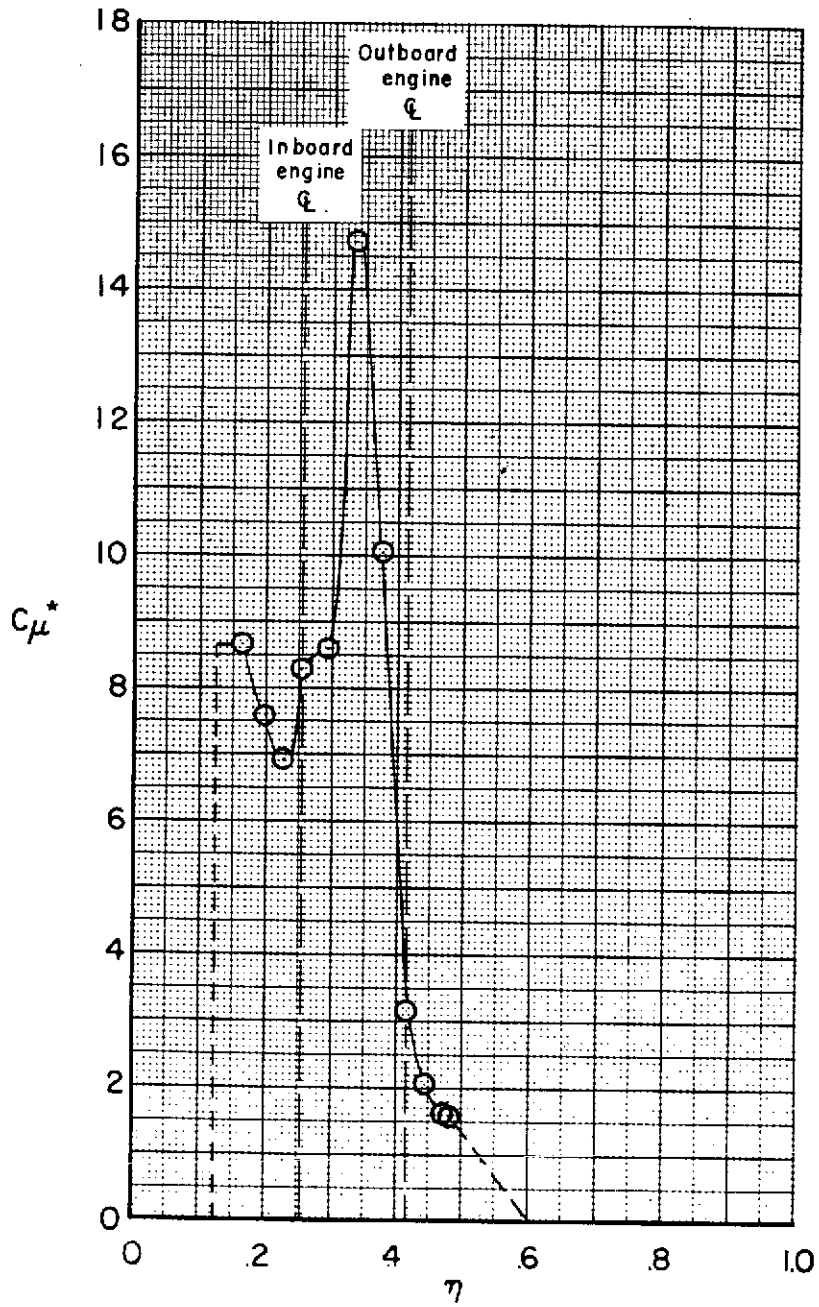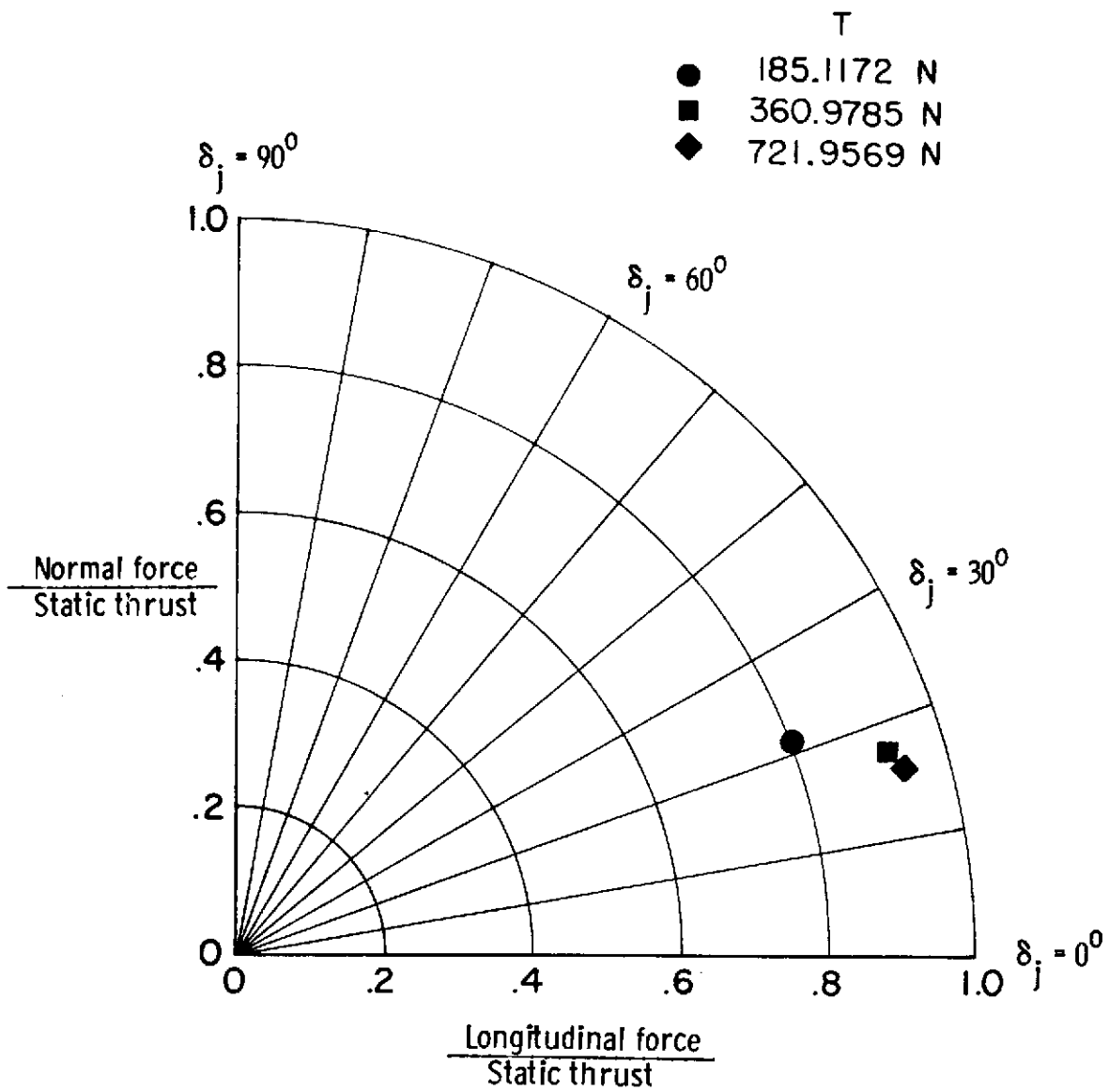
(c) $\alpha = 12^{O}$.
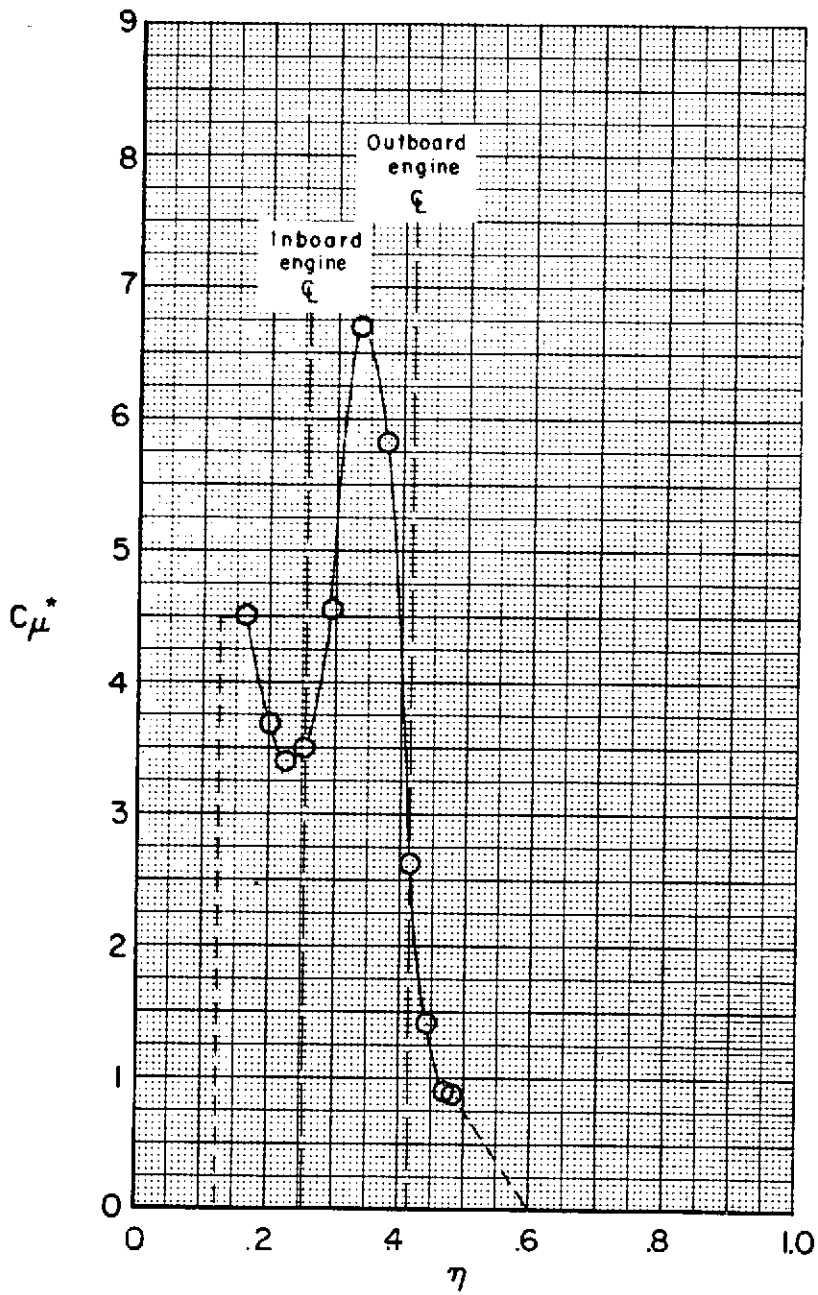
Figure 150.- Continued.

(d) $\alpha = 16^{O}$.

Figure 150.- Concluded.

(a)  $\alpha = 0^O$.

Figure 151.- Experimental momentum coefficient distribution for a
thrust coefficient of 3.90.

(b)  $\alpha = 8^{O}$.

Figure 151.- Concluded.

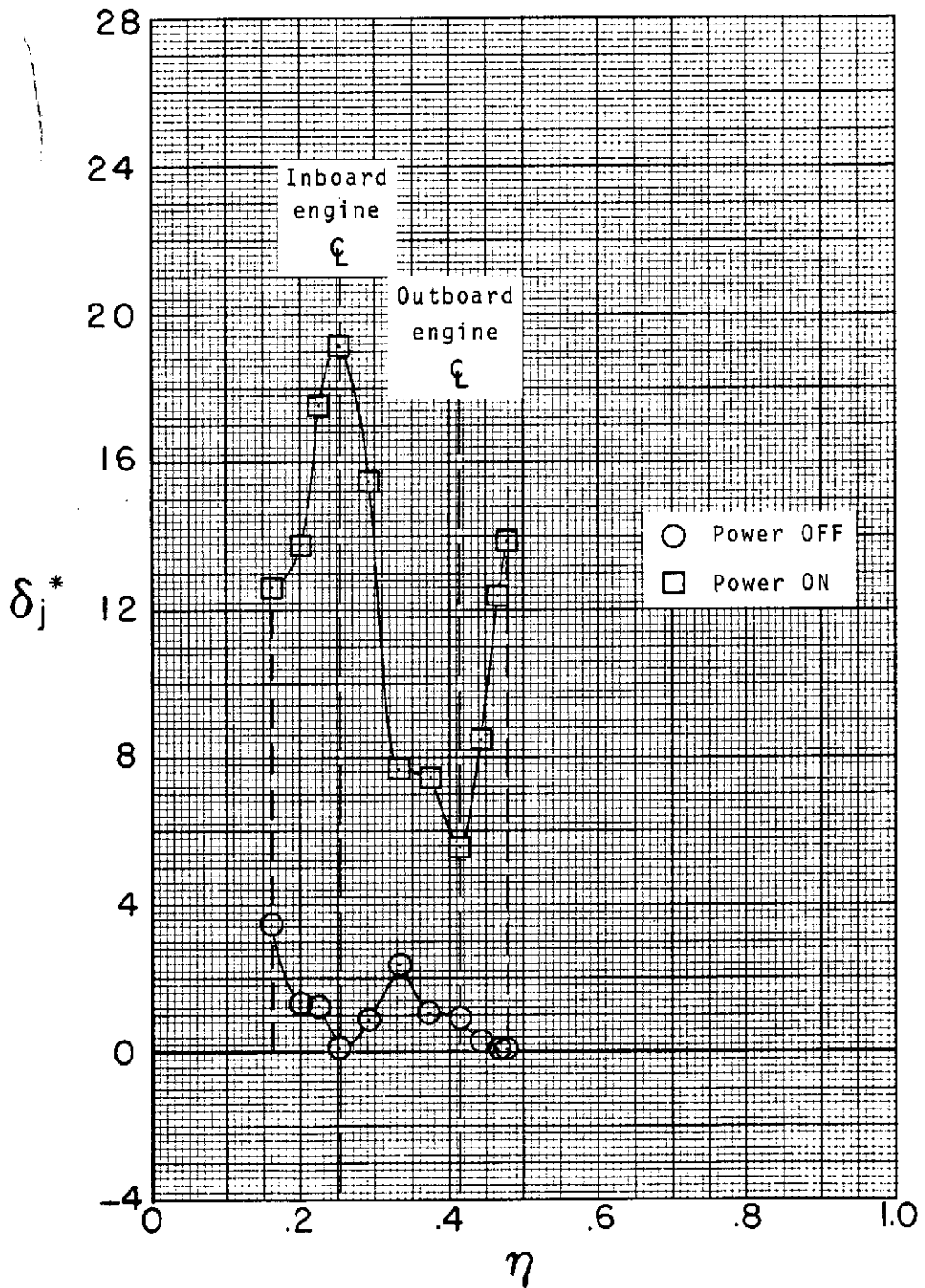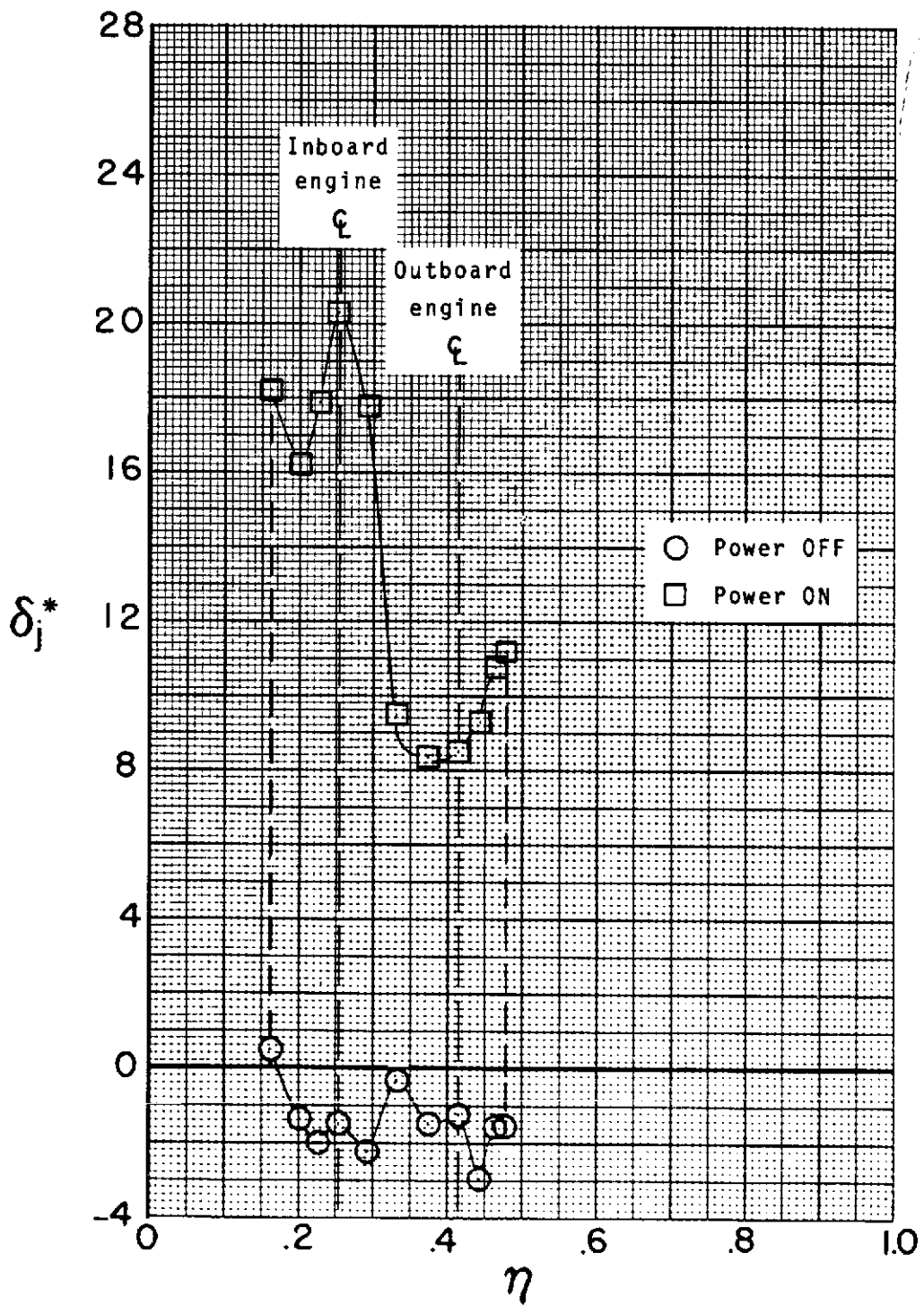Figure 152.- Summary of static turning angles and thrust recovery factor.
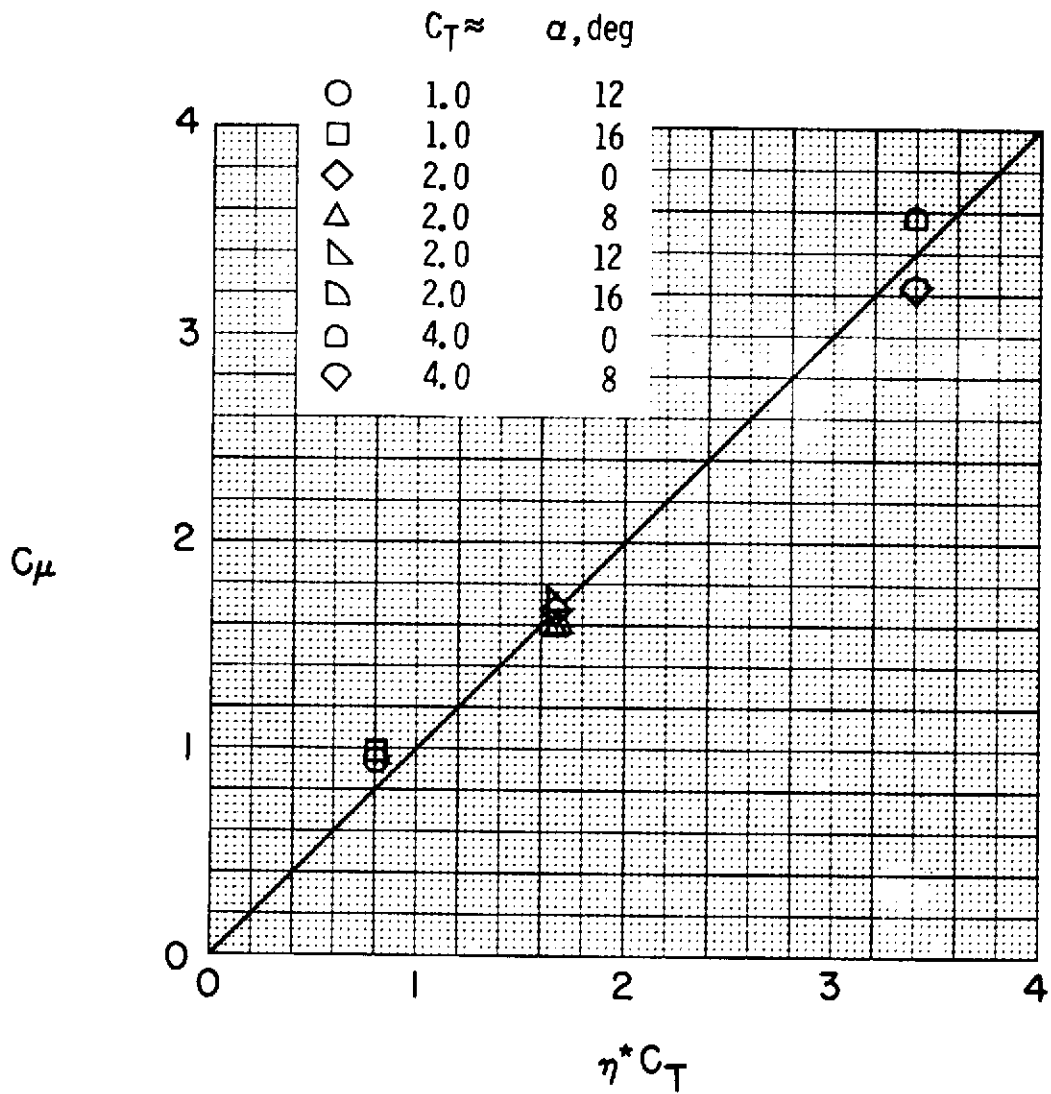
Figure 153.- Comparison of momentum coefficient obtained from the wake-survey measurements at the flap trailing edge with the modified thrust coefficient obtained from static turning data.
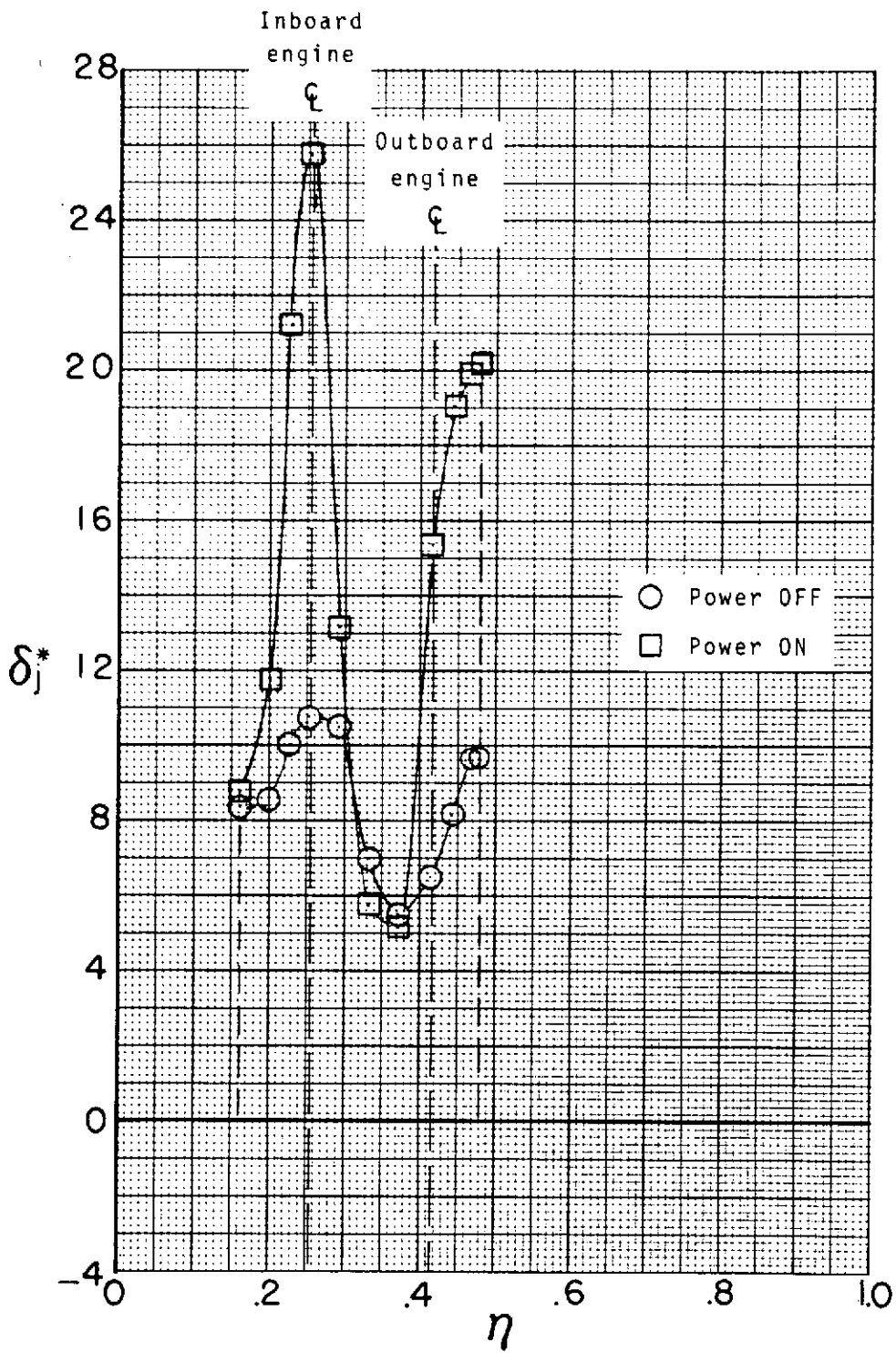
(a)  $\alpha = 12^{\circ}$.

Figure 154.- Experimental jet-deflection angle for a thrust
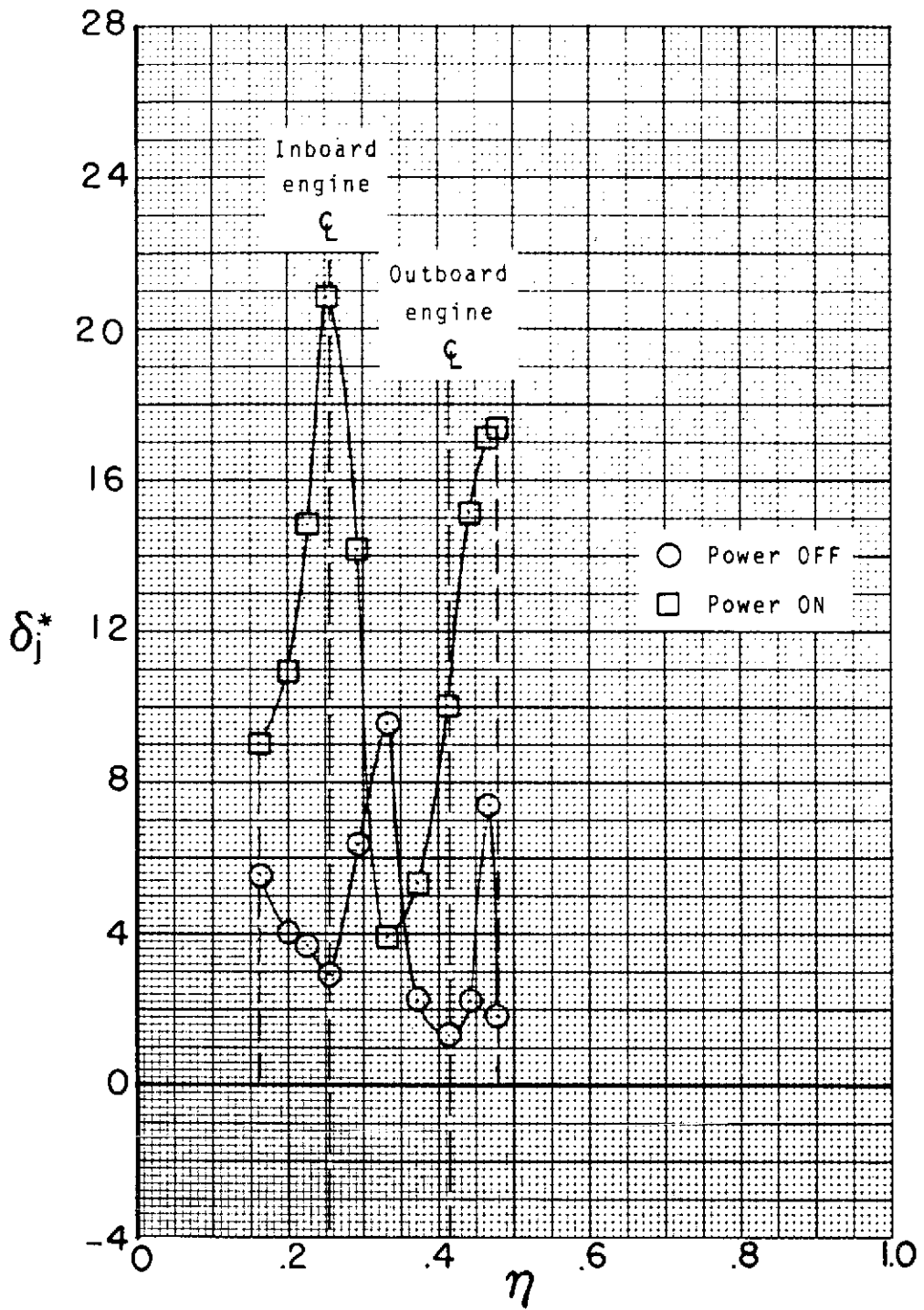coefficient of 1.0.

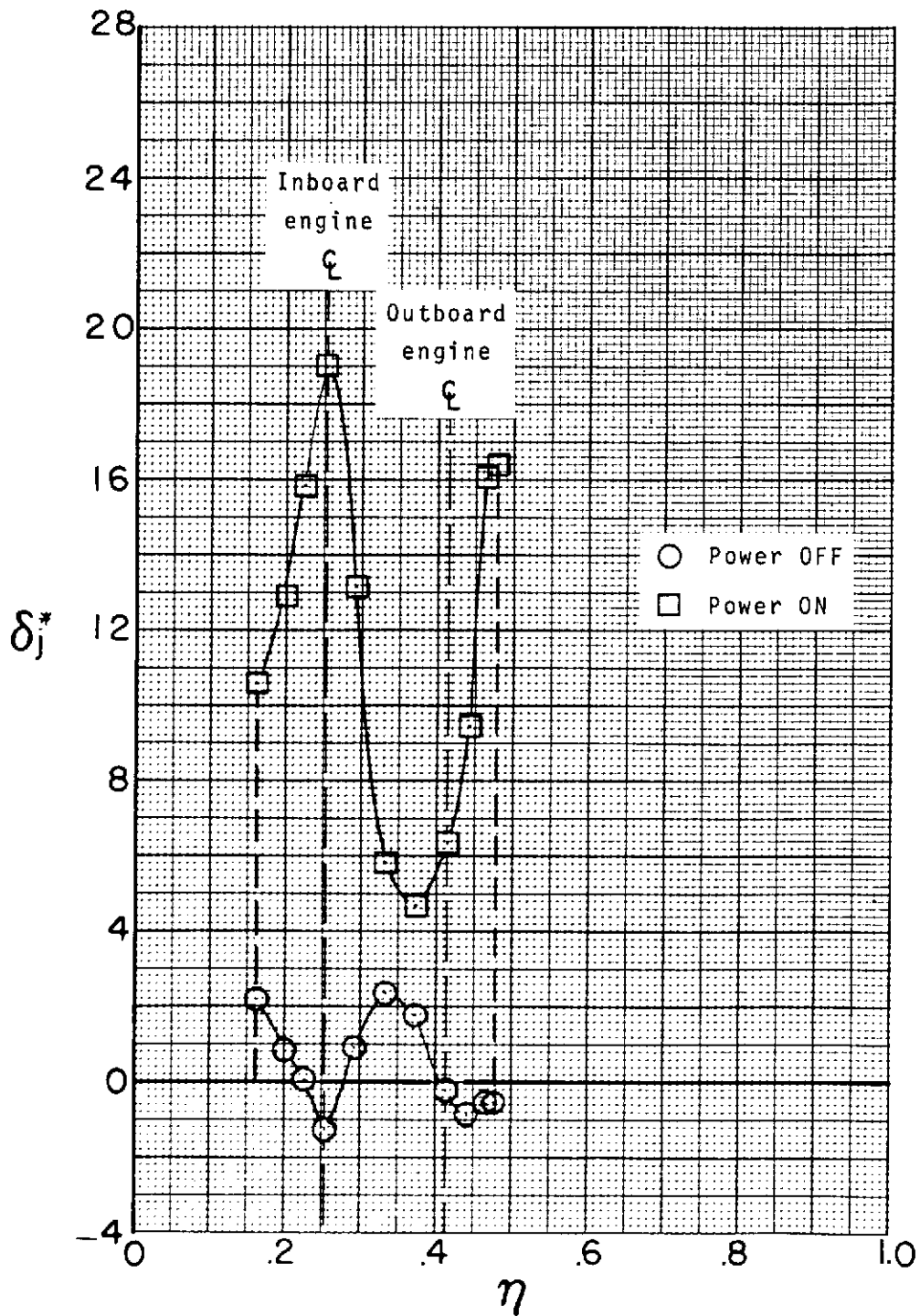(b)  $\alpha = 16^\circ$.

Figure 154.- Concluded.

(a)  $\alpha = 0^o$.

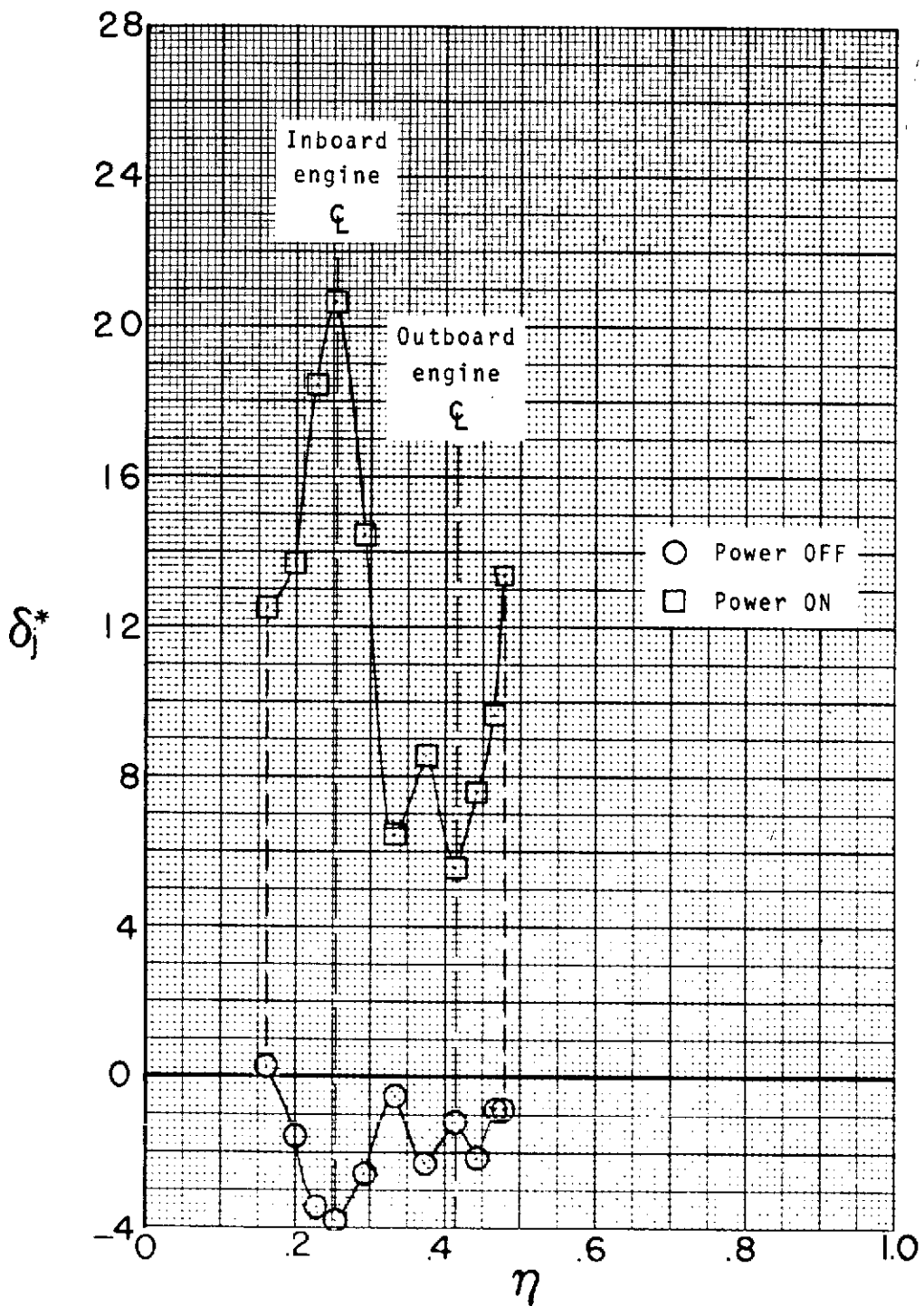Figure 155.- Experimental jet-deflection angle for a thrust coefficient of 1.95.

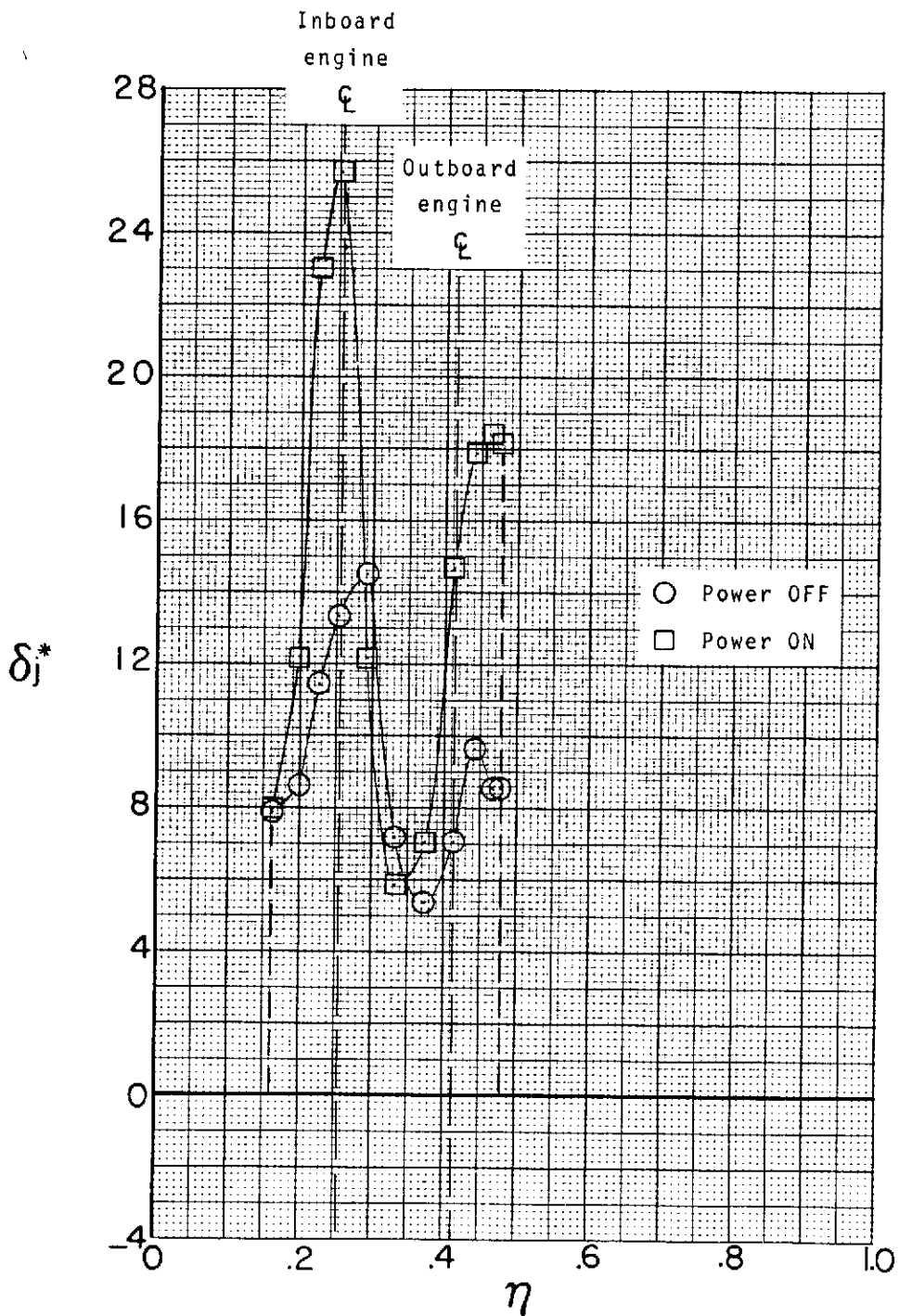(b) $\alpha = 8^{\circ}$.

Figure 155.- Continued.

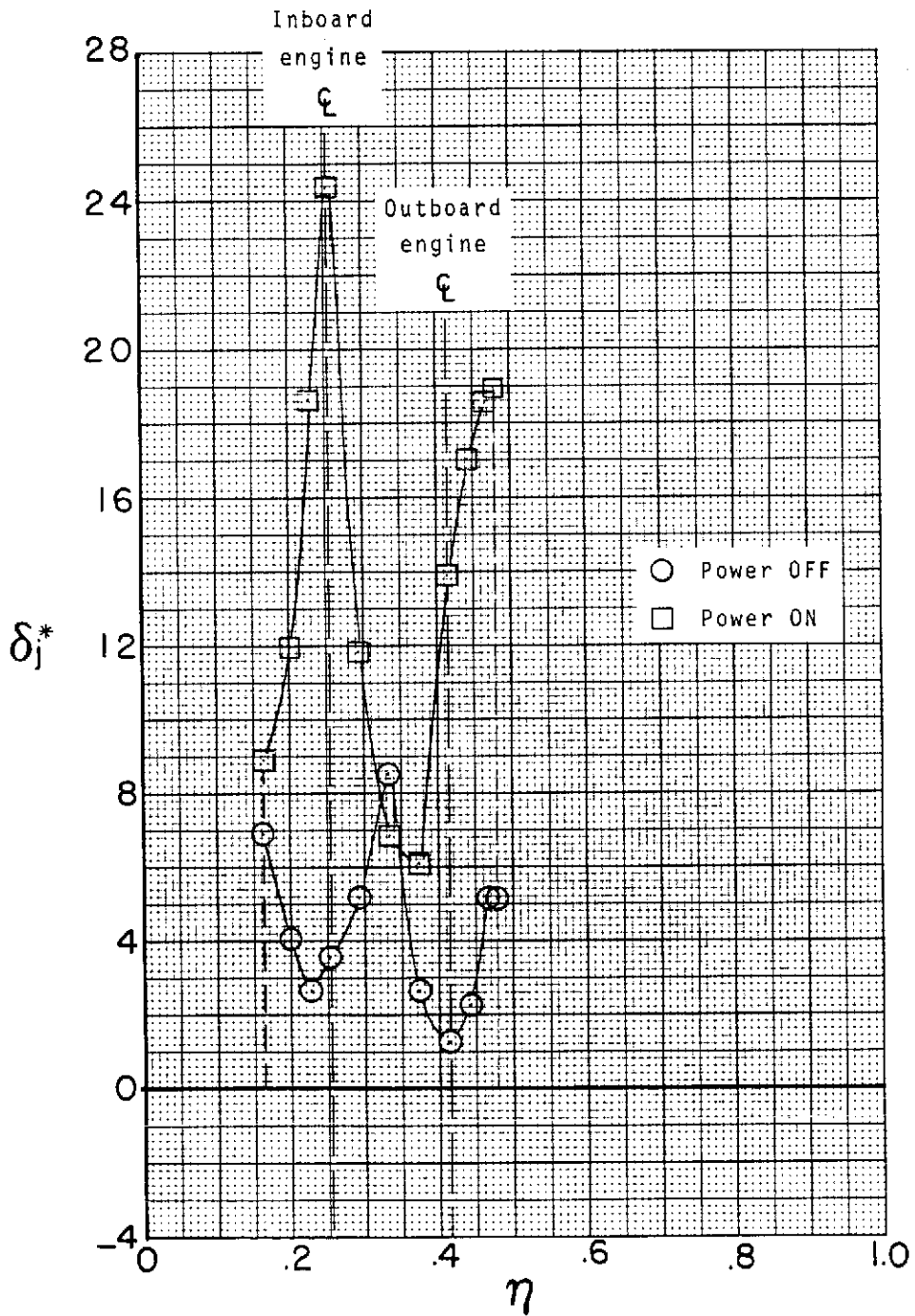(c)  $\alpha = 12^{\circ}$.

Figure 155.- Continued.

(d) $\alpha = 16^\circ$.
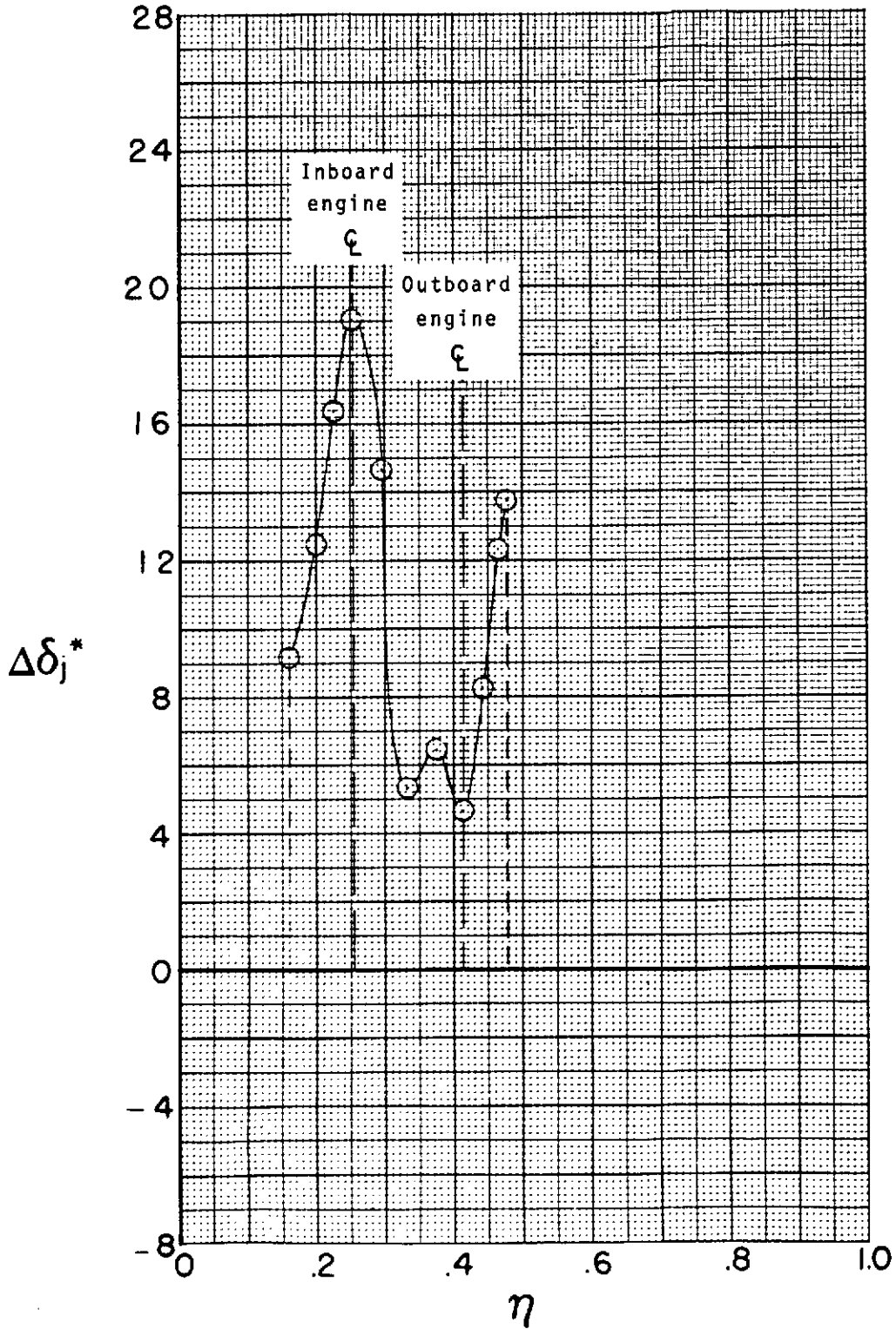
Figure 155.- Concluded.

(a) $\alpha = 0^\circ$.

Figure 156.- Experimental jet-deflection angle for a thrust coefficient of 3.90.
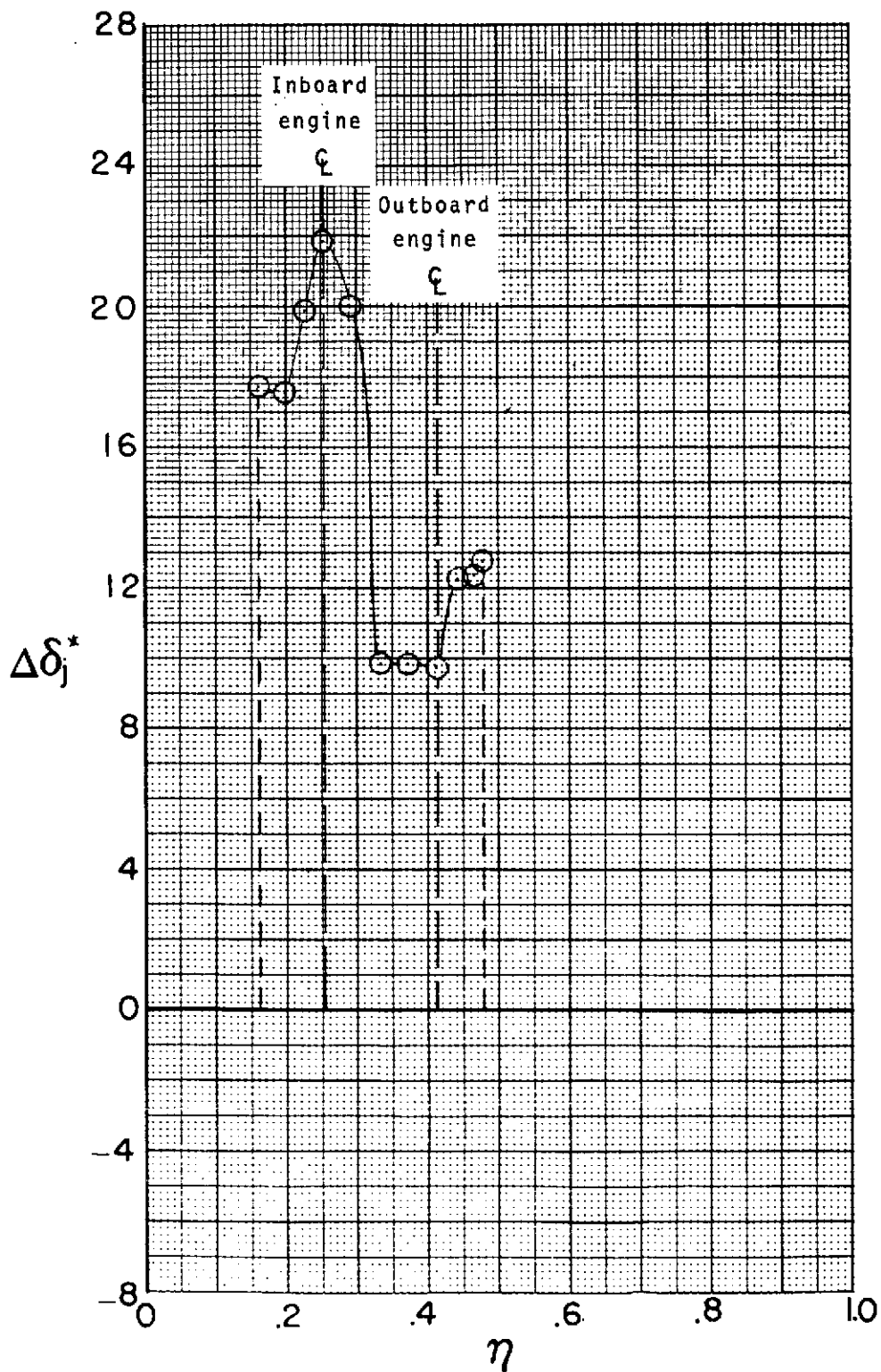
(b) $\alpha = 8^\circ$.
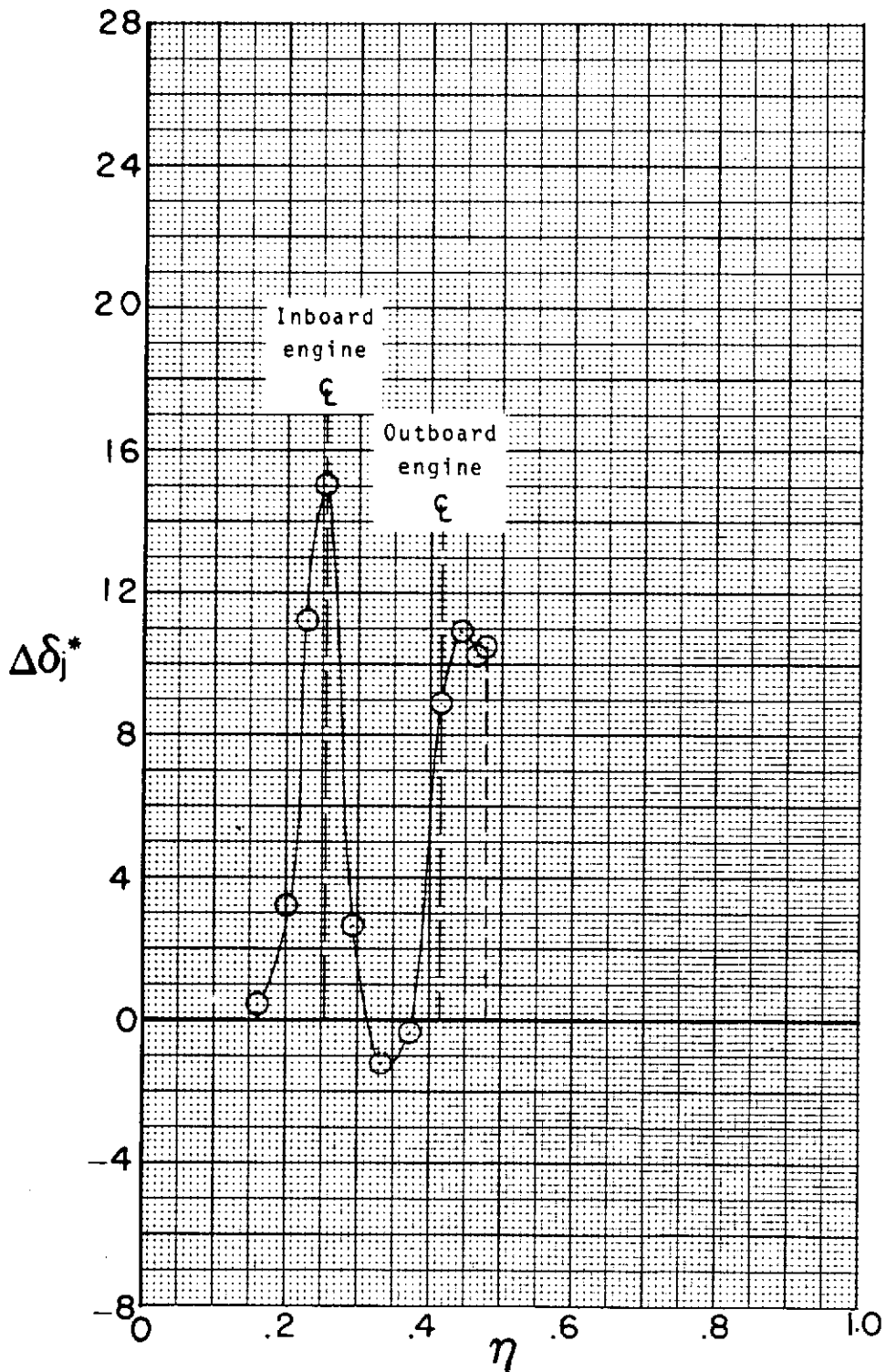
Figure 156.- Concluded.

(a)  $\alpha = 12^{\circ}$.

Figure 157.- Change in experimental jet-deflection angle due
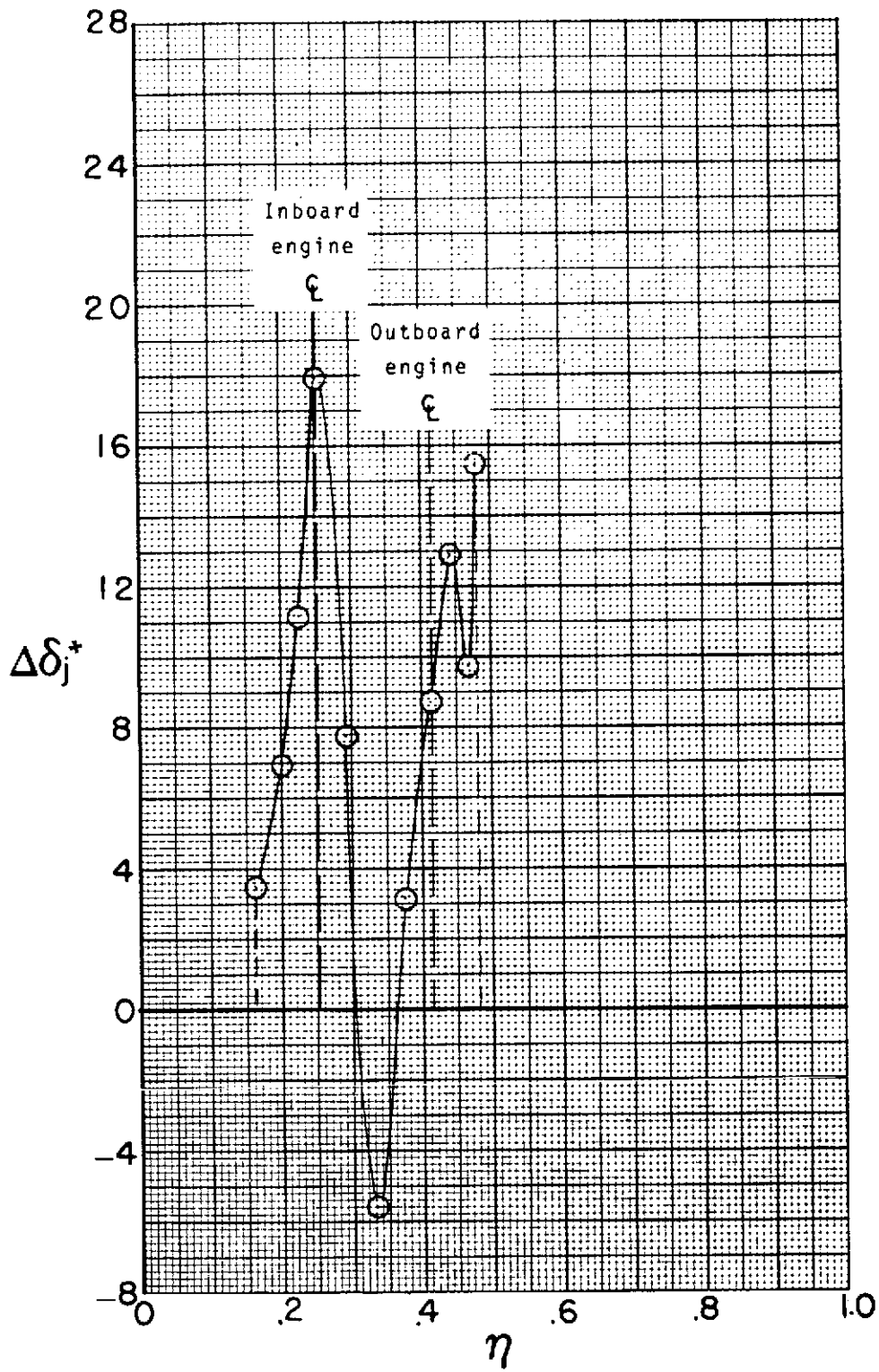to power for a thrust coefficient of 1.0.
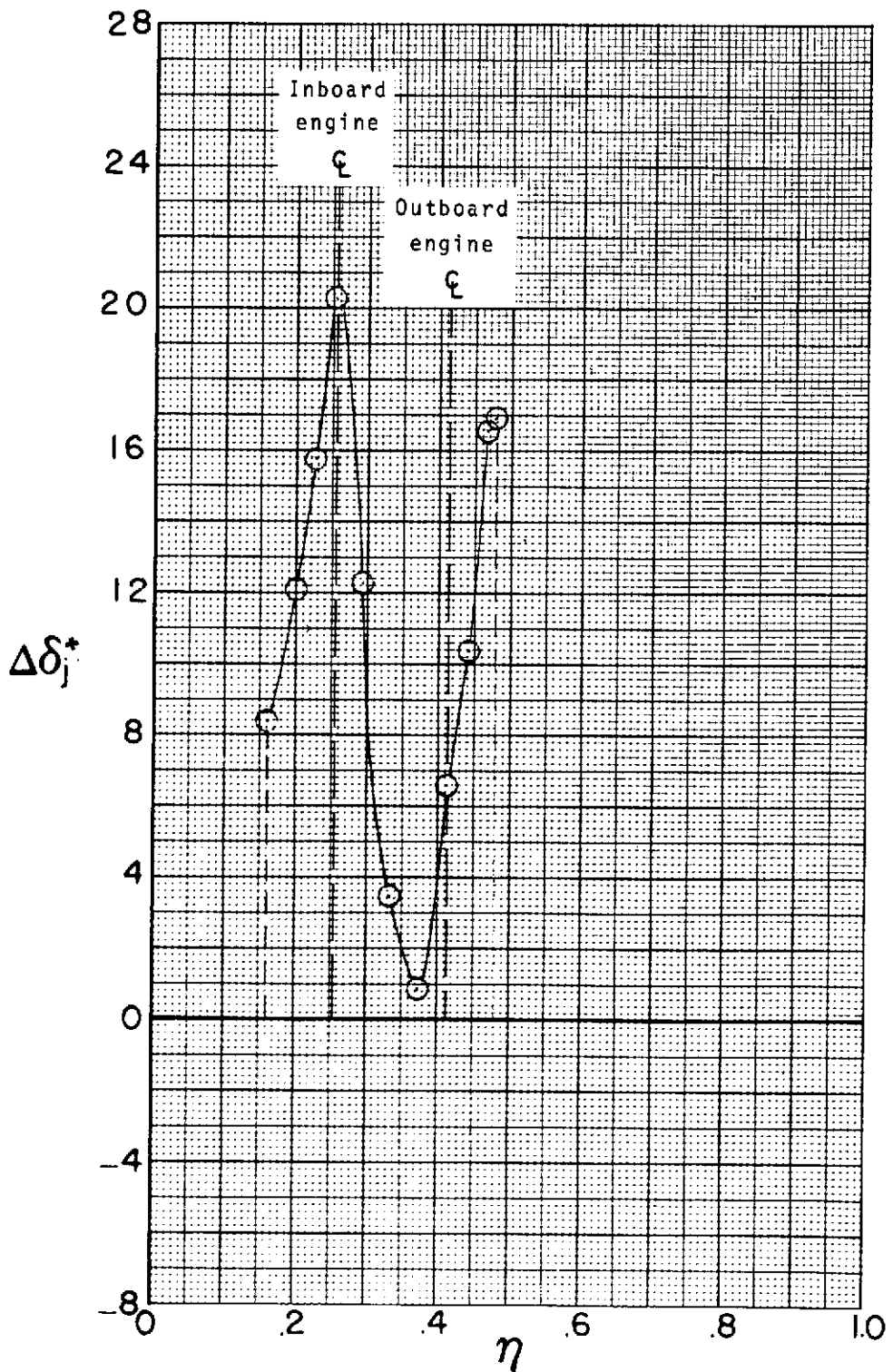
(b) $\alpha = 16^o$.

Figure 157.- Concluded.

(a)  $\alpha = 0^{\circ}$.

Figure 158.- Change in experimental jet-deflection angle due to
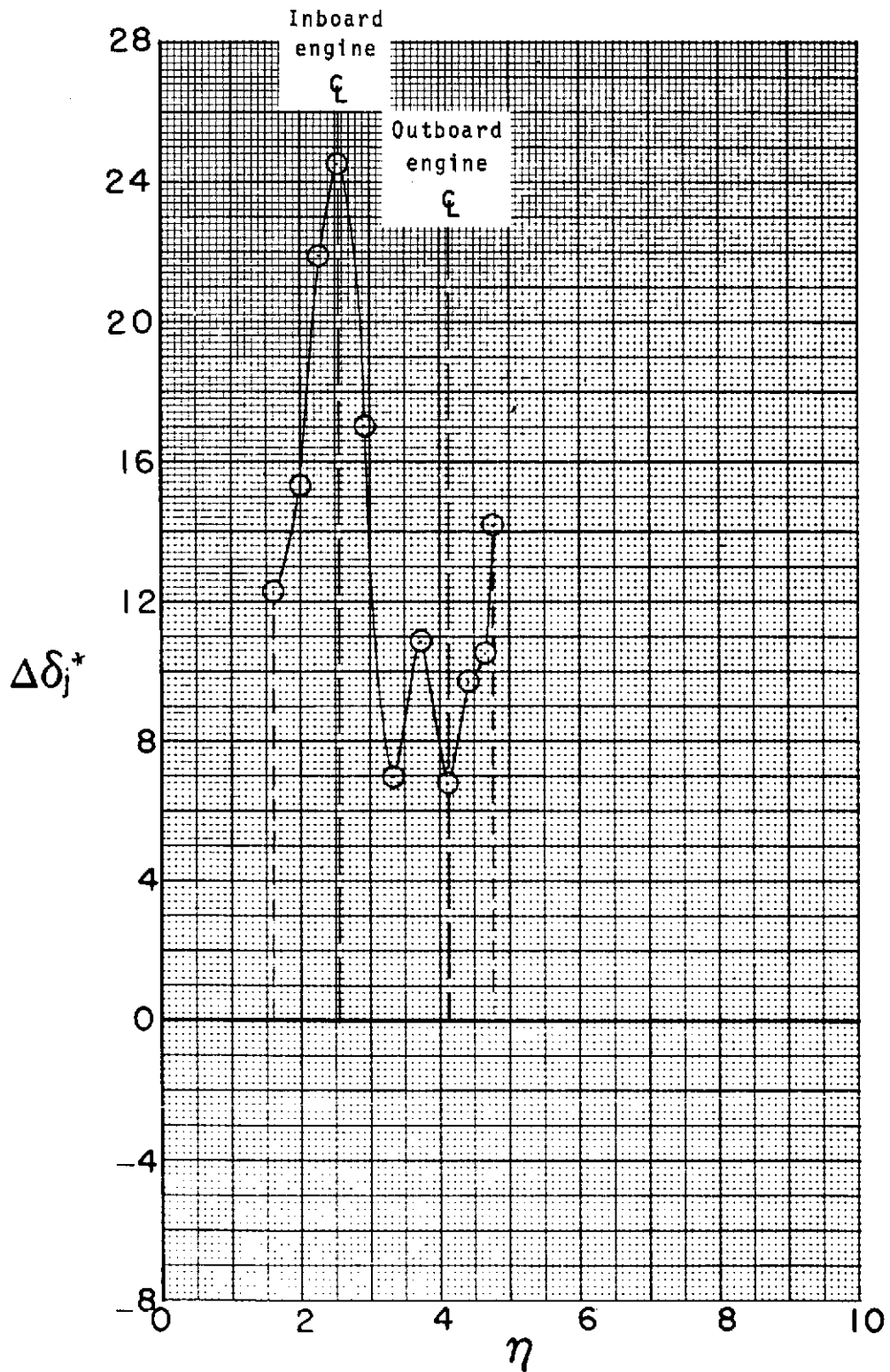power for a thrust coefficient of 1.95.

(b)  $\alpha = 8°$.

Figure 158.- Continued.

(c)  $\alpha = 12^O$.

Figure 158.- Continued.

(d)  $\alpha = 16^O$.

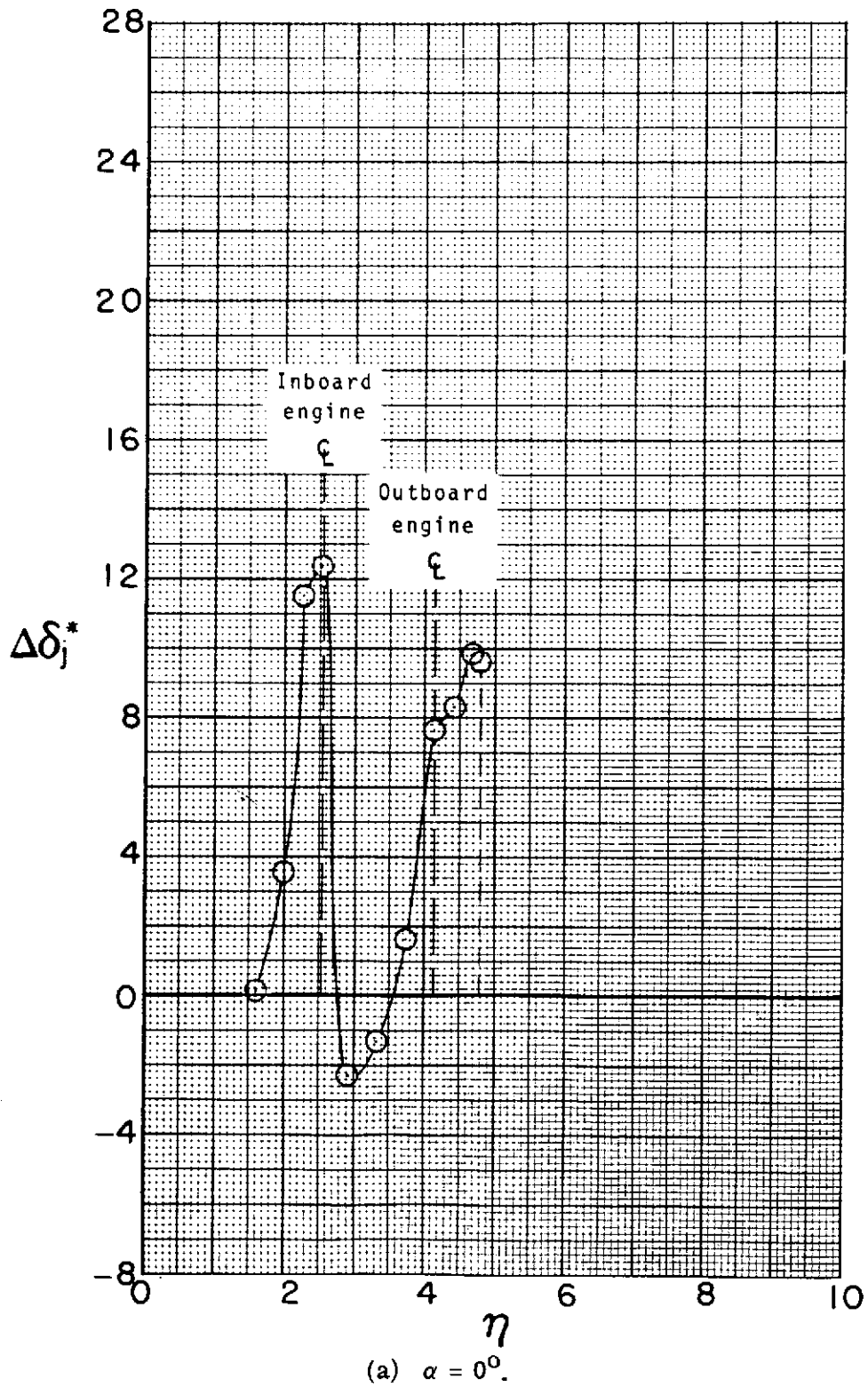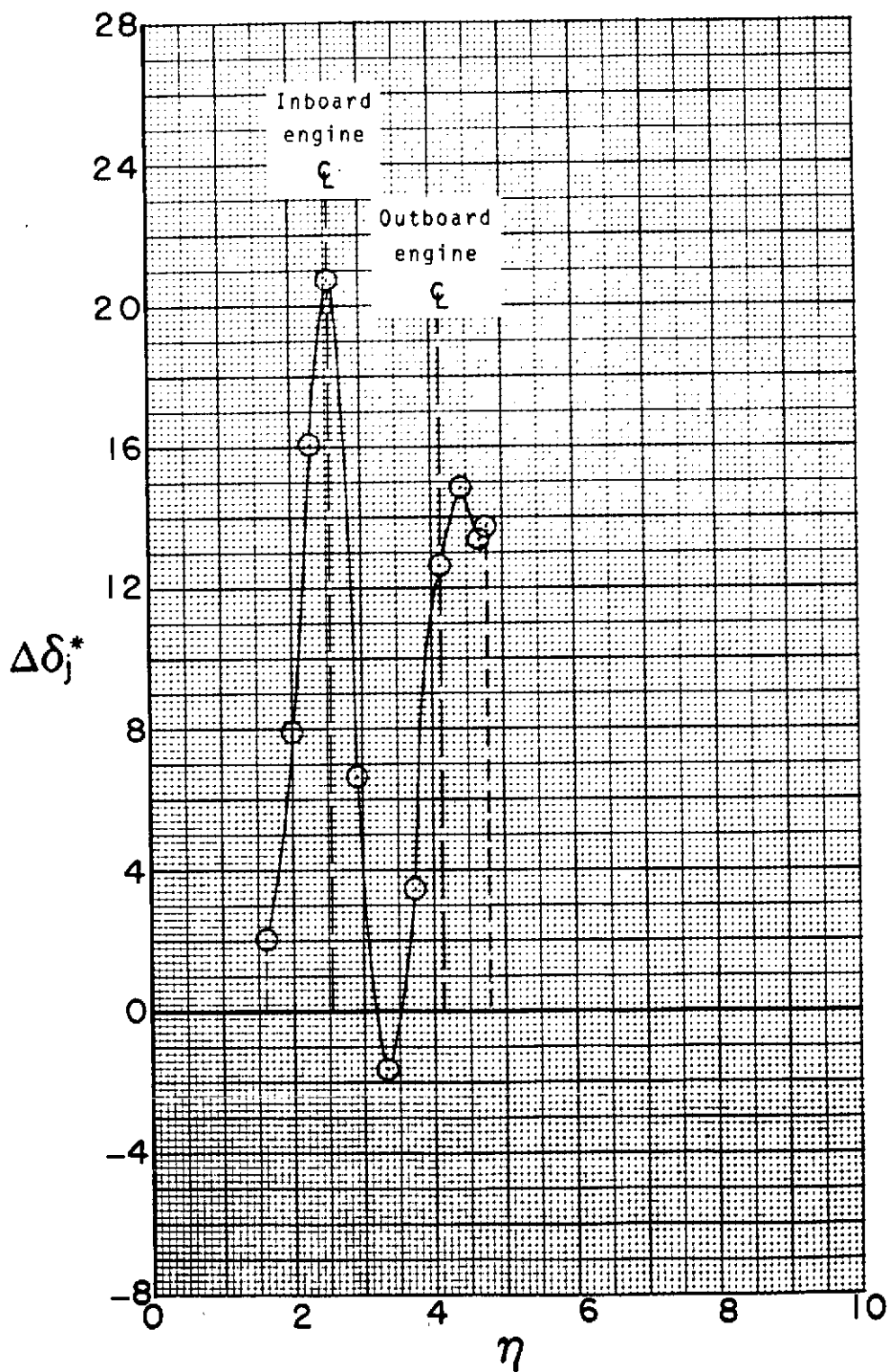Figure 158.- Concluded.

(a)  $\alpha = 0^{\circ}$.

Figure 159.- Change in experimental jet-deflection angle due to
power for a thrust coefficient of 3.90.

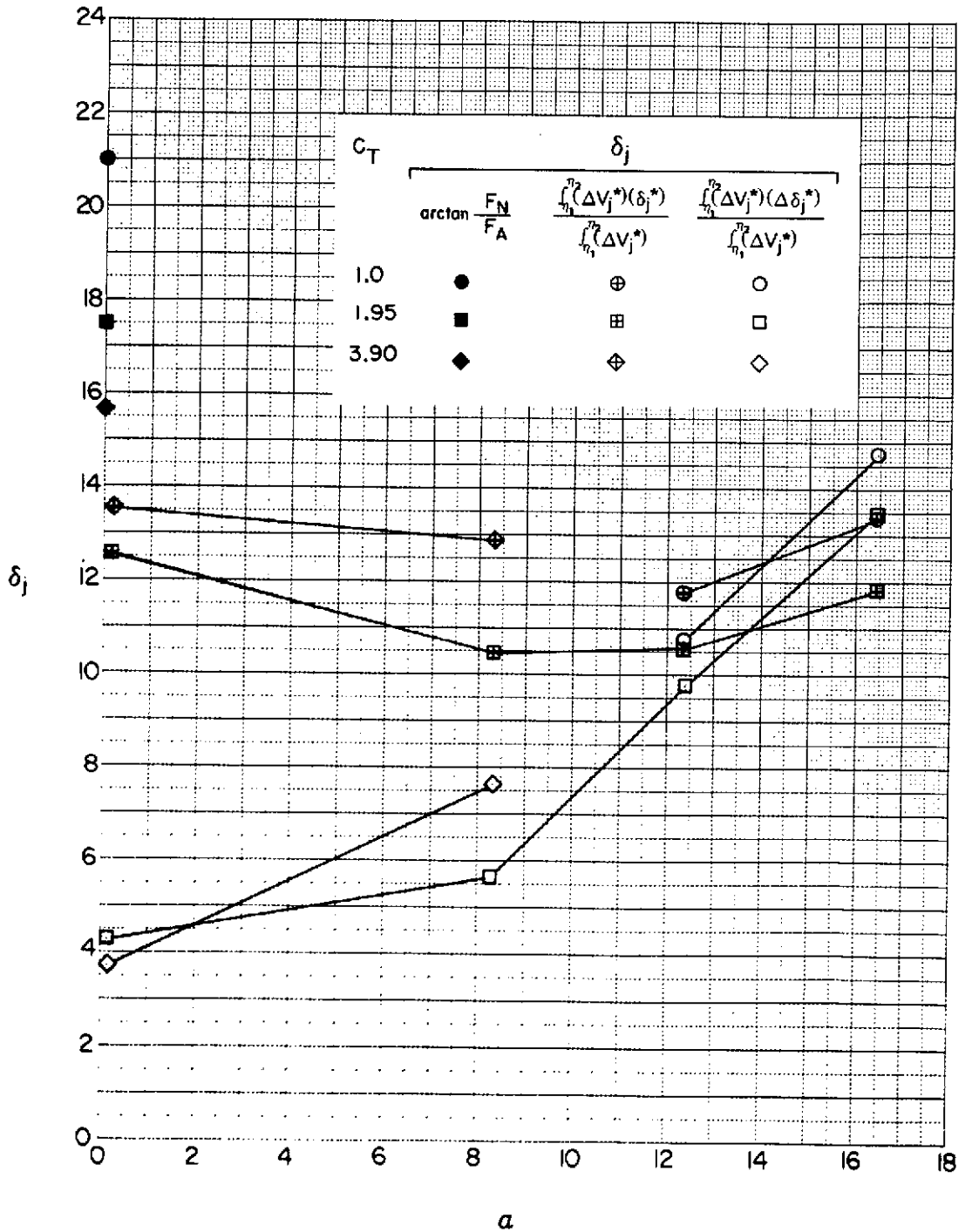(b) $\alpha = 8^\circ$.

Figure 159.- Concluded.

Figure 160.- Comparison of jet-deflection angles from wake survey
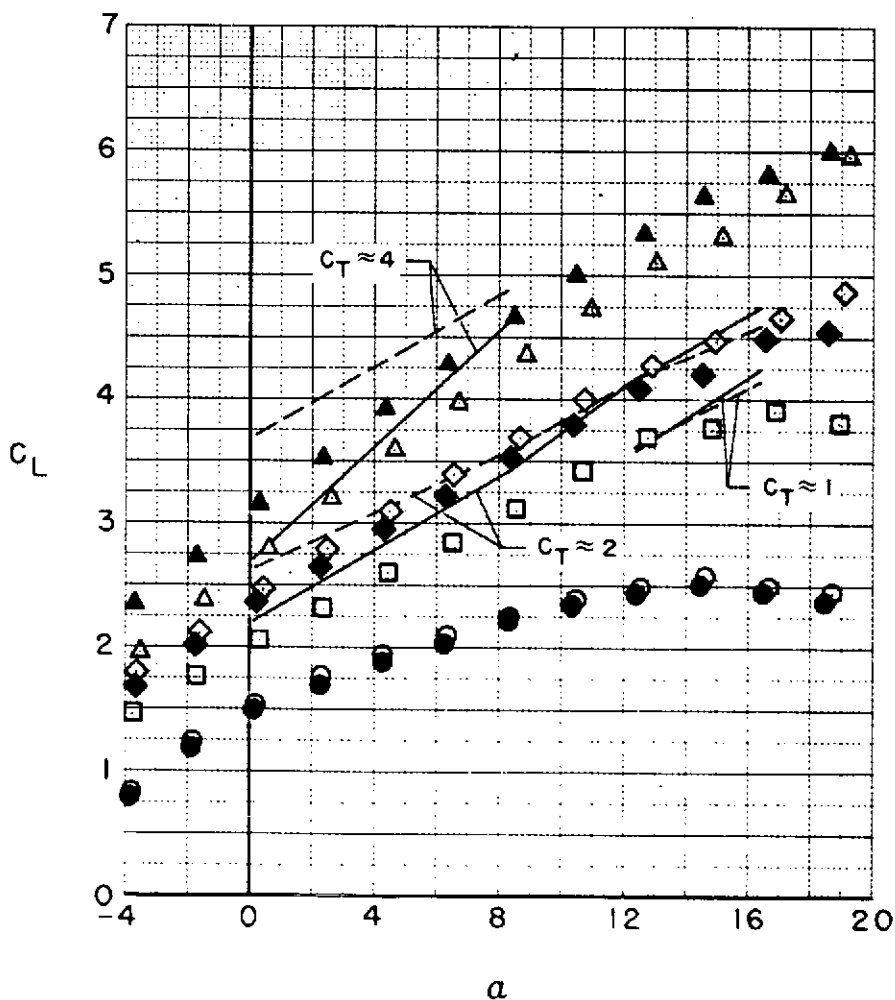with jet-deflection angles from static turning tests.

Figure 161.- Comparisons of theoretical estimations with experimental data.